THE TLR9 SIGNALLING PATHWAY IS A DOUBLE-EDGED SWORD IN THE FAILING HEART

Mistry, Trusha Jayantilal

Awarding institution:
King's College London

THE TLR9 SIGNALLING PATHWAY IS A DOUBLE-EDGED SWORD IN THE FAILING HEART

Trusha J Mistry

Submitted for the degree of

Doctor of Philosophy

from King's College London

January 2016

Supervisors : Professor Kinya Otsu & Dr Alison Brewer

Abstract

Common causes for heart failure (HF) include hypertension and myocardial infarction (MI). Although inflammation is associated with HF, the processes that initiate myocardial inflammation remain unknown. The immune sensor, toll-like receptor (TLR)-9 is involved in pressure overload-induced myocardial inflammation and cardiac remodelling. Various cellular pathways are activated after pressure overload, including the β-adrenergic receptor (β-AR) signalling cascade. Furthermore, the role of TLR9-mediated inflammation after MI is yet to be determined. Therefore, this thesis aimed to elucidate the pathophysiological relevance of TLR9-mediated inflammation in HF induced by chronic β-AR activation and MI.

WT and TLR9KO mice were implanted with minipumps infusing 50 mg/kg/day isoprenaline (Iso) over 4 weeks. Cardiac dysfunction, chamber dilatation, hypertension, heart weight gain and tachycardia were observed in Iso-infused WT and TLR9KO mice. The extent of fibrosis, inflammation and apoptosis were similar between WT and TLR9KO mice after Iso infusion. Interestingly, Iso-infused TLR9KO mice exhibited improved cardiac function and reduced heart weight gain compared to Iso-infused WT mice, suggesting that TLR9 influences β-AR-induced cardiac remodelling. Further investigation of the Iso infusion model found that Iso-induced cardiac dysfunction and tachycardia were recoverable 1 day after removal of Iso. Whilst metabolism, oxidative stress, calcium signalling and mitochondrial structure were maintained after Iso infusion, increased degradation of IκB was observed.

To evaluate the role of TLR9-mediated inflammation after MI, WT and TLR9KO mice were subjected to coronary artery ligation. Interestingly, the mortality of TLR9KO mice 4 days after MI was significantly higher than WT mice due to cardiac rupture. There were no differences in inflammation between MI-operated WT and TLR9KO mice. However, decreased mRNA of *Timp1* and fewer fibroblasts and myofibroblasts were observed in MI-operated TLR9KO mice compared to WT mice, suggesting a life-preserving role of TLR9 in tissue repair.

These findings indicate novel roles of TLR9, independent of its inflammatory function and demonstrate its double-edged nature within the failing heart.

Declaration of independent work

I, the author of thesis, declare that the work presented in this thesis was conducted by me, except where indicated in the text.

Trusha Mistry

Acknowledgements

First and foremost I would like to thank my primary supervisor, Professor Kinya Otsu for all of his expertise, support and guidance that he has provided throughout this PhD project. Additionally, I would like to thank Dr Alison Brewer for her patience and encouragement in driving this project.

My sincere thanks go to Dr Kazuhiko Nishida, Dr Manabu Taneike, Dr Shigemiki Omiya and Dr Yosuke Omori for their advice and assistance throughout my PhD.

I would like to thank all of the people that I have worked with who have made my PhD much more enjoyable. My sincere thanks goes to Dr Elham Zarrinpashneh, Dr Nooreen Shaikh, Dr Can Zhou, Ms Ruth Austin, Mr Francesco Nicolini, Ms Shana de Silva and Ms Amber Emmerson who have supported and encouraged me throughout this PhD journey and brightened my time at the JBC.

To my brother, extended family and friends, thank you for providing support and guidance. Dipen, I will be forever grateful to you for the advice and encouragement that you have provided and for inspiring me through the toughest of times. Finally I would like to dedicate this thesis to my parents, who have provided me with continuous love, advice and encouragement and have really supported me during this PhD.

Table of Contents

Table of Figures

Table of Tables

Abbreviations

α-SMA	Alpha-smooth muscle actin
β-AR	Beta – adrenergic receptor
βMHC	Beta myosin heavy chain
AC	Adenylate cyclase
ACE	Angiotensin converting enzyme
ADP	Adenosine diphosphate
AMP	Adenosine monophosphate
AMPK	Adenosine monophosphate-activated protein kinase
Ang II	Angiotensin II
ANOVA	Analysis of variance
ANF	Atrial natriuretic factor
AR	Adrenergic receptors
ASC	Apoptosis-associated speck-like protein containing a caspase recruitment domain
ATP	Adenosine triphosphate
BNP	Brain natriuretic peptide
BP	Blood pressure
BSA	Bovine serum albumin
BW	Body weight
cAMP	Cyclic adenosine monophosphate
CaM	Calmodulin
CaMKII	Calcium / calmodulin-dependent protein kinase II
CICR	Calcium induced calcium release
CF	Cardiac fibroblasts
CO	Cardiac output
CoA	Coenzyme A
CpG	DNA motif in which cytosine triphosphate deoxynucleotide is followed by guanine triphosphate deoxynucleotide
CPT	Carnitine palmitoyltransferase
CSA	Cross-sectional area
CVD	Cardiovascular disease
Cyt c	Cytochrome C
DAB	Diaminobenzidine
DAMP	Danger associated molecular pattern
DAPI	Diamidino-2-pheylindoledihydrochloride
DCM	Dilated cardiomyopathy
DISC	Death-inducing signalling complex
DMEM	Dulbecco’s modified eagle’s medium
DNase II	Deoxyribonuclease
ECG	Electrocardiography
Echo	Echocardiography
ECM	Extracellular matrix
EDTA	Ethylenediaminetetraacetic acid

EF	Ejection fraction
FA	Fatty acids
FA	Formaldehyde
FADD	Fas-associated protein with death domain
FADH	Flavin adenine dinucleotide
FITC	Fluorescein isothiocyanate
FS	Fractional shortening
G6P	Glucose-6-phosphate
GLUT	Glucose transporters
GPCR	G-protein coupled receptor
GRK	G-protein coupled receptor kinases
H & E	Haematoxylin and eosin
HCM	Hypertrophic cardiomyopathy
HF	Heart failure
HFpEF	Heart failure with preserved ejection fraction
HFrEF	Heart failure with reduced ejection fraction
HR	Heart rate
HW	Heart weight
IAP	Inhibitor of apoptosis
IF	Immunofluorescence
IFN	Interferon
IHC	Immunohistochemistry
IκB	Inhibitor of kappa-B
IKK	Inhibitor of kappa B kinase
IL	Interleukin
IP	Intraperitoneal
I/R	Ischemia-reperfusion
IRAK	IL1R-associated kinase
IRF	Interferon regulatory factor
ISF	Isoflurane
Iso	Isoprenaline
IVSd	End-diastolic interventricular septum
IVSs	End-systolic interventricular septum
KO	Knockout
LAD	Left anterior descending
LDH	Lactate dehydrogenase
LRR	Leucine rich region
Liver W	Liver weight
LTCC	L-type calcium channel
Lung W	Lung weight
LV	Left ventricle
LVIDd	End-diastolic left ventricle internal diameter
LVIDs	End-systolic left ventricle internal diameter
LVPWd	End-diastolic left ventricle posterior wall
LVPWs	End-systolic left ventricle posterior wall

MAPK	Mitogen-activated protein kinases
MBP	Mean blood pressure
mtDNA	Mitochondrial DNA
MI	Myocardial infarction
MMP	Matrix metalloproteinases
MPT	Mitochondrial permeability transition
mPTP	Mitochondrial permeability transition pore
MRI	Magnetic resonance imaging
MT	Mason trichrome
NADH	Nicotinamide adenine dinucleotide
NCX	Sodium calcium exchanger
NFκB	Nuclear factor kappa-light-chain-enhancer of activated B cells
NLR	NOD-like receptors
NOD	Nucleotide-binding oligomerisation domain
ODN	Oligonucleotide
OMM	Outer mitochondrial membrane
PAMP	Pathogen associated molecular pattern
PBS	Phosphate buffered saline
PCR	Polymerase chain reaction
PFA	Paraformaldehyde
PI	Proteinase inhibitors
PKA	Protein kinase A
PKC	Protein kinase C
PLN	Phospholamban
PPARα	Peroxisome proliferator-activated receptor alpha
PPP	Pentose phosphate pathway
PRR	Pattern recognitions receptors
qRT-PCR	Quantitative real time polymerase chain reaction
RAAS	Renin angiotensin aldosterone system
RIP	Receptor-interacting protein
ROS	reactive oxygen species
RT	Reverse transcription
RT	Room temperature
RyR	Ryanodine receptor
SC	Subcutaneous
SDS	Sodium dodecyl sulphate
SDS-PAGE	Sodium dodecyl sulphate polyacrylamide gel electrophoresis
SEM	Standard error mean
SERCA	Sarco/endoplasmic reticulum calcium ATPase
SIC	Stress-induced (or takotsubo) cardiomyopathy
SR	Sarcoplasmic reticulum
SV	Stroke volume
TAC	Transverse aortic constriction

TBE	Tris buffered ethylenediaminetetraacetic acid
TBS	Tris buffered saline
TCA	Tricarboxylic acid
TE	Tris-ethylenediaminetetraacetic acid
TEM	Transmission electron microscopy
TGF	Transforming growth factor
TIC	Tachycardia induced cardiomyopathy
TIMP	Tissue inhibitors of metalloproteinases
TIR	Toll and interleukin-1 receptor
TL	Tibia length
TLR	Toll like receptor
TM	Transmembrane
TNF	Tumour necrosis factor
TNF-R	Tumour necrosis factor receptor
Tpn	Troponin
TRADD	Tumour necrosis factor receptor type 1-associated death domain
TRAF	Tumour necrosis factor receptor associated factor
TRITC	Tetramethylrhodamine
TUNEL	Terminal deoxynucleotiyl transferase dUTP nick end labelling
VOCC	Voltage operated calcium channels
W	Weight
WGA	Wheat germ agglutinin
WT	Wild-type

1 Introduction

1.1 The heart

The heart is a simple, yet extraordinary organ, which operates as a mechanical pump propelling oxygen- and nutrient- rich blood around the body to supply metabolising tissues with the necessary nutrients. The muscular component of the heart is architecturally diverse and is composed of a myriad of different cell types with 30% being cardiomyocytes [1, 2]. Other cells that reside in myocardial tissue include fibroblasts, endothelial cells, pericytes, vascular smooth muscle cells and tissue-residing macrophages [1, 3]. Collectively, these cells maintain the electrical, chemical and biomechanical functions of the heart. Furthermore, a number of extracellular matrix (ECM) components provide structural integrity and scaffolding [4, 5] while gap junctions between cardiomyocytes electrochemically integrate the contraction of neighbouring cells. Cardiomyocytes are terminally differentiated, contractile cells that possess repeating units of sarcomeres, consisting of actin and myosin among other contractile proteins [2]. The movement of actin and myosin filaments, mediated by adenosine triphosphate (ATP) and calcium, provide the molecular basis for cardiomyocyte contraction [6, 7, 8]. With ATP and calcium fundamental for cardiomyocyte contractile function, the cardiomyocyte possesses many ATP-generating mitochondria whilst the sarcoplasmic reticulum (SR) is a major calcium store. Therefore, both ATP production and calcium handling are tightly regulated to preserve the pumping nature of the myocardium.

1.2 Heart failure (HF)

Within the UK, HF is a leading cause of morbidity and mortality with 900,000 people currently diagnosed with this complex clinical syndrome [9]. HF occurs when the heart fails to pump blood adequately to meet the demands of metabolising tissues [10]. This condition may originate from structural cardiac abnormalities or it may arise as an indirect consequence of other conditions including chronic hypertension, myocardial infarction (MI) and cardiomyopathies [11, 12, 13]. As these conditions increase cardiac workload, the heart induces compensatory mechanisms, to increase cardiac function and decrease wall tension [14]. Unfortunately, over time, these adaptations decrease myocardial contractility and are detrimental to the heart [15]. Structural and/or functional cardiac abnormalities lead to myocyte dysfunction, death and/or ventricular remodelling which may contribute to HF [16]. Among the many biochemical abnormalities associated with the progression of HF, are the elevated levels of circulating catecholamines [17, 18] and proinflammatory cytokines such as tumour necrosis factor (TNFα) [19], interleukin 6 (IL6) and IL1β [20, 21] as well as impaired β-adrenergic receptor (β-AR) signalling [18, 22].

HF can be classified according to the length of its progression (acute versus chronic), the location of the dysfunction (left-sided versus right-sided) and the phase within the cardiac cycle that is disrupted (systolic versus diastolic) [23]. Chronic HF cases are more common than acute incidents [23] and right-sided HF, observed by systemic congestion, commonly transpires following left-sided HF, indicated by pulmonary oedema [23]. Systolic HF can be diagnosed when ventricles contract abnormally, such that blood is pumped into the circulation with insufficient force, leading to symptoms such as pulmonary congestion [24]. Further, if the myocardium is too stiff and incapable of relaxing fully, then

insufficient blood enters the ventricles, referred to as diastolic dysfunction [24]. Clinically, these conditions may manifest with reduced ejection fraction (HFrEF) or with preserved ejection fraction (HFpEF), which have distinct pathophysiologies [25, 26].

Current medications for HF patients help to attenuate the symptoms, impede the progression of the condition and improve the quality and length of life. Common treatments include β-AR blockers (β-blockers) [27], angiotensin-converting-enzyme (ACE)-inhibitors [28], angiotensin II (Ang II) type 1 receptor blockers and lifestyle changes [16]. Even with current therapeutics, prognosis is still poor. With the number of cases of HF anticipated to increase, it becomes increasingly important to comprehend the molecular mechanisms of this condition, such that this may aid the development of novel and effective treatments.

1.2.1 MI

As mentioned earlier, the susceptibility to develop HF increases after MI. The most common cause of MI is atherosclerotic narrowing of coronary arteries associated with plaque rupture, completely blocking the blood flow through the coronary artery [29]. This denies the provision of oxygen and nutrients to actively contracting cardiomyocytes, ceasing ATP generation by oxidative phosphorylation. As the contractile function of cardiomyocytes corresponds to the rate of ATP formation, the inability to generate ATP equates to depressed contractile function, which reduces blood pressure (BP), cardiac output (CO) and stroke volume (SV).

An estimated 1 billion cardiac cells can be lost in a typical MI [30]. Cells begin to die within the first few hours, by necrosis and apoptosis, leading to an infarct.

Dying cells alter the electrical conductivity of the heart and release creatinine kinase, lactate dehydrogenase (LDH), troponin T (TpnT) or TpnI. Clinically, these electrophysiological and biochemical abnormalities can be detected and are routinely used to diagnose MI [31].

In response to these dying cells, a wound healing response is initiated to remove debris and dead cells, promote tissue repair and stimulate scar formation. This can be separated into 3 distinct, yet overlapping phases [32]. The initial inflammatory response is associated with cytokine and chemokine expression along with infiltration of leukocytes to mediate clearance of dead cells and tissue debris [33]. This is followed by the proliferative phase in which inflammation is supressed and fibroblasts and myofibroblasts secrete matrix proteins to mediate remodelling of the ECM and scar formation. Lastly, the maturation phase is characterised by apoptosis of the participating cells, leaving a cross-linked collagen scar. Furthermore, myocyte and ECM remodelling of the infarct regions leads to infarct expansion, thinning of the myocardium and chamber dilatation [34, 35].

This permanent damage to the myocardium increases the susceptibility of developing life-threatening arrhythmias and/or inducing rupture of the cardiac wall after acute MI, which accounts for 5 - 20% of hospital deaths after MI [36].

Reperfusion is the only option to salvage an ischemic tissue and is achieved by thrombolytic treatment or by percutaneous coronary intervention through surgical insertion of a coronary balloon or stent. However, in the early moments of reperfusion, significant reversible and irreversible damage is also initiated, known as ischemia-reperfusion (I/R) injury (**section 1.6.4.1**).

1.2.2 Hypertension

BP, the force at which blood is propelled out of the heart and into the major arteries, is regulated by several factors including humoral mediators, blood vessel elasticity and neural stimulation, such as the renin-angiotensin-aldosterone system (RAAS) [37]. In developed countries, hypertension affects 20 – 50% of adults and contributes to 49% of all heart diseases, including HF [38]. Under hypertensive conditions, pressure on the left ventricle (LV) escalates leading to myocardial stiffness and cardiac hypertrophy. Renal sodium retention, stress associated with central and sympathetic nervous system activity along with the loss of elasticity and contractile nature of the vasculature are proposed causes of hypertension [37]. Fortunately, hypertension can be managed with the use of ACE inhibitors and Ang II type 1 receptor blockers, which inhibit RAAS-induced vasoconstriction [39, 40]. However, if left untreated, hypertension can have serious consequences since it is an adverse risk factor for MI, HF, stroke and vascular diseases [37, 39].

1.2.3 Cardiomyopathies

Cardiomyopathies are diseases of the myocardium that have not arisen from pericardial, hypertensive or valvular disorders. Although cardiomyopathies may transpire from a multitude of factors, such as alcohol, toxins or viral infection [41, 42, 43], the best-described cases are congenital with more than 900 acknowledged genetic mutations [44], of which 400 have been identified in 13 sarcomeric proteins [43].

The most prevalent type of cardiomyopathy is dilated cardiomyopathy (DCM) [45], in which one or both ventricular chambers are dilated, with thinner walls and larger, more spherical chambers. Whilst the volume of the chamber increases,

the systolic function declines. Molecular features of DCM include apoptosis, fibrosis, wall stiffness and inflammatory cell infiltration [45]. In the case of hypertrophic cardiomyopathy (HCM), patients exhibit asymmetrical thickening of the septum, increasing myocardial muscle mass, but reduced chamber size [46, 47]. Enlarged and misaligned (myocardial disarray) cardiomyocytes in conjunction with interstitial fibrosis and inflammation has been described in HCM patients [43, 48]. Alas, both DCM and HCM can progress to HF.

1.2.3.1 Reversible cardiomyopathies

Cardiomyopathies with transient LV dysfunction possess several phenotypic characteristics that are associated with HF and MI. However, the remodelling associated with HF and MI is irreversible, whilst features of the cardiomyopathies discussed below are recoverable.

Tachycardia-induced cardiomyopathy (TIC) is associated with prolonged elevated heart rate (HR) or irregular heart rhythm. Haemodynamic features of TIC include fleeting systolic dysfunction, LV chamber dilatation, neurohormonal activation, reduced CO, increased ventricular filling pressures and increased vascular resistance [49, 50, 51]. At the molecular level, TIC is associated with cellular elongation, myofibril misalignment, disorganisation of the ECM, loss of sarcomeric structure and mitochondrial morphological and functional defects [51, 52, 53]. Abnormal calcium handling, myocardial energy depletion, myocardial ischemia and ECM remodelling are proposed to induce TIC [50, 54, 55, 56, 57]. Taking HR cadence and duration of tachycardia into consideration, TIC increases the risk of HF, although tachycardia can be controlled with medication.

Another cardiomyopathy associated with transient LV function is stress-induced or takotsubo cardiomyopathy (SIC). In this condition, LV dysfunction is

associated with regional wall abnormalities, such as akinesia or hyperkinesia in apical, midventricular and/or basal regions [58, 59]. This condition is precipitated by intense emotional or physical stress and is usually accompanied by a surge in catecholamine levels [60, 61]. Lethal complications can include arrhythmias, cardiogenic shock and ventricular rupture. Ventricular ballooning, electrocardiography (ECG) abnormalities and a slight elevation of cardiac enzymes are prominent features of this condition together with leukocyte infiltration, contraction band necrosis, clustering of mitochondria of variable shapes and sizes and enlargement of ECM [61, 62, 63, 64]. Several pathological mechanisms have been proposed including multivessel vasospasm, catecholamine-induced cardiomyocyte stunning and increased ventricular afterload [58, 59]. The favoured hypothesis proposes that catecholamine-induced cardiomyocyte stunning induces the switching of β2-AR signalling from Ga_s to Gi (**section 1.6.1**), which mediates anti-apoptotic and negative inotropic effects [65].

Most surprisingly, after functional recovery the changes in myocardial composition and appearance can be restored to normal. Further study is required to understand the molecular processes involved in the recovery of the cardiac function in these reversible cardiomyopathies, these potential, which could have extensive implications for HF and cardiovascular disease (CVD) therapies.

1.3 Myocardial injury and cardiac remodelling

Cardiac remodelling may be defined as the molecular, cellular and interstitial modifications that manifest after myocardial stress or injury, leading to morphological and functional modulations to the heart [66]. Cardiac remodelling involves amendments to the ECM and to cardiomyocytes, such as shape and size, in addition to changes in wall thickness, scar formation, chamber dilatation, cell death and fibrosis, which modify the overall structure and function of the myocardium (**figure 1.1**) [66, 67]. Cardiac remodelling is a dynamic and time-dependent process and is influenced by haemodynamic load, neurohormonal activation as well as other hormones, peptides and cytokines [66].

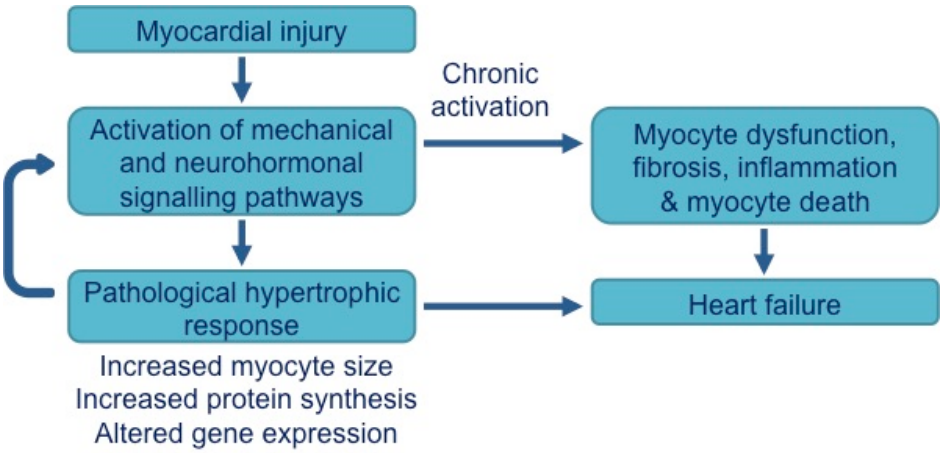

Figure 1.1 Cardiac remodelling response.
Injury to the myocardium activates mechanical and neurohormonal signalling pathways to aid and enhance the cardiac workload. Stimulation of these signalling pathways leads to pathological hypertrophy. Initially this response is beneficial to the heart but over a prolonged period, it leads to myocyte dysfunction, fibrosis, inflammation and myocyte cell death, all of which contribute to heart failure. Adapted from [68].

1.3.1 Hypertrophic responses

Under conditions such as hypertension or during exercise, the heart must adapt to conduct the extra work, normalise the load and reduce wall stress. The hypertrophic response is initiated, enlarging the size of cardiomyocytes leading to increased wall thickness [2]. The initial decline in cardiac function is remedied

with an improvement in contractile function of the cardiac muscle, decreasing ventricular wall tension [69]. Depending on the type of stress, the heart may undergo 2 types of hypertrophic responses: physiological cardiac hypertrophy and pathological cardiac hypertrophy [2, 14, 70] (**figure 1.2**).

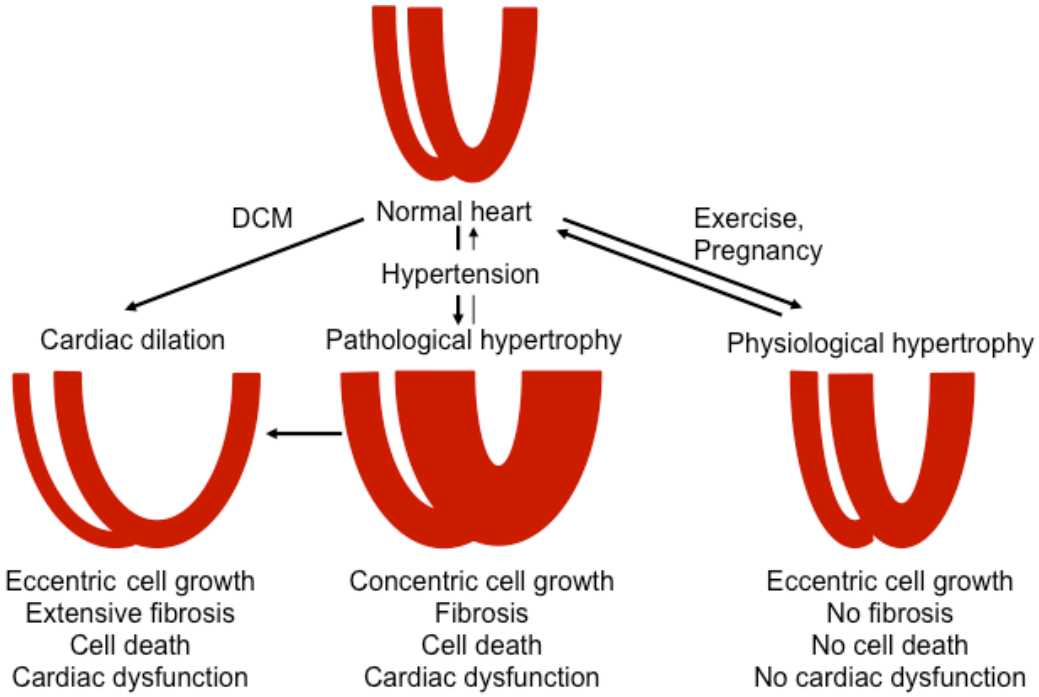

Figure 1.2 Cardiac hypertrophic responses.
The adaptive and reversible physiological hypertrophic response to exercise and pregnancy leads to eccentric cell growth and maintained cardiac function. Pathological hypertrophy induces concentric hypertrophy which initially improves cardiac function. Over time, cardiac remodeling is detrimental as fibrosis and cell death impair cardiac function. Cardiac dilation may occur from normal hearts under conditions such as dilated cardiomyopathy (DCM) or from severe pathological hypertrophy. Adapted from [14].

During exercise or pregnancy, the heart undergoes a physiological hypertrophic response, which is mediated through insulin-like growth factor 1 and transduced downstream by phosphoinositide 3-kinase-Akt signalling [9, 71, 72]. A uniform cardiac growth response is observed, with sarcomeres added in series elongating the cardiomyocytes which is known as eccentric hypertrophy (**figure 1.2**). There is a matched increase in ventricular wall thickness and chamber

dimensions. This adaptive response is accompanied with normal or enhanced cardiac function [69].

Pathological cardiac hypertrophy may evolve from sustained hypertension or cardiomyopathies (**figure 1.2**). Stimulation of biomechanical and stretch sensitive mechanisms in addition to neurohormonal signalling (such as proinflammatory cytokines, hormones and growth factors) activate pathways that mediate pathological cardiac growth. This includes induction of mitogen-activated protein kinases (MAPK) signalling through ERK1/2 [73, 74] in addition to stimulation of protein phosphatase, calcineurin [75, 76] and calcium/calmodulin-dependent protein kinase II (CaMKII) [77, 78] to evoke the changes associated with pathological cardiac hypertrophy. These modifications include increased size of the cardiomyocytes, increased protein synthesis and reactivation of the foetal gene program, including atrial natriuretic factor (ANF), brain natriuretic peptide (BNP) and β myosin heavy chain (βMHC) [70, 79]. Cardiomyocytes undergo concentric hypertrophy, with sarcomeres added in parallel, widening the cardiomyocyte, which physiologically corresponds to thicker ventricular and septal walls and a decrease in chamber dimensions. These changes are initially compensatory which improve the pumping function of the heart [80]. Over time, the compensatory state becomes maladaptive with impaired cardiac function, increasing the risk of adverse cardiac events [9, 80, 81]. The reasons for the change from compensated to decompensated state remain unclear. However it maybe associated with the remodelling of the myocardium such as ECM adaptations, fibrosis and cell death, along with alterations in the expression of proteins involved in electrochemical (EC) coupling and changes to the energetic and metabolic state of the cardiomyocyte [66, 70, 82].

Cardiac dilation has a similar, yet more severe phenotype compared with pathological hypertrophy and this has been noted to be a feature of the transition from the compensatory state to the decompensated phase (**figure 1.2**). Signalling is mediated through the MEK5-ERK5 proteins of the MAPK family as well as calcineurin and CaMKII [70, 83, 84] and is associated with eccentric hypertrophy inducing dilatory growth of the cardiac muscle [14]. Cardiac dysfunction, fibrosis and cell death along with ECM remodelling are apparent in this phenotype.

1.3.2 Fibroblasts, myofibroblasts, ECM remodelling and fibrosis

Within the heart, the ECM is a network that encompasses and interconnects myocytes and non-myocytes, providing structural support and a means to distribute force through the myocardium. The ECM is comprised of a fibrillar collagen network with elastin, fibrillin, fibronectin, laminin, proteoglycans and glycosaminoglycans components [5, 85]. The arrangement of the collagen fibres provides scaffolding for adjoining myocytes and connections to sarcomeric proteins through the integrin family [4, 86].

Interruptions within the ECM network disrupt myocardial structure and support, subjecting cardiomyocytes to abnormal stresses and strains that perturb myocardial geometry and function. The ECM is maintained by cardiac fibroblasts (CFs), through their ability to synthesise and deposit ECM proteins and create and secrete matrix-degrading enzymes, a process known as ECM remodelling [4, 5, 85].

Fibroblasts are highly heterogeneous cells, with distinctive phenotypic properties and functions in different organs or under various physiological conditions. These flat and spindle-shaped cells with multiple protrusions, usually

of mesenchymal origin [87], are derived from mesangioblasts, monocytes, fibrocytes and pericytes [88] (**figure 1.3**). Additional sources of fibroblasts include epicardial and endocardial cells, which undergo epithelial-mesenchymal [89] and endothelial-mesenchymal transformations [90].

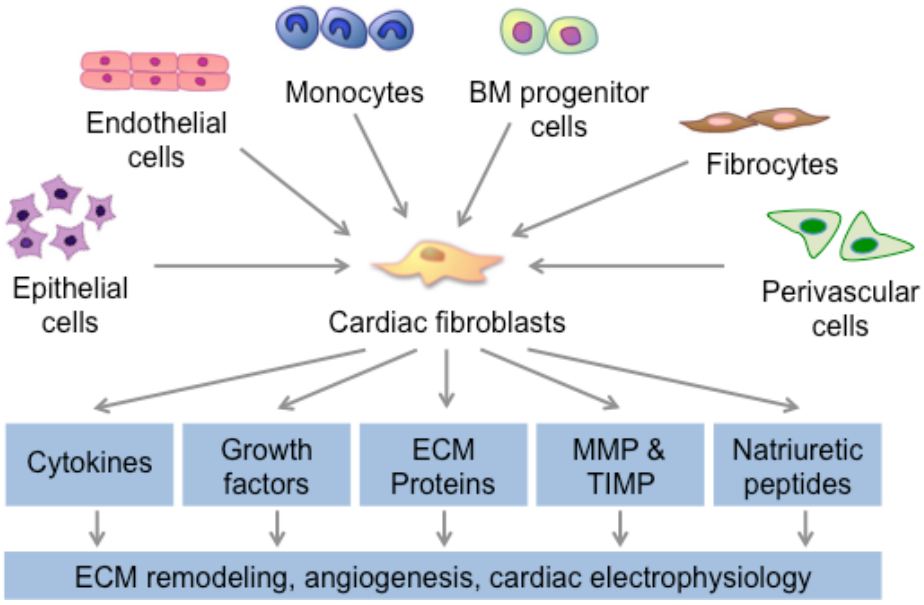

Figure 1.3 The sources and functions of cardiac fibroblasts (CFs).
CFs are sourced from a variety of cells, such as epithelial cells and endothelial cells, and possess the ability to perform multiple functions in physiological and pathological settings. CFs are capable of producing and secreting many mediators which facilitate processes such as ECM remodelling, angiogenesis and angiogenesis. Adapted from [5].

CFs are described as 'sentinels', sensing changes in the environment and reacting to preserve organ function [5]. In the myocardium, CFs reside in the cardiac interstitium and are organised in sheets and strands that run parallel with myofibres to maintain continuity between cells and the overall structural integrity of the heart [91, 92]. These cells contribute to structural, mechanical, biochemical and electrical properties of heart, with a particular role in maintaining and remodelling the ECM [85].

Another subset of cells observed during cardiac remodelling are myofibroblasts. In comparison to fibroblasts, these cells possess enhanced migratory,

proliferative, contractile and secretory properties [85, 93]. The main distinction from fibroblasts is the expression of contractile proteins such as alpha smooth muscle actin (α-SMA) within myofibroblasts [32, 93, 94]. Myofibroblasts are necessary for tissue repair and scarring and are therefore not expressed within the healthy myocardium, but appear after injury [95]. Their contractile nature is proposed to aid wound closure and provide structural integrity to cardiac scar tissue [96, 97].

Myofibroblasts can differentiate from fibroblasts, progenitor stem cells and endothelial cells [88] and are induced by transforming growth factor beta (TGFβ), cytokines, ECM and growth factors. While several studies have suggested that CFs differentiate into myofibroblasts, other studies have opposed this view [93, 98, 99], therefore further study is required to clarify the sources of CFs.

CFs and myofibroblasts play a key role during the pathological remodelling of the heart. CFs are activated by a variety of pathological stimuli including myocardial injury, oxidative stress, mechanical stress and autocrine and paracrine mediators including cytokines [85]. After injury, the number of fibroblasts and myofibroblasts increase and migrate to the site of injury guided by a chemokine gradient to promote wound healing and scar formation [32]. Together fibroblasts and myofibroblasts facilitate remodelling of the ECM by synthesising and secreting ECM proteins, cytokines, growth factors and matrix metalloproteinases (MMPs). Initial fibroblast activation and proliferation are essential for reparative wound healing and maintaining cardiac function, however the persistence of fibroblasts after injury leads to fibrotic scaring and adverse remodelling which diminish cardiac function [85, 100].

1.3.2.1 ECM remodelling

The ECM is a dynamic network that is altered in response to pathological stress, which can impact the morphology and function of the heart. MMPs are predominantly responsible for the degradation of the ECM. Whilst, these zinc-dependent proteases degrade a wide spectrum of ECM proteins, each MMP has its own specificity and the 26 currently known members of the human MMP family are classified into 5 different groups based on substrate specificity and structure [101]. The non-membrane MMPs are secreted as zymogens (pro-MMPs) and are activated by cleavage of the amino-terminal propeptide domain by serine proteases [102].

All cells in the myocardium can express MMPs and the members reported to contribute to myocardial remodelling are MMP1, MMP3, MMP8, MMP13, MMP2, MMP9, MMP12, MMP28 and MT1-MMP [5, 103, 104, 105].

To prevent excessive degradation of ECM, MMP expression is tightly regulated by tissue inhibitors of metalloproteinases (TIMPs). There are 4 known members (TIMP 1 - 4) which bind to the active site of MMPs with a 1:1 stoichiometry, blocking access to substrates [102]. In addition, TIMPs are able to bind to the latent forms of MMPs to prevent auto-activation [106]. Though constitutively expressed, TIMPs are differentially expressed in various cells and tissues and TIMP4 is most predominantly expressed in human myocardial tissue [107, 108].

Whilst growth factors and cytokines IL1β and TNFα can induce synthesis and activity of MMPs [109, 110], these 2 mediators have additionally been reported to induce expression of TIMP1 and TIMP2 [111]. Furthermore, *in vitro* studies have suggested that TIMP1 and TIMP2 may stimulate growth of fibroblasts [112].

In humans, alterations in MMP and TIMP expression have been noted in different cardiac diseases, including HF. In patients with end-stage DCM,

decreased MMP1 alongside increased MMP3, MMP9, TIMP1 and TIMP2 was reported [113]. It has been stated that TIMP1 levels were increased in diseased hearts [114] whilst hypertensive patients with pathological hypertrophy have reduced plasma levels of MMP1, MMP2 and MMP9, alongside elevated TIMP1 expression [115, 116]. Elevated levels of MMP2, MMP9 and TIMP1 have been detected in MI patients [117]. Furthermore plasma MMP9 is recognised as a prognostic marker for the indication of late-onset HF [118]. Thus, ECM remodelling mediated by MMP activity and TIMP expression is a crucial mediator for the pathogenesis of HF.

1.3.2.2 Fibrosis

After injury to the myocardium, ECM components are deposited by both fibroblasts and myofibroblasts to promote scar formation and maintain myocardial integrity. However, excessive deposition of ECM proteins and accumulation of fibroblasts, is perceived as scarring and is known as fibrosis [88]. Cardiac fibrosis leads to distorted organ architecture, stiffness, impaired myocardial mechano-electrical coupling leading to systolic and diastolic dysfunction and increased risk of arrhythmias [119]. It has also been reported that fibrosis induces pathological signalling leading to progressive HF [88]. Hyperactive fibroblasts and failure to terminate the wound healing response are the predominant causes for the scarring and the unfavourable remodelling associated with fibrosis [100, 120, 121].

Whilst TNFα and interferon gamma (IFNγ) are recognised as being anti-fibrotic, TGFβ, a profibrotic cytokine, is a vital contributor to the development of cardiac fibrosis [122, 123, 124]. TGFβ has been demonstrated to stimulate transformation of fibroblasts to myofibroblasts and increase ECM protein synthesis [93, 122].

In HF patients, increases in collagen, fibronectin, laminin and vimentin have been detected [125]. The extent of fibrosis negatively correlates with ejection fraction (EF) and altered myocardial structure [5, 88]. Nonetheless, the amino- and carboxyl- terminal properties of collagen type 1 and collagen type 3, are considered biomarkers of collagen synthesis [126] and in hypertensive and HF patients, these markers have been associated with severity of fibrosis and contractile function [127, 128].

1.3.3 Cell death

Cell death is a prominent characteristic of various CVDs including MI and HF [129, 130]. Cardiomyocyte cell death occurs primarily by 2 recognised forms of cell death; programmed necrosis and apoptosis. Though, the characteristics and signal transduction of these pathways are distinct, there are some overlapping features. Both necrosis and apoptosis are activated through cell-surface receptors, referred to as the extrinsic pathway or by the intrinsic pathway, which primarily involves the mitochondria [130, 131].

Apoptosis is defined as programmed cell death [129, 131]. This regulated process is essential during embryonic development and for tissue homeostasis. Cytoplasmic shrinkage, plasma membrane blebbing, nuclear condensation and DNA fragmentation alongside the presence of membrane-enclosed apoptotic bodies are central features of apoptosis [132, 133]. Phagocytosis of apoptotic cells by macrophages and neighbouring cells maintain an efficient clean-up process.

Apoptosis is mediated by cysteine proteases, known as caspases, that are synthesised as zymogens (procaspase) and activated upon cleavage [134]. Caspases are classed as either upstream initiator caspases (caspase -2, -8, -9, -10) or downstream caspases (caspase -3, -6, -7). Initiator caspases cleave and

activate downstream caspases, which subsequently amplify the pro-apoptotic signal by cleaving other apoptotic mediators and cutting many cellular structural and regulatory proteins [129].

Stimulation of the extrinsic pathway is facilitated through death-ligands such as Fas ligand and TNFα (**figure 1.4**) [129, 131, 135]. Activation of the receptor induces the formation of the death-inducing signalling complex (DISC). Fas-associated death domain (FADD) is recruited and binds procaspase -8 or -10 [136]. These caspases are activated through forced proximation [137] and released from the DISC to cleave and activate procaspase -3 and -7, which subsequently cleave cellular proteins. However, activation of the extrinsic pathway is insufficient for complete cell death and requires amplification from the intrinsic pathway [129].

The intrinsic pathway is activated by inadequate nutrients/survival factors, hypoxia, oxidative stress, DNA damage and chemical and physical toxins [131] (**figure 1.4**). This process is mediated by the Bcl-2 family of proteins [138], which induces permeabilisation of the outer mitochondrial membrane, known as mitochondrial permeability transition (MPT). MPT enables release of mitochondrial apoptogens, such as cytochrome c, second mitochondria-derived activator of caspases (Smac/DIABLO) and Omi/HtrA2 into the cytosol [129, 131]. Cytochrome c along with ATP and apoptotic protease activating factor 1 (Apaf1) associate to form the apoptosome, which binds, cleaves and activates caspase-9 which in turn, cleaves and activates downstream caspases [139]. Both Smac/DIABLO and Omi/HtrA2 inhibit IAP (inhibitors of apoptosis) [140, 141] whilst DNA fragmentation, a feature of apoptosis, is mediated by apoptosis inducing factor and endonuclease G [142]. Inadequate, excessive or inappropriate apoptosis may contribute to the pathogenesis of disease.

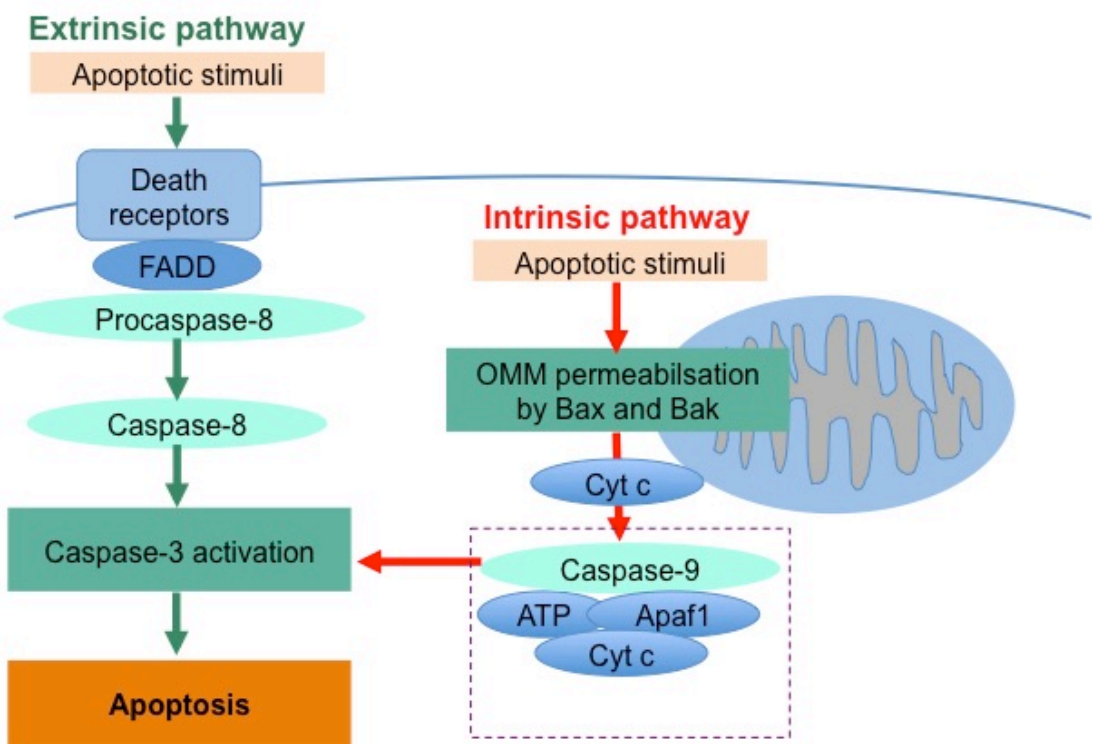

Figure 1.4 Apoptotic pathways in cardiomyocytes.
Apoptosis is induced by intrinsic and extrinsic stimuli. The extrinsic pathway is facilitated through death receptors such as Fas and tumour necrosis factor receptors (TNF-R). Binding of the ligand enables binding of Fas-associated death domain (FADD) which binds procaspase -8 or -10. Activation of these caspases enables cleavage and activation of procaspase -3. The intrinsic pathway is stimulated by inadequate nutrients, oxidative stress, DNA damage and toxins and is mediated by the Bcl-2 family of proteins. Permeabilisation of the outer mitochondrial membrane (OMM) by Bax and Bak, allows release of mitochondrial apoptogens, including cytochrome c (Cyt c). Cyt c along with ATP and apoptotic protease activating factor 1 (Apaf1) form the apoptosome, which binds, cleaves and activates caspase-9 which in turn, cleaves and activates downstream caspases, leading to apoptosis. Adapted from [131].

Necrosis is actively executed by cells [131] and features of this cell death pathway include depletion of cellular ATP and swelling of the cell and organelles, which leads to the collapse of cellular homoeostasis [129, 143]. Loss of plasma membrane integrity enables the release of cellular contents into the extracellular space, evoking an inflammatory response (**section 1.5.1**). Therefore necrosis completely opposes the tidy nature of apoptosis.

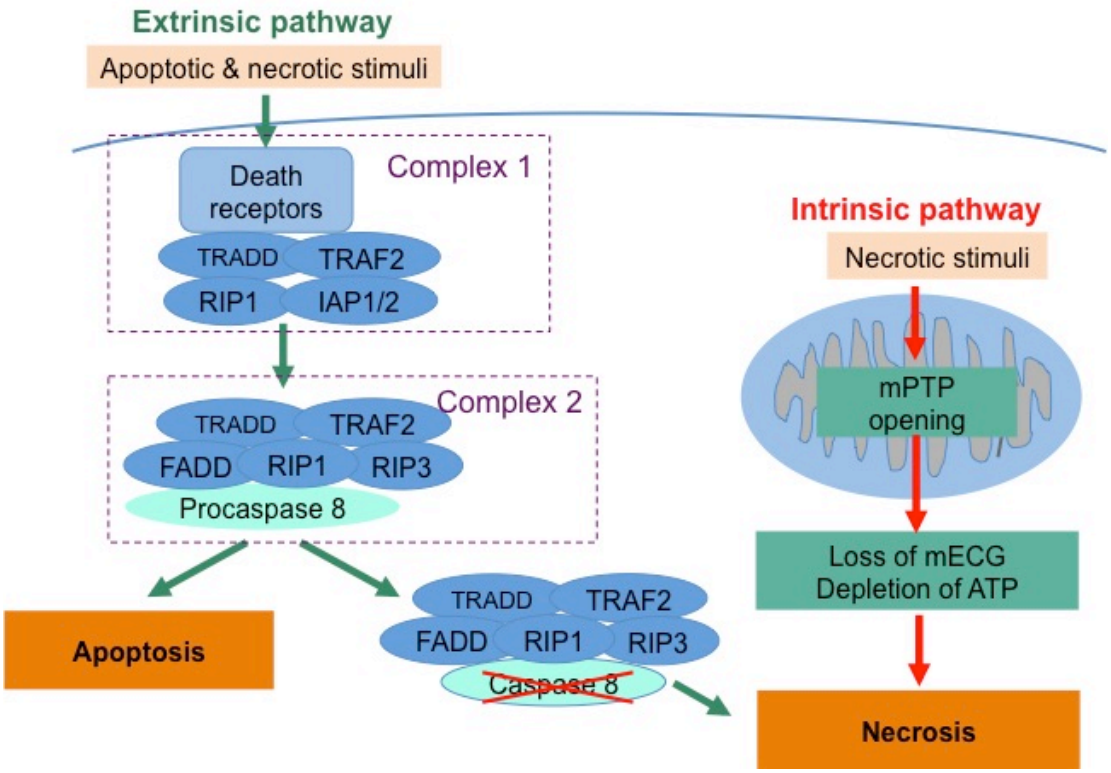

Figure 1.5 Necrotic pathways in cardiomyocytes
Necrosis is induced by intrinsic and extrinsic stimuli. The extrinsic pathway is mediated through the tumour necrosis factor receptor (TNF-R). Binding of TNFα to TNF-R recruits TNF-R associated death domain (TRADD), receptor-interacting protein 1 (RIP1), TNF-R-associated factor 2 (TRAF2), inhibitors of apoptosis 1 (IAP1) and IAP2, which collectively form complex 1. Dissociation of the multiprotein complex from the receptor, deubiquitination of RIP1 and recruitment of FADD, RIP3 and caspase-8 forms complex 2. This leads to activation of apoptosis via caspase-8 stimulation. Inhibition of caspase-8 induces cross-phosphorylation of RIP1 and RIP3, which progresses to necrosis through mechanisms that are unclear. The intrinsic pathway activated by elevated matrix calcium concentration, ROS, or depletion of ATP opens the mitochondrial permeability transition pore (mPTP). Subsequent swelling of the mitochondria and loss of mitochondrial electrochemical gradient (mECG) across the membrane halts oxidative phosphorylation. Following this, the cell undergoes necrosis. Adapted from [131].

Necrosis is triggered by nutrient stress, heat shock or exposure to harsh environments. The extrinsic pathway involves 2 complexes and is mediated through the TNF receptor (TNF-R) [144]. Binding of the death ligand, TNFα to its receptor recruits TNF-R associated death domain (TRADD), receptor-interacting protein 1 (RIP1), TNF-R-associated factor 2 (TRAF2), IAP1 and IAP2, which collectively form complex 1 (**figure 1.5**). IAP1 and IAP2

ubiquitinate RIP1 [145] which permits recruitment of TAK1 and through a series of phosphorylation steps enables translocation of nuclear factor kappa-light-chain-enhancer of activated B cells (NFκB) into the nucleus to stimulate transcription of survival factors [146]. Complex I transitions into complex II when the multiprotein complex dissociates from the receptor, undergoes endocytosis followed by deubiquitination of RIP1 and recruitment of FADD, RIP3 and caspase-8 [131, 144]. Cleavage and activation of caspase-8 stimulates apoptosis whereas inhibited caspase-8 leads to cross-phosphorylation of RIP1 and RIP3, which progresses to necrosis through mechanisms that are unclear [129, 131, 144].

The intrinsic necrotic pathway is mediated by the opening of the mitochondrial permeability transition pore (mPTP) which is caused by necrotic stimuli, elevated matrix calcium or phosphate concentration, by reactive oxygen species (ROS) or depletion of ATP [131] (**figure 1.5**). This opening leads to mitochondrial swelling and loss of electrochemical gradient across the membrane, halting oxidative phosphorylation. Following this, the cell undergoes necrosis.

1.3.3.1 Cell death in MI and HF

In animal models to induce MI or I/R injury, apoptosis and necrosis of myocytes and non-myocytes have been detected in the ischemic area. It has been reported that apoptosis peaks 4.5 hours after permanent coronary occlusion whilst necrosis peaks at 24 hours [147]. Upon reperfusion, the rate of apoptosis is increased (I/R injury) whilst aspects of I/R injury, including ROS and normalisation of intracellular acidosis (**section 1.6.4.1**), may trigger opening of the mPTP, leading to necrosis [129].

Compared to the acute and potentially immense cell death post-MI, cell death in HF is a chronic process and is modestly elevated. Both apoptosis and necrosis

are upregulated in HF. The rates of apoptosis in patients with end-stage HF are 0.12 – 0.70 % [148], which questions if this low percentage of apoptosis may contribute to the pathogenesis of HF. It has also been suggested that necrosis was more frequent than apoptosis in HF patients [149]. Interestingly others have reported that in HF patients, cardiomyocyte death with autophagic features occurred at a rate of 0.03% compared to 0.002% for apoptosis [150]. Clearly, further studies are required to understand myocardial cell death and its contribution to the pathogenesis of HF.

1.4 Autophagy

Autophagy is a highly conserved process that can be described as an intracellular recycling process in which organelles, proteins and lipids are catabolised by lysosomal degradation. Under basal conditions, low levels of autophagy sustain the turnover of organelles and regulate protein and organelle abundance and quality [151]. Autophagy is considered as a cell survival mechanism and is activated upon nutrient deprivation, hypoxia and oxidative stress, to replenish initial constituents.

Whilst there are 3 main forms of autophagy, macroautophagy is most prevalent. Macroautophagy is mediated through the formation of an invaginated, double-membrane vesicle, known as an autophagosome, that encapsulates engulfed material (**figure 1.6**). Lysosomes containing degradative lysosomal enzymes fuse with an autophagosome to form an autophagolysosome and the contents are then degraded.

Within the heart, autophagy is a cytoprotective mechanism that maintains cellular homeostasis and therefore inadequate autophagy may lead to an accumulation of harmful proteins, protein aggregates and damaged organelles [152]. However excessive self-degradation of essential cellular constituents

promotes cell death [153]. As mentioned, autophagic structures have been observed in dying and dead cardiomyocytes [129, 150] and in the cardiomyocytes of animal models such as UM-7.1 cardiomyopathic hamsters [154]. This process is not well understood, and it remains unknown whether autophagy is a sign of failed cardiomyocyte repair or a suicide pathway for failing cardiomyocytes.

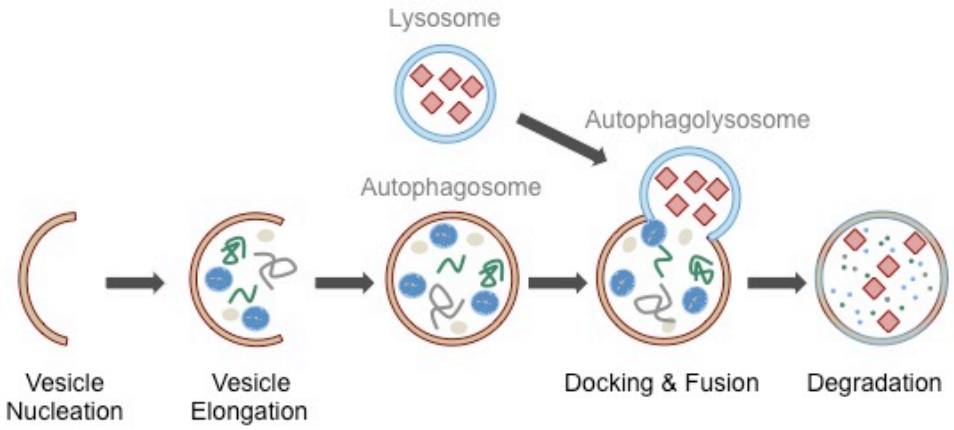

Figure 1.6 The formation of autophagosomes.
The membrane elongates and encapsulates cytosolic constituents, including proteins and organelles in a double membrane vesicle, known as an autophagosome. Lysosomes containing lysosomal enzymes dock and fuse with autophagosome to form an autophagolysosome and the contents are degraded. Adapted from [155].

Autophagy has been observed in pathological cardiac hypertrophy, MI and HF [151]. Interestingly, whilst total protein abundance increases during pathological hypertrophy, it was reported that autophagic activity was diminished after pressure overload [152, 156, 157].

Under ischemic and/or hypoxic conditions autophagy is activated, although in models to induce MI or I/R injury, the underlying pathways and functional consequences differ. During ischemia, activation of adenosine monophosphate-activated protein kinase (AMPK) leads to induction of autophagy whilst after reperfusion, autophagic activity is elevated and associated with Beclin-1 abundance [158]. Therefore it may be considered that autophagic activity during

ischemia is protective [159], whereas during reperfusion, autophagy is excessively stimulated, possibly leading to cell death.

Autophagy is upregulated in HF and failing hearts exhibit an increased number of autophagosomes [150]. Diminished expression of markers of autophagy after mechanical unloading of the failing human heart by LV assist devices [160] suggested that autophagy may be an adaptive mechanism in the failing heart [151]. Whether this increase in autophagy in the pathogenesis of HF is protective and associated with cell-survival or deleterious and related to cell death mechanism remains unclear.

1.5 Inflammation

The immune system possesses a variety of strategies to defend the body against invasion and attack by pathogens and tumours[161] alongside the capability to promote tissue repair after injury. Responses of the immune system can be partitioned into 2 categories: the acute, abrupt innate response and the slower, more specific adaptive immune response. Inflammation is a common, initial, fast-acting innate immune defence mechanism that removes injurious stimuli and initiates the healing process[162]. The inflammatory response facilitates matrix deposition, removal of dead cells and debris, granulation tissue formation and the secretion of cytokine and growth factors [163].

Detection of foreign substances or injurious stimuli by the complement system or tissue-residing macrophages stimulates the release of chemokines, IL8 and proinflammatory cytokines, IL1 and TNFα. Complement activation triggers degranulation of mast cells, releasing histamine and prostaglandins into the extracellular space. The secretion of these mediators instigates dilation of local blood vessels and permeabilisation of capillaries, leading to the increased

recruitment and extravasation of leukocytes, mainly neutrophils and monocytes to the area[164]. These cells contribute to the inflammatory response by secreting inflammatory cytokines and chemokines and using their artillery of weapons to combat the invasive agent or phagocytose foreign material or dying cells. Inflammation persists until anti-inflammatory mediators suppress it. Excessive inflammation can result in damage to the host tissues and lead to neurodegenerative and autoimmune disorders[164]. Therefore, inflammation must be tightly regulated to maintain homeostasis and prevent additional tissue damage.

Within the heart, macrophages reside near endothelial cells or within the interstitial space [165]. While, there are a few dendritic cells and mast cells, there are no neutrophils. Cells of the myocardium (cardiomyocytes, endothelial cells, fibroblasts) in additional to inflammatory cells (leukocytes, platelets, macrophages) contribute to cardiac inflammation. However, the intricate mechanisms responsible for initiating and integrating inflammatory responses within the heart remain poorly defined.

1.5.1 Toll-like receptors (TLRs)

Macrophages and dendritic cells are important sensors for detecting infectious material. Infectious material is sensed by pattern recognition receptors (PRRs) located at the plasma membrane or intracellularly in the cytoplasm or within endosomes. Binding of the ligand to the receptors triggers a signalling cascade to mediate a co-ordinated and well-orchestrated inflammatory response.

These PRRs recognise foreign, non-self pathogen-associated molecular patterns (PAMPs) as well as endogenous, host-derived danger-associated molecular patterns (DAMPs) such as heat shock proteins and mitochondrial

DNA (mtDNA) [103, 161]. DAMPs are proposed to act as 'danger' signals and are released during cellular injury or death. A subset of PRRs includes the transmembrane (TM) proteins, Toll-like receptors (TLRs). There are 10 TLR members in humans, with each TLR specifically recognising a different PAMP or DAMP (TLR ligand). The leucine-rich regions (LRR) within structurally conserved TLRs mediate recognition of TLR ligands whilst the cytoplasmic-facing Toll and IL1 receptor-like (TIR) domains associate with an assortment of signalling proteins to activate intracellular signalling upon receptor stimulation (**figure 1.7**). TLRs have cell-specific expression and are either expressed at the plasma membrane or on endosomal membranes[166]. Activation of TLRs instigates an intracellular signalling pathway with each TLR having a specific response, but all activate the inflammatory cascade[167]. The inflammatory response evoked by TLRs can be acute or chronic. However TLRs have been reported to possess pro- or anti- apoptotic features alongside the intriguing ability to supress an inflammatory response [168].

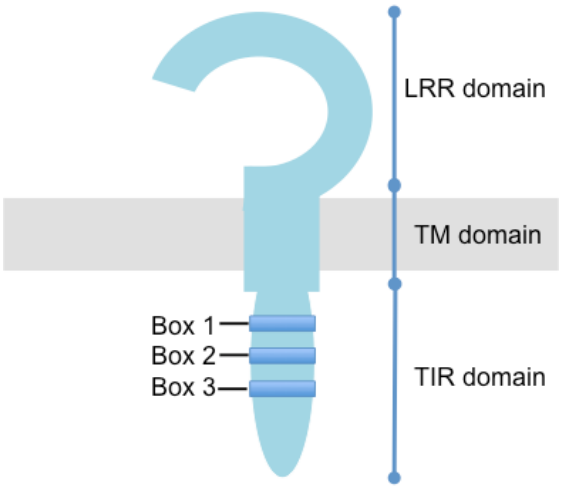

Figure 1.7 Structure of toll-like receptors (TLRs).
Pattern-recognition receptors such as TLRs are transmembrane (TM) receptors that recognise exogenous pathogen associated molecular patterns and endogenous danger associated molecular patterns. This is mediated by the leucine rich region (LRR) within the N-terminal domain which activates an intracellular signalling cascade though its C-terminal TIR (Toll and IL1 receptor-like) domain.

In addition to TLRs, other PRRs include C-type lectins, and cytosolic proteins retinoic acid-inducible gene (RIG)-like receptors and nucleotide-binding oligomerisation domain (NOD)-like receptors (NLRs) [169]. NLRs associate with apoptosis-associated speck-like protein containing a caspases recruitment domain (ASC) and caspase-1 to form a cytosolic multiprotein complex, known as an inflammasome [170]. Formation of this complex can be activated by a variety of stimuli including ATP, asbestos urate crystals, microbial entities, ROS and mtDNA and these complexes are vital defenses against pathogens. Inflammasomes are capable of cleaving pro-IL1β and pro-IL18 into active IL1β and IL18, using the protease action of caspase-1 [171]. Both these cytokines are crucial in the attack against pathogens, recruiting leukocytes and stimulating a powerful inflammatory response.

1.5.2 TLR9 signalling

Whilst TLRs are preferentially expressed in immune cells, TLRs 1-10 are also expressed within the myocardium, with TLR4, a lipopolysaccharide detector, most abundantly expressed [172]. In addition to TLR4, there are several reports regarding the role of TLR2 (lipoproteins sensor) and TLR3 (endosomal double stranded RNA detector) in models of cardiac-related injury. However it has previously been reported that TLR9 could potentially stimulate inflammation that may contribute to the pathogenesis of HF [173] (**section 1.5.3.1**). Several reports have demonstrated that TLR9 is expressed in cardiomyocytes, cardiac fibroblasts and tissue-residing macrophages [174, 175, 176]. Therefore there is particular interest in TLR9, an endosomal receptor that recognises unmethylated DNA motifs in which cytosine triphosphate deoxynucleotide is followed by guanine triphosphate deoxynucleotide (CpG), which are found

within bacterial and viral DNA [166, 177]. Though the human genome possesses CpG motifs, these are often methylated and are not recognised by TLR9. In contrast, unmethylated CpG motifs are capable of evoking a robust immunostimulatory response. TLR9 is also activated by the DAMP, mtDNA [178], which also possesses inflammogenic unmethylated CpG motifs.

Unmethylated CpG motifs bind to the TLR9 receptor, leading to the recruitment of the adaptor protein MyD88 to the TIR domain (**figure 1.8**) [179]. MyD88 recruits several other signalling intermediates to form a signalling complex, including serine/threonine kinase, IL1R-associated kinase (IRAK)-1, IRAK-4 and TRAF6 [179]. From this signalling complex, the inhibitor of kappa B kinase (IKK) complex consisting of IKKα, IKKβ and IKKγ is activated which in turn phosphorylates inhibitor of kappa B (IκBα). This leads to ubiquitin-mediated degradation of IκBα and the liberation of the transcription factor, NFκB, which is now free to translocate into the nucleus. TRAF6 facilitates the entry of interferon regulatory factor (IRF)-5 into the nucleus [180] whilst IRF7 is translocated into the nucleus through association between TRAF3, IRAK1, IKKα and MyD88 [167]. NFκB, IRF5 and IRF7 initiate transcription of proinflammatory cytokines such as IL1 and IL6 and type 1 IFNs, IFNα and IFNβ [181]. The transcription and induction of cytokines is a vital step for commencing and maintaining an inflammatory response.

The downstream signalling of the other TLRs are all MyD88-dependent, excluding TLR3 [172]. However other adaptor proteins and signalling intermediates are utilised to derive different responses for each distinct receptor.

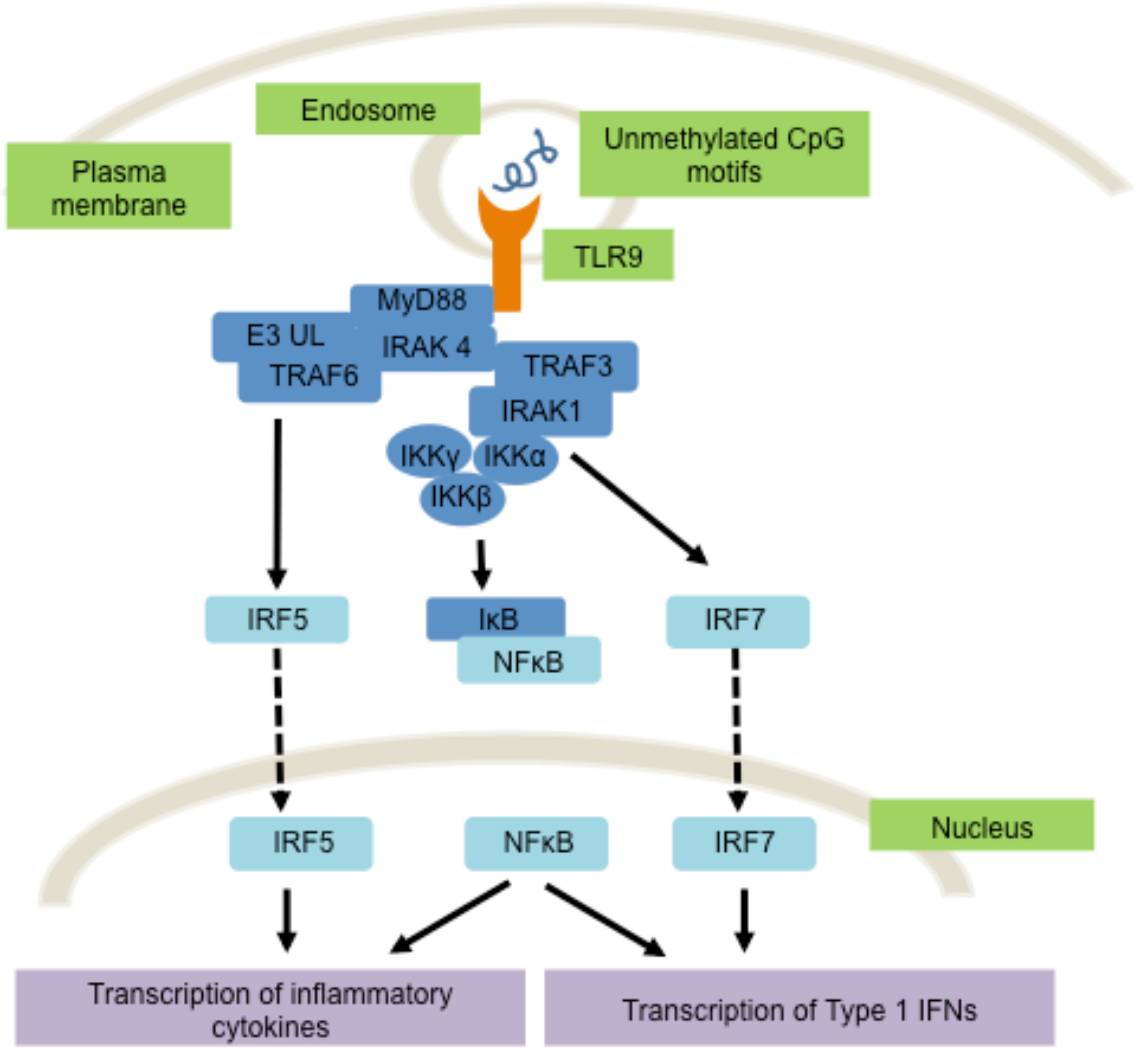

Figure 1.8 Toll-like receptor 9 (TLR9) signalling.
Endosomal located TLR9 recognises unmethylated CpG motifs on DNA. Activation of TLR9 leads to the recruitment of the adaptor protein MyD88, which forms a complex with IL-1R-associated kinase (IRAK)-4, E3 ubiquitin ligase (E3UL) and TNFR-associated factor 6 (TRAF6). E3 ligase ubiquitinates TRAF 6 enabling regulatory proteins of TAK1, TAB2 and TAB3 to bind to the ubiquitinated sites of TRAF 6 (not shown). Activated TAK1 phosphorylates IκB kinase (IKK)-β within the IKK complex, which in turn phosphorylates the inhibitor of kappa B (IκBα). This phosphorylation leads to degradation of IκBα via the ubiquitin–proteasome system and the release of NFκB. NFκB translocates into the nucleus and activates the transcription of proinflammatory cytokine genes and type 1 interferons. TRAF6 activates interferon regulatory factor (IRF)-5 to enter into the nucleus and activate the transcription of proinflammatory cytokine genes. In addition, MyD88 also forms a signalling complex with TRAF3, IRAK1 and IKKα. Phosphorylation of IRF7 by IRAK1 or IKKα enables entry of IRF7 into the nucleus which initiates transcription of type 1 interferons. Adapted from [167].

While, the inflammatory nature of TLR9 has been well-studied, evidence suggests that TLR9 does not instigate autoimmune or virus-induced myocarditis [169, 182]. Moreover, recent reports have proposed a novel role of TLR9 for modulating energy metabolism [183] through inhibition of sarcoendoplasmic reticulum calcium ATPase 2 (SERCA2) in cardiomyocytes as a protective mechanism against stress [184]. In addition, downstream mediators of TLR9 signalling, NFκB, TNFα and IL6 have multiple roles. Both NFκB and TNFα have been reported to be pro-survival and induce and mediate pathological hypertrophy responses [185, 186, 187], yet retain the capability to stimulate apoptotic and inflammatory effects. This demonstrates the range of actions of cytokines and transcription factors and the need to contemplate the initial stimuli as well as the immediate upstream and downstream signalling components of the inflammatory cascade.

1.5.3 Inflammation in MI and HF

Inflammation is a contributing factor to the pathophysiology of cardiac diseases and remodelling. Short-term activation of TLR signalling induces cytoprotective responses within the heart, whereas long-term TLR signalling is maladaptive leading to cell death, ECM degradation and fibrosis, which alter cardiac morphology and function [172]. This highlights the double-edged nature of inflammation and the balance between insufficient and excessive inflammation.

After myocardial injury such as MI, ECM degradation and cardiomyocyte death induce the release of mediators which activate innate immune sensors, instigating an inflammatory response. In addition, the release of DAMPs from necrotic cells leads to PRR and inflammasome activation, inflammation and

necrosis. These pro-inflammatory activities mediate the clearance of dead cells and debris and initiate the repair and remodelling responses.

In chronic HF patients, increased levels of circulating proinflammatory cytokines, such as TNFα[19], IL6 and IL1β[20, 21] correlate with the progression and severity of the condition and could be considered as independent predictors of prognosis. Several studies have shown that β-blockers possess anti-inflammatory properties [188, 189] emphasising the potential benefits of developing treatments to modulate inflammation within HF patients. Unfortunately, clinical trials that modulate the inflammatory response through anticytokine and immunomodulatory therapy in HF patients have been disappointing. Therapies designed to target TNFα include an anti-TNF antibody (infliximab) [190] and soluble TNF inhibitory receptors (etanercept) [191], both of which were promising in preclinical models, but were unsuccessful in clinical trials. Both thalidomide [192, 193] and pentoxifylline [194, 195] (a xanthine derivative) have multiple modes of immunomodulatory actions including minimising the effects of TNFα. However clinical data have been mixed. Experimental studies targeting leukocyte-mediated inflammation (activation, adhesion and extravasation) in reperfused myocardium were extremely successful, with marked reductions in infarct size and prevented extension of ischemic cardiomyocyte injury [196, 197]. However in MI-patients, these treatments were unsuccessful [198]. Though it remains unknown why these treatments failed in clinical trials, one possible reason why these therapies were unsuccessful could be the temporal and spatial aspects of inflammation. There are acute and chronic inflammatory responses with different types and numbers/levels of cells, cytokines and other inflammatory mediators observed during these diverse stages of an inflammatory response [20, 172]. An example includes the multi-phase inflammatory response observed after

MI (discussed in **chapter 5**). Furthermore, cytokines are reported to be temporally regulated by circadian regulations (mediated by circulating hormones) which also be another contributing factor [199]. Also, different tissue compartments may yield differential immune responses, therefore a general and systemic approach to targeting myocardial inflammation may not be appropriate and a more targeted approach (in terms of specific timing and location) may be more successful in treating HF.

Thus the ineffectiveness of these therapies demonstrates the need to understand the mechanisms of inflammation. An additional layer of complexity is added by the complicated and varied nature of inflammation and inflammatory mediators in injury and repair. It has been proposed that interactions of the immune system with the neurohormonal system may induce systemic inflammation observed in HF [21], amid one study suggesting that proinflammatory cytokines may uncouple β-ARs [200].

1.5.3.1 Autophagy, TLR9 and HF

Inflammation has been implicated with the pathogenesis of HF, yet exposure to infectious agents is unlikely to be the causative agent. Therefore the prospect of sterile inflammation or inflammation without a foreign component was suggested [20]. Release of host cellular components including DAMPs into the extracellular environment from necrotic cells could be one form of sterile stimuli alongside mechanical trauma, ischemia and toxins. It has previously been reported that partially digested mtDNA arising from incomplete stress-induced autophagy triggered chronic myocardial inflammation and HF [173].

Cardiac-specific deletion of deoxyribonuclease (DNase) II, an acidic DNase in the lysosome accumulated mitochondrial DNA within autophagosomes

provoked a robust inflammatory response after pressure overload. Interestingly, inhibition or genetic-ablation of TLR9 attenuated this cardiac inflammation and dysfunction associated with this model, indicating that this inflammatory response was mediated through TLR9 [173]. Therefore, these findings suggest that mtDNA that escapes autophagy induces TLR9-mediated inflammation and HF, suggesting a potential pathway for stress-induced sterile inflammation that may contribute to the pathogenesis of HF.

The role of TLR9 within the myocardium is an avenue of current interest. Pressure overload induced myocardial inflammation and cardiac remodelling is mediated by TLR9 [173]. TLR9-deficient mice subjected to pressure overload, displayed reduced cardiac dilatation, hypertrophy, fibrosis and pulmonary congestion together with improved cardiac function compared to WT mice. Synthetic oligonucleotides (ODN) containing CpG motifs are used to study the effects of TLR9 stimulation. Priming or administering (before or after induction of hypertrophy) mice with CpG-ODN attenuated the development of hypertrophy and HF [174, 201]. Furthermore in a septic model, it was reported that bacterial DNA induced myocardial inflammation and reduced cardiomyocyte contractility [202] and that *in vivo* inhibition of TLR9 ablated that dysfunction [203]. Therefore TLR9 may be an important sensor within the healthy and stressed myocardium and its potential role within sterile inflammation may contribute to HF.

An alternative mechanism of sterile inflammation involves the inflammasome . Within the myocardium, NOD1 and NLRP3 have been shown to participate within inflammasomes [170]. mtDNA and ROS have been reported to activate the NLRP3 inflammasome and reports of activated NLRP3 inflammasome after ischemia and I/R injury indicate that this complex had adverse consequences on cardiac remodelling [169].

1.6 Mechanisms of HF

As mentioned previously, there is an assortment of biochemical and mechanical abnormalities associated with HF. Besides cardiac remodelling, additional characteristics of HF include alterations in the expression and downstream signalling of the β-ARs, calcium handling, metabolism and oxidative stress [66, 204, 205, 206, 207]. These features are discussed below as well as their contributions to the progression of HF.

1.6.1 β-AR signalling

As a component of the neurohormonal system, the sympathetic nervous system interacts with the cardiovascular system through AR. This interaction occurs is mediated by the release of the neurotransmitters, epinephrine and norepinephrine to modulate myocardial performance [204].

Within the human body, there are 2 types of AR– α and β [208, 209], with 3 different β-AR sub-types (β1, β2, β3). Though, α1- and β- ARs are expressed in the myocardium, 75% of β-ARs are β1-AR receptors [210]. Since β1-AR is the most abundant sub-type within the myocardium, this section will focus on the signalling pathway downstream of this receptor.

β-ARs are G-protein coupled receptors (GPCRs) possessing 7 TM helices that associate with an intracellular G-protein [208, 211]. The heterotrimeric G-protein contains 3 polypeptides chains, α, β, γ, that form 2 distinct subunits: Gα and Gβγ [212]. In the guanosine diphosphate (GDP)-bound state, Gα and Gβγ form a functionally inactive heterotrimer (**figure 1.9**). When the receptor is activated and undergoes a conformational change, the G-protein exchanges GDP for guanosine triphosphate (GTP). The G-protein dissociates into 2 subunits, Gα-GTP and Gβγ, which subsequently activates downstream signalling molecules.

Both β1- and β2- ARs have a $G\alpha_s$ stimulatory subunit which activates adenylate cyclase upon receptor stimulation [204, 211]. This leads to an increase in cyclic adenosine monophosphate (cAMP) levels and activation of protein kinase A (PKA). This serine/threonine kinase targets many proteins including metabolic enzymes, ion channels and transcription factors.

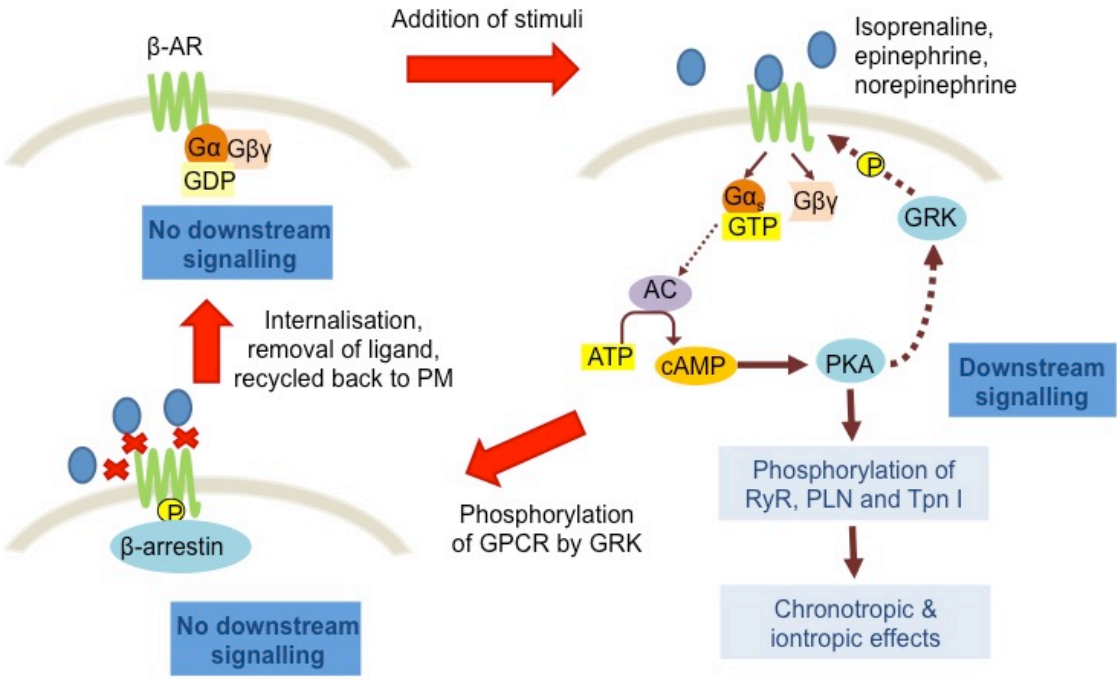

Figure 1.9 β-adrenergic receptor (β-AR) signalling.
In the inactive state, guanosine diphosphate (GDP) is bound to the G-protein ($G\alpha_s/G\beta\gamma$). However, binding of the ligand to the β-AR leads to nucleotide exchange to guanosine triphosphate (GTP) and dissociation of $G\alpha_s$ and Gβγ. The $G\alpha_s$ subunit activates adenylate cyclase (AC), increasing cyclic adenosine monophosphate (cAMP) levels. This subsequently stimulates protein kinase A (PKA) which phosphorylates the ryanodine receptor (RyR), phospholamban (PLN) and contractile proteins (troponin (Tpn) I), leading to positive inotropic and chronotropic effects. However PKA phosphorylates G-protein-coupled receptor kinases (GRKs), which can phosphorylate a ligand-bound β-AR that enable binding of β-arrestin to the third intracellular loop and the carboxyl tail of the receptor. This leads to the internalisation of the receptor into the cytosol, where the ligand and β-arrestin are removed and the receptor is returned to the plasma membrane (PM). Additionally, hydrolysis of GTP by GTPases enables reformation of the heterotrimeric G-protein and inactivates downstream signalling. Adenosine triphosphate (ATP), sarcoendoplasmic reticulum calcium ATPase (SERCA), sarcoendoplasmic reticulum (SR). Adapted from [204].

Within cardiomyocytes, PKA phosphorylates L-type voltage-operated calcium channels (VOCC) at the plasma membrane, ryanodine receptors (RyR) and phospholamban (PLN) at the SR membrane, contractile proteins (Tpn I) and G-protein-coupled receptor kinases (GRKs) [213, 214]. Thus, activation of β1-ARs contributes to enhanced calcium activity within the cytosol, increased contractile force of the muscle (positive inotropic effect) and elevated HR (positive chronotropic effect), leading to increased CO [204, 214]. In addition, the Gβγ subunit induces phosphorylation and activation of ERK1/2, which activates the cardiac hypertrophy response downstream of the β-AR [215]. β2-ARs may also couple to $G\alpha_{i,}$ an inhibitory subunit which diminishes adenylate cyclase activity and has anti-apoptotic properties [216]. Therefore, β-AR signalling is essential for maintaining cardiac function in response to stress, a condition which activates AR signalling.

High levels of catecholamines are toxic to cardiomyocytes as enhanced calcium activity may induce apoptosis through calcineurin activation [217]. Therefore, β-AR activation is tightly regulated. Feedback mechanisms downstream of ARs include receptor phosphorylation by several kinases including PKA and protein kinase C (PKC), but is largely executed by serine/threonine targeting GRKs [213]. GRK2 (β-ARK1) is predominantly expressed in the myocardium, alongside GRK3 (β-ARK2), GRK5 and GRK6 [218]. Phosphorylation of activated ARs enables binding of β-arrestin to the receptor, preventing the coupling of $G\alpha_s$ to the receptor [204, 214, 219]. This loss of functional β-AR signalling is known as short-term desensitisation. Long-term desensitisation involves internalisation of the receptor and regulated gene expression of the receptor and downstream signalling proteins [204].

1.6.1.1 β-AR signalling in HF

β-AR signalling is dramatically changed during HF. Initial strain on the heart decreases CO, triggering the release of epinephrine and levels of circulating catecholamines are increased in HF patients [17, 18]. Activation of the β-ARs stimulates myocyte contractility and HR to maintain CO, as part of a compensatory mechanism [220]. This initially is favourable, however long term β-AR stimulation leads to β-AR decoupling, β-AR desensitisation and internalisation of β-ARs from the plasma membrane of cardiomyocytes [183]. Thus, interactions between the sympathetic nervous system and the myocardium are minimised, with a direct impact on myocardial performance in terms of calcium handling and cardiomyocyte contractility [204, 214, 219]. Calcium mishandling and the subsequent activation of apoptosis contribute to the progression of HF [204, 214, 219]. At a molecular level, the expression of β1-AR declines whilst β2-AR expression is maintained changing the ratio of β1-ARs : β2-ARs from 70:30 to 50:50 [210]. In addition, myocardial GRK2 [221, 222] and $G\alpha_i$ [223] levels are significantly elevated in human HF, which may contribute to the loss of β-AR responsiveness observed in this condition. In addition, several *in vitro* studies have shown immunomodulatory effects of β-AR activation, linking immune modulation, excessive catecholamine stimulation and β-AR signalling [224, 225]. Thus, β-AR signalling is thoroughly compromised in HF.

1.6.2 Calcium handling

Calcium is a critical regulator of cardiomyocyte contractile function, connecting the electrochemical signals that saturate the heart to the overall contraction of the myocardium. The major participants of calcium homeostasis and handling include RyRs, VOCCs and calcium pumps and transporters [205, 225].

As a wave of electrical excitation spreads across the heart, the plasma membrane of cardiomyocytes becomes depolarised. L-type VOCC, located within the T-tubules open to admit a small amount of calcium into the cytosol that binds to the cytosolic face of the RyR [226] (**figure 1.10**). This causes RyRs to open, leading to an influx of calcium into the cytosol from the SR, referred to as calcium-induced calcium release (CICR) [227]. Additionally, a small amount of calcium is imported from extracellular sources. Cytoplasmic calcium concentration increases 100-fold and binds to the contractile protein, Tpn C stimulating myocardial contraction.

Relaxation is mediated by the closure of calcium entry channels and calcium is rapidly imported into the SR by SERCA or exported into the extracellular space by sodium calcium exchanger (NCX) [205, 225]. Therefore, the amplitude and duration of a calcium transient can modulate the rate, magnitude and duration of each contraction and so calcium handling proteins are tightly regulated.

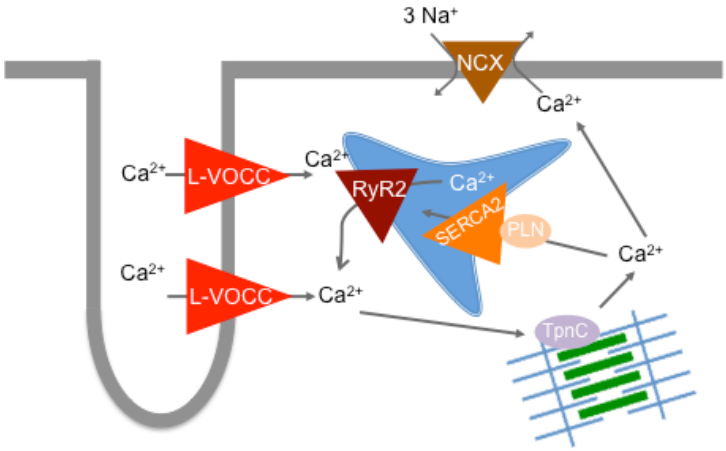

Figure 1.10 Calcium handling.
Upon cellular depolarisation, L-type voltage-operated calcium channels (VOCC), located within the T-tubules open to admit a small amount of calcium into the cytosol. This calcium binds to the cytosolic face of the RyR, causing the channel to open and an influx of calcium into the cytosol from the SR, known as calcium induced calcium release (CICR). An increase of 100-fold in calcium cytosolic concentration enables myocardial contraction though association with Troponin C (TpnC). Upon relaxation, calcium is quickly transported into the SR by ATP-dependent function of sarcoendoplasmic reticulum calcium ATPase (SERCA) or exported into the extracellular space by sodium calcium exchanger (NCX).

The opening of L-type VOCC upon membrane depolarisation is vital for the initial entry of calcium, which acts as the trigger for SR calcium release. PKA-dependent phosphorylation increases channel activity [228] whilst the effects of PKC phosphorylation remain unknown. Inactivation of the L-type VOCC is mediated by membrane repolarisation and calcium dependent inactivation controlled by calmodulin (CaM) and CaMKII [229].

The RyR are located close to T-tubules to facilitate CICR. RyR2 is the prevalent cardiac isoform that associates to form a tetrameric complex with each monomer weighing 500 kDa. In addition, RyR2 acts as a scaffolding protein with a multitude of accessory proteins. The structure of the RyR was recently published [230, 231] and the mechanism of CICR may soon be established. Currently it is hypothesised that the initial binding of calcium causes conformational changes, twisting the TM region to open the ion pore, to allow influx of calcium into cytosol from SR [232].

RyR2 activity is tightly regulated by several mechanisms. Whilst PKA and CaMKII phosphorylation increases RyR activity, protein phosphatases PP1 and PP2 decrease calcium activity [233, 234]. Both the calcium-binding proteins, calsequestrin and calmodulin, are capable of binding to RyR2, decreasing calcium efflux through these channels [229].

Uptake of calcium into the SR is mediated by SERCA using energy from ATP hydrolysis. Though 3 isoforms of SERCA have been identified, SERCA2 is the major form expressed in cardiomyocytes [235]. SERCA activity directly influences cytosolic calcium content and the rate of myocardial relaxation. SERCA activity is regulated by the 52 amino acid TM protein, PLN [229]. Unphosphorylated monomers of PLN associate with SERCA2 diminishing the affinity of SERCA2 for calcium. However, phosphorylation of PLN induces formation of a pentamer

and relieves inhibition of SERCA2, leading to increased SERCA2 activity and SR calcium accumulation. Phosphorylation of PLN is mediated by CaMKII or cAMP dependent kinases at Serine-16 (PKA) or at Threonine-17 (PKC) [236]. Modulation of PLN-mediated SERCA inhibition is a major mechanism for acute enhancement of cardiac function following β-AR activation.

The NCX located on the plasma membrane uses the electrochemical gradient to expel 1 calcium ion whilst importing 3 sodium ions. The NCX can be reversed following depolarisation, leading to calcium entry and sodium efflux [229]. Although phosphorylation of NCX by PKC and PKA has been described [237, 238], the effects remain unknown, though it is established that interactions with TM protein, phospholemman inhibits NCX activity [239].

Subtle modifications in calcium regulatory and handling proteins as a result of mutation, disease or chronic changes in haemodynamic demand have profound consequences for cardiomyocyte function. During adaptive hypertrophy, increases in the amplitude of calcium transients and sparks as well as enhanced SR store loading have been reported [2, 70, 229]. Elevated SERCA2 activity is proposed to be caused by increased SERCA expression, decreased PLN expression and increased PLN phosphorylation. In addition, a decrease in NCX current and an increase in RyR activity have been noted in this adaptive phase [208].

As the heart progresses to failure, further changes in calcium handling are observed and a general decrease in the amplitude of calcium transient has been noted [205]. The density of the L-type VOCC is reduced in HF samples, though the calcium current is maintained by PKA-mediated phosphorylation of the channels [240]. In addition, it has been proposed that abnormal RyR2 function is involved in dysregulated calcium handling in HF, with hyperphosphorylation of

RyR2 triggering spontaneous RyR2-mediated SR calcium leakage. This leads to depressed SR calcium content and delayed myocardial contraction which may contribute to the development of ventricular tachycardia [205, 241].

Most studies have found that SERCA activity is reduced in HF, which increases diastolic calcium levels (associated with diastolic dysfunction), prolongs myocyte relaxation and reduces SR calcium content (reduced systolic performance) [205, 229, 242, 243]. This could be due to the abundance of PLN, reduced phosphorylation of PLN and the expression of SERCA, which have all been detected in failing heart samples.

Further, the abundance and activity of the NCX is increased in HF [205, 244] and its activity to remove cytoplasmic calcium is increased, which is likely to be due to the impaired SERCA2 activity. Also, reverse-mode NCX activity has been reported which may contribute to diastolic dysfunction [244].

Thus calcium handling is essential to maintaining cardiomyocyte function and alterations in the expression, activity and post-translational modifications of the proteins involved greatly influence the progression of HF.

1.6.3 Metabolism

Due to the contractile nature of the myocardium, cardiomyocytes require a constant supply of ATP. Therefore ATP consumption in myocardial tissue is very high and turnover is rapid. However a low intracellular content means that ATP can be completely consumed within seconds if ATP production is interrupted. As myocardial contraction directly correlates with the rate of ATP generation, impairments in ATP generation may induce contractile dysfunction.

Under normoxic conditions, oxidative phosphorylation in the mitochondria of a healthy heart generates more than 95% of cardiac ATP [245]. The remaining 5%

is obtained from glycolysis and to a lesser extent, the tricarboxylic (TCA) cycle. Electrons power oxidative phosphorylation, which are derived from dehydrogenation reactions that occur during β-oxidation, TCA cycle, glycolysis and pyruvate decarboxylation (**figure 1.11**). The electron-carrying intermediates, nicotinamide adenine dinucleotide (NADH) and flavin adenine dinucleotide (FADH2), acquire electrons from carbon fuels and transfer them to the oxidative phosphorylation machinery. In a healthy heart, β-oxidation of fatty acids (FAs) is the dominant source of electrons, providing 60-90% of cardiac ATP whilst the remaining proportion is derived from carbohydrates, (glucose, pyruvate and lactate), amino acids and ketones [246, 247]. The metabolic flexibility to utilise different carbon sources permits changes to substrate utilisation in response to altered substrate availability or altered regulation of metabolic pathways.

As mentioned above, FAs are crucial for ATP generation [248]. Free FAs are transported into the cytosol by transporter proteins, where they are esterified into fatty acyl-coenzyme A (CoA) [249] (**figure 1.11**). This is then transported across the mitochondrial membrane by carnitine palmitoyltransferase 1 (CPT1) and CPT2 [250]. Once inside the mitochondria, Acyl-CoA undergoes β-oxidation, generating acetyl-CoA, NADH and $FADH_2$. Acetyl-CoA feeds into the TCA cycle whilst NADH and $FADH_2$ fuel mitochondrial oxidative phosphorylation.

Aside from FAs, the other major carbon source utilised within the myocardium is glucose, which can be derived from glycogen stores. However the majority of glucose is absorbed from the blood, facilitated by insulin-independent glucose transporters 1 (GLUT1) and insulin-sensitive GLUT4 [251] (**figure 1.11**). Once in the cytosol, glucose is phosphorylated to glucose-6-phosphate (G6P).

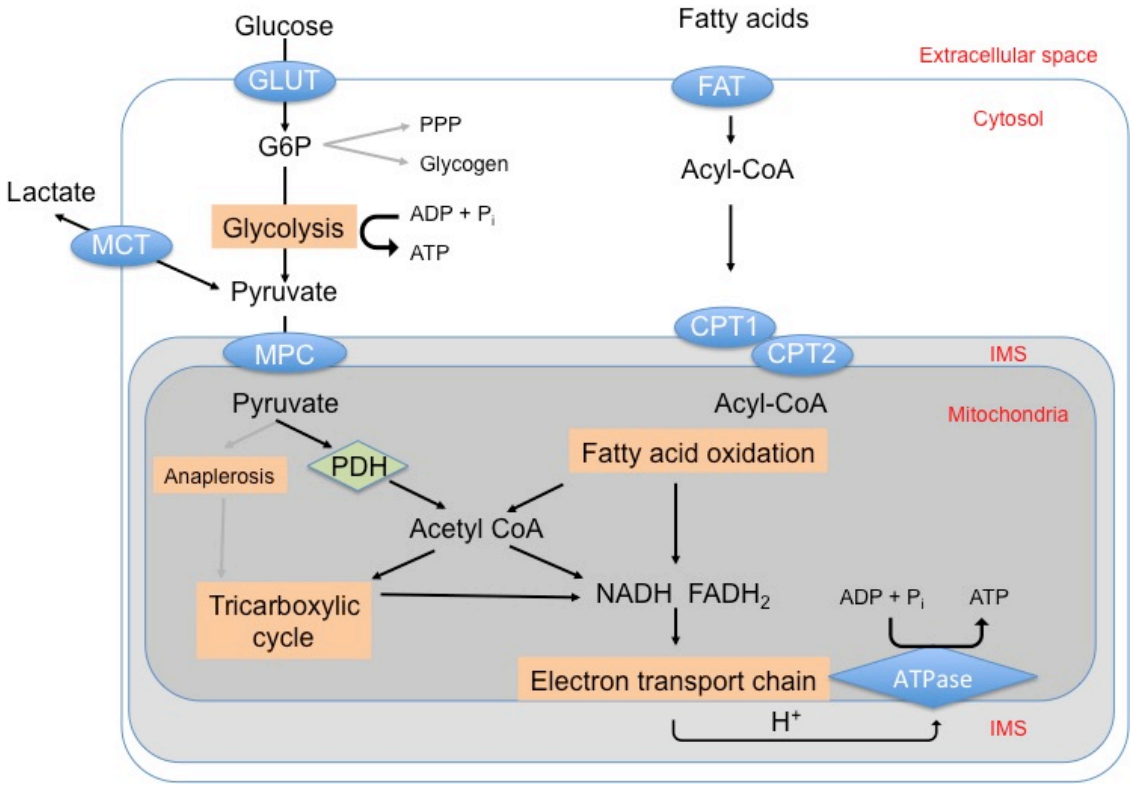

Figure 1.11 Metabolic pathways in cardiomyocytes.
Both glucose and fatty acids (FAs) are metabolic sources of electrons used to power the electron transport chain to generate ATP. The majority of cardiac metabolism is mediated by FA oxidation. FAs enter the cytosol by FA transporter (FAT) proteins and esterified into fatty acyl-coenzyme A (CoA). Fatty acyl-CoA is transported across the mitochondrial membrane by carnitine palmitoyltransferase 1 (CPT1) and CPT2 and undergoes β-oxidation of FAs, generating acetyl-CoA. Acetyl-CoA is also generated from glucose, which is transported into the cytosol by glucose transporters (GLUT) and directly phosphorylated to glucose-6-phosphate (G6P). G6P can be used for glycogen synthesis and the pentose phosphate pathway (PPP) but the majority is directed towards glycolysis, which yields pyruvate. Pyruvate is either converted to lactate which is exported from the cell by monocarboxylate transporter (MCT) or pyruvate is transported into the mitochondria by the mitochondrial pyruvate carrier (MPC) to undergo pyruvate decarboxylation by pyruvate dehydrogenase (PDH) producing acetyl-CoA. Generation of acetyl-CoA is used to fuel the TCA cycle. Electrons from nicotinamide adenine dinucleotide (NADH) and flavin adenine dinucleotide ($FADH_2$) are imparted to the electron transport chain, which generates an electrochemical gradient to power ATPase, yielding ATP. IMS = intermitochondrial space. Adapted from [248].

G6P can be further used in a multitude of pathways, such as glycogen synthesis and the pentose phosphate pathway (PPP). Usually, G6P undergoes glycolysis, yielding pyruvate, NADH and small amount of ATP. This ATP is thought to be used for calcium uptake into the SR by SERCA activity and

diastolic relaxation [248, 251]. The pyruvate is then either converted to lactate by LDH (anaerobic metabolism) or transported into the mitochondria to undergo oxidation to acetyl-CoA.

As mentioned, both β-oxidation of FAs and pyruvate decarboxylation yield acetyl-CoA, which is consumed by the TCA cycle to provide additional sources of electrons. In addition, the carbon intermediates of the TCA cycle are replenished by anaplerosis, a crucial process in the heart [252].

Thus, the regulation of myocardial metabolism is linked to carbon substrate concentration, hormones, coronary flow, inotropic state and the nutritional status of tissue.

1.6.3.1 Metabolism in HF

Many studies have proposed that impaired substrate metabolism contributes to contractile dysfunction and progressive LV remodelling [2, 66, 206, 251]. However, metabolic phenotypes differ between HF of different causes and at different stage of HF. During compensated hypertrophy, glycolysis modestly increases [253]. When hypertrophy becomes maladaptive and systolic dysfunction occurs, the myocardium switches to a preference for carbohydrate sources [206, 245, 248, 251]. The foetal heart preferentially utilises carbohydrates sources, which is also observed during cardiac hypertrophy, consistent with re-expression of foetal genes. In addition, there is accelerated glycolysis and a higher rate of glucose uptake but surprisingly no changes in expression of glycolytic enzymes [254]. However there are no changes in glucose oxidation, although increased activity of LDH has been reported alongside elevated efflux of lactate from the myocardium [251].

Conversely, FA uptake and oxidation are reduced in HF [248]. The expression of enzymes involved in these processes such as, long chain acyl CoA dehydrogenase, medium chain acyl CoA dehydrogenase as well as FA transporter, CPT1b, are reduced in compensated hypertrophied hearts and dysfunctional hearts though no changes in CPT1a are seen [255, 256]. Changes in FA oxidation have been suggested to be caused by reduced expression of peroxisome proliferator-activated receptor alpha (PPARα) [257]. This nuclear receptor is upregulated by FA levels and promotes FA uptake and oxidation and reduced expression of PPARα has been reported in HF [258]. Additionally, studies in HF patients exhibit diminished ATP content, increased ADP levels and reduced activity of the oxidative phosphorylation machinery [245, 259, 260] alongside transcriptional regulation of genes involved in mitochondrial oxidative metabolism [257]. Commonly the change in substrate preference from FAs to glucose does not occur until end-stage HF, but is dependent upon the aetiology of the condition [245, 248].

1.6.4 Redox signalling and oxidative stress

Redox signalling involves the oxidation or reduction of cellular signalling pathway components by reactive species. This process is involved in electrochemical coupling and cell differentiation and is further associated with pathological processes such as adaptation to hypoxia/ischemia, cardiac remodelling (fibrosis, hypertrophy, cell death), calcium dysregulation and contractile dysfunction [207].

Oxidative stress occurs when the production of reactive species exceed the capacity of antioxidant defence. Reactive species include ROS, which encompasses both highly reactive, unstable, free radicals (superoxide and

hydroxyl radicals) and less reactive, more stable non-radical forms (hydrogen peroxide) [261].

ROS are by-products of aerobic metabolism, therefore highly metabolising tissues, such as the myocardium, are abundant with ROS. In the myocardium, sources of ROS include NADPH oxidases, xanthine oxidase and the electron transport chain [207, 261]. However, minimal levels of ROS are maintained by the presence of antioxidant mediators and the enzymes, superoxide dismutases, catalases and peroxidases.

Oxidative stress is an intrinsic mechanism in cardiac remodelling and in the development of cardiac hypertrophy and HF, contributing to the structural and functional changes associated with these conditions [2, 66, 261]. Increased oxidative stress leads to oxidation and damage of macromolecules (DNA, lipids and proteins), membranes and enzymes involved in cellular structure, function and homeostasis [262, 263]. In addition, ROS regulate growth and hypertrophic pathways, thereby promoting cardiomyocyte remodelling [207, 261]. Both collagen synthesis and MMP activity are regulated by oxidative stress [207, 264, 265]. ROS can initiate apoptosis and necrosis whilst other studies suggest that ROS alter calcium transients and electrochemical coupling by increasing the activity of NCX leading to calcium overload [266]. Thus oxidative stress and increased ROS production may have adverse effects on cardiac remodelling.

Systemic and myocardial oxidative stress have been noted in HF patients. These include increases in lipid peroxidation, circulating levels of myeloperoxidase and 8-isoprostanes in addition to increased oxidation of glycoproteins, protein and DNA [267, 268, 269, 270]. Therefore measurements of markers of oxidative stress such as pentosidine, 8-oxo-2'-deoxyguanosine (8-OH-dG) and uric acid are routinely used in HF patients [271, 272, 273].

1.6.4.1 Ischemia

Myocardial ischemia occurs when there is an inadequate supply of blood to the heart. This is commonly caused by blocked or reduced blood flow, halting oxidative phosphorylation within cardiomyocytes. Cellular ATP is depleted which has disastrous ramifications on cardiomyocytes in terms of relaxation of myofilaments. In addition, reduction in glycogen stocks, disruption of the ionic equilibrium and cellular swelling are consequences of ischemia and diminished ATP levels. Ischemia is prominent during cardiac remodelling and evokes LV dysfunction, enhanced levels of catecholamines, apoptosis and stunning / hibernation of cardiomyocytes [274] (**figure 1.12a**).

Due to cessation of aerobic respiration, there is a shift towards anaerobic respiration, depleting glycogen stores and an accumulation of hydrogen ions, inducing tissue acidosis [263, 275]. To counteract the acidosis, the sodium-hydrogen exchanger is activated, with an efflux of hydrogen ions balanced by the influx of sodium ions. However the increasing cytosolic sodium concentration stimulates the reverse action of the NCX, leading to an influx of calcium into the cytoplasm [263]. Due to ATP depletion, SERCA activity is unavailable, leading to a build-up of calcium ions in the cytoplasm, which activates numerous intracellular degradative enzymes that damage cellular structures and can lead to cell death. Calcium is passively imported into the mitochondrial matrix by the mitochondrial calcium uniporter and mitochondrial calcium overload is a stimuli for MPT, leading to apoptosis [130, 276] (**figure 1.12a**). If the ischemia is severe and ionic imbalances are sustained, this cytosolic and mitochondrial calcium overload will induce irreversible cellular injury.

Reperfusion of an ischemic tissue may reverse these effects and restore normal myocyte contractile function, if the duration of ischemia is brief. However, it was

demonstrated that reperfused myocardium displayed greater pathological injuries, such as myocyte swelling, plasma membrane disruption and dense mitochondrial bodies compared to non-reperfused myocardium that was subjected to the same ischemic duration [277]. Thus the concept of I/R injury was established in which reperfusion itself, triggers myocardial injury beyond that caused by ischemia. Prime mediators of I/R injury include the rapid correction of intracellular acidosis, myocyte calcium overload and oxidative stress [278] (**figure 1.12b**). Under ischemia, acidosis reduces the reverse activity of NCX, inhibits MPT and prevents the activation of cytoskeletal-degrading calcium-dependent proteases, known as calpains [279]. However upon reperfusion, the washout of hydrogen ions alleviates acidotic inhibition, inducing injury of reperfused myocytes. Upon reperfusion, myocyte calcium overload after ischemia is not amended, but is further exacerbated [263]. The washout of hydrogen ions favours sodium-hydrogen exchanger activity, with an influx of sodium ions, which activates the reverse action of the NCX. The resulting elevated cytosolic calcium levels lead to cytosolic and mitochondrial calcium overload, inducing cardiomyocyte injury by MPT induction, activation of calpains and myocyte hypercontracture [278]. Additionally, reperfusion of ischemic tissue results in a sudden burst of ROS which overwhelms the capacity of the cell to scavenge these intermediates, evoking a state of oxidative stress [274, 280]. ROS are capable of inducing MPT which enables the release of additional free radicals that can trigger MPT in other mitochondria, termed 'ROS-induced ROS release' [281]. Moreover, ROS damage calcium handling proteins, lipids and DNA thereby contributing to calcium overload, lipid peroxidation, protein cross-linkage and DNA oxidation. There are multiple sources of increased ROS in the reperfused cardiomyocyte. A major contributor of ROS after reperfusion is xanthine oxidase

as well as the electron transport chain as a result of incomplete reduction of oxygen [280]. Additionally, I/R injury results in the influx of leukocytes which generate more ROS through NADPH oxidase activation [207, 263, 280].

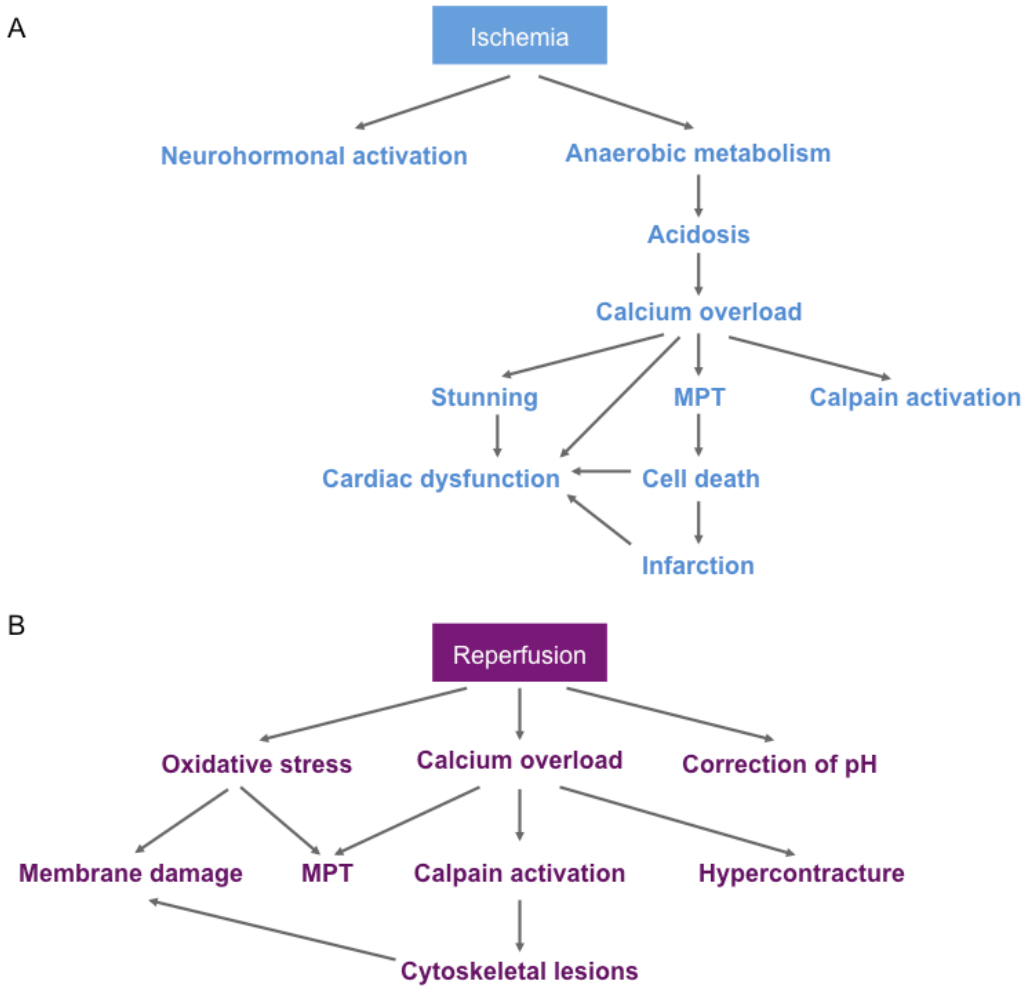

Figure 1.12 Damaging pathways of ischemia and ischemia-reperfusion (I/R) injury
A, Ischemia leads to neurohormonal activation and anaerobic metabolism, of which the latter induces acidosis, which activates sodium-hydrogen exchanger (importing sodium and exporting protons) and the reverse action of the sodium-calcium exchanger (importing calcium and exporting sodium) which subsequently leads to calcium overload. This results in myocardial stunning and induction of mitochondrial permeability transition (MPT), leading to apoptosis and activation of calpains, which degrade cellular structural and functional proteins. B, Reperfusion of an ischemic tissue leads to correction of intracellular pH and ROS generation inducing a state of oxidative stress. These ROS damage membranes and induce MPT. In addition reperfusion enhances calcium overload, by favouring sodium-hydrogen exchanger activity which further increase intracellular calcium levels, by the reverse action of the sodium-calcium exchanger. Increased calcium levels lead to MPT induction, activation of calpains and cytoskeletal lesions. Adapted from [263].

1.7 Animal models of HF

Despite advancements in understanding the molecular processes that contribute to the pathogenesis and progression of HF, prognosis remains poor with current treatments. However, with the incidence of HF anticipated to increase, it is necessary to comprehend the mechanisms of this syndrome to develop novel therapies for treatment. In this context, animal models have a major role in devising potential therapeutic strategies.

A wide variety of animals, including dogs, rabbits and rats, have been used to model a wide variety of cardiac-related diseases. However the popularity of the mouse has leapt in the last two decades since its genome was successfully sequenced, which has enabled researchers to manipulate the murine genome, generating mice of different genetic backgrounds (knockouts, overexpression, knockins). This technology has enabled researchers to further understand the role of particular proteins within the healthy and injured (using models discussed below) heart. Several pre-clinical hypertrophy and HF models have been established in mice including transverse aortic constriction (TAC), coronary artery ligation to induce MI and catecholamine infusion [282, 283, 284]. Disadvantages of using mice include the ethical dilemma of using animals as well as the initiating cause and speed at which hypertrophy and HF develop. In humans, these conditions may progress naturally over months to years, whereas in mice these conditions (hypertension, pressure overload) are synthetically orchestrated to occur over a period of days to weeks. Other disadvantages of using mice include the differences in HR (human = 60 - 100 bpm, mouse = 500 - 600 bpm) and lifespan (human = 70 years, mouse = 2 - 3 years). However, compared to other animal species, mice have large litters, short gestation times, low maintenance and housing expenses and recent

technological advancements to measure haemodynamic parameters in small animals have prevailed. Thus, alongside the ability to manipulate the murine genome, the mouse has become a popular choice for studying the pathogenesis of HF and models using mice have provided much knowledge about the heart and the mechanisms by which the heart progresses to failure.

1.7.1 Model of pressure overload-induced remodelling

Hypertensive patients develop hypertrophy as a result of perpetually increased afterload. In these situations, the LV elevates the systolic BP to eject an adequate SV, known as pressure overload. Banding of the ascending, transverse or descending aorta is established as a preclinical model of pressure overload [285] and can be used to study the progression of hypertrophy to HF. Additionally, the tightness of banding can be modified to derive different HF phenotypes (compensatory hypertrophy, decompensated hypertrophy, acute HF) with different timecourses [286]. Low mortality and cardiac remodelling are associated with this model [287].

1.7.2 Model of volume overload-induced remodelling

Patients with chronic mitral or atrial regurgitation acquire a constantly elevated LV cavity volume, known as volume overload. Under these conditions, CO is maintained by elevated SV, which is sustained by an increase in preload. Over time, the myocardium dilates and end-diastolic volume increases. In mice, to mimic the progression of volume overload to HF, an aortocaval shunt can be created between the abdominal aorta and inferior vena cava [288]. This model induces eccentric cardiac hypertrophy, developing into cardiac dilatation and inducing cell death [287].

1.7.3 Models of MI and I/R injury

MI is a unique stress of the myocardium associated with increased preload, increased afterload and cardiac remodelling. Ligation of the left anterior descending (LAD) coronary artery can be used to investigate the remodelling after MI [289], and its pathogenesis to HF. Wall thinning, infarct development and activation of wound repair responses are attributes of this model, alongside the haemodynamic changes seen in MI patients.

Research into the mechanisms that induce I/R injury is an area of active interest due to the poor recovery of ischemic tissue. Models of reperfusion after ischemia have been established to study the mechanisms of I/R and myocardial stunning [290, 291]. I/R injury can be performed *in vivo* with ligation executed as described above with a small tube present to ease relief of the occlusion and enable reperfusion. This model is associated with the typical features of I/R injury including infiltration of inflammatory cells, attenuated fibrotic remodelling and enhanced neovascularisation [292]. Additionally, I/R injury can be examined *ex vivo* using the Langendorf system [293]. The heart is explanted and mounted onto a perfusion system and supplied with nutrients to maintain cellular energetics. This system is capable of evaluating the pathophysiological and electrophysiological consequences of I/R injury.

1.7.4 Neurohormonal models

As mentioned previously, enhanced activation of the sympathetic nervous system is commonly observed in HF patients and is proposed to contribute to cardiac dysfunction. Elevated levels of catecholamines are observed in these patients [17, 18, 22] as well as alterations in the expression of the associated receptors.

Catecholamines are an organic chemical group, which encompasses endogenous signalling hormones, epinephrine and dopamine as well as synthetic entities such as isoproterenol (Iso). Within the body, catecholamines act as signalling molecules that bind to ARs to prepare the body for physical action. As mentioned in **section 1.6.1**, the adrenergic signalling cascade plays a fundamental role in hypertrophy and its development to HF.

In addition to Ang II or insulin-like growth factor 1 infusion, Iso is commonly used to investigate pathological ventricular remodelling associated with hypertrophy [282]. Although Iso is structurally similar to epinephrine, it has a higher affinity for the β-AR than epinephrine and norepinephrine [294]. Over the past sixty years, Iso infusion has been implemented as a successful model of hypertrophy with infusion inducing LV hypertrophy, fibrosis and cell death in rats and dogs [295, 296, 297, 298].

As a β-AR stimulant (β-stimulant), Iso binds to β-ARs and activates intracellular signalling pathways downstream of these receptors. However, chronic infusion of catecholamines impairs the β-AR signalling pathway with reports of desensitised adrenergic receptors and calcium mishandling [299, 300]. Furthermore, increased proinflammatory cytokine expression, lipid peroxidation and diminished FA and glucose metabolism have all been detected after Iso treatment [224, 301, 302]. Thus infusion of Iso has multiple effects on the myocardium.

Although, infusion of Iso is frequently used to model hypertrophy, several studies have used Iso to induce HF [303, 304]. Iso can be administered by intraperitoneal injection or by implantation of an osmotic minipump and may therefore be considered less invasive than the methods described above. This

model provides a platform to study the effects of catecholamines and the β-AR signalling pathway in the development of hypertrophy and its progression to HF.

1.8 Study rationale

Sterile inflammation has been reported to contribute to the pathogenesis and progression of HF [20, 169], yet the processes that initiate and execute myocardial inflammation remain unknown. The endosomal immune sensor, TLR9 is reported to be involved in pressure overload-induced myocardial inflammation and cardiac remodelling [173]. However, the mechanisms and interactions by which TLR9 induces these responses after pressure overload remain unstudied. Various cellular pathways are activated after pressure overload, including the β-AR signalling cascade, which is impaired in HF and has immunomodulatory roles [224, 225]. Therefore TLR9 may potentially interact with the β-AR signalling cascade to induce myocardial inflammation and may also impact other cardiac remodelling processes such as fibrosis, hypertrophy and cardiac function.

Another common trigger of HF is MI, in which a robust inflammatory is observed and is reported to play a crucial role during LV remodelling post-MI by aiding the clearance of dead cells and promoting tissue repair. However, as mentioned, the processes that initiate and execute myocardial inflammation remain unknown. Although, the impact of TLR9 stimulation on LV remodelling after MI has not yet been studied, increased levels of circulating mtDNA have been detected in acute MI patients [305]. This finding suggests a stimuli that could potentially activate a TLR9-dependant inflammatory response post-MI and warrants further evaluation.

1.8.1 Aims

Therefore, the overall aim of this thesis was to investigate the role of the immune sensor, TLR9 in the pathogenesis of HF and its contribution to the associated inflammatory response. This thesis focussed upon TLR9-mediated inflammation in the context of β-AR signalling cascade and post-MI using mouse models.

Therefore the general hypothesis for this thesis is that TLR9-mediated inflammation contributes to myocardial inflammation observed in Iso-induced HF and MI-induced HF.

Chapter 3 focuses on possible associations between TLR9-mediated inflammation and the β-AR signalling cascade, using a β-stimulant infusion model. Further characterisation of this model is performed in chapter 4, in which alterations in oxidative stress, mitochondrial morphology and function and metabolism are investigated. Finally, chapter 5 examines the contribution of TLR9-associated inflammation in the aftermath of MI. Collectively these chapters aim to increase the understanding of inflammatory processes within the myocardium and its contribution to the development of HF.

2 Methods

2.1 Animal work

All procedures were performed in accordance with the Guidance on the Operation of the Animals (Scientific Procedures) Act, 1986 (UK Home Office). Global TLR9-deficient (TLR9KO) mice were kindly provided by Professor Shizuo Akira (Osaka University, Japan) [177]. In these mice, a 1 kb genomic DNA sequence that encoded for the LRR of murine TLR9 was replaced with a neomycin cassette (**figure 2.1**). These mice had previously been backcrossed with C57Bl/6 mice for more than 5 generations, so C57BL/6 mice could be used as wild-type (WT) controls. C57Bl/6 mice, hereafter referred to as WT mice, were ordered from Harlan Laboratories whilst TLR9KO mice were bred and housed on site. Mice were accommodated in a temperature and humidity controlled animal facility, with 12-hour light/dark cycles and were given unrestricted access to water and standard laboratory chow.

For Isoprenaline (Iso) related experiments in chapters 3 and 4, 10 – 11-week-old, 24 – 27 g WT and TLR9KO male mice were used whilst MI-related experiments in chapter 5 were performed with 8 – 10-week-old WT and TLR9KO male mice. All experiments were performed in a blinded manner using a coding system to minimise bias. Mice were coded prior to treatment, therefore it was unknown to the experimental operator during the experiment the genetic background and treatment for each mice / sample. The treatment and genetic background was disclosed upon conclusion of the physiological, biochemical or histological experiment.

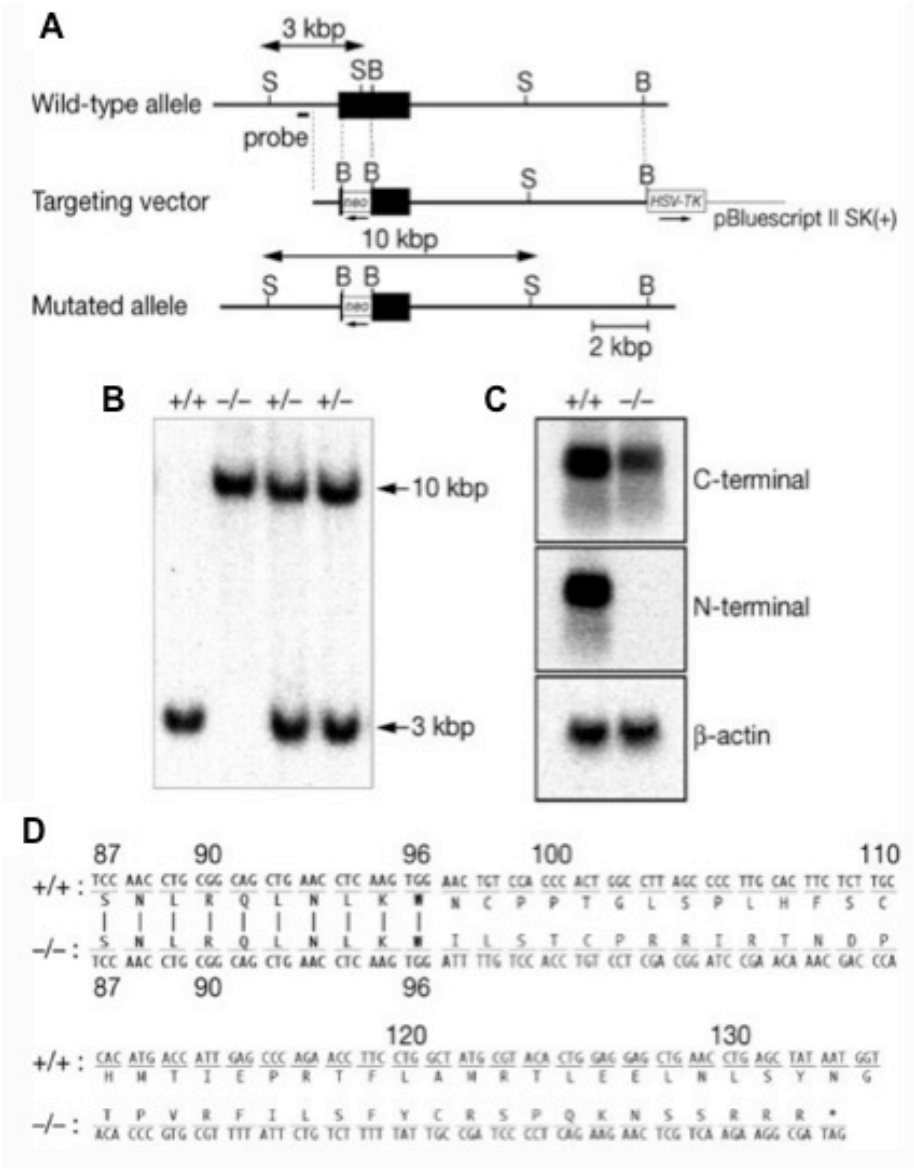

Figure 2.1 Targeted disruption of the murine gene encoding *Tlr9* used to generate a conventional TLR9-deficient mouse line.
Figure taken from Hemmi *et al* (2000) [177]. A, Maps of the TLR9 genome, the targeting vector and the predicted disrupted gene. In the targeting vector, 1 kbp of the coding exon (closed box) was replaced with a neomycin cassette and novel restriction enzyme sites : B, *Bam*HI; S, *Sca*I. B, Southern blot analysis of offspring from the heterozygote intercrosses. Extracted DNA was digested with *Sca*I and hybridised with the radiolabelled probe indicated in A. Wild-type (WT) mice (+/+) gave a single 3 kbp band, a 10 kbp band for TLR9KO mice (-/-) and both bands for heterozygous mice (+/-). C, Northern blot analysis of splenocytes from WT (+/+) and TLR9KO (-/-) mice. Samples were hybridised using a probe targeting the TLR9 N-terminal or C-terminal portions. The N-terminal probe bound to WT samples but did not bind to TLR9KO samples, confirming recombination of the *Tlr9* encoding allele. D, Comparison of the predicted amino-acid sequences between WT (+/+) and TLR9KO (-/-) cDNA highlight the introduction of a new stop codon in TLR9KO cDNA to cause premature translational termination to generate a shorter form of TLR9. The numbers indicate predicted amino acid positions within WT TLR9.

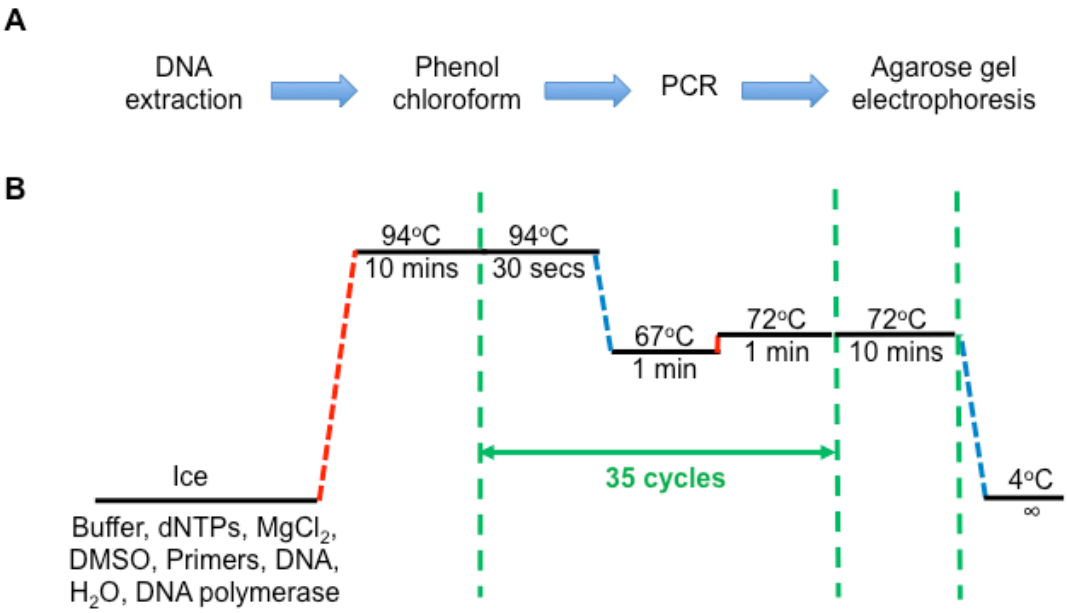

Figure 2.2 Genotyping procedure of TLR9KO mice.
A, Steps performed to genotype TLR9KO mice. B, PCR (polymerase chain reaction) programme. On ice, extracted DNA was combined with AmpliTaq Gold Buffer, deoxynucleotide triphosphates (dNTPs), magnesium chloride ($MgCl_2$), dimethyl sulphoxide (DMSO), primers (Table 2.1), autoclaved water and AmpliTaq Gold DNA polymerase. Samples were heated to 94°C for 10 minutes, then 35 cycles of 94 °C for 30 seconds, cooling to 67°C for 1 minute and heating to 72°C for 1 minute. After the repeated cycles, the samples were held at 72°C for 10 minutes.

2.1.1 Genotyping of TLR9KO mice

The breeding strategy to produce TLR9KO mice was designed so that only TLR9KO mice were generated. Homozygous knockout (TLR9KO) mice were bred with TLR9KO mice, to yield only TLR9KO mice (see **figure 3.5**). Ear biopsies were taken from mice before surgery and after harvesting to confirm the genotype of the mouse. An outline of the procedure used to genotype these mice is presented in **figure 2.2a**.

2.1.1.1 DNA extraction

Ear biopsies were added to coded tubes containing 10 µM NaOH (Sigma Aldrich, S8045), vortexed and left to incubate at 95°C for 30 minutes to lyse samples. Next, 0.1 M Tris-HCl (pH 8.0) (Trizma base, Sigma Aldrich, T1503;

36% hydrochloric acid, Alfa Aesar, L13091) was added and the samples were vortexed and centrifuged at 13,400 g for 10 minutes at room temperature (RT). The supernatant containing genomic DNA was isolated and put into a new tube. To increase the purity of the genomic DNA for polymerase chain reaction (PCR), double the volume of Tris- Ethylenediaminetetraacetic acid (EDTA) buffer (TE) (10 mM Tris, 1 mM EDTA (Sigma Aldrich, ED2SS)) was added to the DNA extracted from ear biopsies. Next, phenol (Sigma Aldrich, P4557) and chloroform : isoamyl alcohol (IAA) were added (chloroform : IAA, 24 : 1, Sigma Aldrich, CO549) and the samples were vortexed for 30 seconds followed by centrifugation for 5 minutes at 15,700 g at 4^{o}C. The top phase of the solution was transferred to a new tube and chloroform : IAA was added. The vortex and centrifugation steps were repeated. The top phase of the solution was transferred to a new tube and 3 M sodium acetate (1/10 of the volume) (Sigma Aldrich, S2889) and 100% ethanol (2.5 x the volume) (Fisher Scientific, E/0650DF/17) was added. The tube was mixed gently and left at -20^{o}C for 30 minutes. The solution was subjected to centrifugation for 30 minutes at 15,700 g at 4^{o}C and the resulting pellet was resuspended in 20 µl TE buffer to obtain pure genomic DNA.

2.1.1.2 PCR and agarose gel electrophoresis

Extracted genomic DNA (purified by phenol chloroform extraction) was diluted 10-fold and 0.5 µl was added to the PCR mixture. This PCR mixture consisted of 1 x AmpliTaq Gold Buffer (Life Technologies, 4398781), 200 µM deoxynucleotide triphosphates (dNTPs) (Life Technologies, 1405147), 2.5 mM $MgCl_2$ (Life Technologies, 4486224), 2.5% dimethyl sulphoxide (DMSO) (Sigma Aldrich, W387520), 0.5 µM of each primer (forward and reverse), autoclaved

water and 2.5 U of AmpliTaq Gold DNA polymerase (Life Technologies, 4311814).

Two mastermixes were prepared; 1 mastermix included primers for WT mice (WT and Extra) and another mastermix contained primers for TLR9KO mice (TLR9KO and extra) (**table 2.1**). The tubes were loaded onto the PCR machine (Veriti thermocycler, Applied Biosystems) and heated to 94^{o}C for 10 minutes and then 35 cycles of heating to 94^{o}C for 30 seconds, cooling to 67^{o}C for 1 minute and heating to 72^{o}C for 1 minute (**figure 2.2b**). After the repeated cycles, the samples remained at 72^{o}C for 10 minutes. Next, PCR samples were diluted 6 times with DNA loading buffer and applied to a 1.5% agarose gel (1.5 g in 100 ml Tris-Borate-EDTA (TBE) (900 mM Tris, 900 mM boric acid (Sigma Aldrich, B7660, 20 mM EDTA))) with a 100 bp ladder (Promega, G2101). Electrophoresis was performed for 30 minutes at 150 V with TBE. Following this, the gel was stained in 0.5 µg/ml ethidium bromide (Sigma Aldrich, E1510) and developed using the gel imager, BioSpectrum AC Imaging System (UVP). Samples were decoded to identify the mice from which the sample was obtained.

Table 2.1 Sequences of primers used to genotype TLR9KO mice.
To confirm the genotype of TLR9KO mice, polymerase chain reactions were performed with DNA extracted from ear biopsies using 2 different primer sets. The first primer set (WT and Extra primers) would only amplify DNA from WT mice whilst the other primer set (TLR9KO and Extra primers) would only amplify DNA from TLR9KO mice.

Primer	Sequence
WT	5'-GAAGGTTCTGG GCTCAATGGTCATGTG-3'
Extra	5'-GCAA TGGAAAGGACTGTCCACTTTGTG-3'
TLR9KO	5'-ATCGCCTTCTATCGCCTTCTTG ACGAG-3'

2.1.2 Surgery

2.1.2.1 Preparation and implantation of minipumps

Osmotic minipumps (model 2004, Alzet) infusing 75 mg/kg/day Iso (isoprenaline hydrochloride, Sigma Aldrich, I5627), 50 mg/kg/day Iso or saline solutions (AquaPharm, XVD587) were primed and implanted as previously described [306]. 40 hours before implantation, minipumps were prepared under sterile conditions and stored in saline at 37^{o}C for priming. The concentration of the Iso solution loaded into the minipumps was calculated to account for the flow rate of the minipumps and body weight of the mice (**figure 2.3**).

A

Weight of mouse (kg)	x	Dose of Iso (mg/kg/day)	=	Daily amount of Iso (mg/day)
Flow rate of minipump (µl/hour)	x	Hours per day	=	Flow rate per day (µl/day)
Daily amount of Iso (mg/day)	÷	Flow rate per day (µl/day)	=	Concentration of Iso (mg/µl)

B

For **25 g** mice, minipumps infusing **50 mg/kg/day** Iso at flow rate **0.25 µL/hour**

0.025 kg x 50 mg/kg/day = 1.25 mg/day

0.25 µl/hour x 24 hours/day = 6 µl/day

1.25 mg/day ÷ 6 µl/day = 0.208 mg/µl
= 208 mg/ml of Iso needed

Figure 2.3 Equations used to determine the concentration of Iso solution required for minipumps.
A, Equations used to calculate the concentration of Iso needed for each experiment. B, Use of the equations to determine the concentration of Iso solution required to deliver 50 mg/kg/day Iso to a 25 g mouse using minipumps with a flow rate of 0.25 µL/hour.

Once the solutions were prepared and filtered, the solutions were loaded into the minipumps according to the manufacturer's protocol using a syringe and the filling tube provided with the minipumps. Once the minipumps were filled with

solution, the filling tube was removed and the flow moderator (provided with the minipumps) was fully inserted into the minipump.

Surgery was performed in a blinded manner to minimise bias. The surgeon (myself) was unaware of which minipump was inserted (saline or Iso) and the genetic background of the mice. Mice were given an intra-peritoneal (IP) injection (6 ml/kg) containing an anaesthetic cocktail (9.3% ketamine (Pfizer, Vetalar) and 9.8% medetimidine (Orion, Domitor)) and analgesia reagents. Hair was shaved from the posterior of the mice above the tail and the skin was cleansed using povidine-iodine (VetaSept) and chlorhexidine (VetaSept).

Loss of the pedal toe reflex ensured that mice were sufficiently anaesthetised. An incision was made subcutaneously (SC) on the back of the mouse close to the tail and a pocket was created for the minipump by inserting jaws of surgical scissors into the incision and performing a spreading motion by opening and closing the jaws. The minipump was implanted and the incision was closed using 5-0 suture (Ethilon, Ethicon). IP injection of the anaesthetic reversal reagent (10% atipamezole (Orion, Antisedan)) was applied to the mouse and mice were left to recover in a warm chamber before returning to their cages.

2.1.2.2 Left anterior descending (LAD) artery ligation

Ligation of the LAD artery was performed by Dr Shigemiki Omiya (King's College London) as previously described [156]. Mice were anaesthetised by IP injection containing an anaesthetic cocktail (6 ml/kg) and also given analgesia. Hair was shaved from the neck area and the left side of the ribcage and the skin was disinfected using povidine-iodine and chlorhexidine. Mice were maintained in supine position and after ensuring that mice were adequately anaesthetised, mice were intubated at 150 strokes per minute (SV 150 µl) using a Type 845

ventilator (MiniVent). A left-sided thoracotomy was performed, carefully pulling aside the pectoralis minor and pectoralis major. Using forceps, an incision was made in the 3rd intercostal space (between the 3rd and 4th rib). The thorax was opened carefully and the LAD coronary artery was located and completely ligated with 1 stitch of 8-0 suture (Ethilon, Ethicon). After ligation, the muscles were carefully repositioned and the skin was closed using 5-0 suture (Ethilon, Ethicon). Anaesthetic reversal reagent was administered to the mice by IP injection and mice were left to recover in a warm chamber before returning to their cages.

2.1.2.2.1 Evans Blue staining

Evans Blue staining was performed by Dr Shigemiki Omiya (King's College London). Directly after LAD ligation, mice were injected with 2% Evan's Blue reagent (Sigma Aldrich, 206334) in saline into the inferior vena cava. Immediately, several organs, including the heart turned blue. The mice were left for 30 seconds to allow complete staining of the myocardium and then the heart was extracted and frozen. Hearts were transversely cut into 6 slices and imaged using a camera (G15, Canon).

2.1.3 *In vivo* and *ex vivo* measurements

2.1.3.1 Echocardiography and BP measurements

Echocardiography using Vevo 2100 Imaging System (Visualsonics) attached to MicroScan transducer (Visualsonics, MS250) was used to study *in vivo* cardiac morphology and function. Echocardiography was either performed using anaesthetised mice using 0.5 - 2% isoflurane (Abbot, 13506) by myself or using conscious mice by Dr Manabu Taneike or Dr Shigemiki Omiya (both from King's

College London). As the mice were coded, the genetic background and treatment for each mouse was unknown to the operator and echocardiography was performed in a blinded manner.

A

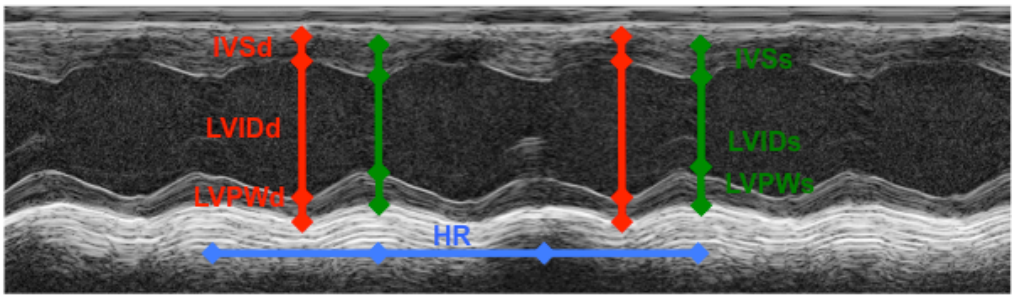

B

$$\text{Ejection fraction (\%)} = 100 \times \left[\frac{[\text{LVEDV} - \text{LVESV}]}{\text{LVEDV}} \right]$$

$$\text{LVEDV} = \text{LVIDd}^3 \times \left[\frac{7}{[2.4 + \text{LVIDd}]} \right]$$

$$\text{LVESV} = \text{LVIDs}^3 \times \left[\frac{7}{[2.4 + \text{LVIDs}]} \right]$$

C

$$\text{Fractional shortening (\%)} = 100 \times \left[\frac{[\text{LVIDd} - \text{LVIDs}]}{\text{LVIDd}} \right]$$

D

$$\text{LV mass (mg)} = 1.053 \times [[\text{LVIDd} + \text{LVPWd} + \text{IVSd}]^3 - \text{LVIDd}^3]$$

Figure 2.4 Analysis of echocardiographic images and formulas used to calculate cardiac parameters.
Vevo 2100 Workstation Software (Visualsonics) was used to analyse short-axis M-mode echocardiographic images. A, The user was able to measure cardiac parameters. End-diastolic measurements are shown in red: Interventricular septal wall thickness (IVSd), Left ventricle internal dimension (LVIDd), Left ventricular posterior wall thickness (LVPWd). End-systolic measurements are shown in green: Interventricular septal wall thickness (IVSs), Left ventricle internal dimension (LVIDs), Left ventricular posterior wall thickness (LVPWs). Heart rate (HR) (blue) was drawn with every contraction cycle. B-D, Measurements from echocardiographic images were used to calculate the ejection fraction (B), fractional shortening (C) and LV mass (D). LVEDV = left ventricular end-diastolic volume, LVESV = left ventricular end-systolic volume.

Preceding echocardiography, hair was removed from the chest using a topical depilatory agent. Under anaesthesia, the body temperature of the mice was maintained at 36.5^{o}C ± 1^{o}C and the respiratory rate kept above 100 breaths per minute. Using Vevo 2100 Workstation Software (Version 1.6.0, Visualsonics), 2 short axis M-mode images were acquired for each animal and each image was analysed during 2 different heartbeats as described in **figure 2.4**.

Non-invasive BP measurements (Kent Scientific, CODA) were performed on pre-warmed conscious mice in a blinded manner (**figure 2.5**). Mice were trained 3 times before taking valid BP measurements. Using the CODA software (Kent Scientific), 3 or more accepted readings (out of 20) were required to calculate an average reading for each mouse.

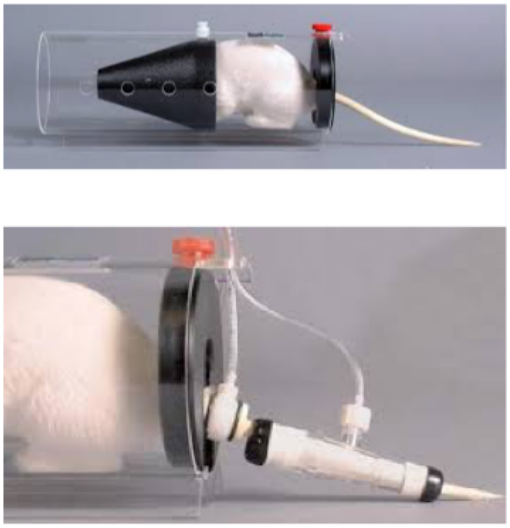

Figure 2.5 Blood pressure (BP) measurements
Mice were warmed to dilate blood vessels and a tail cuff was applied to the mouse, that was linked to a laptop that recorded the BP readings.

2.1.3.2 Cardiac magnetic resonance imaging (MRI)

Cardiac MRI, 7 Tesla horizontal MR scanner (Varian) was performed by Dr Andrea Protti (King's College London) as previously described [307, 308]. The operator was blinded to the genetic background of the mice and mice were anaethetised with 1.5% isoflurane, maintained at 37^{o}C and set in the prone

position. 30 µl bolus of 0.5 mmol/kg gadolinium-diethylenetriaminepentaacetic acid (Gd-DPTA) (Magnevist, Schering Healthcare) was injected IP into the mice. 2 metallic needles were placed SC in the front paws to monitor the electrocardiogram.

Acquired images were analysed using a semiautomated in-house-developed cardiac preclinical computer software program [307, 308] to calculate cardiac functional parameters and infarct size (**figure 2.6**). Using ImageJ software (version 1.46r, NIH), the thickness of the free wall was calculated.

A

$$\text{Infarct size} = \frac{\left[\sum_{\text{Apex}}^{\text{Base}} \left[\frac{\text{Area}_{\text{inf}}}{\text{Area}_{\text{tot}}}\right] X\ 100\right]}{\text{Number of slices}}$$

B

$$\text{Stroke volume (µl)} = \text{LVEDV - LVESV}$$

C

$$\text{LV mass (g)} = \gamma \sum_{\text{Apex}}^{\text{Base}} \left[\text{Epicardial volume} - \text{Endocardial volume}\right] \text{x slide thickness}$$

Figure 2.6 Equations used to analyse cardiac MRI images.
Semiautomated in-house-developed cardiac preclinical computer software program was used to analyse cardiac MRI images [307, 308]. Equations used to measure the (A) infarct size. Area_{inf} = End-diastolic infarct area, Area_{tot} = End-diastolic total LV area. (B) Stroke volume and (C) LV mass. γ = specific gravity of the myocardium (1.055 g/cm^2).

2.1.3.3 Gravimetric data collection

Animals were culled by cervical dislocation. Promptly, the chest was opened and the hearts was harvested and washed in ice-cold phosphate buffered saline (PBS) (Sigma Aldrich, P4417). The heart was weighed and segmented for further analyses (**figure 2.7**). In addition measurements of lung weight, liver weight, minipump weight and tibia length were recorded during harvesting.

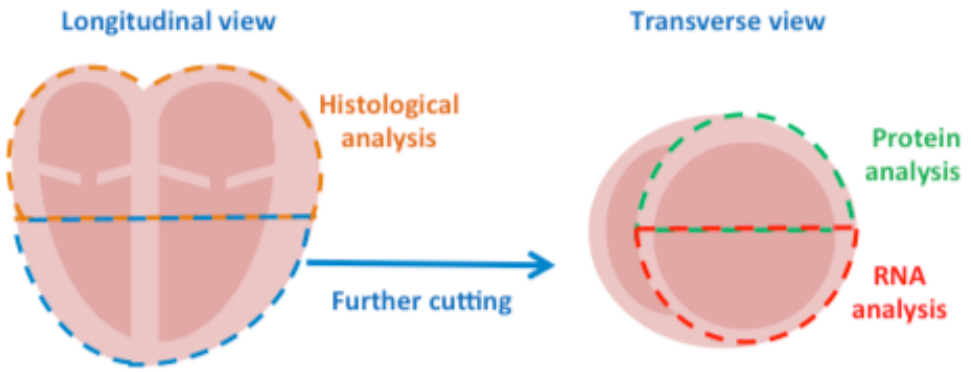

Figure 2.7 Segmentation of a murine heart.
Upon harvesting, the heart was excised from the body, washed in ice-cold PBS, and sliced horizontally in the middle and the top half was submitted for histological analyses. The right ventricle was removed from the residual heart piece (bottom half) and the remaining left ventricle was cut into two from an aerial view, with both halves containing septal and lateral walls. Only samples of left ventricles were submitted for biochemical analyses.

2.2 Histological analysis

After harvesting, coded heart samples for paraffin embedding were fixed in 4% paraformaldehyde (PFA) (Sigma Aldrich, P6148) overnight at 4°C. Next day, the heart samples were washed 3 times with PBS. The hearts were stored in 70% ethanol at 4°C and submitted for processing. After processing, the heart samples were embedded in paraffin and 6 µm sections were cut using the microtome (Leica, RM2125). The sections were heated to 42°C for 5 minutes in a water-bath (RA Lamb, E65), collected using Superfrost Plus slides (Thermo Scientific, 10149870) and heated to 40°C for 30 minutes (RA Lamb, E18.1) and left at RT overnight. Prior to staining, the paraffin embedded heart sections were deparaffinised in xylene (Scientific Laboratory Supplies, 534056) twice and rehydrated using decreasing concentrations of ethanol (100% twice, 95%, 80%, 70%) and distilled H_2O (dH_2O) with each incubation lasting 5 minutes.

The heart tissue reserved for cryosections were stored in Shandon Cryomatrix compound (Thermo Scientific, 6769006) after harvesting and frozen using

isopropanol (Sigma Aldrich, I9516) and dry ice. The coded samples were sectioned using the cryostat (Thermo Scientific, HM560) at a thickness of 6 µm and stored at -80^{o}C. Prior to staining, the sections were dried at RT for 30 minutes, fixed in acetone (Sigma Aldrich, 34850) for 15 minutes at 4^{o}C and washed with PBS 3 times for 5 minutes. Slides were decoded upon termination of the experiment to disclose the genetic background and treatment for each sample.

2.2.1 Haematoxylin and Eosin (H & E) staining

H & E staining was performed using paraffin-embedded and cryo- sections. After being prepared as described in **section 2.2**, the sections were treated with haematoxylin (Thermo Scientific, LAMB-230-D) for 3 minutes and rinsed with tap water. Sections were dipped 12 times in acid ethanol (1:400 concentrated HCl in 70% ethanol) and rinsed in dH_2O. Eosin (Thermo Scientific, LAMB-100-D) was used as a counterstain for 30 seconds, before dehydrating with 3 washes of 5 minutes using 95% and 100% ethanol. Slides were treated with xylene twice for 15 minutes and mounted with coverslips (Fisher, 12373128) using DPX mountant (Sigma Aldrich, 06522) and left to dry overnight. The slides were imaged using a brightfield microscope (Zeiss, Axioskop 2) at 50 x and 200 x magnification.

2.2.2 Wheat Germ Agglutinin (WGA) staining

After fixing the cryosections (**section 2.2**), slides were washed using tap water for 5 minutes. After drawing a circle around the specimen using a PAP pen (Life Technologies, 00-8899), the sections were incubated with 0.1% bovine serum albumin (BSA) (Sigma Aldrich, A7906) in PBS for 5 minutes. Once the BSA

solution was removed, the section was incubated with FITC-lectin conjugate (diluted 100-fold with 0.1% BSA solution) (Sigma Aldrich, L4895) at RT for 1 hour. Sections were washed 3 times with 0.1% BSA solution for 5 minutes and finally rinsed with PBS. The slides were mounted using Vectashield mounting medium for fluorescence with DAPI (Vector Laboratories, H-1200) and sealed using nail polish. 5 images per heart section were acquired using Volocity software (version 6.3, Perkin Elmer) on the fluorescent microscope (IX81, Olympus) at 200 x magnification. Using ImageJ, the cardiomyocyte cross-sectional area (CSA) of 20 cells per image was measured. Cardiomyocytes that were measured were round in shape with the nucleus in the middle of the cell (**figure 2.8**).

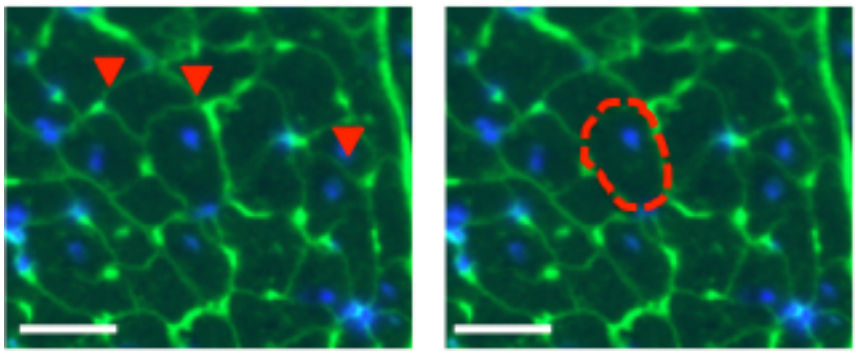

Figure 2.8 Analysis of wheat germ agglutinin (WGA) staining to measure cardiomyocyte cross-sectional area (CSA).
Images of WGA staining to illustrate the round shape (red) and central position of the nuclei within cardiomyocytes (left) selected for analysis to measure the cardiomyocyte CSA (right). Scale bar = 30 µm. Green signal (FITC, lectin), blue signal (DAPI, DNA).

2.2.3 Immunohistochemistry (IHC)

After myocardial cryosections were fixed (**section 2.2**), a circle was drawn around the specimen using a PAP pen and the sections were blocked with 3% skimmed milk powder reagent (Biorad, 170-6404) diluted in PBS for 30 minutes at RT. This was followed by an overnight incubation at 4^{o}C with the primary antibody (**table 2.4**), diluted in blocking reagent. The next day, slides were

washed in PBS 3 times for 5 minutes and endogenous peroxidases were deactivated using 0.3% H_2O_2 in methanol (Pedrogen, Sigma Aldrich, 31642; Methanol, Fisher Scientific, M/3900/17) for 30 minutes at RT. A 15 minutes wash with PBS was followed by incubation with the secondary antibody (**table 2.5**) in blocking reagent at RT for 30 minutes. Sections were washed 3 times for 5 minutes using PBS and then incubated with ABC reagent (Vector, PK-6101) at RT for 20 minutes. Slides were washed twice for 5 minutes in PBS and incubated with 3,3'-diaminobenzidine (DAB) (Vector, DAB SK-4100). Washing in PBS halted the reaction and slides were counterstained with haematoxylin for 3 minutes. Slides were washed in pre-warmed dH_2O for 10 minutes, dehydrated and mounted using DPX. Slides were left to dry overnight and were imaged on the brightfield microscope at 200 x and 400 x magnification. The number of DAB-positive cells were calculated from 5 images per section and expressed as cells per mm^2. Negative controls were performed without any primary antibody to confirm the specificity of antibody.

2.2.4 Masson's Trichrome (MT) staining

MT kit (Polysciences Inc, 25088-1) was used for this procedure and followed according to the manufacturers instructions. Slides were mounted with DPX mountant and left to dry overnight. Slides were viewed on the brightfield microscope and images were taken at 200 x magnification. Analysis of 5 images per heart section was performed using ImageJ software to determine the fibrotic area (blue signal) per image and this was expressed as a percentage.

2.2.5 Picrosirius Red staining

Paraffin-embedded heart sections were prepared as described in **section 2.2.** Slides were subjected to 0.2% phosphomolybdic acid (Sigma Aldrich, 79560) for 2 minutes, rinsed and incubated in 0.1% picrosirius red diluted in saturated picric acid (Direct Red 80, Sigma Aldrich, 43665; saturated picric acid, Sigma Aldrich, 80456) for 2 hours at RT. The slides were washed twice with acidified water (1:200 dilution of acetic acid (Scientific Laboratory Supplies, CHE1016)), dehydrated using 95% ethanol twice and 100% ethanol twice. Slides were cleared with xylene twice for 15 minutes and mounted using DPX and left overnight to dry. Brightfield images were acquired using the IX81 microscope (Olympus) at 50 x magnification. Using the tilestitch feature, an image was formed of the entire heart section. ImageJ software was used to analyse the amount of fibrosis, by splitting the image into different colour channels. The fibrotic area and the total area of the heart section were measured and the fibrotic area was expressed as a percentage of the total area of the heart.

2.2.6 TUNEL staining

After deparaffinising and hydrating paraffin-embedded sections (**section 2.2**), slides were incubated with 50 µg/ml proteinase K (Sigma Aldrich, P2308) diluted in PBS, for 30 minutes at RT. Myocardial cryosections were fixed using 4% PFA for 1 hour at RT and were permeabilised using 0.25% Triton X-100 (Sigma Aldrich, X100) for 20 minutes. Both paraffin-embedded- and cryo-sections were washed twice in PBS and incubated with α-sarcomeric actin antibody (diluted 1:500 in 1% BSA with 0.1% Triton X-100 in PBS) (Sigma Aldrich, A2172) at RT. After 50 minutes incubation, the samples were washed 4 times with PBS and each section was incubated with 5 µl Texas RED Anti-

mouse IgM (Vector Laboratories, TI-2020), 45 µl labeling safe buffer and 5 µl TdT enzyme (both from In Situ Apoptosis Detection Kit, Clontech, MK500). This incubation was performed at 37^{o}C in a light-shielded humidity chamber for 1 hour and then washed 4 times with PBS. The slides were mounted with DAPI containing mounting media and sealed using nail varnish. For the positive control, the section was incubated with 300 U/ml Dnase I (Sigma Aldrich, DN25), diluted in 1 mg/ml BSA in 50 mM Tris-HCl (pH7.5) for 30 minutes at RT, prior to incubation with anti-α-sarcomeric actin. Slides were viewed using the fluorescent microscope. Images were taken in 5 random regions of the section at 200 x magnification and the number of DAPI nuclei per image was calculated using Volocity. The number of TUNEL-positive cells was counted in the whole heart section and expressed at number of TUNEL-positive cells per 10^5 cells.

2.2.7 Oil Red O staining

Frozen cryosections were warmed to RT whilst Oil Red O stock solution (0.3% in isopropanol; Sigma Aldrich, O0625) was diluted 6:4 with dH_2O (Oil Red O working solution). This solution was vortexed, left for 10 minutes and filtered. After air-drying the slides, the sections were fixed with 10% formaldehyde (FA) (Sigma Aldrich, F8775) for 10 minutes on ice. Following this, the samples were washed twice for 5 minutes with dH_2O. Slides were then stained with the Oil Red O working solution for 10 minutes and washed in running tap water for 10 minutes. Slides were counterstained with haematoxylin for 5 minutes and washed again with running tap water for 10 minutes. Slides were mounted using DPX. 5 brightfield images were attained per section at 200 x magnification. Images were analysed using ImageJ software by splitting the image into different colour channels. Lipid deposition (marked in red) was calculated and

the total area of the heart section was measured and the lipid deposition was expressed as a percentage.

2.2.8 Immunofluorescence (IF) staining

After cryosections were defrosted and fixed (**section 2.2**), a circle was drawn around the section using a PAP pen. Sections were blocked with 2% skimmed milk diluted in PBS, for 30 minutes at RT. Next the samples were left in primary antibody (**table 2.4**) diluted in the blocking reagent overnight at 4^{o}C. Next day, the slides were washed 3 times in PBS for 5 minutes. Subsequently, sections were incubated with secondary antibody (**table 2.5)** diluted in blocking reagent at RT for 1 hour under light-shielded conditions. Sections were washed 3 times in PBS for 5 minutes and mounted using ProLong Gold Antifade Reagent with DAPI (Life Technologies, P36935) and left in a dark place overnight. 5 images per heart section were acquired using the fluorescent microscope at 200 x magnification. The number of α-SMA and double positive (α-SMA and Ki67) cells were counted per image using Volocity and expressed as positive cells per mm^2.

2.3 RNA extraction and quantitative-real-time PCR (qRT-PCR)

2.3.1 RNA extraction

Frozen heart tissue were coded (to minimise bias) and homogenised at 25 Hz for 1 minute with 1 ml TRIzol (Life Technologies, 15596) using MM400 homogeniser (Retsch). The solution was pipetted into a clean tube and incubated RT for 5 minutes. Chloroform (200 µl) (Sigma Aldrich, C2432) was added and shaken vigorously for 15 seconds. The solution was left at RT for 5 minutes, followed by centrifugation at 12,000 g for 15 minutes at 4 ^{o}C. The upper aqueous phase was placed into a clean labelled tube and 500 µl

isopropanol was added and the tube was inverted several times. After 10 minutes incubation at RT, the tubes were centrifuged at 12,000 g for 10 minutes at 4^{o}C. The supernatant was discarded and the pellet was washed with 1 ml 70% ethanol. The tubes were briefly vortexed and centrifuged at 7,500 g for 5 minutes at 4^{o}C. The supernatant was removed and the pellet was left to airdry. The pellet was resuspended in 30 µl RNase / DNase free H_2O (Gibco, 10977-035) and incubated at 55^{o}C for 10 minutes.

2.3.2 Complementary DNA (cDNA) synthesis and qRT-PCR

Total RNA concentration was measured using Nanodrop 2000 (Thermo Scienitifc). Total RNA (500 ng) was incubated with 100 ng random primers (Life Technologies, 48190-011), 0.5 mM dNTPs (Life Technologies, N8080260) and dH_2O and heated to 65^{o}C for 5 minutes. Samples were chilled on ice whilst 5 x first strand buffer (Life Technologies, y02321) and 0.01 M dithiothreitol (Life Technologies, y00147) was added. Samples were incubated at 25^{o}C for 2 minutes. After adding 100 U Superscript II reverse transcriptase (Life Technologies, 18064), samples were incubated at 25^{o}C for 10 minutes, 42^{o}C for 50 minutes and 70^{o}C for 15 minutes using Veriti thermocycler (Applied Biosystems) (**figure 2.9**).

cDNA samples were diluted 10-fold. For standards, 2 µl of each sample was combined in another tube and diluted accordingly (1 x, 4 x, 16 x and 64 x). cDNA was submitted for qRT-PCR analysis using 2 x Power SyBr Green Mastermix (Life Technologies, 4367660), 0.5 µM forward and reverse primers and dH_2O in a 96 well plate. The plate was sealed and qRT-PCR was performed on StepOnePlus machine (Applied Biosystems) with the programme set at 95^{o}C for 10 minutes, then 40 cycles of 95^{o}C for 15 seconds and 60^{o}C for

1 minute (**figure 2.10**). Samples were decoded to identify the mouse genotype and treatment. A list of qRT-PCR primers used in this thesis are detailed in **table 2.2**.

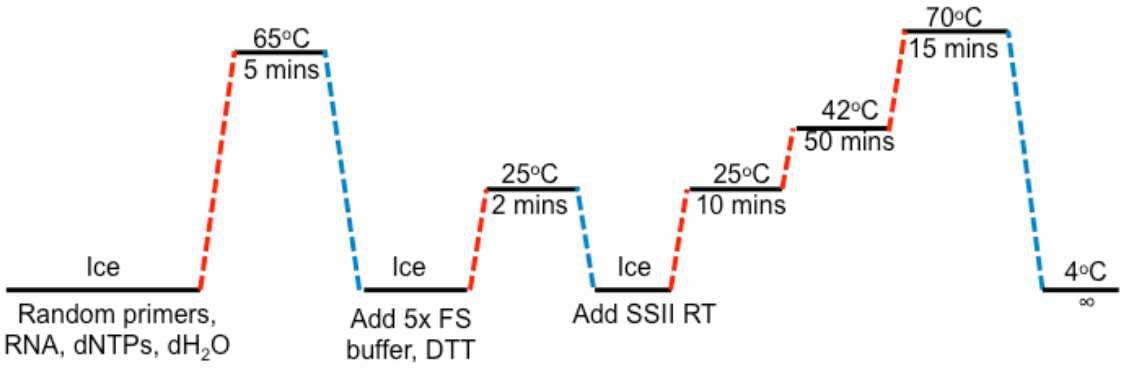

Figure 2.9 Reverse Transcription (RT) programme using Superscript II.
Total RNA (500 ng) was mixed with random primers, deoxynucleotide triphosphates (dNTPs) and dH_2O. After heating to 65°C for 5 minutes, 5x First Strand (FS) Buffer and dithiothreitol (DTT) were added on ice. Samples were heated to at 25°C for 2 minutes. Superscript II Reverse Transcriptase (SSII RT) was added and the samples were incubated at 25°C for 10 minutes, 42°C for 50 minutes and 70°C for 15 minutes.

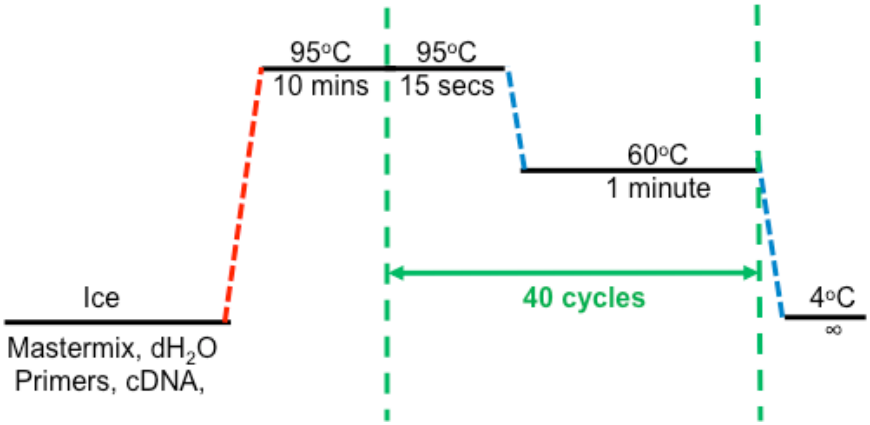

Figure 2.10 qRT-PCR programme.
Ten-fold diluted cDNA was mixed with Power SyBr Green Mastermix, 0.5 µM forward and reverse primers and dH_2O. This solution was heated to 95°C for 10 minutes, then 40 cycles of 95°C for 15 seconds and 60°C for 1 minute.

2.4 SDS-PAGE and Western blotting

Protease inhibitors (PI) (Sigma Aldrich, P8340) were diluted 100 x in lysis buffer (**table 2.3**). Lysis buffer with PI was added to tubes containing frozen harvested LV samples. Samples were homogenised at 25 Hz for 1 minute and pipetted into a clean tube. 0.1% Triton X-100 in PBS (Sigma Aldrich, X-100) was added and samples were left on ice for 30 minutes, followed by 10 minutes centrifugation at 8,000 rpm at 4 ^{o}C. The supernatant was collected. 10 µl of the supernatant was diluted 10-fold and used for protein quantification using Pierce BCA assay kit (Thermo Scientific Pierce, 13276818). After measuring the protein concentration, 20 – 40 µg protein was mixed with 5 x sample buffer (**table 2.3**) with 5% 2-mercaptoethanol (Sigma Aldrich, M3148). Samples were either heated to 95^{o}C for 5 minutes or left at RT for 30 minutes. Samples were loaded onto 5%, 10% and 15% SDS gels (**table 2.3**) with running buffer (**table 2.3**) and Precision Plus Protein Dual Xtra Standards (Biorad, 161-0377) and SDS-PAGE was performed for 2 hours at 120 V. Proteins were transferred from SDS-PAGE onto nitrocellulose membrane (Fisher Scientific, 15269794) at 0.1 A for 100 minutes with transfer buffer (**table 2.3**) using the wet transfer method. After transfer, the membrane was rinsed twice with TBS (**table 2.3**) and blocked for 1 hour at RT using the Odyssey blocking buffer (LI-COR Biosciences, 927-40000) or 5% milk powder. After blocking, membranes were washed with TBS-T (**table 2.3**) 4 times, each wash lasting 5 minutes. This was followed by overnight incubation at 4^{o}C with the primary antibody diluted in the blocking reagent. Next day, the membranes were washed as described earlier, followed by secondary antibody incubation at RT for 1 hour. Membranes were washed as before and developed using the Odyssey Clx imager (LI-COR Biosciences). Image Studio Lite software (version 5.2, LI-COR Biosciences) was used to

analyse images and perform densimetric analysis. Primary and secondary antibodies used for Western blotting are listed in **table 2.4** and **2.5**.

2.5 Transmission electron microscopy (TEM)

Mice were given an IP injection containing 75 IU heparin. After 20 minutes, mice were anaesthetised using an IP injection of sodium pentobarbital (50 mg/kg body weight) (Animalcare Ltd, Pentoject). Once the mice were adequately anaesthetised (with loss of the pedal toe reflex), the chest was opened. The apex of the LV was punctured by a needle that was connected to the PHD2000 pump (Harvard Apparatus) delivering wash solution (100 mM piperazine-N,N′-bis (2-ethanesulfonic acid (PIPES)) at 90 - 100 mmHg (flow rate 5 ml/min). Immediately after starting perfusion, the right atrium was snipped to allow blood/perfusate to leave the circulation. After 2 minutes, the fixative (0.1% sodium nitrate, 2% PFA, 2% glutaraldehyde, 100 mM PIPES) was perfused through the animal for 5 minutes. Following this, the heart was excised and sliced transversally. Slices were kept in buffer overnight and next morning, the hearts were washed with 100 mM PIPES 3 times. Samples were taken to the Centre of Ultrasound Imaging (King's College London) and Dr Gema Vizcay and Ms Leanne Glover kindly dehydrated, sectioned and stained the samples as well as providing the fixative and wash buffer. Images were taken on TEM (H7650, Hitachi).

2.6 Phospholamban overexpression studies

2.6.1 Bacterial transformation

Whilst the DNA plasmid solution was chilled on ice, DH5α competent cells (Invitrogen, 18258) were also thawed on ice. Once thawed, the cells were

added to the DNA solution (1,000 ng) and mixed by gentle pipetting. The mixture was left on ice for 30 minutes and then heat-shocked at 42^{o}C for 45 seconds. Immediately after, the samples were placed on ice for 2 minutes and 1 ml of SOC (SOB media with 20 mM magnesium and 20 mM glucose) was added. The samples were incubated at 37^{o}C for 1 hour, followed by centrifugation at 5,900 g for 1 minute. The majority of the supernatant was removed, leaving approximately 100 µl which was used to resuspend the pellet. This solution was placed onto RT antibiotic-containing agar plates (ampicillin (10 mg / 100 ml) (Sigma Aldrich, A9393) or chloramphenicol (1.25 mg / 100 ml) (Sigma Aldrich, C0378)) (Bacto Agar, BD Biosciences, 214010; LB Broth Merck, VM1540485) and spread across the surface. The plates were left to incubate at 37^{o}C overnight.

2.6.2 Miniprep and DNA sequencing

The day after transformation, colonies were picked using sterile toothpicks and incubated in individual tubes containing LB Broth with antibiotic ((ampicillin (10 mg / 100 ml) or chloramphenicol (1.25 mg / 100 ml)) and left to grow overnight at 37^{o}C. Next day, plasmid DNA was isolated from the cloudy LB Broth solution by using the QIAprep Spin Miniprep Kit (Qiagen, 27106). The protocol from the kit was followed and the DNA was eluted in 30 µl dH_2O. The DNA concentration and the 260/280 ratio was determined by the Nanodrop 2000. For DNA sequencing, samples were diluted to 100 ng/µl and dispatched to Source Bioscience for sequencing.

2.6.3 Enzyme digestion and ligation

Buffers (NEB) for enzyme digestion was selected according to NEBuffer performance chart for restriction enzymes (NEB). 2 µl buffer, 250 µg DNA and 1,000 units of each restriction enzyme for double digestion was combined and made up to 20 µl with RNase/DNase free H_2O and left for 1 hour at 37^oC. After digestion, 6 x DNA loading buffer was added to the samples and loaded onto a 1% agarose gel (1 g agarose in 100 ml TBE) and subjected to electrophoresis for 30 minutes at 150 V in TBE. After gel electrophoresis, samples were stained with ethidium bromide. Digested bands were observed using a transilluminator (UVP) and were excised from the gel. The digested DNA was isolated from the agarose gel using QIAquick gel extraction kit (Qiagen, 28706) and the DNA was eluted in 30 µl dH_2O.

Ligation of digested products was performed using the Mighty Mix DNA ligation kit (Clontech, 6023). Eluted DNA (vector) was diluted at 1:3 ratio with the eluted DNA (insert) and 2 x ligation mix was added (final volume 20 µl) and the solution was left at 16^oC overnight. The next day, 1 µl of the ligation mixture was transformed into DH5α cells.

2.6.4 Cell Culture

Human embryonic kidney (HEK)-293A cells (American Type Culture Collection) were kindly provided by Mr Francesco Nicolini (King's College London). Cells were cultured in 75 cm^2 flasks (Thermo Scientific, 178905) with DMEM medium (Sigma Aldrich, D6546) containing 10% foetal bovine serum (Gibco, 10270-106) and 1% penicillin-streptomycin-glutamine (Sigma Aldrich, G1146). Cells were incubated at 37^oC with 5% CO_2.

When cells reached approximately 80% confluency, cells were passaged. Media was aspirated off the cells and 5 ml PBS (Sigma Aldrich, D8637) was used to rinse the cells. 5 ml 0.5 M EDTA was added to the cells and left for 5 minutes at 37^{o}C. 5 ml culture media was added and the suspended cell solution was centrifuged at 100 g for 5 minutes. The supernatant was discarded and the pellet (cells) was resuspended with 1 ml of pre-warmed culture media. This cell mixture was diluted 20 x in 20 ml of culture media and seeded into a new flask.

2.6.5 Transfection

HEK293A cells were seeded at 2.5 x 10^5 cells per well in 6-well plates (in 3ml culture media) and left to incubate for 24 hours. Next day, cells were transfected with FuGENE HD (Promega, E2311) and plasmid DNA (3 µg) (ratio of transfection reagent : DNA plasmid was 3:1). Cells were harvested for 24 and 48 hours after transfection and the protein was isolated. Wells were aspirated, leaving 1 ml that was used to scrape the cells. The cell suspension was pipetted into clean tubes and centrifuged at 15,700 g for 5 minutes at 4^{o}C. The supernatant was discarded and the pellet was resuspended in 50 µl ice-cold lysis buffer containing PI (diluted 100 x). Immediately samples were sonicated for 10 seconds, followed by centrifugation at 15,700 g for 5 minutes at 4^{o}C. The pellet was discarded and the protein concentration of the supernatant was determined and Western blotting was performed as described in **section 2.4**.

2.7 Statistical analysis

Results are shown as the mean ± standard error mean (SEM) and the data were analysed using Graph Pad Prism (Graph Pad Software Inc, version 5.0). Paired data was assessed using Student's *t*-test analysis. Comparing 3 sets of data were analysed using one-way analysis of variance (ANOVA) with the

Bonferroni post hoc test whereas two-way ANOVA with the Bonferroni post-hoc test was used for comparing 4 sets of data made up of 2 distinct groups (for example WT and KO, with Saline and Iso treatments). Repeated measures analysis was used on results in experiments in which parameters were measured at 2 different time points using the same samples. A value of $p<0.05$ was considered statistically significant.

Table 2.2 qRT-PCR primers.
Forward and reverse primer sequences that were used in this thesis to study the mRNA expression of various markers.

Gene of interest	Direction of primer	Sequence
Acaca	F	GAGAGGGGTCAAGTCCTTCC
	R	CTGCTGCCGTCATAAGACAA
Acacb	F	GGGCTCCCTGGATGACAAC
	R	GCTCTTCCGGGAGGAGTTCT
Adrb1	F	GTCATGGGATTGCTGGTGGT
	R	GCAAACTCTGGTAGCGAAAGG
Adrb2	F	GACAGCGACTTCTTGCTGG
	R	CGTCCCGTTCCTGAGTGAC
Atp2a2	F	TCGACCAGTCAATTCTTACAGG
	R	CAGGGACAGGGTCAGTATGC
Ccl2	F	CCACTCACCTGCTGCTACTCAT
	R	TGGTGATCCTCTTGTAGCTCTCC
Ccl5	F	GCTGCTTTGCCTACCTCTCC
	R	TCGAGTGACAAACACGACTGC
Col1a2	F	ACGCGGACTCTGTTGCTGCT
	R	GCGGGACCCCTTTGTCCACG
Col3a1	F	CCCGGGTGCTCCTGGACAGA
	R	CACCCTGAGGACCAGGCGGA
Cpt1	F	GTGACTGGTGGGAGGAATAC
	R	GAGCATCTCCATGGCGTAG
Cpt2	F	CAGTGCACAGAAGCCTCTCTTG
	R	CTTCCCAATGCCGTTCTCAA
Crat	F	TGCTGCCAGAACCGTGGT
	R	TCCAGGGATTGCTGAAGTGG
Fasn	F	TTGCTGGCACTACAGAATGC
	R	AACAGCCTCAGAGCGACAAT
Hif1a	F	CCCATTCCTCATCCGTCAA
	R	CCGGCTCATAACCCATCAA
Hmox1	F	CAGGATTTGTCAGAGGCCCTGAAGG
	R	TGTGGTACAGGGAGGCCATCACC
Ifnb1	F	CTTCTCCGTCATCTCCATAGGG
	R	CACAGCCCTCTCCATCAACT
Ifny	F	CGGCACAGTCATTGAAAGCCTA
	R	GTTGCTGATGGCCTGATTGTC
Il1b	F	AAGAGCTTCAGGCAGGCAGTATCA
	R	TAATGGGAACGTCACACACCAGCA
Il6	F	ACAACCACGGCCTTCCCTACTT
	R	CACGATTTCCCAGAGAACATGTG
Il10	F	CGGCACAGTCATTGAAAGCCTA
	R	GTTGCTGATGGCCTGATTGTC

Gene of interest	Direction of primer	Sequence
Il12b	F	AGACATGGAGTCATAGGCTCTG
	R	CCATTTTCCTTCTTGTGGAGCA
Gapdh	F	CATGGCCTTCCGTGTTCCTA
	R	CCTGCTTCACCACCTTCTTGAT
Gclc	F	GTTATGGCTTTGAGTGCTGCAT
	R	ATCACTCCCCAGCGACAATC
Gsta2	F	CAGAGTCCGGAAGATTTGGA
	R	GAGGCTGCTGATTCTGCTCT
Ldha	F	GGCACTGACGCAGACAAG
	R	AGCTTGATCACCTCGTAGGC
Mmp2	F	GATAACCTGGATGCCGTCGTG
	R	CTTCACGCTCTTGAGACTTTGGTTC
Mmp9	F	GAAGGCAAACCCTGTGTGTT
	R	AGAGTACTGCTTGCCCAGGA
Myh7	F	ATGTGCCGGACCTTGGAAG
	R	CCTCGGGTTAGCTGAGAGATCA
Nppa	F	TCGTCTTGGCCTTTTGGCT
	R	TCCAGGTGGTCTAGCAGGTTCT
Nppb	F	AAGTCCTAGCCAGTCTCCAGA
	R	GAGCTGTCTCTGGGCCATTTC
Pdha1	F	TGTGACCTTCATCGGCTAGAA
	R	TGATCCGCCTTTAGCTCCATC
Pdk1	F	GGACTTCGGGTCAGTGAATGC
	R	TCCTGAGAAGATTGTCGGGGA
Pdk4	F	CCGCTTAGTGAACACTCCTTC
	R	TGACCAGCGTGTCTACAAACT
Ppargc1a	F	AATCAGACCTGACACAACGC
	R	GCATTCCTCAATTTCACCAA
Slc2a1	F	ATGGATCCCAGCAGCAAG
	R	CCAGTGTTATAGCCGAACTGC
Slc2a4	F	GACGGACACTCCATCTGTTG
	R	GCCACGATCGAGACATAGC
Sod2	F	GTGTCTGTGGGAGTCCAAGG
	R	AGCGGAATAAGGCCTGTTGT
Tgfb1	F	CTCCCGTGGCTTCTAGTGC
	R	GCCTTAGTTTGGACAGGATCTG
Tgfb2	F	TGGCTTCACCACAAACAGAG
	R	GTGCCATCAATACCTGCAAA
Timp1	F	GTAAGGCCTGTAGCTGTGCC
	R	GTCTCGTTGATTTCTGGGGA
Timp2	F	CACAGACTTCAGCGAATGGA
	R	CTTGGGAAGCTTGAGAGTGG
Timp3	F	CAGCCCTGTGATACTTGGGT
	R	CAAGCTTCCAGCCAAACTTC

Gene of interest	Direction of primer	Sequence
Timp4	F	ACCTCCGGAAGGAGTACGTT
	R	TTATCTGGCAGCAACACAGC
Tnfa	F	TCCCAGGTTCTCTTCAAGGGA
	R	GGTGAGGAGCACGTAGTCGG
Txnrd1	F	GGTCCTATGACTTCGACCTG
	R	AGTCGGTGTGACAAAATCCAAG

Table 2.3 List of solutions used for protein extraction and Western blotting.

Buffer	Ingredients
Lysis buffer (100 ml)	5 ml 1 M Tris-Cl (pH 7.4), 15 ml 1 M NaCl, 200 µl 0.5 M EDTA, 1 ml 0.1 M EGTA, 500 µl 0.5 M Na-orthovanadate, 500 µl 0.5 M Na-pyrophosphate, 500 µl 0.2 M β-glycerophosphate
Sample Buffer (100 ml)	10 ml 0.1% bromophenol blue, 5 ml 1 M sodium phosphate buffer (pH 7.0), 50 ml glycerol, 2% SDS
SDS-PAGE buffer (1 L)	3 g Tris, 14.5 g glycine, 1 g powdered SDS
Transfer buffer (1 L)	2.9 g Tris, 14.5 g glycine, 200 ml methanol
TBS (1L)	2.42 g Tris, 8 g NaCl, pH to 7.4 using HCl
TBST (1 L)	TBS with 0.1% Tween
5% SDS-PAGE resolving gel (6 ml)	1 ml 30% acrylamide/bis, 1.5 ml 1.5 M Tris HCl (pH 8.8), 30 µl 20% SDS, 45 µl 10% ammonium persulphate, 15 µl TEMED
10% SDS-PAGE resolving gel (6 ml)	2 ml 30% acrylamide/bis, 1.5 ml 1.5 M Tris HCl (pH 8.8), 30 µl 20% SDS, 45 µl 10% ammonium persulphate, 15 µl TEMED
15% SDS-PAGE resolving gel (6 ml)	3 ml 30% acrylamide/bis, 1.5 ml 1.5 M Tris HCl (pH 8.8), 30 µl 20% SDS, 45 µl 10% ammonium persulphate, 15 µl TEMED
Stacking gel (6 ml)	0.9 ml 30% acrylamide/bis, 1.5 ml 0.5 M Tris HCl (pH 6.8), 30 µl 20% SDS, 45 µl 10% ammonium persulphate, 20 µl TEMED

Table 2.4 List of primary antibodies used in this study
These antibodies were used for immunohistochemical (IHC), immunofluorescence (IF) and western blotting (WB) experiments. Markers used for IHC include : CD3 = T-cell marker, CD45 = leukocyte marker, CD68 = macrophage marker, FSP1 (fibroblast specific protein 1)= fibroblast marker, Ly6G/C= neutrophil marker. Markers used for IF include : α-SMA (α-smooth muscle actin) = myofibroblast marker, Ki67 = proliferation marker. AMPK = adenosine monophosphate-activated protein kinase, Iκb = inhibitor of kappa b, PLN = phospholamban, SERCA2 = sarco(endo)plasmic reticulum calcium ATPase 2.

	Antibody	Dilution	Company and catalogue number
IHC	Rabbit anti-mouse CD3	1:100	Abcam, ab16669
	Rat anti-mouse CD45	1:100	R&D Systems, MAB114
	Rat anti-mouse CD68	1:100	AbD Serotec, MCA1957GA
	Rabbit anti-mouse FSP1	1:2000	Abcam, ab27957
	Rat anti-mouse Ly6G and Ly6C	1:50	BD Pharmigen, 550291
IF	Goat anti-mouse α-SMA	1:50	Abcam, ab21027
	Rabbit anti-mouse Ki67	1:500	Abcam, ab15580
WB	Mouse anti-mouse α-actinin	1:1000	Sigma, A5044
	Rabbit anti-mouse pAMPKα (Thr172)	1:1000	CST, 2535
	Rabbit anti-mouse AMPKα	1:1000	CST, 2532
	Rabbit anti-mouse Caspase-3	1:1000	CST, 9665
	Mouse anti-mouse Desmin	1:100	Dako, M0760
	Mouse anti-mouse pIκb	1:1000	CST, 9246
	Rabbit anti-mouse Iκb	1:1000	CST, 9242
	Mouse anti-mouse PLN	1:500	Thermo Scientific, MA3-922
	Goat anti-mouse pPLN	1:500	Santa Cruz, sc-12963
	Goat anti-mouse SERCA2	1:1000	Santa Cruz, sc-8094
	Mouse anti-mouse α-tubulin	1:5000	CST, 3873

Table 2.5 List of secondary antibodies used in this investigation.

	Antibody	Dilution	Company and catalogue number
IHC	Biotinylated goat anti-rabbit IgG	1:200	Vector Laboratories, PK-6101
	Mouse adsorbed biotinylated rabbit anti-rat IgG	3:200	Vector Laboratories, BA-4001
IF	Alexa Fluor® 568 donkey anti-goat, orange-red	10 µg/ml	Thermo Scientific, A-11057
	Alexa Fluor® 488 chicken anti-rabbit, green	10 µg/ml	Thermo Scientific, A-21441
WB	IR dye 700 goat anti-mouse	1:15000	LI-COR, 926-68020
	IR dye 800 goat anti-rabbit	1:15000	LI-COR, 926-32211
	IR dye 800 donkey anti-goat	1:15000	LI-COR, 926-32214
	IR dye 800 donkey anti-mouse	1:15000	LI-COR, 926-32212

3 Cardiac effects of TLR9 after chronic β-AR stimulation

3.1 Introduction

The pathogenesis and progression of HF is associated with increased levels of pro-inflammatory cytokines [19, 20], impaired β-AR signalling [22, 210] and increased levels of circulating catecholamines [18, 309]. However, the processes that initiate inflammatory responses within the heart remain undefined [20]. As mentioned, one investigation demonstrated that mtDNA binds to the immune sensor and inflammatory instigator, TLR9, within cardiomyocytes, inducing myocarditis and dilated cardiomyopathy [173]. Furthermore, the same study reported that TLR9KO mice, subjected to TAC, exhibited reduced cardiac dilatation, cardiac hypertrophy, fibrosis, inflammation and pulmonary congestion together with improved cardiac function compared to control mice. Together, these 2 findings propose a potential role of TLR9 in the pathogenesis of HF, although the intricate mechanisms by which TLR9-mediated inflammation provoke deterioration of the failing heart remains unanswered.

In both clinical HF cases and preclinical models, cardiomyocyte overload instigates various cellular responses, through the activation of several signalling pathways, including the clinically vital, neurohormonal β-AR signalling cascade. Currently, inhibition of this signalling pathway by β-blockers remains a prevalent treatment for HF, emphasising the influence of this pathway in the pathogenesis of HF. Thorough examination of this pathway has identified chronotropic and inotropic responses after β-AR stimulation and several studies have demonstrated that β-AR signalling possesses immunomodulatory effects alongside the reported anti-inflammatory properties of β-blockers [224, 225, 310]. These reports indicate a potential relationship between inflammation and the β-AR signalling cascade, which may contribute to the pathogenesis of HF. With

the accumulating evidence discussed above, advocating that TLR9 contributes to the advancement of HF, it was hypothesised that the immune sensor, TLR9, potentially interacts with the β-AR signalling cascade, leading to myocardial inflammation and DCM.

The aim of this study was to develop a murine model of HF, induced by Iso infusion, to explore the relationship between TLR9-mediated inflammation and the β-AR signalling pathway, in the pathogenesis of HF. Differences in the cardiac phenotype of WT and TLR9KO mice, subjected to this model would thereby inform on this association.

3.2 Results

3.2.1 Conception of an Iso infusion model

Infusion of the β-stimulant Iso has frequently been used as a model of cardiac hypertrophy and cardiac dysfunction [299, 306, 311]. With its reported capability to induce myocardial inflammation [224], Iso was considered an appropriate model for investigating the association between the β-AR signalling cascade and TLR9-mediated inflammation. Various doses of Iso between 5-30 mg/kg/day for 1 day up to 2 weeks [312, 313, 314] have been utilised as models of hypertrophy. However, previous data from my laboratory group demonstrated that in WT mice ($Capns1^{+/+}$), 50 mg/kg/day Iso for 2 weeks increased posterior wall thickness whilst maintaining cardiac function (**figure 3.1**), suggesting that these WT mice were in the compensated phase of cardiac hypertrophy which had not yet progressed to HF [306]. Other doses of Iso was used by my laboratory prior to this study to determine the optimal Iso dose to induce hypertrophy (data not shown) and 50 mg/kg/day Iso for 2 weeks was found to be the most suitable.

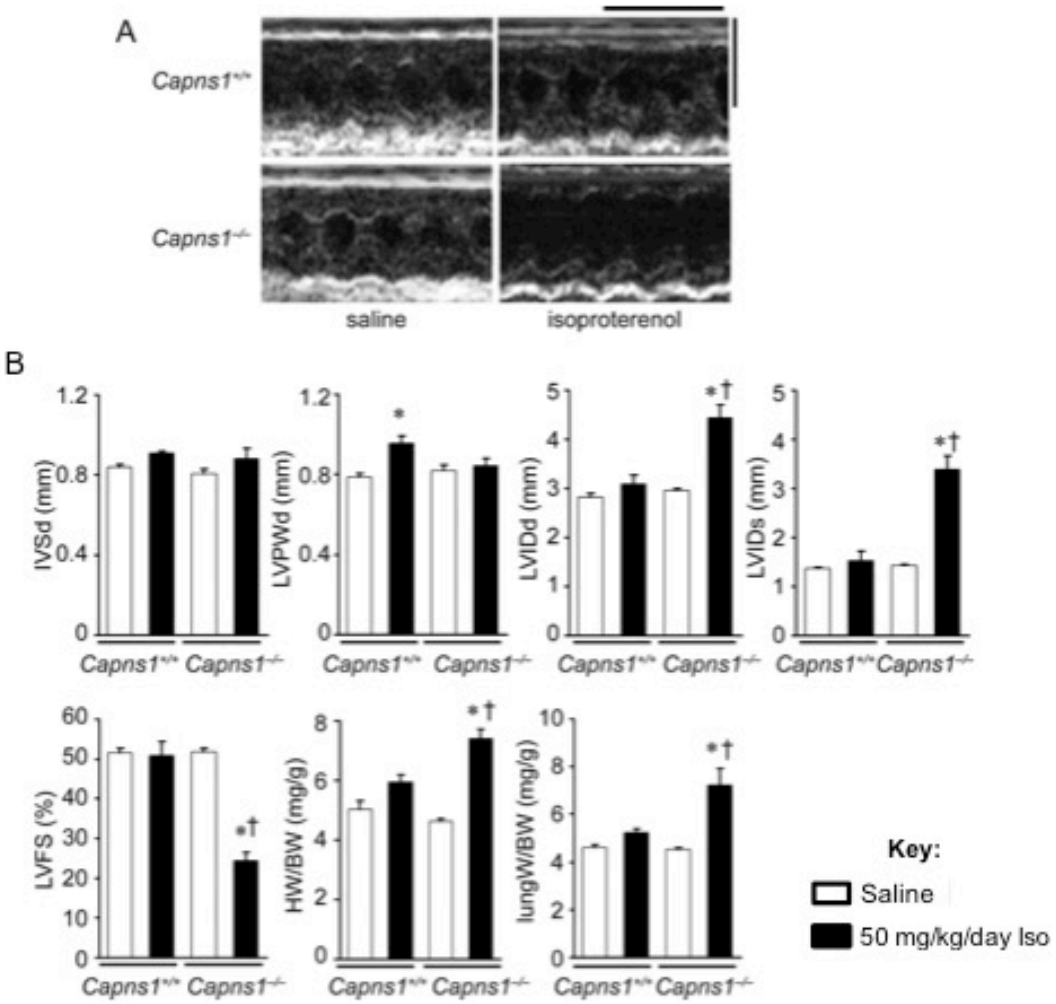

Figure 3.1 Mild cardiac hypertrophy observed in WT (Capsn1$^{+/+}$) mice after 2 weeks infusion of 50 mg/kg/day Iso.
Data taken from Taneike *et al* (2011) [306]. A, Transthoracic M-mode echocardiography after 2 weeks infusion of Iso in calpain small 1 (*Capsn1*) genetically modified mice. Scale bars = 0.2 s and 5 mm, respectively. B, Echocardiographic and physiological parameters show increased end-diastolic posterior wall thickness (LVPWd) in *Capsn1*$^{+/+}$ (WT) mice, though no changes were observed in left ventricular fractional shortening (LVFS) or heart weight / body weight (HW/BW) ratio. This indicates the initiation of the early stages of pathological hypertrophy in these WT (*Capsn1*$^{+/+}$) mice after 2 weeks infusion of 50 mg/kg/day Iso. Values expressed as mean ± S.E.M (*n* = 4 per group); Saline (open bars), Iso (closed bars). **p*<0.05 versus the corresponding saline-treated group; †, *p*<0.05 versus Iso-treated *Capns1*$^{+/+}$ mice. IVSd = End-diastolic interventricular septal wall thickness; LVPWd = LV posterior wall thickness; LVIDd = End-diastolic LV internal dimension; LVIDs = End-systolic LV internal dimension; LVFS = LV fractional shortening.

As cardiac hypertrophy typically progresses to HF [80], it was anticipated that a higher and prolonged dose of Iso, compared to this previous study using 50 mg/kg/day Iso for 2 weeks conducted by my laboratory group (**figure 3.1**),

would result in HF. Therefore, taking these previous findings from my laboratory into account, 10 - 11 week-old C57Bl/6 male mice were implanted with osmotic minipumps infusing 75 mg/kg/day Iso, 50 mg/kg/day Iso or saline (as control) for 4 weeks to determine a suitable dose and duration of Iso infusion to induce HF (**figure 3.2**). For this series of experiments, cardiac morphology and function was assessed by echocardiography 2 and 4 weeks after minipump implantation. Mice were sacrificed 4 weeks after minipump implantation, to obtain physiological measurements.

Figure 3.2 Timeline of *in vivo* procedures for the pilot study.
To determine a suitable timecourse and concentration of Iso infusion for a model of heart failure, 10 – 11-week old WT male mice were implanted with minipumps infusing 75 mg/kg/day Iso, 50 mg/kg/day Iso or saline. Mice were subjected to echocardiography (echo) 2 and 4 weeks post-implantation. The mice were sacrificed on day 29.

3.2.1.1 4 weeks treatment of 50 and 75 mg/kg/day Iso induced cardiac dilatation and dysfunction.

Study of cardiac structure and function *in vivo* was facilitated by M-mode echocardiography, which was performed on conscious mice using the LV short axis view (refer to **section 2.1.3.1**). Minor changes in echocardiographic parameters were observed 2 weeks after Iso infusion at both doses compared to saline-infused mice (**figure 3.3**). Nonetheless, 4 weeks after Iso infusion, end-diastolic and end-systolic measurements of the LV chamber (LVIDd and LVIDs) were increased, compared with saline treatment, indicative of LV cardiac

chamber dilatation (**figure 3.3c**). No significant changes were observed in end-diastolic and end-systolic septal or posterior wall thickness (IVSd, IVSs, LVPWd and LVPWs) after 4 weeks of Iso infusion (**figure 3.3a-b**). Cardiac function, depicted by EF* and fractional shortening (FS)†, deteriorated 4 weeks after Iso infusion (**figure 3.3d**) compared with mice treated with saline. In addition, LV mass was increased after 4 weeks of Iso treatment compared to saline-treated mice (**figure 3.3f**). Most surprisingly, the heart rate (HR) remained unchanged at both doses of Iso compared to saline-infused mice, at all timepoints (**figure 3.3e**).

No differences in echocardiographic parameters were noted between mice treated with 50 mg/kg/day Iso and those administered with 75 mg/kg/day Iso, after 4 weeks of minipump infusion (**figure 3.3**), suggesting both doses of Iso induce chamber dilatation and cardiac dysfunction to a similar extent.

3.2.1.2 50 mg/kg/day Iso increased heart weight and lung weight.

After 4 weeks of infusion of 75 mg/kg day Iso, 50 mg/kg/day Iso or saline, the mice were sacrificed and the heart, lung and liver tissues were harvested and weighed and the tibia lengths were recorded in order to determine any physiological variations induced by Iso treatment. Mice infused with 50 mg/kg/day Iso gained body weight compared with saline-treated mice (**figure 3.4a**), though there were no significant differences in the tibia lengths between all groups (**figure 3.4b**). Therefore, all parameters were standardised to tibia length to account for the size of the mouse.

---

* Compared to saline-treated mice, EF decreased by 25.47% and 26.65% in mice treated with 50 mg/kg/day Iso and 75 mg/kg/day Iso, respectively.

† FS decreased by 20.50% and 21.94 % in mice treated with 50 mg/kg/day Iso and 75 mg/kg/day Iso, compared to saline-treated mice.

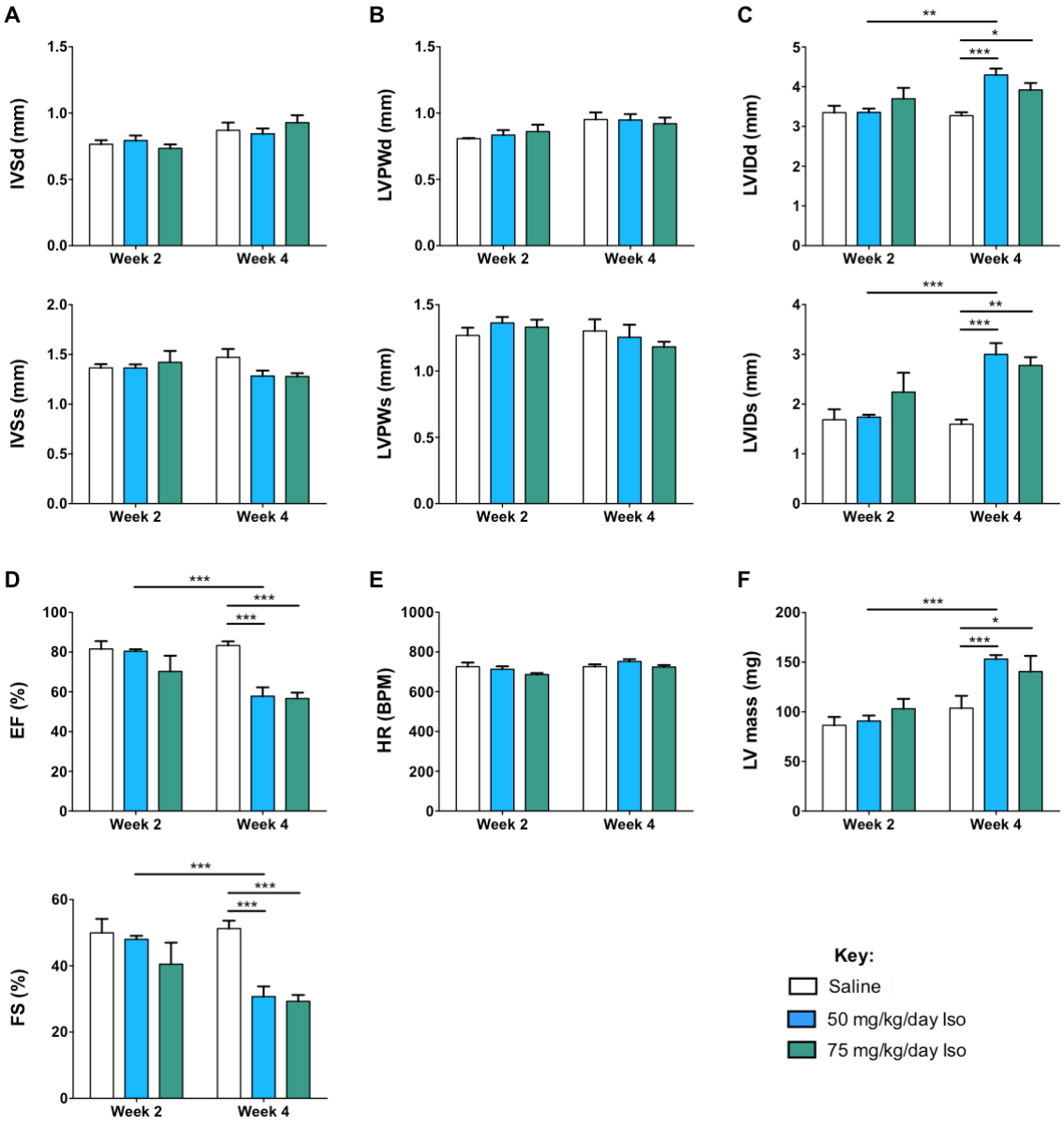

Figure 3.3 4 weeks infusion of Iso induced dilated cardiomyopathy.
Echocardiographic measurements of conscious WT mice 2 and 4 weeks after implantation with minipumps infusing 75 mg/kg/day Iso (green), 50 mg/kg/day Iso (blue) or saline (white). A, IVSd = End-diastolic interventricular septal wall thickness, IVSs = End-systolic interventricular septal wall thickness. B, LVPWd = End-diastolic left ventricular posterior wall thickness, LVPWs = End-systolic left ventricular posterior wall thickness. C, LVIDd = End-diastolic left ventricle internal dimension, LVIDs = End-systolic left ventricle internal dimension. D, EF = Ejection fraction, FS = Fractional shortening. E, HR = Heart rate. F = LV mass. No changes in echocardiographic parameters were observed after 2 weeks infusion, however after 4 weeks infusion, Iso induced chamber dilatation and cardiac dysfunction. Saline *n*= 4; 50 mg/kg/day Iso *n*= 7; 75 mg/kg/day Iso, *n*= 4. Data were analysed by two-way ANOVA with bonferroni's post-hoc test. **p*<0.05, ***p*<0.01, ****p*<0.001.

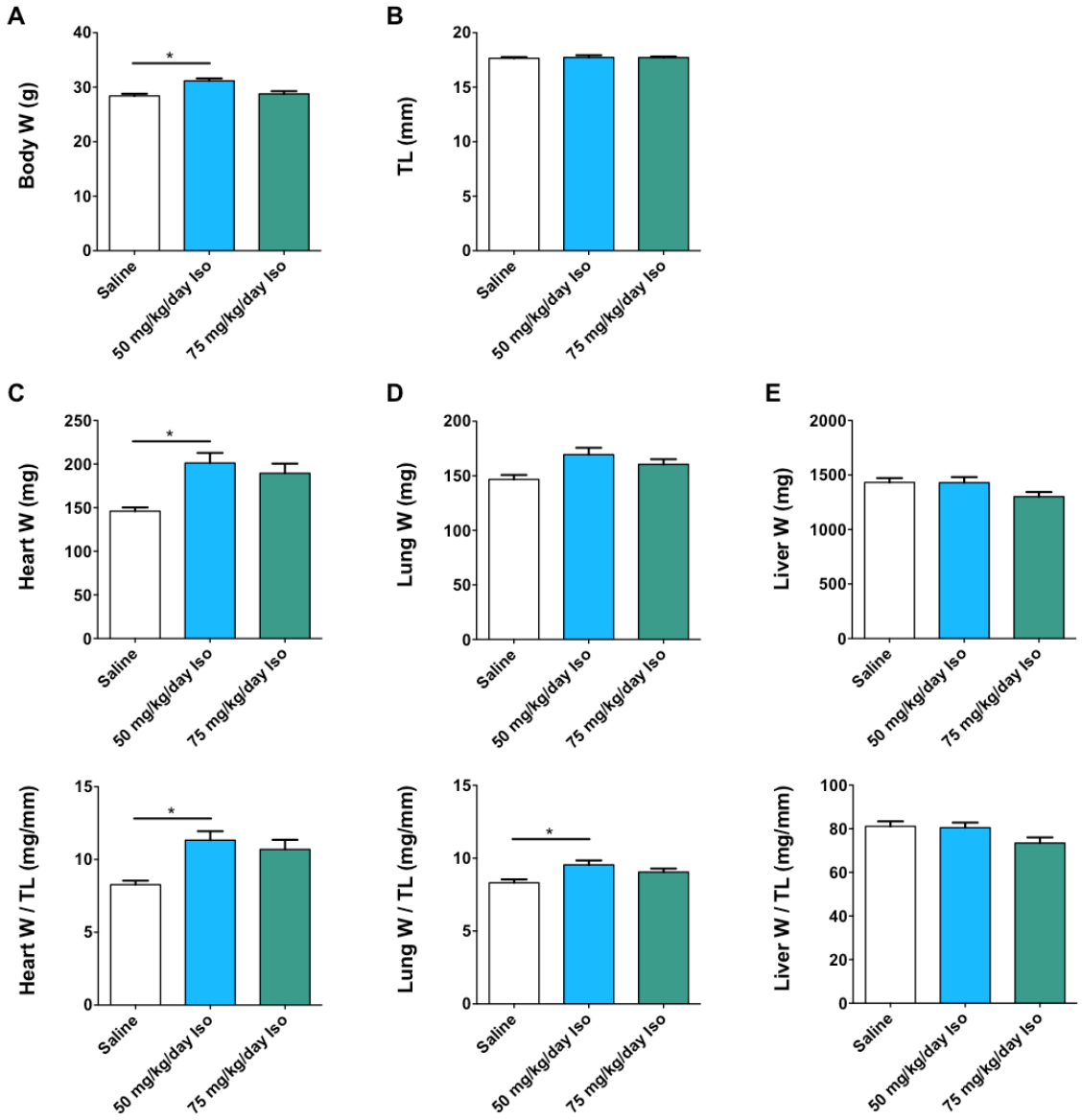

Figure 3.4 Physiological analysis revealed that 50 mg/kg/day Iso increased heart weight and lung weight.
Mice fitted with minipumps infusing 75 mg/kg/day Iso, 50 mg/kg/day Iso or saline were harvested 29 days after implantation and physiological parameters were examined. A, Body weight. B, Tibia length (TL). C, Heart weight and heart weight / TL. D, Lung weight and lung weight / TL. E, Liver weight and liver weight / TL. Mice treated with 50 mg/kg day Iso increased body weight, heart weight / TL and lung weight / TL compared to saline-treated mice, whereas no difference was seen with mice infused with 75 mg/kg day Iso. Saline (white), *n*= 4; 50 mg/kg/day Iso (blue) *n*= 7; 75 mg/kg/day Iso (green) *n*= 4. Data were analysed by one-way ANOVA with bonferroni's post-hoc test. *p<0.05. W = Weight.

Increased heart weight and increased heart weight / tibia length was noted in the mice infused with 50 mg/kg/day Iso compared to saline, implying induction of cardiac hypertrophy in these mice (**figure 3.4c**). Lung weight / tibia length was significantly increased in mice treated with 50 mg/kg/day Iso mice compared to saline-treated mice (**figure 3.4d**), indicating pulmonary congestion, a common feature of left-sided HF. No differences in liver weight or liver weight / tibia length were observed after 4 weeks of Iso infusion, compared to saline-treated mice (**figure 3.4e**). No significant alterations were detected in the physiological parameters, between mice treated for 4 weeks with saline and 75 mg/kg day Iso or between mice infused with 75 mg/kg day Iso and 50 mg/kg/day Iso for 4 weeks (**figure 3.4)**.

3.2.1.3 Summary of pilot study.

The aim of the pilot study was to determine a suitable dose and timecourse of Iso that could be employed as a model of HF for further investigations. From preceding studies, it was anticipated that 4 weeks infusion of Iso would lead to tachycardia, cardiac hypertrophy, chamber dilatation, body weight gain, pulmonary congestion alongside excessive cardiac dysfunction as previously reported [80, 295, 313, 315, 316, 317, 318].

In the pilot study, the echocardiographic data displayed no significant changes in the cardiac morphology and function after 2 weeks infusion of Iso at both doses compared to saline-infused mice. Whilst, 4 weeks treatment of Iso at both doses was sufficient to induce LV chamber dilatation, cardiac dysfunction and increased LV mass compared to saline controls, the wall thicknesses and HR after 4 weeks of Iso treatment was unexpectedly comparable to saline treated-mice (**table 3.1, see section 3.3.1 for further discussion**).

Table 3.1 Summary table of pilot study.
Table to show differences in echocardiographic and physiological parameters between 2 different doses of Iso, 50 and 75 mg/kg/day detailed in **figures 3.3** and **3.4**. 50 mg/kg/day Iso-infused mice induced more physiological changes over 4 weeks than mice treated with 75 mg/kg/day Iso. ✓ = significant difference compared to saline-treated mice, X = no difference compared to saline-infused mice. PI = pump implantation, LVIDd = End-diastolic left ventricle internal dimension, LVIDs = End-systolic left ventricle internal dimension, EF = Ejection fraction, FS = Fractional shortening, IVSd = End-diastolic interventricular septal wall thickness, LVPWd = End-diastolic left ventricular posterior wall thickness, W = Weight, TL = Tibia length.

Phenotype	50 mg/kg/day Iso	75 mg/kg/day Iso
Chamber dilatation		
Increased LVIDd and LVIDs	✓ 4 weeks after PI	✓ 4 weeks after PI
Cardiac dysfunction		
Decreased EF and FS	✓ 4 weeks after PI	✓ 4 weeks after PI
Cardiac hypertrophy		
Increased IVSd and LVPWd	X	X
Increased LV mass	✓ 4 weeks after PI	✓ 4 weeks after PI
Increased Heart W:TL	✓ 4 weeks harvest	X
Body weight		
Increased Body W	✓ 4 weeks harvest	X
Pulmonary congestion		
Increased Lung W:TL	✓ 4 weeks harvest	X

Increased body weight, increased heart weight and pulmonary congestion were indicated by the physiological data obtained from mice infused for 4 weeks with 50 mg/kg/day Iso compared with saline (**table 3.1**). However, no significant difference was observed in the physiological parameters between mice infused with 75 mg/kg day Iso and mice treated with saline. These surprising findings suggest that 50 mg/kg/day Iso induced more significant physiological alterations than 75 mg/kg/day Iso infusion, although there were no significant differences between mice infused with 50 mg/kg/day Iso or 75 mg/kg/day Iso in all echocardiographic and physiological parameters (**table 3.1).** As it was hypothesised that a higher dose of Iso infusion would result in a stronger

dysfunctional phenotype, this finding is highly unexpected and is discussed further in **section 3.3.1.**

Also the measurements of cardiac hypertrophy remain inconclusive as no changes to wall thickness was observed by echocardiography, although increased heart weight was noted. Further molecular analyses are required to determine the induction of cardiac hypertrophy. Although pulmonary congestion was observed after Iso infusion, the extent of cardiac dysfunction after Iso infusion within this model was not severe enough to induce HF [11, 23, 319, 320], suggesting that this model is representative of mild cardiac dysfunction with pulmonary congestion.

Collectively, the pilot study found that 50 mg/kg/day Iso for 4 weeks induced more physiological changes than 75 mg/kg/day Iso. Although severe cardiac dysfunction and HF was not observed in this model, 50 mg/kg/day Iso (referred to as Iso) for 4 weeks was chosen to evaluate the association between TLR9 and β-AR-signalling as it may provide an insight on the impact of excessive and chronic β-AR signalling that may contribute to the progression to HF. Therefore, the condition induced by Iso (chamber dilatation, cardiac dysfunction, increased heart weight, weight gain and pulmonary congestion) was referred to as β–stimulant-induced cardiomyopathy.

A limitation of the pilot study was the lack of echocardiographic data preceding minipump implantation. Therefore pre-implantation echocardiography was performed in all future experiments to verify no differences between mice prior to surgery. Furthermore, as the HR was unchanged between saline- and Iso-infused hearts, BP was assessed to monitor the physiological effects of Iso in the following experiments.

3.2.2 Investigation of the affiliation between TLR9-mediated inflammation and β-AR signalling.

To explore the potential relationship between TLR9-medaited inflammation and the β−AR signalling pathway, the experimental model of β–stimulant-induced cardiomyopathy devised in the pilot study was implemented to global TLR9KO mice, kindly provided by Professor Shizuo Akira (Osaka University, Japan) [177].

3.2.2.1 Genotyping of WT and TLR9KO mice.

As mentioned in **section 2.1.1** TLR9KO mice were previously backcrossed with C57Bl/6 mice, warranting the use of C57BL/6 mice as WT controls. The breeding strategy intercrossed homozygous knockout (TLR9KO) mice with TLR9KO mice to yield only TLR9KO mice (**figure 3.5**).

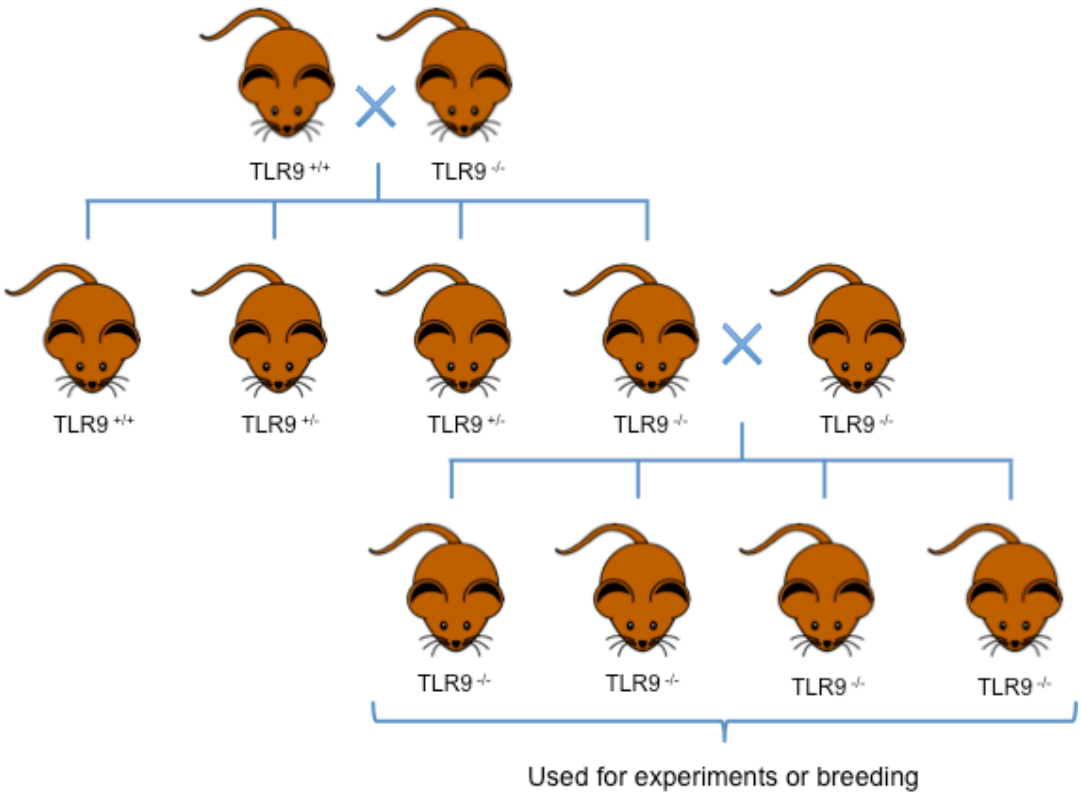

Figure 3.5 Breeding strategy for TLR9KO mice.
TLR9KO mice that were backcrossed with C57Bl/6 mice were kindly donated by Professor Shizuo Akira (Osaka University, Japan). Due to demand for TLR9KO ($TLR9^{-/-}$) mice, TLR9KO were bred with TLR9KO to produce only TLR9KO mice. These mice were used for experiments in this chapter and chapter 5.

To confirm the genotype of the WT and TLR9KO mice utilised in these experiments, DNA was extracted from ear biopsies of the mice and submitted for PCR with 2 separate primer combinations. The first primer assortment (WT) recognised the WT DNA sequence whilst the other primer set (TLR9KO) targeted the neomycin cassette within TLR9KO mice (**table 2.1**). The genotyping results of WT and TLR9KO mice utilised in this series of experiments are displayed in **figure 3.6**.

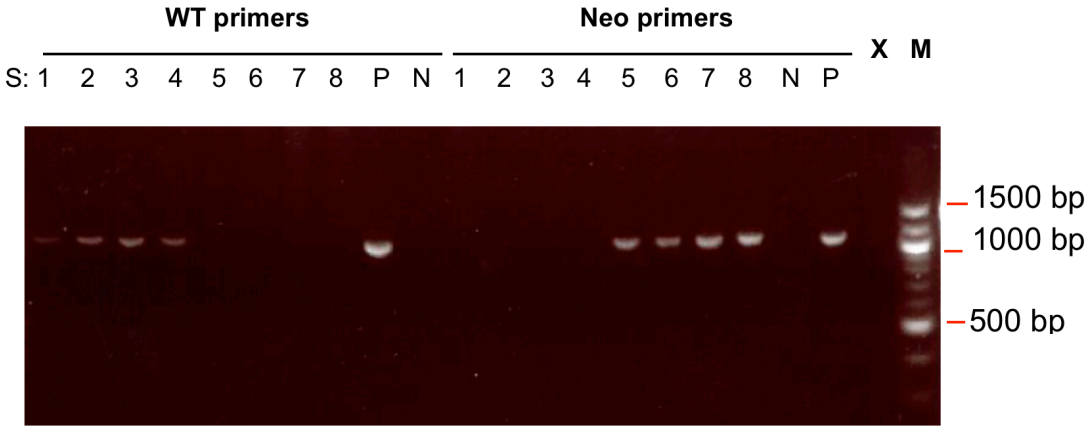

Figure 3.6 Genotyping results of WT (C57Bl/6) and TLR9KO mice.
PCR was performed using WT primers or TLR9KO primers (**table 2.1**) on DNA extracted from ear biopsies from WT and TLR9KO mice. Samples were loaded onto a 1.5% agarose gel. WT primers amplified a 1.2 kbp region from WT DNA, which was not amplified using DNA from TLR9KO mice. Conversely, the TLR9KO primers targeted a 1.2 kbp region in the genome of TLR9KO mice, whereas no amplification was seen using WT DNA. If mice were heterozygous, then both WT and TLR9KO primer sets would amplify the DNA. Therefore, samples (S) 1 - 4 have a 1.2 kbp band using WT primers and no band using the Neo primers indicating that these mice are WT. Samples 5 - 8 display a 1.2 kbp band amplified with the TLR9KO primers, but no band using the WT primers indicating that these are TLR9KO mice. M= marker (100 bp ladder), X= empty well, P = positive control, N = negative control

3.2.2.2 WT and TLR9KO mice displayed no differences in echocardiographic and physiological parameters at baseline.

To compare the cardiac structure and function between WT and TLR9KO mice at baseline, 10 - 11 week-old male mice were subjected to anaesthetised echocardiography using 1.5% isoflurane. The following day, mice were

harvested for physiological analyses. No significant differences in cardiac structure and function relayed by the echocardiographic data or physiological measurements were observed between WT and TLR9KO mice at baseline (**table 3.2 and 3.3**).

Table 3.2 No differences in echocardiographic parameters at baseline between WT and TLR9KO mice.
Anaesthetised echocardiography was performed on 10-week-old WT and TLR9KO mice to assess cardiac morphology and performance. No differences were observed in all echocardiographic parameters at baseline. Data were analysed by t-test. IVSd = End-diastolic interventricular septal wall thickness, LVPWd = End-diastolic left ventricular posterior wall thickness, LVIDd = End-diastolic left ventricle internal dimension, IVSs = End-systolic interventricular septal wall thickness, LVPWs = End-systolic left ventricular posterior wall thickness, LVIDs = End-systolic left ventricle internal dimension, EF = Ejection fraction, FS = Fractional shortening, HR = Heart rate. Sig. = significance, n.s = no significance.

Echocardiographic parameters	WT (*n*= 6)	TLR9KO (*n*= 6)	*P* value	Sig.
IVSd (mm)	0.70 ± 0.01	0.70 ± 0.01	0.99	n.s
IVSs (mm)	1.00 ± 0.02	1.03 ± 0.02	0.20	n.s
LVIDd (mm)	3.90 ± 0.02	3.85 ± 0.03	0.26	n.s
LVIDs (mm)	2.69 ± 0.02	2.64 ± 0.03	0.25	n.s
LVPWd (mm)	0.82 ± 0.02	0.81 ± 0.03	0.91	n.s
LVPWs (mm)	1.08 ± 0.04	1.02 ± 0.01	0.19	n.s
EF (%)	59.49 ± 0.54	60.03 ± 0.57	0.50	n.s
FS (%)	31.10 ± 0.37	31.45 ± 0.38	0.53	n.s
HR (BPM)	447.83 ± 9.80	464.00 ± 22.42	0.52	n.s
LV mass (mg)	104.85 ± 3.17	102.17 ± 3.26	0.57	n.s

Table 3.3 Physiological parameters were similar between WT and TLR9KO mice at baseline.
Physiological parameters were measured from 10-week-old WT and TLR9KO mice, demonstrating no differences between the 2 groups of mice at baseline. Data were analysed by student t-test. BP = blood pressure, Sig. = significance, n.s = no significance.

Physiological parameters	WT (*n*= 6)	TLR9KO (*n*= 6)	*P* value	Sig.
Body weight (g)	25.75 ± 0.42	26.00 ± 0.39	0.67	n.s
Systolic BP (mmHg)	95.01 ± 3.49	96.94 ± 3.86	0.72	n.s
Diastolic BP (mmHg)	68.14 ± 3.02	69.50 ± 3.02	0.76	n.s
Heart weight (mg)	142.88 ± 4.29	141.12 ± 4.98	0.79	n.s
Lung weight (mg)	146.07 ± 2.92	152.67 ± 4.78	0.27	n.s
Liver weight (mg)	1231.62 ± 22.25	1339.17 ± 76.25	0.21	n.s
Tibia length (mm)	17.57 ± 0.22	17.76 ± 0.12	0.46	n.s
Heart weight / Body weight ratio (mg/g)	5.67 ± 0.19	5.31 ± 0.19	0.21	n.s
Heart weight / Tibia length ratio (mg/mm)	8.15 ± 0.33	7.95 ± 0.28	0.65	n.s
Lung weight / Body weight ratio (mg/g)	5.80 ± 0.16	5.62 ± 0.08	0.33	n.s
Lung weight / Tibia length ratio (mg/mm)	8.32 ± 0.17	8.59 ± 0.24	0.37	n.s
Liver weight / Body weight ratio (mg/g)	48.94 ± 1.50	49.54 ± 3.24	0.87	n.s
Liver weight / Tibia length ratio (mg/mm)	70.17 ± 1.54	75.43 ± 4.27	0.27	n.s

3.2.2.3 Cardiac function was modestly salvaged in TLR9KO mice after Iso infusion.

Prior to minipump implantation, echocardiography and BP measurements were performed on WT and TLR9KO mice (**figure 3.7**), followed by implantation of minipumps to infuse either 50 mg/kg/day Iso or saline. Echocardiography was performed under anaesthesia using 1.5% isoflurane whilst BP measurements were performed on conscious mice. 4 weeks after implantation, mice were subjected to echocardiography and BP measurements and harvested for further analyses.

Figure 3.7 Timeline of *in vivo* procedures.
10-11-week-old WT and TLR9KO male mice (24 - 27 g) were subjected to echocardiography (echo) and blood pressure (BP) measurements pre-implantation. The mice were fitted with minipumps infusing 50 mg/kg/day Iso or saline. 4 weeks later, echo and BP measurements were performed and the mice were sacrificed the day after.

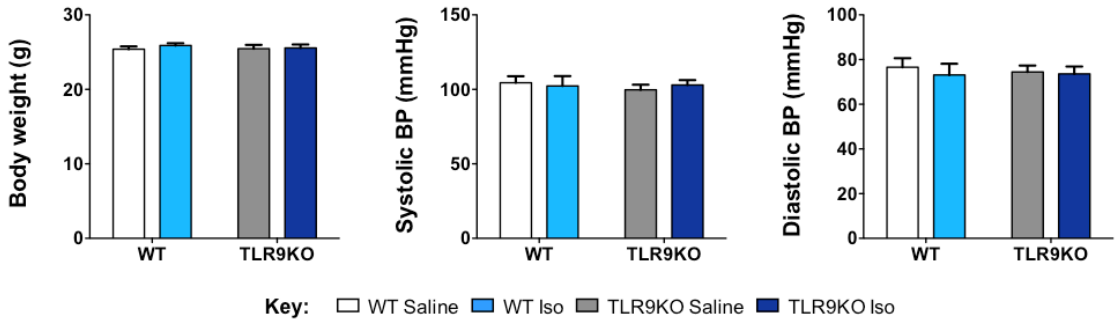

Figure 3.8 No differences in physiological parameters pre-implantation between WT and TLR9KO mice.
The body weight and blood pressure (BP) measurements showed no difference prior to implantation. WT saline (white), WT Iso (light blue), TLR9KO saline (grey), TLR9KO Iso (dark blue); *n*= 8 for all groups. Data were analysed by two-way ANOVA with bonferroni's post-hoc test.

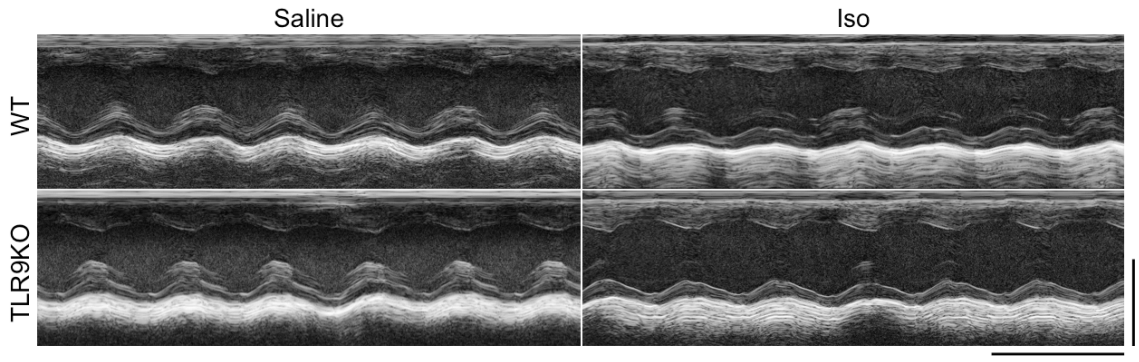

Figure 3.9 Transthoracic M-mode echocardiography pre-implantation showed no differences in cardiac morphology between WT and TLR9KO mice.
Transthoracic M-mode echocardiography pre-implantation displayed no difference in cardiac morphology and function between WT and TLR9KO mice. *n*= 8 for all groups. Scale bars = 0.2 s and 5 mm respectively.

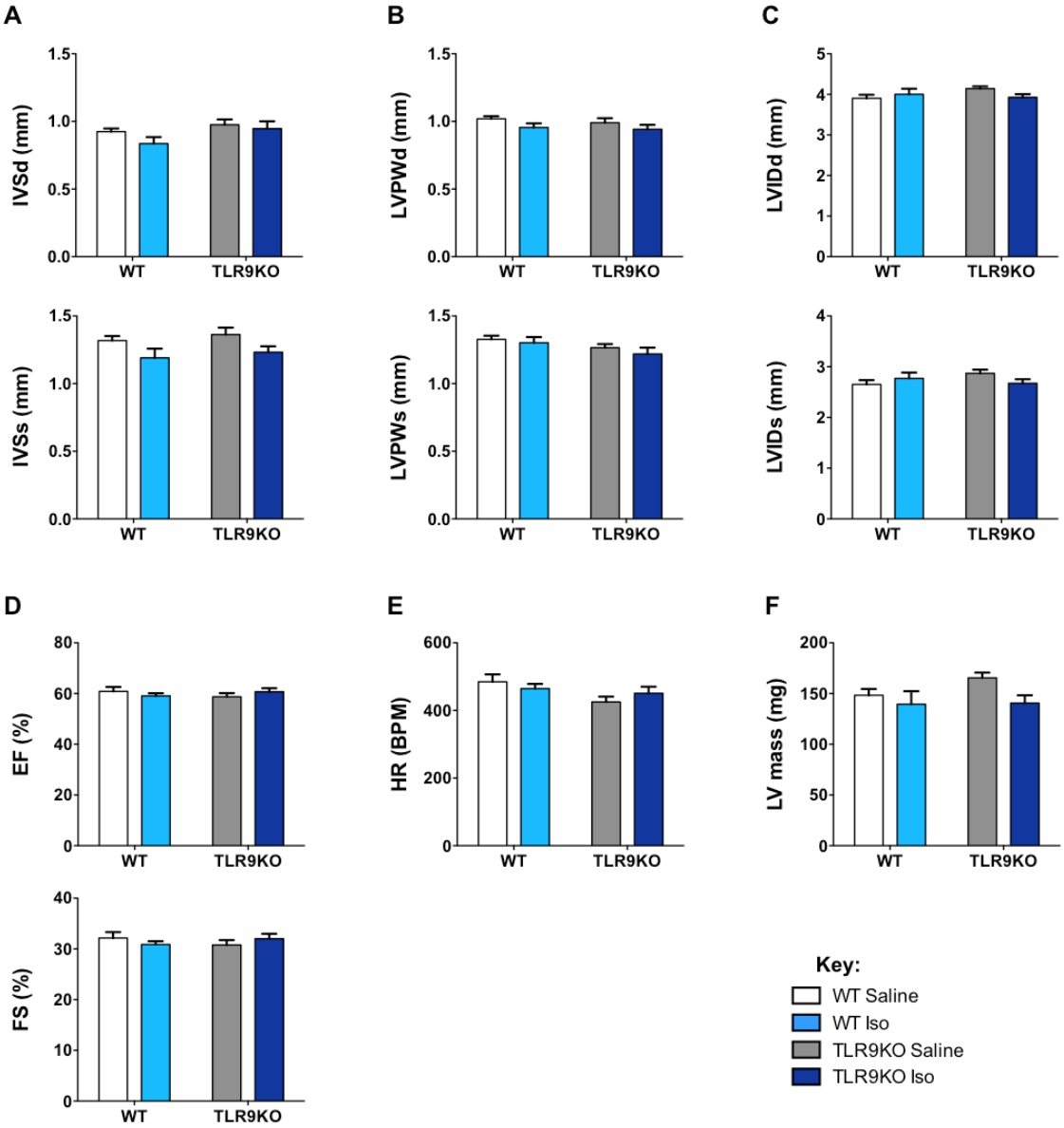

Figure 3.10 No difference in echocardiographic parameters pre-implantation.
Anaesthetised echocardiography was performed on WT and TLR9KO prior to minipump implantation. A, IVSd = End-diastolic interventricular septal wall thickness, IVSs = End-systolic interventricular septal wall thickness. B, LVPWd = End-diastolic left ventricular posterior wall thickness, LVPWs = End-systolic left ventricular posterior wall thickness. C, LVIDd = End-diastolic left ventricle internal dimension, LVIDs = End-systolic left ventricle internal dimension. D, EF = Ejection fraction, FS = Fractional shortening. E, HR = Heart rate. F = LV mass. No differences were observed in cardiac structural and functional parameters. WT saline (white), WT Iso (light blue), TLR9KO saline (grey), TLR9KO Iso (dark blue); *n*= 8 for all groups. Data were analysed by two-way ANOVA with bonferroni's post-hoc test.

As expected, there were no differences in echocardiographic, body weight or BP parameters pre-implantation between WT and TLR9KO mice (**figures 3.8, 3.9 and 3.10**). Moreover, 4 weeks after minipump implantation, systolic BP, diastolic BP and body weight were significantly increased in WT mice after Iso infusion, compared to saline-treated mice (**figure 3.11**), indicating hypertension and weight gain. Additionally, these changes were also observed in TLR9KO mice with the same treatment, though there were no differences in these parameters between Iso-infused WT and TLR9KO mice. Tachycardia with an elevated HR of approximately 190 bpm was observed in Iso-infused WT mice compared to saline-treated mice, which was additionally observed in TLR9KO mice after Iso infusion (**figure 3.12 and 3.13e**). There was also a significant increase in the LVPWd in WT mice after Iso infusion, compared to saline treated mice, but no difference between saline- and Iso- treated TLR9KO mice (**figure 3.13b**). Considering that echocardiographic parameters are HR dependent alongside elevation of the HR by 44% in both WT and TLR9KO Iso-infused mice, compared to saline-treated mice, it was technically challenging to compare and interpret the data between saline- and Iso- infused mice.

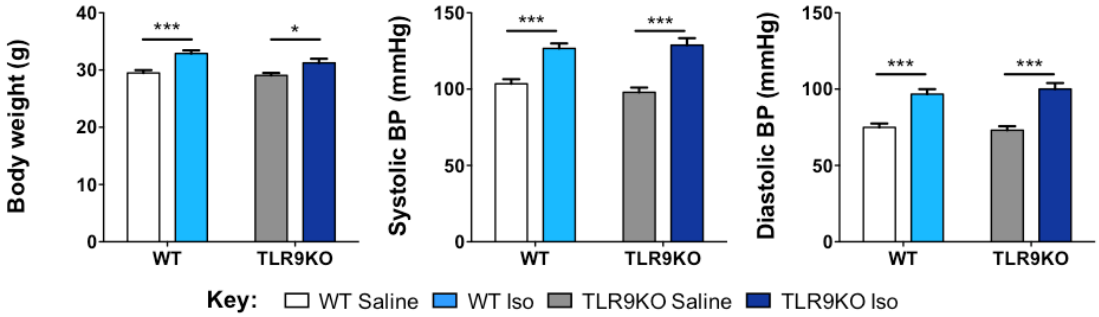

Figure 3.11 Iso induced physiological changes after 4 weeks infusion in WT and TLR9KO mice.
After 4 weeks infusion of Iso, the body weight and BP were increased in WT and TLR9KO mice. WT saline (white), WT Iso (light blue), TLR9KO saline (grey), TLR9KO Iso (dark blue); *n*= 8 for all groups. Data were analysed by two-way ANOVA with bonferroni's post-hoc test. **p*<0.05, ****p*<0.001.

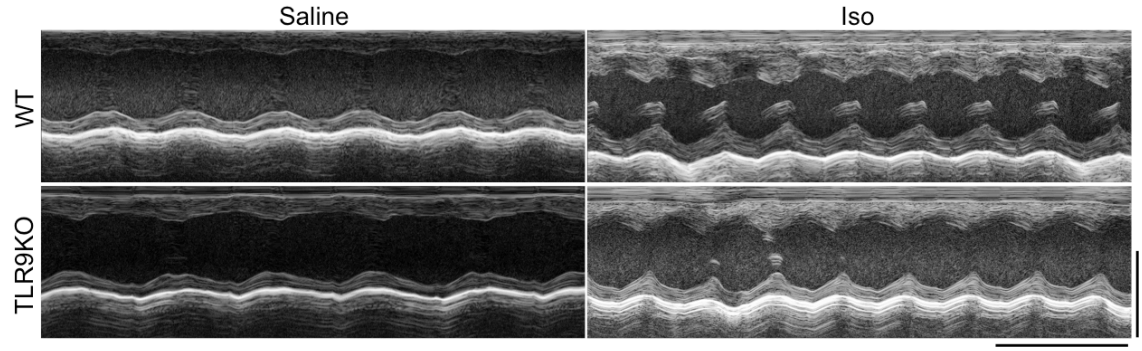

Figure 3.12 Transthoracic M-mode echocardiography indicated tachycardia in mice subjected to Iso treatment.
Transthoracic M-mode echocardiography after 4 weeks infusion of Iso in WT and TLR9KO mice revealed increased heart rate in mice treated with Iso. Scale bars = 0.2 s and 5 mm respectively. *n*= 8 for all groups.

Therefore, echocardiography was also performed using different percentages of isoflurane (ISF) to achieve heart rates within a range of 450 – 550 BPM (**figure 3.14**). Using this method, Iso infusion in WT mice increased LVPWd, LVIDd, LVIDs and LV mass and reduced EF and FS, compared to saline-treated mice which suggested induction of cardiac hypertrophy, chamber dilatation and cardiac dysfunction after Iso infusion in WT mice (**figure 3.15**). Whilst Iso infusion in TLR9KO mice exhibited chamber dilatation (**figure 3.15c**), comparable to WT mice after Iso infusion, LVPWd or LV mass were not increased compared to saline-treated TLR9KO mice (**figure 3.15b, f**). Additionally, the cardiac function was modestly improved in the Iso-infused TLR9KO mice compared with WT mice infused with Iso (**figure 3.15d**). These exciting findings insinuate that Iso-induced cardiac dysfunction and thickened walls were partially blunted in TLR9KO mice, compared to WT mice suggesting that TLR9 may influence cardiac function and potentially cardiac hypertrophy (though further investigation is required) through interactions with the β-AR.

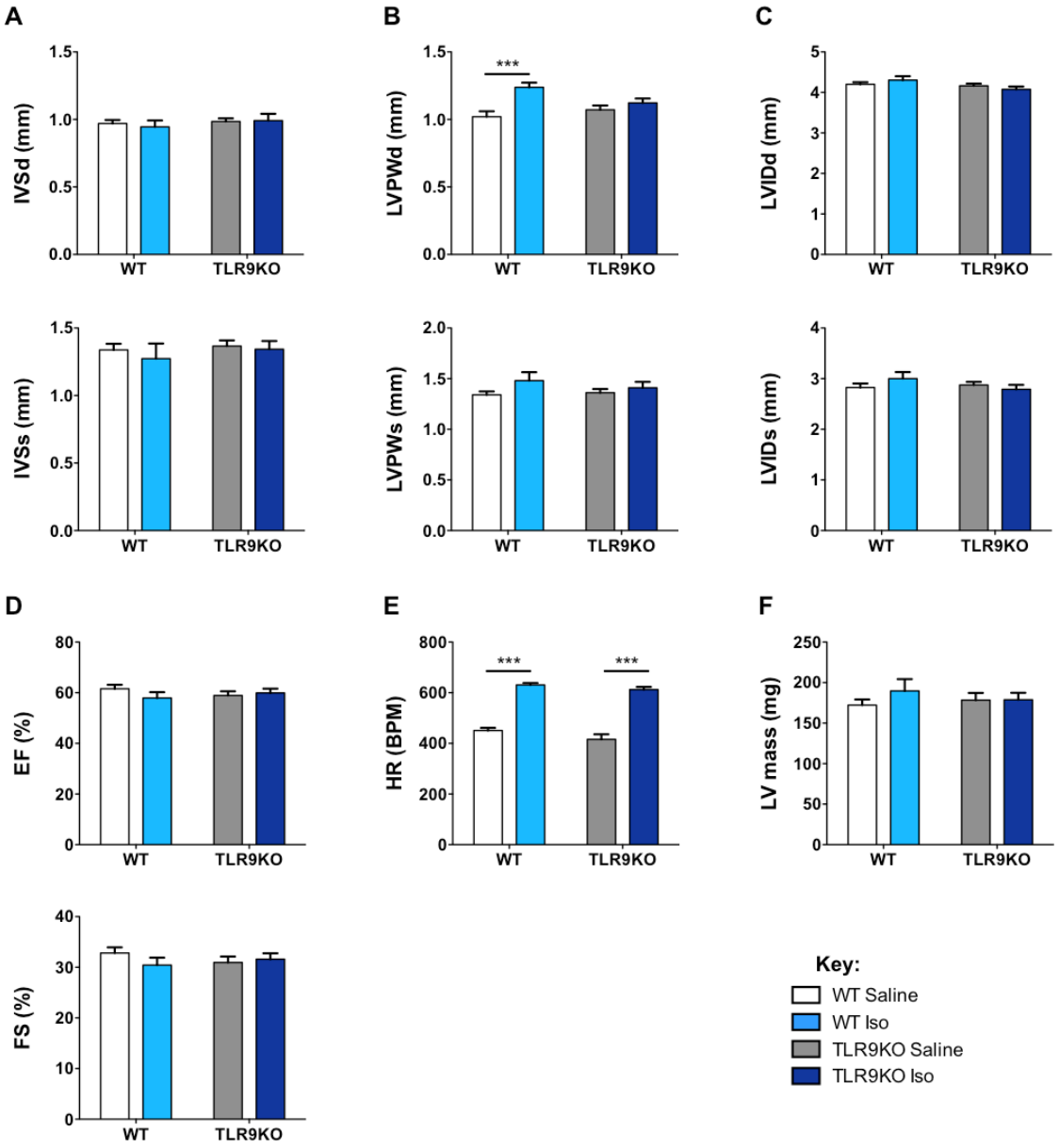

Figure 3.13 Tachycardia was observed in Iso- infused WT and TLR9KO mice.

Echocardiographic measurements were performed under anaesthesia using 1.5% isoflurane on WT and TLR9KO mice after 4 weeks infusion of Iso. A, IVSd = End-diastolic interventricular septal wall thickness, IVSs = End-systolic interventricular septal wall thickness. B, LVPWd = End-diastolic left ventricular posterior wall thickness, LVPWs = End-systolic left ventricular posterior wall thickness. C, LVIDd = End-diastolic left ventricle internal dimension, LVIDs = End-systolic left ventricle internal dimension. D, EF = Ejection fraction, FS = Fractional shortening. E, HR = Heart rate. F = LV mass. HR was increased by approximately 190 BPM in WT and TLR9KO Iso-infused mice compared to saline-infused mice. WT saline (white), WT Iso (light blue), TLR9KO saline (grey), TLR9KO Iso (dark blue); *n*= 8 for all groups. Data were analysed by two-way ANOVA with bonferroni's post-hoc test. ****p*<0.001.

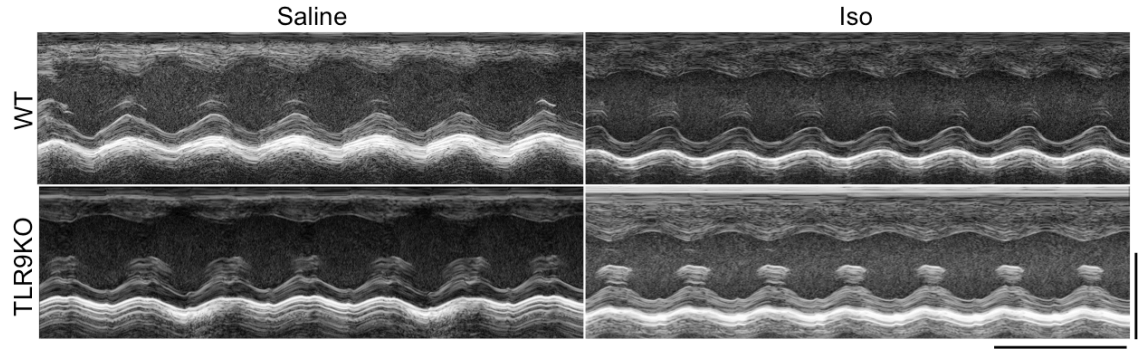

Figure 3.14 Transthoracic M-mode echocardiography using echocardiographic method 2 exhibited dilated cardiomyopathy after Iso infusion in WT and TLR9KO mice.

Transthoracic M-mode echocardiography after 4 weeks infusion of Iso or saline in WT and TLR9KO mice. Anaesthetised echocardiography was performed using different percentages of isoflurane to bring heart rates to between 450 and 550 bpm. Scale bars = 0.2 s and 5 mm respectively. *n*= 8 for all groups

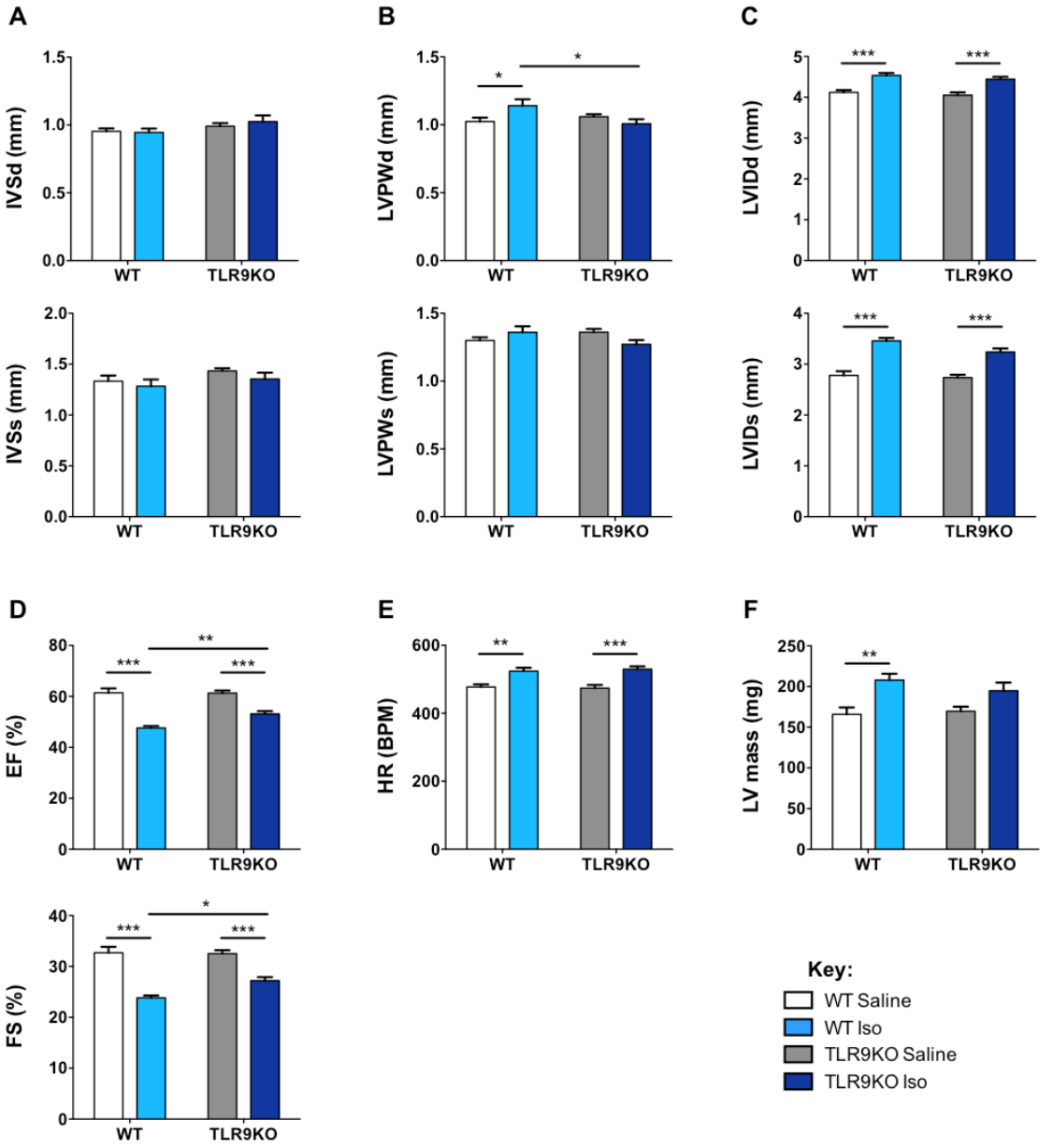

Figure 3.15 Performing echocardiography to match heart rates (HRs) revealed a rescue of cardiac function in TLR9KO mice after Iso infusion. Anaesthetised echocardiography was performed using different percentages of isoflurane to bring HRs to between 450 and 550 bpm. A, IVSd = End-diastolic interventricular septal wall thickness, IVSs = End-systolic interventricular septal wall thickness. B, LVPWd = End-diastolic left ventricular posterior wall thickness, LVPWs = End-systolic left ventricular posterior wall thickness. C, LVIDd = End-diastolic left ventricle internal dimension, LVIDs = End-systolic left ventricle internal dimension. D, EF = Ejection fraction, FS = Fractional shortening. E, HR. F = LV mass. Though chamber dilatation and cardiac dysfunction were observed in WT and TLR9KO Iso infused mice, there was partial recovery of LVPWd thickness and cardiac function after Iso infusion in TLR9KO mice compared with WT mice. WT saline (white), WT Iso (light blue), TLR9KO saline (grey), TLR9KO Iso (dark blue); *n*= 8 for all groups. Data were analysed by two-way ANOVA. **p*<0.05, ***p*<0.01, ****p*<0.001.

3.2.2.4 Blunted gain of heart weight after Iso infusion in TLR9KO mice.

After 4 weeks of saline or Iso infusion, WT and TLR9KO mice were sacrificed and their organs were harvested for physiological analyses. Compared to saline-treated mice, Iso infusion in WT mice induced body weight gain, yet did not affect the tibia length (**figure 3.16a-b**). Heart, lung and liver weights normalised to tibia length were significantly upregulated in Iso-infused WT mice compared to saline-treated mice (**figure 3.16c-e**), indicative of cardiac hypertrophy, pulmonary congestion and systemic congestion.

TLR9KO mice presented similar changes in physiological parameters as WT mice after Iso treatment. The heart weight / tibia length was increased in both WT and TLR9KO mice after Iso infusion, however, most intriguingly the increase in this parameter was significantly less in Iso-infused TLR9KO mice compared to WT Iso- infused mice (**figure 3.16c**). Therefore these findings suggest that after Iso infusion, both WT and TLR9KO mice induce body weight gain, pulmonary congestion and systemic congestion to a similar extent, yet TLR9KO mice were less susceptible to Iso-induced heart weight gain than WT mice. These exciting findings suggest that TLR9 may influence the progression of cardiac hypertrophy (although molecular analyses is required).

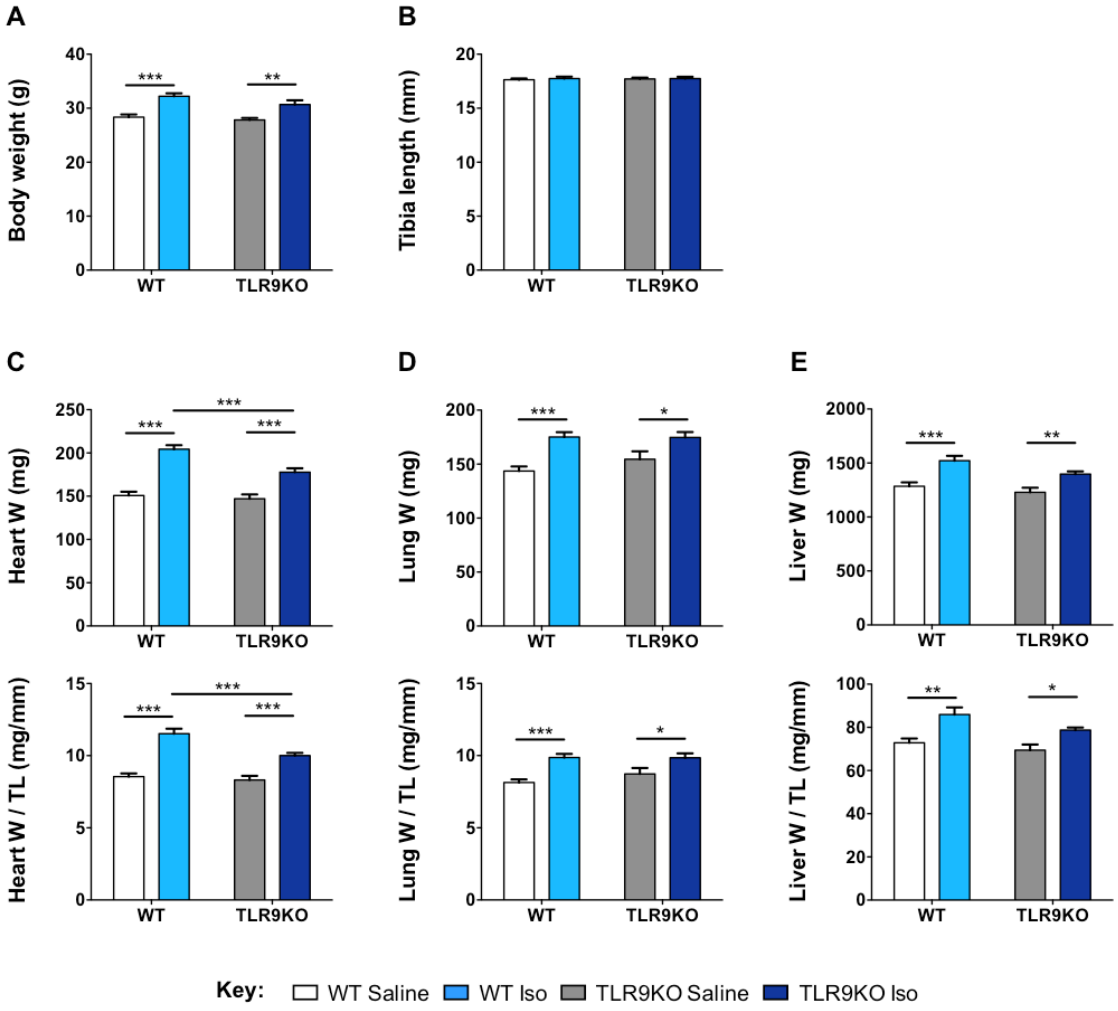

Figure 3.16 Less gain in heart weight in TLR9KO mice infused with 50 mg/kg/day Iso for 4 weeks compared with WT mice.
Physiological parameters were measured in WT and TLR9KO mice after 4 weeks Iso infusion. A, Body weight. B, Tibia length (TL). C, Heart weight and heart weight / TL. D, Lung weight and lung weight / TL. E, Liver weight and liver weight / TL. WT and TLR9KO mice subjected to Iso infusion gained weight and the mass of the heart, liver and lungs were increased compared with saline-treated mice. However, the gain in heart weight was reduced in TLR9KO-Iso infused mice compared with WT Iso-treated mice. WT saline (white), WT Iso (light blue), TLR9KO saline (grey), TLR9KO Iso (dark blue); *n*= 8 for all groups. Data were analysed by two-way ANOVA with bonferroni's post-hoc test. **p*<0.05, ***p*<0.01, ****p*<0.001. W = Weight.

3.2.2.5 Investigation of the hypertrophic response after Iso infusion in WT and TLR9KO mice

Several preceding studies demonstrated that Iso induces cardiac hypertrophy [295, 296, 311]. At the cellular level, this is characterised by increased cardiomyocyte CSA, re-expression of foetal genes and elevated protein synthesis. Moreover, these changes are also detected in the failing heart. Thus, to study if the hypertrophic response was activated after Iso infusion in WT and TLR9KO mice, staining with H & E and WGA was performed to measure cardiomyocyte CSA, alongside qRT-PCR to monitor changes in foetal gene expression.

3.2.2.5.1 Increased cardiomyocyte CSA after Iso infusion in WT mice.

Samples for histological analysis were harvested from WT and TLR9KO mice after Iso infusion. Initially, these heart samples were embedded in paraffin, sectioned and stained with H & E. Unfortunately in all of the paraffin-embedded sections, large spaces between cardiomyocytes were observed (**figure 3.17a**), that were speculated to be a consequence of artefacts in the fixation or embedding procedures. In an attempt to optimise the paraffin-embedding protocol, different fixation protocols were performed, modifying the concentration of fixatives (PFA or FA), the period of fixation (4 or 24 hours) and temperatures (4^{o}C or RT). Despite these adjustments, the gaps between cardiomyocytes were still apparent (**figure 3.17b**).

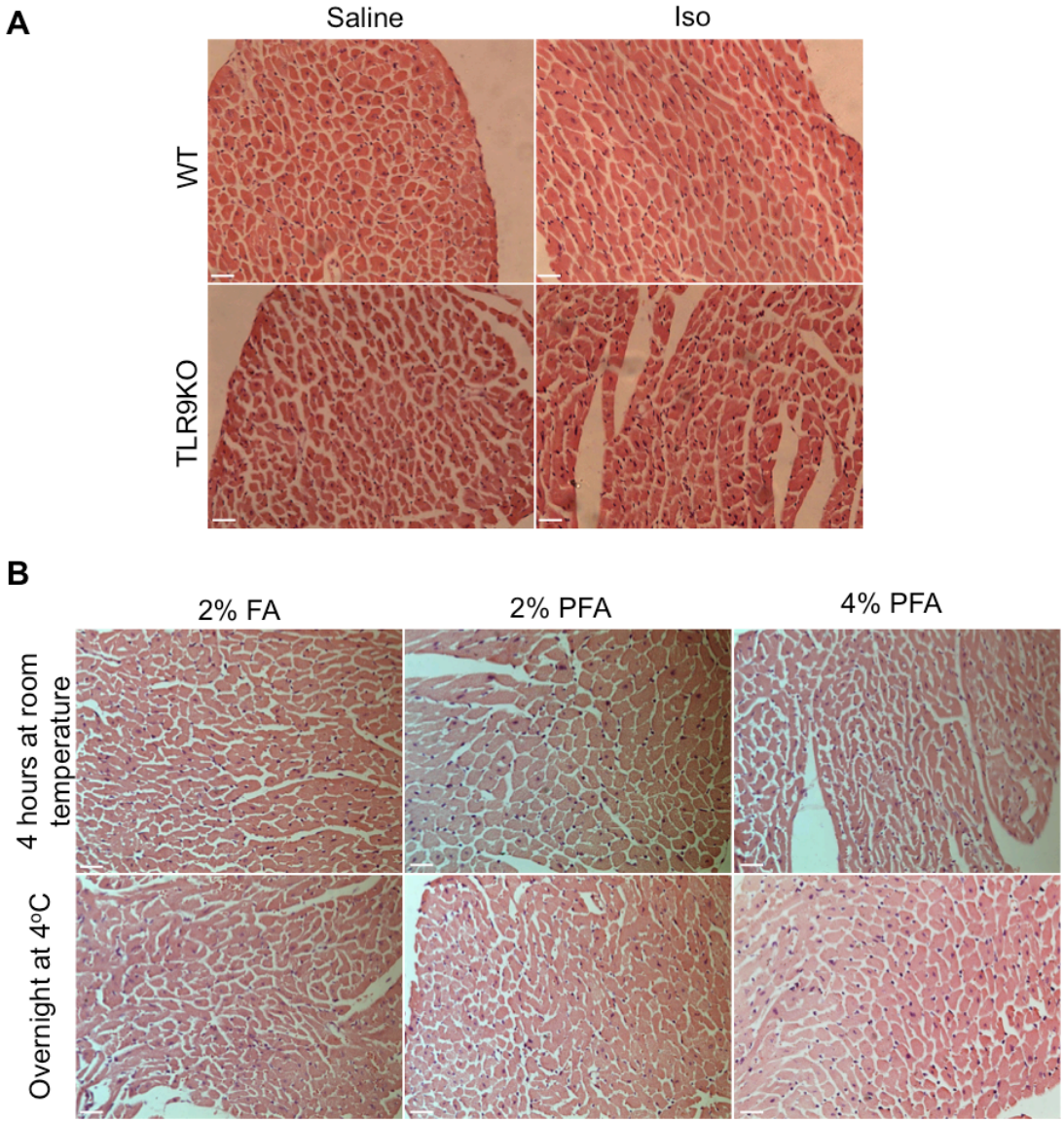

Figure 3.17 Optimising the fixation conditions for paraffin embedding did not resolve the breaching of cardiomyocytes.
A, Hematoxylin and Eosin (H & E) staining on paraffin embedded heart sections from WT and TLR9KO mice infused for 4 weeks with 50 mg/kg/day Iso or saline revealed gaps between cardiomyocytes. B, Heart sections using different fixation conditions (fixatives, temperatures and durations) were subjected to H & E staining. PFA= paraformaldehyde. Images taken at 200x magnification, scale bar = 30 µm.

As paraffin-embedded samples were unsuitable for staining, H & E staining was performed on cryosections of hearts of WT and TLR9KO mice after Iso infusion. The staining suggests there was an increase in the CSA after Iso infusion in both WT and TLR9KO mice (**figure 3.18**) (data not quantified). To quantitate the changes in cardiomyocyte CSA after Iso treatment, WGA staining was

performed and the CSA of 100 cardiomyocytes per section was measured using Image J software. Analysis of CSA measurements exhibited a significant increase in the cardiomyocyte CSA after Iso infusion in WT mice, compared to saline-treated mice, indicative of cardiac hypertrophy (**figure 3.19**). In contrast, no differences were observed between saline- and Iso- infused TLR9KO mice or between Iso-treated WT and TLR9KO mice. Although these current findings suggests a blunted cardiac hypertrophic response in TLR9KO mice subjected to Iso, compared to WT mice, further samples are required to confirm this finding as the *p* value for TLR9KO subjected to saline and Iso treatment is close to significance (p value = 0.079).

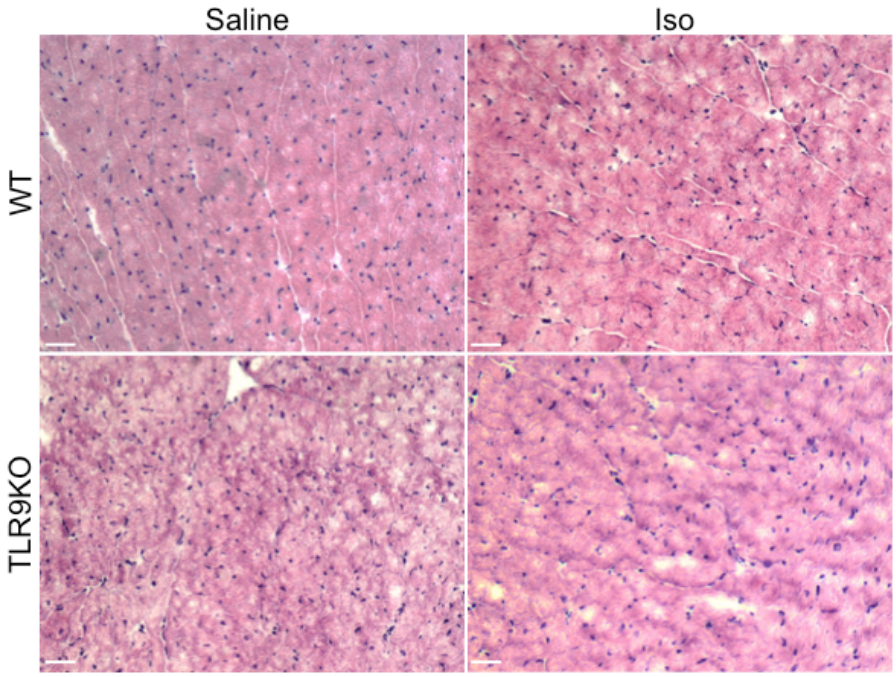

Figure 3.18 Haematoxylin & Eosin (H & E) staining using cryosections of hearts from WT and TLR9KO mice infused with Iso for 4 weeks.
H & E staining on cryosections of heart tissue from WT and TLR9KO mice infused for 4 weeks with 50 mg/kg/day Iso or saline. Cardiomyocyte cross-sectional area (CSA) appears to be increased in Iso infused mice. *n* = 5 for all groups. Scale bar = 30 µm.

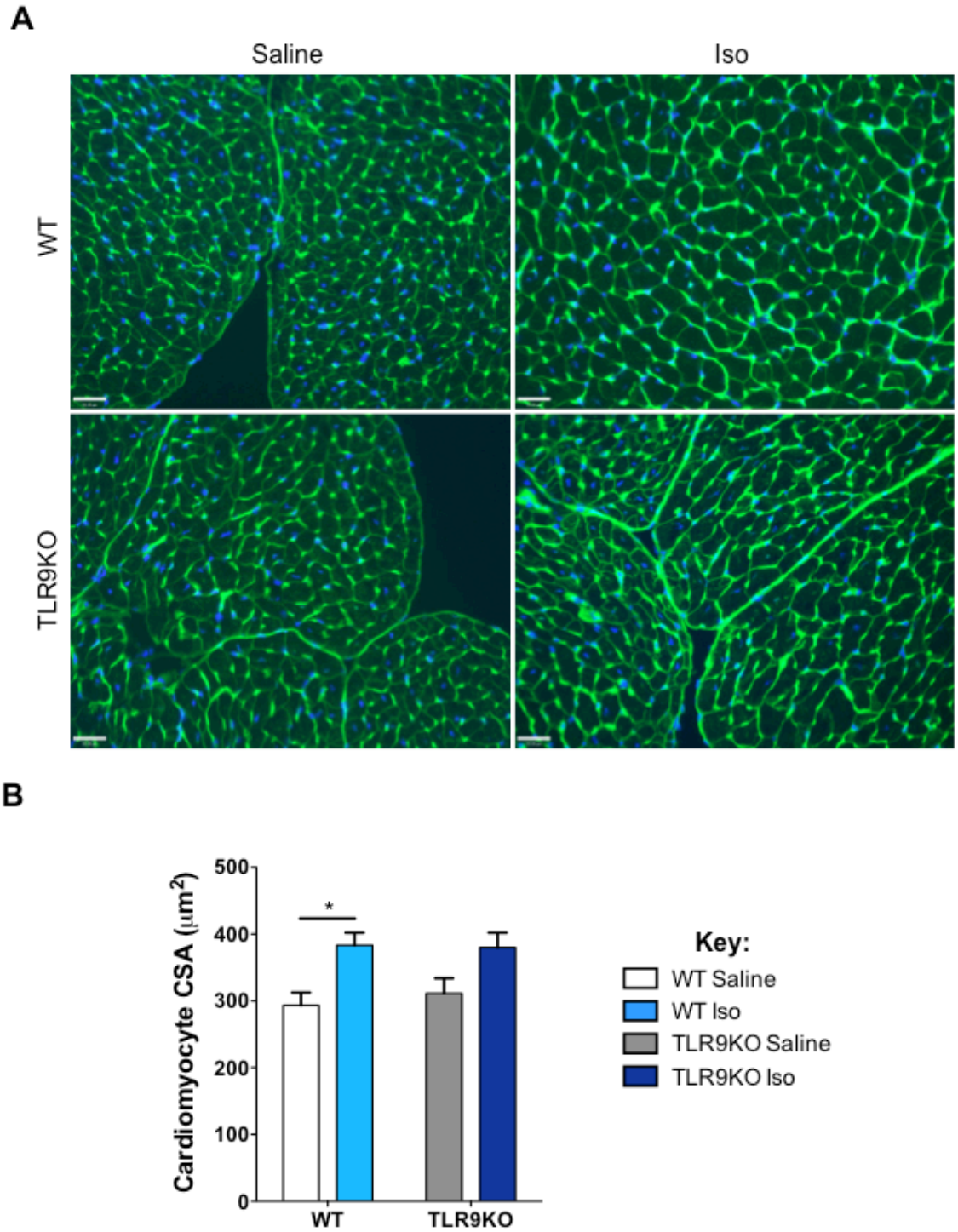

Figure 3.19 Wheat germ agglutinin (WGA) staining presented an increase in cardiomyocyte cross-sectional area (CSA) in WT mice infused with Iso, but no difference in the TLR9KO mice.

A, WGA staining was performed on cryosections on myocardium harvested from WT and TLR9KO mice after 4 weeks of Iso infusion. Scale bar = 30 μm. B, Quantification of cardiomyocyte CSA revealed an increase in WT mice treated with Iso compared with saline treated mice, which was not observed with the TLR9KO mice infused with Iso. Green signal (FITC, lectin), blue signal (DAPI, DNA). WT saline (white), WT Iso (light blue), TLR9KO saline (grey), TLR9KO Iso (dark blue); n= 5 for all groups. Values expressed as mean ± SEM. Data were analysed by two-way ANOVA with bonferroni's post-hoc test. *p<0.05. p value for TLR9KO saline versus TLR9KO iso is 0.079.

3.2.2.5.2 Iso infusion did not induce expression of foetal genes.

The mRNA levels of foetal genes, natriuretic peptide A (*Nppa), Nppb* and myosin heavy chain 7 beta (*Myh7)* were evaluated by qRT-PCR using LV samples of WT and TLR9KO mice after Iso infusion. Most unexpectedly, *Nppa* expression was significantly reduced after Iso infusion in WT mice, compared to saline-treated mice (**figure 3.20**). However this surprising change was not observed between TLR9 saline- and Iso- treated mice. Furthermore, no differences in *Nppb* and *Myh7* expression were detected between saline- and Iso- treated WT mice, which was analogous to TLR9KO mice after Iso infusion.

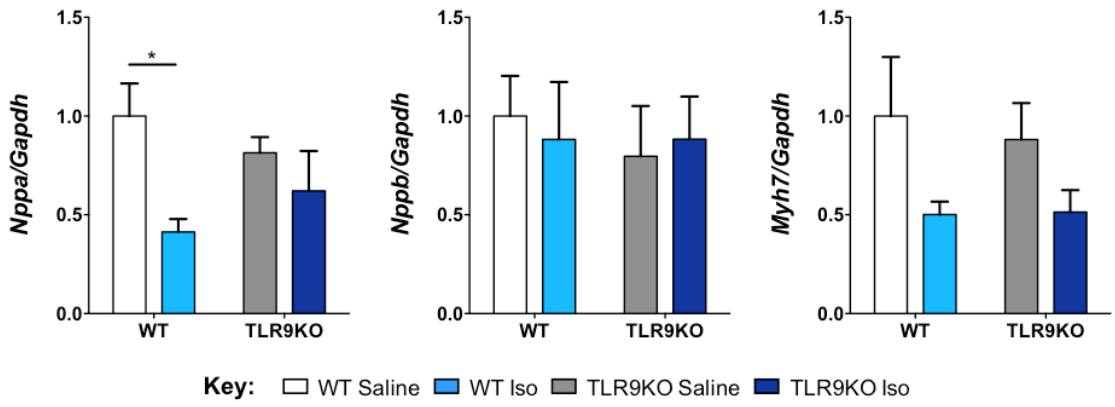

Figure 3.20 Foetal genes were not induced in the myocardium of WT and TLR9KO mice after Iso infusion.
qRT-PCR analysis was performed on left ventricular cDNA samples of WT and TLR9KO mice subjected to 4 weeks treatment of Iso. Levels of natriuretic peptide A *(Nppa)* were reduced in WT iso-infused mice compared with WT saline-infused mice, whereas no difference was seen in TLR9KO mice. Expression of *Nppb* and myosin heavy chain 7 beta *(Myh7)* remained indifferent after Iso infusion in WT and TLR9KO mice. Glyceraldehyde 3-phosphate dehydrogenase *(Gapdh)* was used as a housekeeping gene. Values expressed as mean ± SEM. WT saline (white), WT Iso (light blue), TLR9KO saline (grey), TLR9KO Iso (dark blue); *n*= 5 for all groups. Data were analysed by two-way ANOVA with bonferroni's post-hoc test. *p<0.05.

3.2.2.5.3 Primers targeting *natriuretic peptide A* were validated.

As the qRT-PCR results regarding *Nppa* expression were unexpected, the primers were validated. Firstly, the quality and purity of the RNA was re-assessed and was adequate for experiments. The reverse transcription and qRT-PCR reaction were repeated, yielding similar results as before. Next, the specificity of the primers used for qRT-PCR was assessed by melt curve analysis. These primers exhibited 1 peak, indicating that the primers amplify a single PCR product (**figure 3.21**). Therefore qRT-PCR was performed using primers targeting *Nppa* and LV homogenates harvested from WT mice subjected to TAC, kindly provided by Dr Manabu Taneike (King's College London) (**figure 3.22a**). As expected, a significant increase was observed in *Nppa* levels, confirming the specificity of these primers. Finally, a Taqman assay for *Nppa* and *Gapdh* was used on samples from WT and TLR9KO mice infused for 4 weeks with Iso or saline, which also demonstrated similar results to the initial data (**figure 3.22b**). Together, these results indicate that *Nppa* expression was not upregulated in this model of β–stimulant-induced cardiomyopathy.

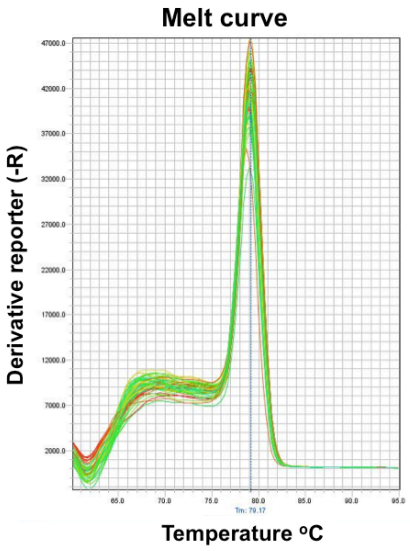

Figure 3.21 Melt curve of natriuretic peptide A targeting primers.
Natriuretic peptide A (*Nppa*) primers were subjected to a melt curve analysis, rendering 1 peak. This confirms that the primers amplify 1 product from DNA and verified the specificity of the primers.

One explanation for the lack of upregulated hypertrophic markers might be the timepoint at which these samples were harvested. Therefore to determine the expression of foetal genes at an earlier timepoint, mice were infused with saline or 50 mg/kg/day Iso for 2 weeks. Although the numbers of experimental replicates were too low to analyse the data statistically, the data from these samples indicate that even at an earlier timepoint, there was no induction of foetal gene expression after Iso infusion (**figure 3.23e-f**). It was also contemplated that the Iso concentration may be excessive. Therefore heart samples were obtained from mice infused for 2 weeks with 30 mg/kg/day Iso, kindly provided by Dr James Clark (King's College London). Although cardiac dysfunction was observed in these mice after Iso infusion (**figure 3.23j**), there was again no difference observed in the expression of hypertrophic markers after Iso infusion (**figure 3.23k-l**). In summary, the findings presented in this section detected no upregulation of hypertrophic markers in samples using different concentrations of Iso for different infusion periods.

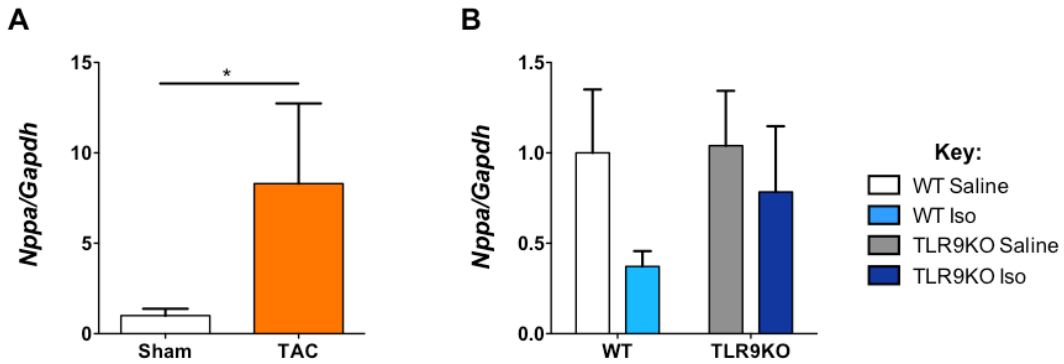

Figure 3.22 Verification of primers targeting natriuretic peptide A.
A, qRT-PCR was performed on cDNA using cardiac homogenates of WT mice subjected to transverse aortic constriction (TAC) from Dr Manabu Taneike (King's College London) using primers targeting natriuretic peptide A (*Nppa*). *Nppa* was induced after pressure overload. Sham (open) and TAC (orange). *n*= 3. B, qRT-PCR was performed using a Taqman assay for *Nppa* on samples from left ventricular samples of WT and TLR9KO mice subjected to 4 weeks treatment of Iso. No difference was observed in all groups. *n*= 5. Values expressed as mean ± SEM. Glyceraldehyde 3-phosphate dehydrogenase *(Gapdh)* was used as a housekeeper. *p<0.05.

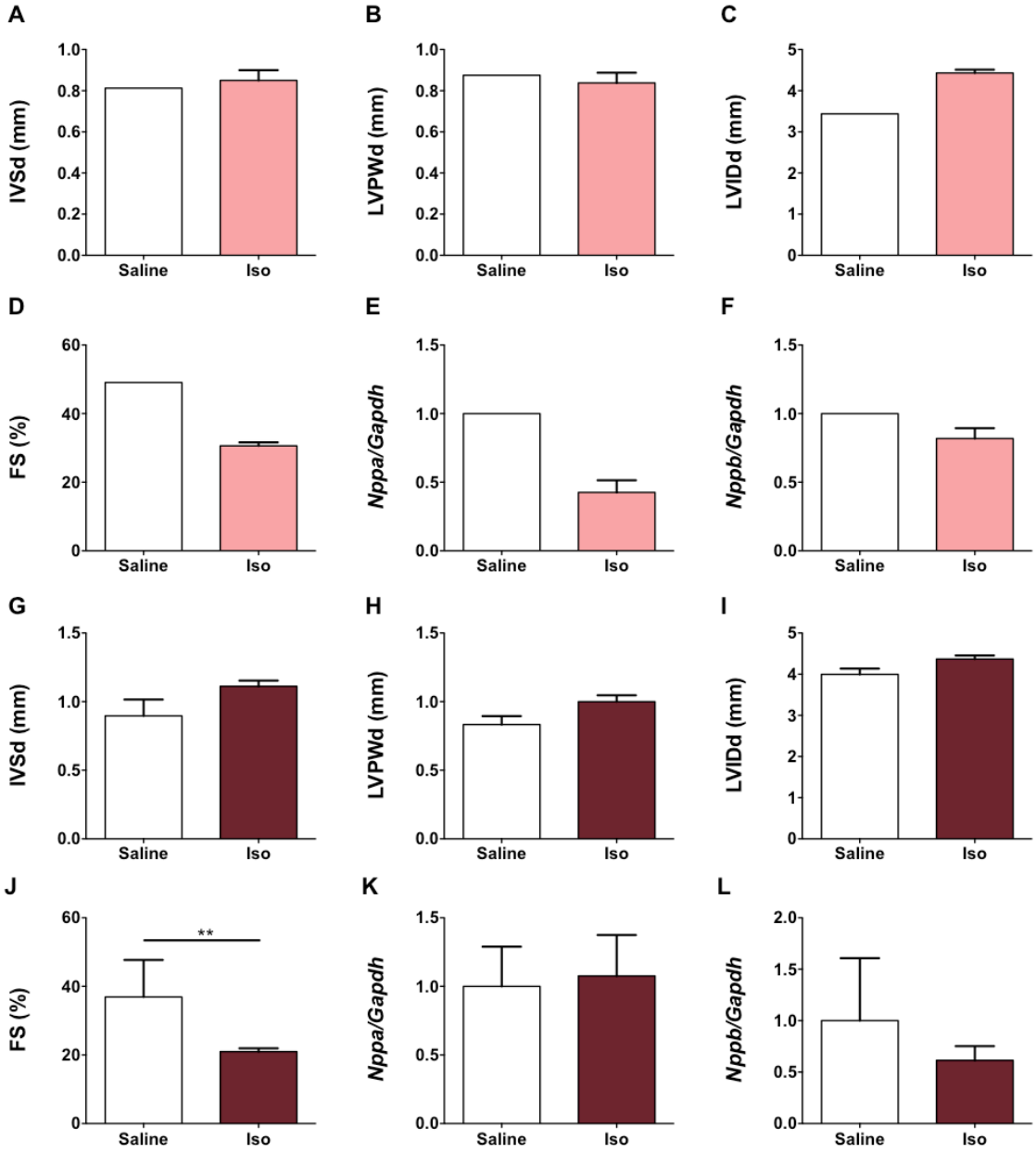

Figure 3.23 Foetal genes expression was not elevated in models using different doses and timecourses of Iso.
The mRNA levels of natriuretic peptide A *(Nppa)* and natriuretic peptide B *(Nppb)* were measured in different models of Iso known to induce hypertrophy. A-F, Data from WT mice subjected to 2 weeks infusion of saline (open bars, *n*= 1) or 50 mg/kg/day Iso (pink bars, *n*= 2). A - D, Echocardiographic parameters. A, IVSd = End-diastolic interventricular septal wall thickness. B, LVPWd = End-diastolic left ventricular posterior wall thickness. C, LVIDd = End-diastolic left ventricle internal dimension. D, FS = Fractional shortening. E and F, mRNA expression of *Nppa* and *Nppb* from cardiac tissue. G - L, Murine heart samples donated by Dr James Clark (King's College London) after 2 weeks infusion of saline (open bars, *n*= 3) or 30 mg/kg/day Iso (red bars, *n*= 4). Data were analysed by student's t-test. G - J, Echocardiographic parameters. K and L, *Nppa* and *Nppb* expression evaluated by qRT-PCR.

3.2.2.6 Examination of the inflammatory response of WT and TLR9KO mice after Iso infusion.

To determine whether TLR9-mediated inflammation contributed to the detrimental role of TLR9 on heart function and weight, the inflammatory response after Iso infusion was examined between WT and TLR9KO mice. IHC staining to detect cell surface markers of inflammatory cells was performed alongside qRT-PCR analyses of the expression of chemokines and pro-inflammatory cytokines.

3.2.2.6.1 No changes in the number of inflammatory cells after Iso treatment in WT and TLR9KO mice.

IHC staining was executed on cryosections of the myocardium obtained from WT and TLR9KO mice infused with saline or Iso for 4 weeks. Expression of CD45, a leukocyte marker that relays information about the general immune response [321] was examined, alongside more specific markers which included CD68, a macrophage marker [322], Ly6G/C, a neutrophil marker [323] and CD3, a T cell marker [324] (**figure 3.24**). To determine if there were any modest changes in the number of infiltrating cells, the number of CD45-positive, CD68-positive, Ly6G/C-positive and CD3-positive cells were quantified from 5 random images acquired per section. However no significant differences in the number of CD45-, CD68-, Ly6G/C- or CD3- positive inflammatory cells were observed between saline- and Iso- treated WT mice (**figure 3.25**). Moreover, the number of these cells was similar between WT and TLR9KO mice treated with saline or Iso. As this data stands, these findings suggest that an inflammatory response was not activated after Iso infusion. However, there are tendencies within the data to suggest that Iso increases the recruitment of CD45-, CD68-, or CD3-

positive inflammatory cells, therefore increasing the number of samples would either prove or disprove this potential trend.

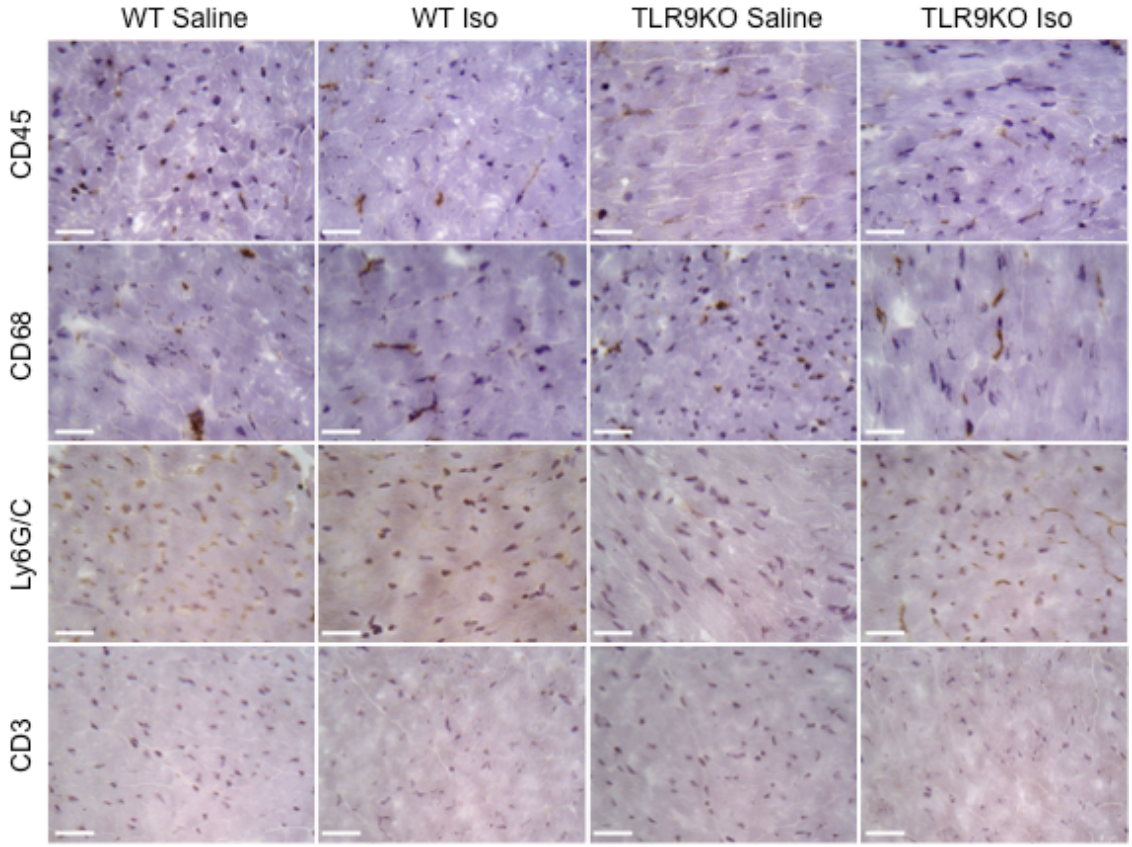

Figure 3.24 Immunohistochemical (IHC) staining suggests no differences in the number of inflammatory cells in the myocardium in WT and TLR9KO mice after Iso treatment.
IHC staining for inflammatory cell markers was performed on cryosections of myocardium harvested from WT and TLR9KO after 4 weeks of Iso infusion. Images acquired at 400x magnification, Scale bar = 30 μm. Staining was performed to detect cells expressing CD45 = leukocytes, CD68 = macrophages, Ly6G/C = neutrophils and CD3 = T-cells. There was no obvious difference in the infiltration of inflammatory cells into the myocardium of WT and TLR9KO mice after Iso infusion. *n*= 3 for all groups.

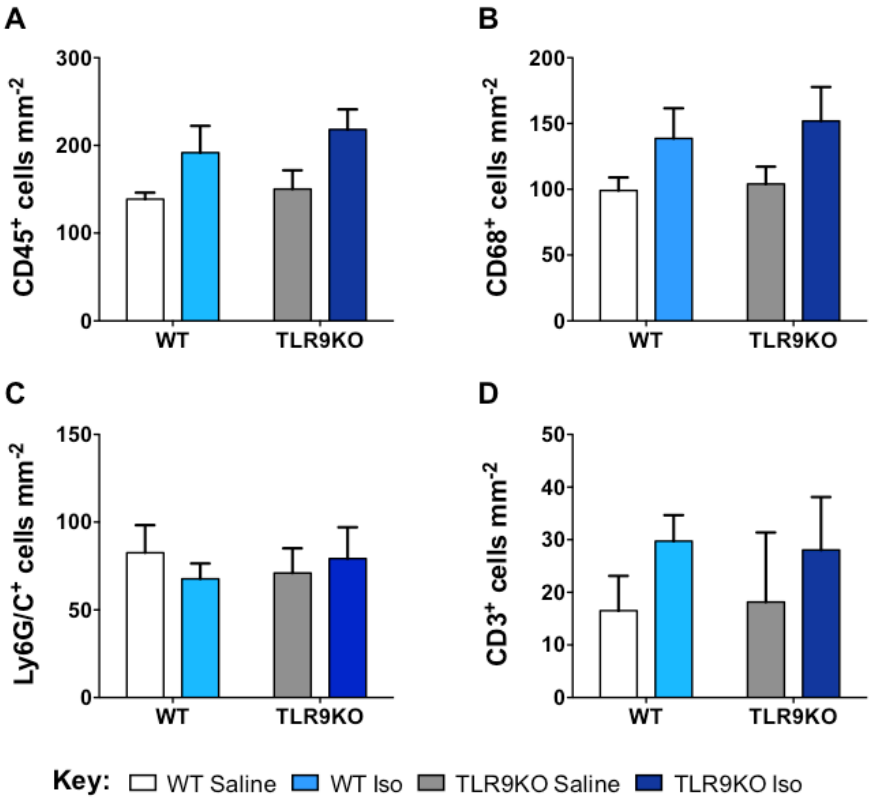

Figure 3.25 No quantifiable changes in the infiltration of inflammatory cells into myocardial tissue after Iso infusion in WT and TLR9KO mice.
To study the infiltration of inflammatory cell markers into the myocardium of WT and TLR9KO after 4 weeks of Iso infusion, IHC staining was performed. The number of 3,3'-Diaminobenzidine (DAB)-positive cells after each stain were counted from 5 images per heart at 400 x magnification and expressed as cells per mm^2. A, CD45 = leukocytes. B, CD68 = macrophages. C, Ly6G/C = neutrophils. D, CD3 = T-cells. No changes were observed in myocardial inflammatory cell infiltration after Iso infusion in WT and TLR9KO mice. WT saline (white), WT Iso (light blue), TLR9KO saline (grey), TLR9KO Iso (dark blue); *n*= 3 for all groups. Values expressed as mean ± SEM. Data were analysed by two-way ANOVA.

3.2.2.6.2 mRNA levels of cytokines and chemokines remained unchanged after Iso infusion.

mRNA levels of the pro-inflammatory cytokines, tumour necrosis factor (*Tnf)-a,* interleukin (*Il)-1b, Il6, Il10, Il12b,* interferon *(Ifn)-b1* and *Ifng* and chemokines, chemokine C-C motif ligand *(Ccl)-2* and *Ccl5* were evaluated by qRT-PCR using LV homogenates harvested from WT and TLR9KO mice infused with Iso.

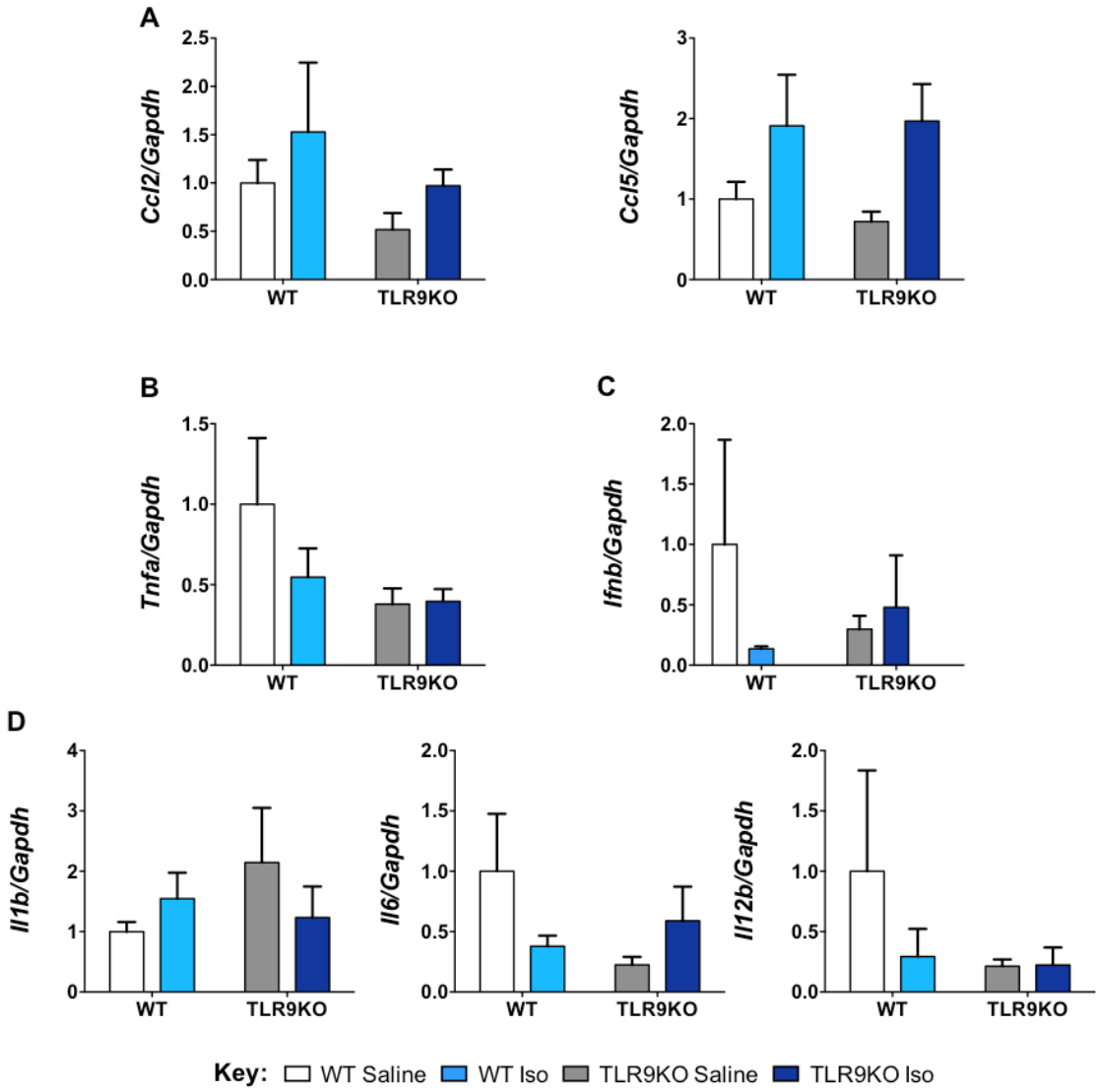

Figure 3.26 mRNA expression of chemokines and cytokines was not upregulated in WT and TLR9KO mice after infusion with Iso.
qRT-PCR analysis was performed on LV samples of WT and TLR9KO mice after 4 weeks of Iso infusion. A, mRNA expression of chemokines. *Ccl5* = chemokine (C-C motif) ligand 5 and *Ccl2.* B - D, Cytokine mRNA expression. B, *Tnfa* = tumour necrosis factor α. C, *Ifnb* = interferon β. D, *Il1b* = interleukin *1*β*, Il6 and Il12b. Gapdh* (Glyceraldehyde 3-phosphate dehydrogenase) was used as a housekeeping gene. No difference in the expression levels of chemokines and cytokines after 4 weeks Iso treatment was observed in WT and TLR9KO mice. *Il10* and *Ifny* were undetectable. Values expressed as mean ± SEM. WT saline (white), WT Iso (light blue), TLR9KO saline (grey), TLR9KO Iso (dark blue); *n*= 5 for all groups. Data were analysed by two-way ANOVA with bonferroni's post-hoc test.

Analysis of these samples determined no differences in the expression of chemokines, *Ccl2* and *Ccl5* (**figure 3.26a**) and cytokines, *Tnfa, Il1b, Il6, Il12b,* and *Ifnb* between WT mice infused with saline and Iso (**figure 3.26 b-d**).

Additionally, there were no differences in the expression of these markers between WT and TLR9KO mice after saline or Iso treatment. *Il10* and *Ifng* were undetectable in all samples (not shown). There were tendencies within the data to suggest that Iso increases the mRNA expression of chemokines, *Ccl2* and *Ccl5* and decreases the expression of cytokines, *Tnfa, Il6, Il12b,* and *Ifnb*. Also there may a decreasing trend in mRNA expression of these cytokines (*Tnfa, Il6, Il12b,* and *Ifnb*) between WT and TLR9KO mice subjected to saline treatment.

Therefore as the data stands, the findings of the IHC staining in section **3.2.2.6.1** and the results presented here indicate that an inflammatory response was not stimulated after Iso infusion and inflammation is unlikely to contribute to TLR9-mediated heart weight gain and dysfunction. However, there are several trends observed within the data (discussed above), therefore more samples are required to prove / disprove these tendencies.

3.2.2.7 Study of the fibrotic response after Iso infusion in WT and TLR9KO mice.

Several reports have demonstrated increased fibrosis after Iso infusion [296, 325, 326], therefore it was questioned whether fibrosis contributes to TLR9-mediated cardiac dysfunction and heart weight gain. Levels of fibrosis were assessed by MT staining and qRT-PCR to determine the mRNA levels of fibrotic markers using samples harvested from WT and TLR9KO mice after Iso infusion.

3.2.2.7.1 MT staining and Picrosirius Red staining indicated no fibrosis after Iso infusion.

MT staining was performed on myocardial cryosections harvested from WT and TLR9KO mice after Iso infusion. Images displayed in **figure 3.27a** surprisingly

suggested no obvious difference in the extent of fibrosis between all groups. Therefore the fibrotic staining was quantified using Image J software to determine any variations. These analyses similarly indicated no differences in the levels of fibrosis between saline- and Iso- treated WT mice (**figure 3.27b**), which was uniform with TLR9KO mice after saline or Iso infusion.

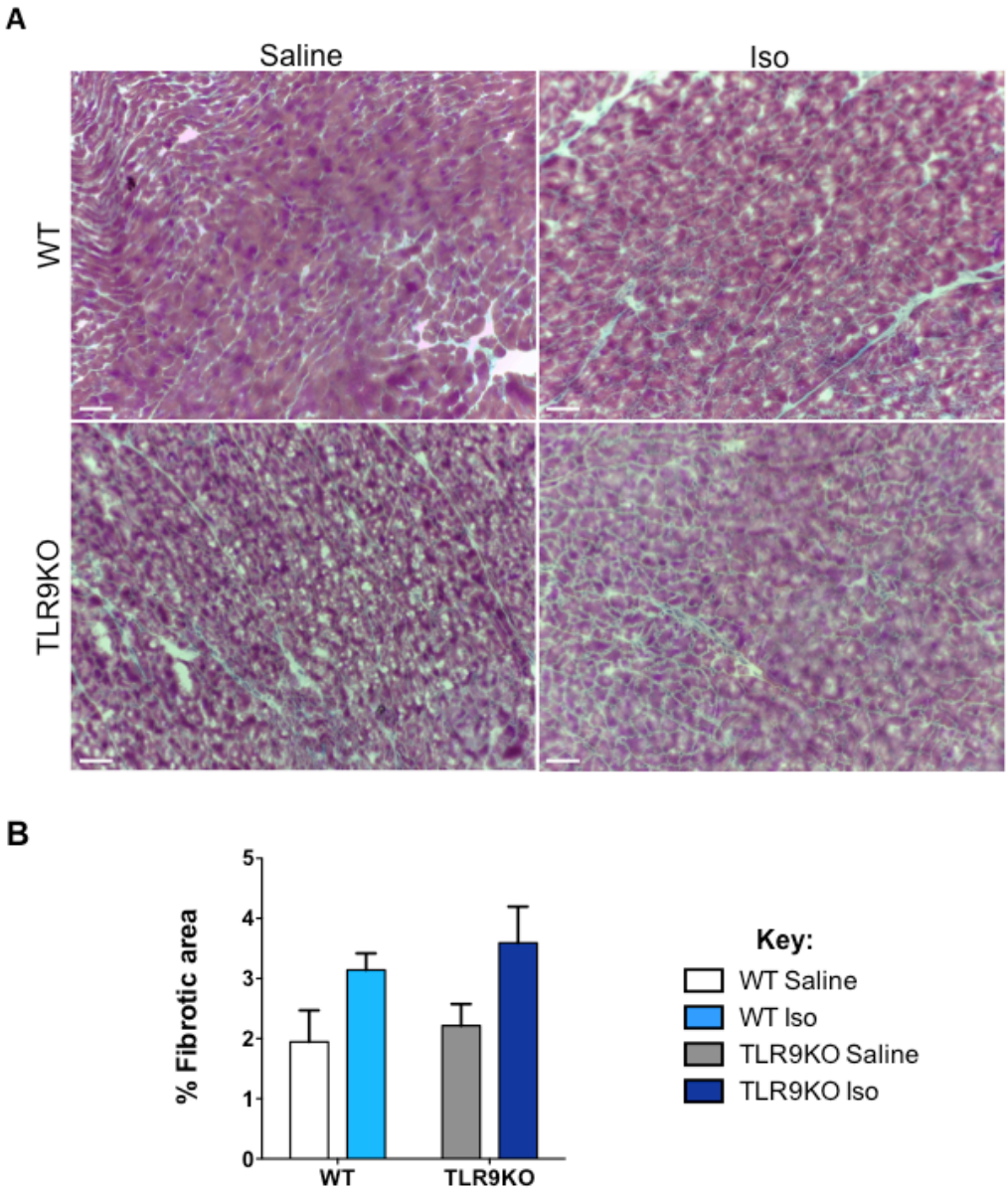

Figure 3.27 Masson's Trichrome staining revealed no difference in cardiac fibrosis in WT and TLR9KO mice after Iso infusion for 4 weeks
No difference in fibrosis was detected in WT and TLR9KO mice after treatment of Iso for 1 month. A, Images of Masson's Trichrome staining. Scale bar = 30 μm. B, Quantification of fibrotic area. Five images per section were analysed using Image J software. Values expressed as mean ± SEM. *n*= 3 per group. Data were analysed by two-way ANOVA with bonferroni's post-hoc test.

As MT staining detected little fibrosis, a more sensitive method, Picrosirius Red staining, was performed to assess the extent of fibrosis between WT saline- and WT Iso- infused mice (**figure 3.28**). Picrosirius Red staining found no significant difference in fibrosis between WT saline and WT Iso-infused hearts, suggesting no induction of fibrosis after Iso infusion. However, both **figures 3.27b and 3.28b** display a trend towards increased levels of fibrosis after Iso infusion in WT mice and TLR9KO mice, therefore more samples are required to confirm this trend.

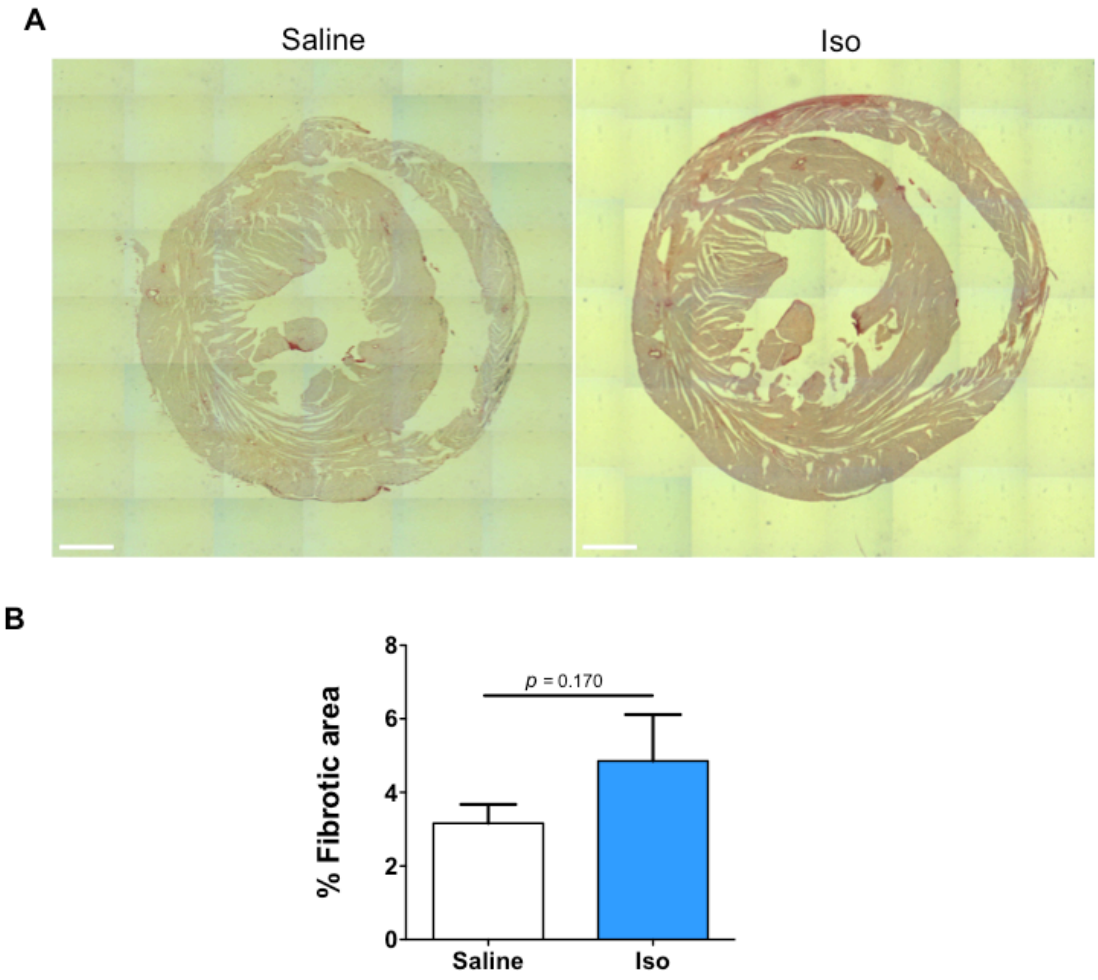

Figure 3.28 Picrosirius Red staining confirmed no changes in fibrosis after Iso infusion in WT mice.
A, Picrosirius Red staining was performed on heart sections of WT mice, showing no difference in fibrosis between saline and Iso-infused animals, corroborating the findings in **figure 3.27.** Scale bar = 500 μm. B, Quantification of fibrotic area. Values expressed as mean ± SEM. Saline = open bars, Iso = blue bars. *n* = 4 for both groups. Data were analysed by Student's t-test.

3.2.2.7.2 *Col1a2* and *Col3a1* mRNA levels were not upregulated after Iso infusion.

The mRNA levels of fibrotic markers, collagen type 1 alpha 2 (*Col1a2*) and collagen type 3 alpha 1 (*Col3a1*) were measured by qRT-PCR using LV homogenates from WT and TLR9KO mice infused with Iso. However there was no significant difference in the expression of the different markers between saline and Iso WT mice, which was comparable with TLR9KO mice after the same treatment (**figure 3.29**). However, **figure 3.29** suggests a trend towards increased expression of fibrotic markers after Iso infusion in WT mice and TLR9KO mice, but more samples are required to verify this tendency.

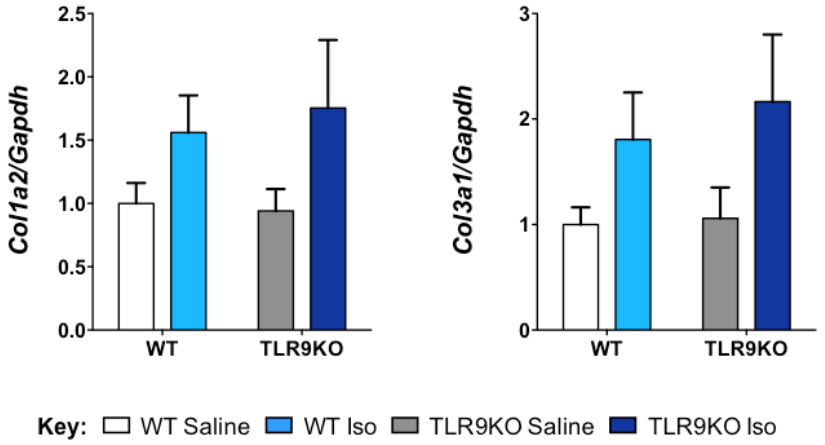

Figure 3.29 No difference in the mRNA levels of fibrotic markers in WT and TLR9KO mice after 4 weeks of Iso treatment.
LV samples of WT and TLR9KO mice subjected to 4 weeks infusion of Iso were used to analyse fibrotic markers by qRT-PCR analysis. Levels of collagen type 1 alpha 2 (*Col1a2*) and *Col3a1* were indifferent between WT and TLR9KO mice after Iso infusion. Glyceraldehyde 3-phosphate dehydrogenase (Gapdh) was used as a housekeeper. Values expressed as mean ± SEM. WT saline (white), WT Iso (light blue), TLR9KO saline (grey), TLR9KO Iso (dark blue); *n*= 5 for all groups. Data were analysed by two-way ANOVA.

This unexpected, uniform expression of fibrotic markers after Iso infusion questioned the accuracy of the primers, therefore qRT-PCR was performed using primers targeting *Col1a2* and *Col3a1* on mRNA isolated from the LV of mice subjected to TAC, kindly provided by Manabu Taneike (King's College

London). An increase in *Col1a2* and *Col3a1* expression was detected in WT mice subjected to TAC compared to sham-operated mice, validating these primers (**figure 3.30**). Hence, these current findings suggest that there was surprisingly no induction of fibrosis after Iso treatment in both WT and TLR9KO mice, however increasing the number of samples may suggest otherwise.

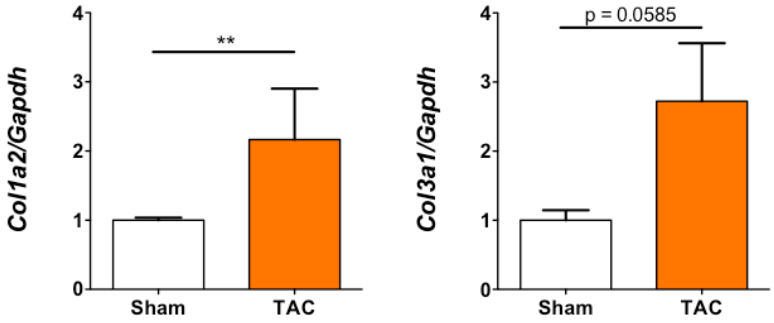

Figure 3.30 Mice subjected to transverse aortic constriction exhibited elevated levels of fibrotic markers,
The effectiveness of the primers targeting fibrotic markers were evaluated using cardiac tissue from WT mice subjected to transverse aortic constriction (TAC) from Dr Manabu Taneike (King's College London) using primers targeting collagen type 1 alpha 2 (*Col1a2*) and *Col3a1*. An increase in the expression of fibrotic markers was observed in TAC operated mice compared with Sham, verifying that the primers work. *n*= 3. Data were analysed by Student's t-test. ***p*<0.01.

3.2.2.8 Study of apoptosis after Iso infusion in WT and TLR9KO mice.

Cell death by apoptosis is another reported consequence of Iso infusion [295]. Therefore to determine whether apoptosis contributed to TLR9-mediated cardiac dysfunction after Iso infusion, terminal deoxynucleotidyl transferase (TdT)-deoxyuridine triphosphate (dUTP) nick end labeling (TUNEL) staining and Western blotting for caspase-3 were performed.

3.2.2.8.1 TUNEL staining indicated no difference in apoptosis after Iso infusion.

Fragmented DNA with nicked ends is a characteristic feature of apoptosis [327]. TUNEL staining uses TdT enzymes to label these nicked ends with dUTP conjugated to fluorophores, thereby signalling activation of cellular apoptosis. TUNEL staining using paraffin-embedded sections was established in my laboratory group [156, 328]. However, cryosections were utilised for histological experiments, due to the issues with paraffin-embedded sections described in **figure 3.17**. Fortunately, the kit used for TUNEL staining provided a protocol for the use of cryosections. The sections were fixed in acetone at 4^{o}C for 15 minutes followed by incubation with the permeabilisation buffer provided with the kit. However there was poor detection of the FITC and DAPI signal using the cryosections compared with the paraffin-embedded sections (**figure 3.31a**). It was speculated that the permeabilisation was inadequate, therefore the sections were permeabilised with 0.25% Triton for 20 minutes (**figure 3.31b**). However this did not improve the signal. Next, the fixation conditions were altered by utilising 4% PFA for 1 hour at RT, followed by permeabilisation in 0.25% Triton for 20 minutes. These conditions proved to be successful (**figure 3.31b**) and were used in subsequent TUNEL staining experiments.

TUNEL staining was performed on cryosections of hearts from WT and TLR9KO mice infused with 50 mg/kg/day Iso or saline for 4 weeks, using the optimised protocol described above. Images of TUNEL-positive cells are displayed in **figure 3.32a**. TUNEL-positive cells were defined as bright FITC signal, which overlapped with the DAPI signal (confirming that this signal was coming from DNA) and also overlay with the TRITC signal, indicating that these cells expressed α-sarcomeric actin, a cardiomyocyte specific marker

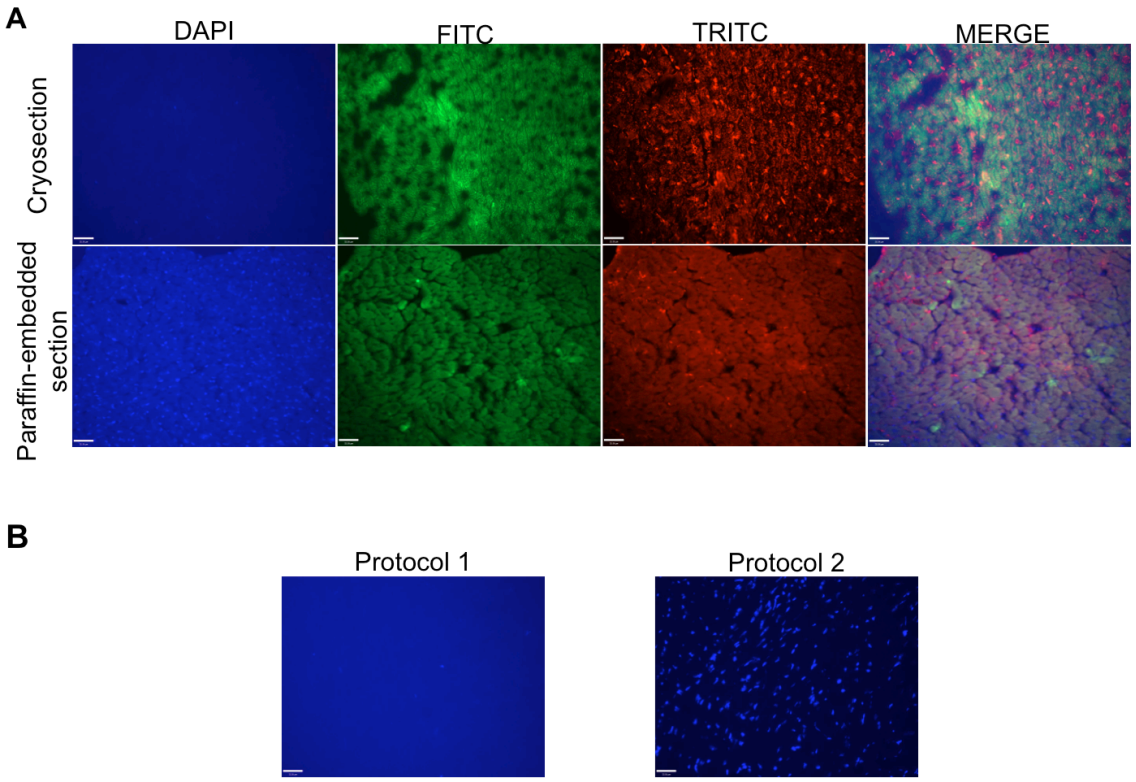

Figure 3.31 Optimisation of TUNEL staining enhanced the DAPI signal. A, TUNEL staining performed on cryosections did not reveal any DAPI signal, whereas paraffin embedded sections showed strong DAPI signal. DAPI (DNA), FITC (TUNEL-positive nuclei), TRITC (α-sarcomeric actin for cardiomyocytes). Scale bar = 30 μm. Thus different fixation and permeabilisation conditions were tested, with protocol 2 being successful. B, DAPI staining was performed on spare cryosections using different fixation and permeabilisation methods. Protocol 1; sections were fixed using acetone for 15 minutes at 4^{o}C and permeabilised using 0.25% Triton X-100, followed by DAPI staining. Protocol 2; 4% PFA for an hour at room temperature and then sections were permeabilised using 0.25% Triton for 20 minutes and stained with DAPI.

The number of TUNEL-positive cardiomyocytes in the entire heart section were counted and expressed as a proportion of the number of TUNEL-positive cells per 10^5 nuclei of cardiomyocytes (**figure 3.32b**). No significant differences in the number of TUNEL-positive cells were observed between WT and TLR9KO mice after Iso infusion, suggesting no stimulation of apoptotic pathways. A tendency towards more TUNEL-positive cells after Iso infusion in WT mice could be suggested from **figure 3.32b,** however more samples are required to confirm this trend.

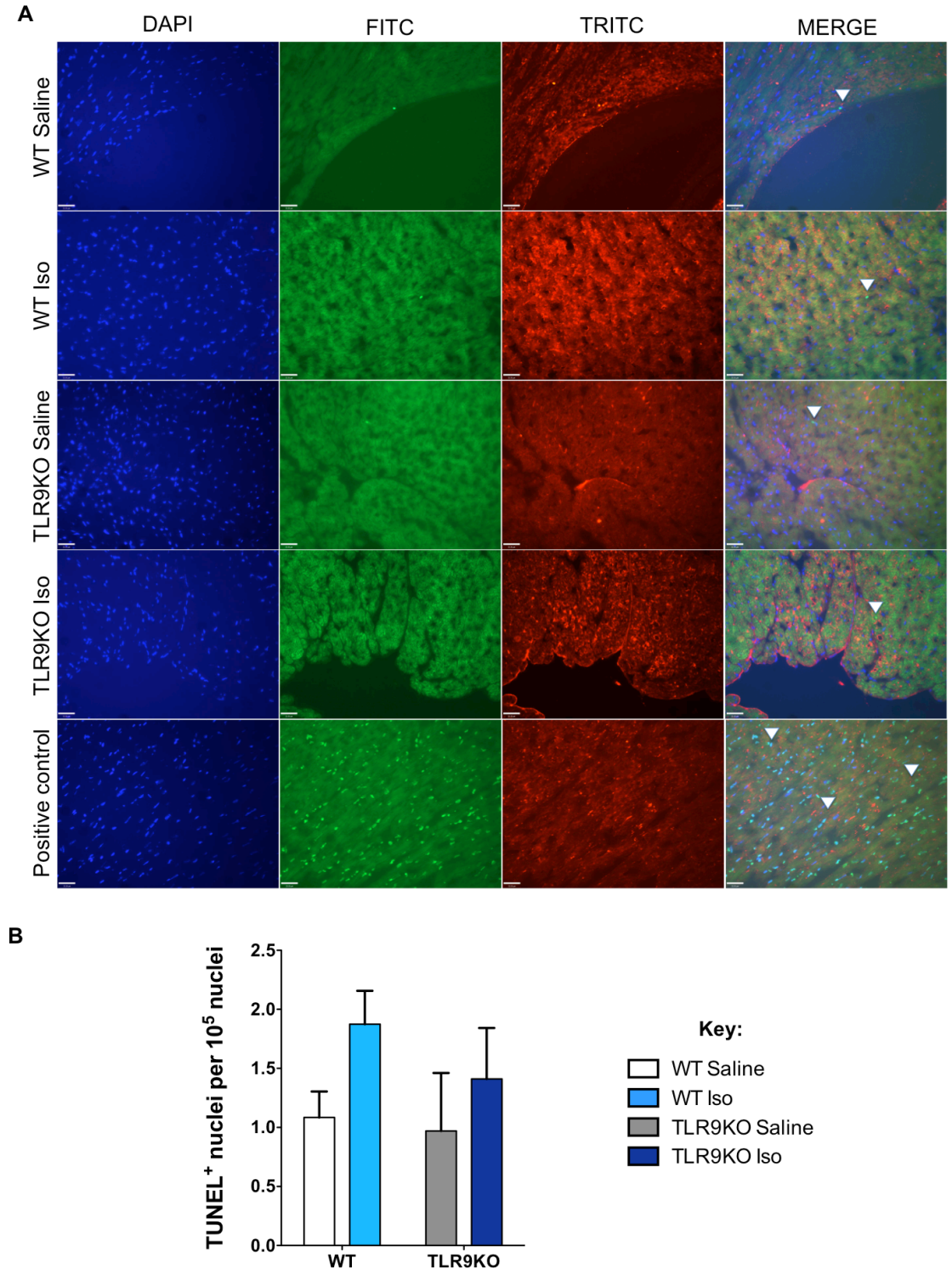

Figure 3.32 TUNEL staining identified no difference in apoptosis in the myocardium of WT and TLR9KO mice infused with Iso.

A, TUNEL staining performed on cryosections of hearts revealed no difference in the number of TUNEL-positive nuclei (white arrows) in the hearts of WT and TLR9KO mice treated with Iso. DAPI (DNA), FITC (TUNEL-positive nuclei), TRITC (α-sarcomeric actin for cardiomyocytes). Positive control section was incubated with DNase I prior to TUNEL staining. Scale bar = 30 μm. B, Quantification of TUNEL-positive cells per 10^5 nuclei, expressed as mean ± SEM. WT saline (white), WT Iso (light blue), TLR9KO saline (grey), TLR9KO Iso (dark blue); *n*= 3 per group. Data were analysed by two-way ANOVA with bonferroni's post-hoc test.

3.2.2.8.2 Cleaved caspase-3 expression was unchanged after Iso infusion.

Upon activation of the apoptotic signalling cascade, initiator caspases cleave the effector caspase, procaspase-3, into its active form, which consequently cleaves cellular contents [129, 131]. Thus the apoptotic response after Iso infusion in WT and TLR9KO mice was examined by Western blot analysis of procaspase-3 and its cleaved form using LV homogenates. There were no differences in the expression of procaspase-3 between WT and TLR9KO mice after Iso infusion (**figure 3.33**). Additionally, there was no detection of the cleaved form of procaspase-3 in all groups, suggesting very little apoptosis in these mice. However more samples are required to support these claims.

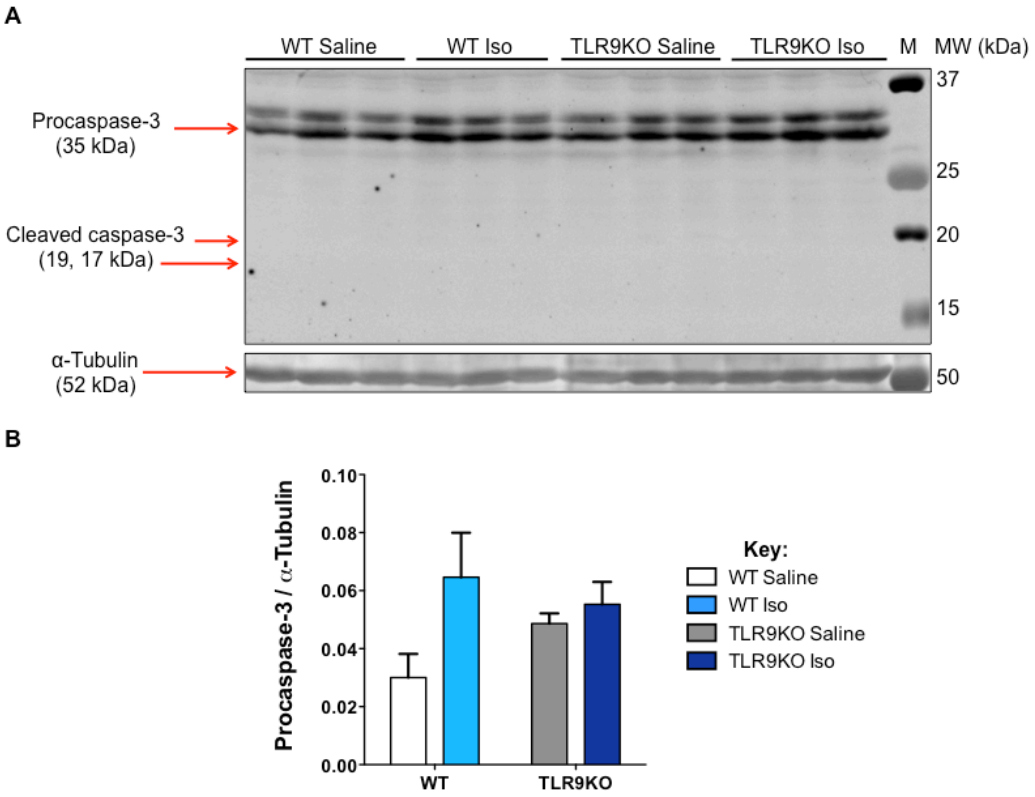

Figure 3.33 No change in caspase-3 activation after Iso infusion in WT and TLR9KO mice.
A, Western blot analysis showed no change in procaspase-3 and cleaved caspase-3 expression in LV homogenates between WT and TLR9KO mice subjected to Iso treatment. M = marker (values in kDa). Red arrows correspond to quantified bands. B, Densimetric analysis. Values displayed as mean ± SEM. WT saline (white), WT Iso (light blue), TLR9KO saline (grey), TLR9KO Iso (dark blue); *n*= 3 for all groups. Data were analysed by two-way ANOVA with bonferroni's post-hoc test.

3.3 Discussion

Collectively, the most important results from this chapter demonstrate that TLR9 induces cardiac dysfunction and heart weight gain, through an association with the β-AR signalling pathway. However, the current data displays that neither, fibrosis, apoptosis or inflammation were involved in TLR9-mediated cardiac dysfunction and heart weight gain. These findings propose a novel role of TLR9, independent of its inflammatory function, which influences cardiac function and heart weight and may prove to be detrimental during the progression of HF. In addition, this chapter has demonstrated that excessive, constant and chronic infusion of Iso does not induce typical HF, but mild cardiac dysfunction and was referred to as β-stimulant-induced cardiomyopathy (**figure 3.34**).

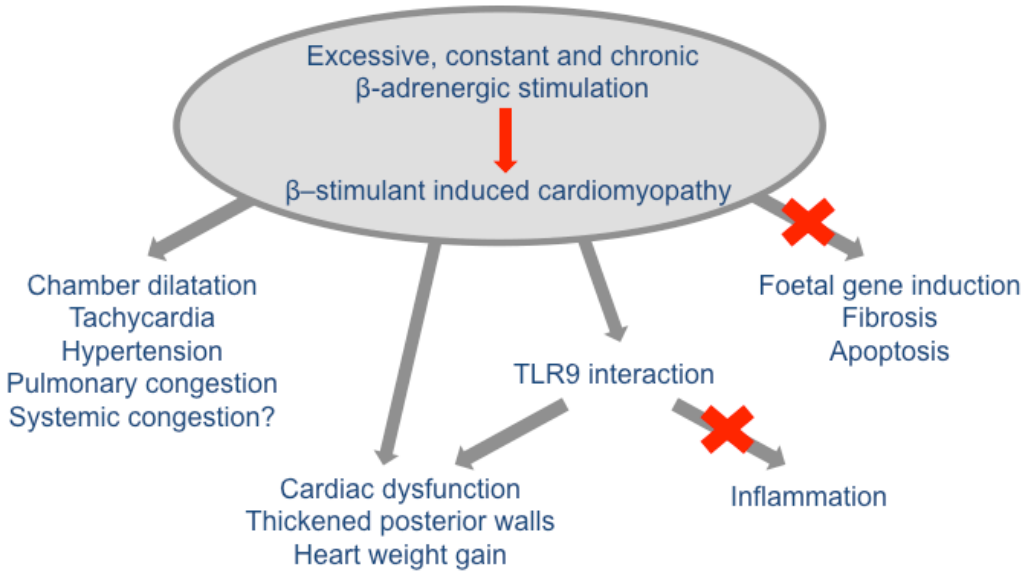

Figure 3.34 Summary findings of this chapter.
Excessive, constant and chronic β-adrenergic receptor (β-AR) stimulation caused β-stimulant-induced cardiomyopathy, which has multiple effects of cardiac function and structure, however, surprisingly did not induce fibrosis, apoptosis or foetal gene expression. The most exciting findings were identifying the influential role of TLR9 on cardiac dysfunction and heart weight.

3.3.1 Iso treatment induced dilated cardiomyopathy.

A pilot study was conducted to determine a suitable timecourse and concentration of Iso to induce HF. Based on previous studies from my research group discussed in **section 3.2.1** [306], 2 doses of Iso were used in this current study, with the expectation that the higher dose would induce a quicker and more robust HF phenotype. As mentioned, well-established traits of Iso infusion, tachycardia, cardiac hypertrophy, LV chamber dilatation, body weight gain, pulmonary congestion alongside cardiac dysfunction, were anticipated outcomes of Iso infusion in this current model [80, 295, 313, 315, 316, 317, 318].

Although cardiac dilatation and dysfunction and increased LV mass were observed 4 weeks after Iso infusion at both doses (**figure 3.3c, d, f**), there were surprisingly no changes in HR or wall thickness (IVSd or LVPWd) parameters after 4 weeks of Iso infusion (**figure 3.3b, e**). For the pilot study, echocardiography was performed on conscious mice with HR between 700 - 800 bpm. With physiological HR values between 500 to 600 bpm [329], it is plausible that the mice were stressed during echocardiography, increasing the levels of circulating catecholamines and elevating the HR. The HR may have reached its maximal value in both saline- and Iso- treated mice thus masking the effects of the Iso treatment. In addition, with such a high HR, there may be difficulties associated with accurately viewing the wall thickness by short axis M-mode echocardiography.

The physiological data from the pilot study indicated weight gain, heart weight gain and pulmonary congestion in mice infused with 50 mg/kg/day Iso for 4 weeks compared to saline-infused mice (**figure 3.4**). However these physiological changes were not observed between mice infused with 75 mg/kg/day Iso and saline, suggesting that 50 mg/kg/day Iso instigated a more

severe phenotype than 75 mg/kg/day Iso. For the 75 mg/kg/day Iso dose, Iso was dissolved at 313 mg/ml, which is close to the maximal solubility capacity of Iso reported by the datasheet (333 mg/ml). Therefore, it is possible that the Iso may have precipitated within the minipumps over the 4 weeks during which they were implanted, rendering the minipump inactive and reducing the concentration of Iso that was infused into the mouse. Therefore the blood concentration of Iso should have been measured in all mice to ensure that the minipumps were working effectively to deliver Iso at the proposed rate.

In the pilot study, Dr Manabu Taneike and Dr Shigemiki Omiya (both from King's College London) performed echocardiography using conscious mice (**figure 3.3**), whereas, in the main study I performed echocardiography on anaesthetised mice (**figures 3.19, 3.10, 3.12 - 3.15**). This alteration was due to different skillsets of the echocardiographic handlers. Nevertheless, the echocardiographic data from both studies yielded different findings and values. As mentioned, the mice were scruffed to perform conscious echocardiography in the pilot study, which may cause stress to the mice and conceal Iso-induced tachycardia. Using anaesthetised echocardiography, increased LVPWd and HR were observed after Iso infusion in WT mice (suggesting cardiac hypertrophy and tachycardia) and not in the pilot study. Although, anaesthesia suppresses cardiac function, the clarity of the images is improved which is used to define the wall thickness and avoids the effects of stress-induced HR changes. This may contribute to the differences seen in LVPWd and HR in the main investigation (**section 6.4 for further discussion**).

However, due to Iso-induced tachycardia, it was difficult to interpret the echocardiographic data obtained under anaesthesia as differences in HR between saline and Iso treated mice were observed when performing

echocardiography using same ISF% and using different ISF% in an attempt to match HRs (**section 6.4 for further discussion**). Alternatively, HR independent indices could have been measured such as myocardial performance index (MPI), isovolumic contraction time (IVCT) and isovolumic relaxation time (IVRT), which could provide information on global systolic and diastolic ventricular function, independent of differences in HR. Also, diastolic cardiac function was not assessed in this Iso infusion model. Performing Doppler echocardiography would provide more information about the overall cardiac structure and function and may identify any issues with ventricular relaxation after Iso infusion.

Furthermore, although cardiac dilatation and dysfunction was observed in both studies, the values of LVIDd and LVIDs are larger in mice in the main study (saline 4.12 mm, 2.78 mm and Iso 4.54 mm, 3.46 mm, respectively[‡]) compared to the pilot study (saline 3.27 mm, 1.60 mm and Iso 4.30 mm, 3.00 mm respectively[§]), which consequently yielded different values for EF and FS (main study: saline 51.24%, 32.69%, Iso 30.7%, 23.82%[*]. Pilot study: saline 83.31%, 61.42%, Iso 57.8%, 47.62%[†]).

Therefore the extent of the change in a particular parameter after Iso infusion differs between the two studies, making it difficult to compare these two studies. However general trends do appear which are comparable between the studies.

One discrepancy between the pilot and main investigation concerns the liver weight after Iso infusion. In the pilot study, there was no difference in liver weight between saline and Iso treated mice (**figure 3.4**) whereas in the main

---

[‡] Values taken from **figure 3.15** after 4 weeks of treatment
[§] Values taken from **figure 3.3** after 4 weeks of treatment
[*] Values taken from **figure 3.15** after 4 weeks of treatment
[†] Values taken from **figure 3.3** after 4 weeks of treatment

study, there was an increase in liver weight in WT mice infused with Iso (**figure 3.16**). Increased liver weight is reminiscent of systemic congestion, which has not been previously reported in mice after Iso infusion. Thus, to determine which result is valid, further study is recommended.

Further, although hypertrophy increases wall thickness and subsequently increases LV mass, echocardiographic assessment of wall thickness and LV mass may be considered an inconclusive and potentially unreliable measure of hypertrophy. Echocardiographic measurements are subjective and dependent upon the position of the mouse, heart and probe as well as the quality of the images. Also, echocardiographic images were acquired from one viewpoint, which were then analysed and the wall thickness and LV mass were calculated. Therefore it is unknown how accurate these measurements are compared to the actual heart measurements as images were taken from one viewpoint and therefore measurements should be taken at different viewpoints to improve the accuracy and reliability of these measurements. Additionally, cardiac hypertrophy can also be demonstrated by physiological and molecular analyses (discussed below) and thereby support the echocardiographic findings if all are in agreement.

3.3.2 Unusual cardiac phenotypes after excessive and chronic infusion of Iso in WT mice.

Iso infusion in mice has been demonstrated to activate the cardiac hypertrophy programme, determined by thickened myocardial walls [330], elevated heart and LV mass [330], increased cardiomyocyte CSA [315] and re-expression of foetal genes [331]. Other reports have discovered the induction of pro-inflammatory cytokines, IL1β, IL6 and TNFα [224] after Iso infusion, in addition to activation of

fibrosis and apoptosis [315]. Thus activation of hypertrophic, fibrotic, inflammatory and apoptotic pathways were investigated after Iso infusion, to determine their contribution to the development of β- stimulant-induced cardiomyopathy.

In terms of the cellular measurements of hypertrophic changes, WGA staining displayed an increase in cardiomyocyte CSA after Iso infusion in WT mice (**figure 3.19**) yet there was no induction of foetal genes (**figure 3.20**). The decrease in *Nppa* expression was most unexpected and was verified by primer validation and Taqman assay (**figure 3.21 and 3.22**). Decreased *Nppa* expression has been reported during pregnancy [332] and one report using an aortocarval shunt model of volume overload exhibited unchanged expression of foetal genes [287]. It remains unknown why *Nppa* expression decreased in this model, however both of these reports suggest that this model of β-stimulant-induced cardiomyopathy may exhibit similar phenotypes to physiological hypertrophy or volume overload models, indicating the uniqueness of this model.

Activation of the cardiac hypertrophy programme after Iso infusion in this model was suggested by thickened posterior walls and increased heart weight. It was also supported by histological data displaying increased cardiomyocyte CSA after Iso infusion, however it has since been advised that prior to harvesting, the mice should be injected with potassium to ensure that the heart rested in diastole so all sections and samples are in the same phase of the cardiac cycle. Therefore this experiment needs to be repeated to confirm these findings.

Using the data from this thesis, it remains questionable whether Iso infusion induced hypertrophy. The qRT-PCR data relayed no induction of foetal genes whilst thickened posterior walls and increased heart weight were observed by echocardiographic and physiological measurement. Measurements of heart

weight / tibia length and cardiomyocyte CSA are regarded as the gold standard for determining the activation of the hypertrophic response therefore this model may potentially induce cardiac hypertrophy, despite the qRT-PCR data, although further experiments are required. However another biochemical measurement of cardiac hypertrophy response would be to study any increments in protein synthesis using a [^{3}H] leucine incorporation study [333], although this would be technically challenging *in vivo*.

Most surprisingly, from the model used in this current study, there was no re-expression of foetal genes, increased inflammation, fibrosis or apoptosis after Iso infusion in either WT or TLR9KO mice relayed by histological analyses (**figures 3.24, 3.25, 3.27, 3.28, 3.32**) and biochemical measurements (**figures 3.20, 3.26, 3.29, 3.33**). With regards to the apoptotic data, previous reports demonstrate that Iso is myotoxic and induces apoptosis and necrosis however the activation of other cell death pathways has not been investigated. Necrosis, necroptosis and pyroptosis all involve inflammation and as **figures 3.24 – 3.26** display no differences in inflammatory responses after Iso treatment, it was unlikely that these other cell death programmes were activated. The lack of fibrosis, foetal gene reactivation, inflammation and apoptosis in this model of β–stimulant-induced cardiomyopathy is highly unusual and opposes previous reports mentioned above. One possible explanation for this could be the low number of samples used for experiments. As mentioned after individual experiments, several trends were observed, however more samples are needed to either prove or disprove these tendencies. Other probable explanations for this could be due to the dose of isoproterenol used (5 – 30 mg/kg/day), duration of treatment (1 day up to 2 weeks), method of administration (injection or continuous infusion using a minipump), age and species of mouse. As a higher

dose and longer timecourse of Iso was used, with 4 weeks of constant infusion, it is plausible that an alternative cardiac response was activated, yielding the unusual response observed. Thus the data from this chapter yielded a model of β-stimulant-induced cardiomyopathy, which does not accurately represent the progression of cardiac hypertrophy to HF.

3.3.3 Detrimental role of TLR9 in β-stimulant-induced cardiomyopathy

It was previously postulated that TLR9-mediated inflammation contributed to the progression of HF induced by pressure overload [173]. Thus this chapter questioned the association between β-AR signalling and TLR9-mediated inflammation and whether this interaction contributes to the development of HF.

The echocardiographic and physiological data revealed many similarities but also a few notable differences between WT and TLR9KO mice after Iso infusion (**figure 3.15**). Intriguingly, there was partial rescue of cardiac function, posterior wall thickness and heart weight gain in TLR9KO mice after Iso infusion, compared to WT mice. The significant improvement in fractional shortening was about 3 - 4% higher than WT mice infused with Iso (**figure 3.15d**) which was a modest improvement, compared with the improvement seen between WT and TLR9KO mice subjected to TAC [173]. Further, between WT Iso- and TLR9KO Iso- infused mice, the difference in LVPWd was 11.6% (**figure 3.15b**) and the heart weight / tibia length ratio was different by 15% (**figure 3.16c**).

These findings demonstrate that TLR9 possesses the ability to influence cardiac function and heart weight, through an association with the β-AR signalling pathway. However, this partial rescue indicates that ablation of TLR9 was not able to fully rescue Iso-induced cardiac dysfunction and heart weight gain,

thereby suggesting that TLR9 partially influences cardiac function and heart weight, in addition to other pathways.

However, the cause of this partial rescue of heart weight gain and cardiac dysfunction in TLR9KO mice after Iso infusion remains unknown, as there were no differences in fibrosis, apoptosis or surprisingly inflammation between WT and TLR9KO (**figures 3.24 – 3.26, 3.27, 3.29, 3.32, 3.33**). Therefore, this data suggests a detrimental role of TLR9 within the heart associated with β-AR signalling, which is independent of its inflammatory function.

A major limitation of this study was the lack of power calculations to ensure that the data was conclusive. In several instances, a higher number of samples were needed to validate the claims made (discussed further in **section 6.4)**. Further, though TLR9KO mice have been bred onto Bl/6 background, littermate controls are the most appropriate control for animal-related experiments and in this study, C57Bl/6 mice were used as WT controls which may considered as another experimental limitation (discussed further in **section 6.4)**. Also, the blood concentration of Iso was not measured in mice treated within Iso. It is plausible that the mice may not be receiving the full dose of Iso and could be one reason for the unexpected findings described in **section 3.3.2**.

Other limitations also include the preparation of samples for histology, the differential echocardiographic methods, use of echocardiography to determine cardiac hypertrophy and lack of diastolic function assessment, which are discussed above in **sections 3.3.1 and 3.3.2.**

Collectively, this chapter has demonstrated that excessive, constant and chronic infusion of Iso induces β-stimulant-induced cardiomyopathy and that TLR9 influences cardiac structure and function, through an association with β-AR signalling.

4 The reversible and NFκB-inducing properties of chronic, constant and excessive β-AR stimulation.

4.1 Introduction

The previous chapter demonstrated that 4 weeks infusion of Iso in mice induced cardiac dysfunction, LV chamber dilatation, hypertension, tachycardia, heart weight gain and pulmonary congestion, collectively referred to as β-stimulant-induced-cardiomyopathy. However the data presented in chapter 3 displayed no induction of foetal genes, fibrosis, inflammation or apoptosis in this model, which conflicted with previous reports [224, 315, 331]. As both a greater dose of Iso and a prolonged time period of administration was utilised in this model compared to previous reports [312, 313, 314], it was plausible that a different cardiac response was activated, which could elicit the responses observed. Therefore, further study of this model was necessary to understand the causes of β-stimulant-induced cardiomyopathy.

As very few structural changes to the myocardium were observed in this model, it was conceivable that Iso was inducing functional modifications, which might be reversed if the Iso was removed. There are several clinical cases of recoverable cardiomyopathies in which cardiac dysfunction is reversed, including TIC, SIC or myocardial stunning/hibernation [50, 334]. Both TIC and SIC are relevant to this model of β-stimulant-induced cardiomyopathy as tachycardia is observed in β-stimulant-induced cardiomyopathy, whilst elevated circulating levels of catecholamines have been recorded in SIC patients and are proposed to induce SIC [334]. Unfortunately, the causes of these clinical conditions remain unknown although alterations in metabolism, ischemia and oxidative stress pathways, β-AR expression and/or calcium handling have been proposed [50, 60,

[335]. These changes are functional adaptations rather than structural modifications and furthermore have been reported to be distorted after Iso infusion [300, 301, 302], pathological hypertrophy [80, 207, 251, 261] and in HF [22, 205, 206, 207, 210, 263].

Rats infused with Iso exhibited diminished LV FA and glucose metabolism [302] whilst systemic β-AR stimulation increased lipolysis with increased lipid uptake and oxidation [336, 337]. It was proposed that excessive amounts of catecholamines for a prolonged period may affect myocardial lipid homeostasis [335]. In addition, depleted energy stores have been reported in TIC patients [50] whilst SIC patients exhibited reduced uptake of FAs and glucose [338, 339]. Therefore, β-stimulant-induced cardiomyopathy could be associated with abnormal metabolism.

It was proposed that chronic rapid HRs may result in ischemia which may induce reversible ventricular dysfunction [50]. In addition, ROS production and activation of oxidative stress pathways are often observed in ischemia-related cardiomyopathies [207, 263] and have additionally been reported in chronically Iso-infused rats [301]. Nuclear factor erythroid 2–related factor 2 (Nrf2)-induced genes, triggered by oxidative stress were reported to be increased in SIC patients [60, 340]. Collectively, these reports suggest that there could be alterations in the expression of ischemic and oxidative stress markers in this model of β-stimulant-induced cardiomyopathy.

Desensitisation of ARs has been previously reported alongside altered ratios of β1-AR : β2-AR expression in samples obtained from HF patients, preclinical models of HF and after chronic Iso infusion [22, 210, 222, 300]. Additionally, diminished calcium transients and decreased SR calcium content were observed in an acute model of Iso infusion [299]. SIC patients exhibited calcium

mishandling with altered expression of the functional proteins involved in this process [341] and it has been proposed that transient contractile dysfunction associated with SIC could be due to decreased calcium handling [59].

It was therefore hypothesised that 4 weeks infusion of Iso may excessively stimulate β-ARs, leading to β-AR desensitisation and calcium overload, decreasing cardiac contractility. Additionally, the reported effects of Iso on oxidative stress and metabolic pathways suggested that changes in metabolism and oxidative stress-related pathways may also contribute to the progression of β-stimulant-induced cardiomyopathy. With these functional adaptations proposed to induce β-stimulant-induced cardiomyopathy, it was further hypothesised that removal of Iso might therefore lead to recovery of the dysfunctional myocardium and an improvement in cardiac function.

Thus the aim of this chapter was to determine the mechanisms that contribute to the phenotype observed in this model of β-stimulant-induced cardiomyopathy, induced by Iso infusion. After determining whether the phenotype was reversible by Iso removal, analysis of the β-AR signalling cascade and metabolic pathways as well as the ischemic and oxidative stress networks were performed using WT C57Bl/6 mice infused with Iso for 4 weeks.

4.2 Results

4.2.1 Iso-induced cardiac dysfunction appears to be reversible in WT mice.

A pilot study was designed and performed to initially test the hypothesis that the cardiac phenotypes observed after Iso infusion were caused by functional and potentially reversible changes within the myocardium. Preceding minipump implantation, echocardiography was performed in WT mice, followed by

implantation of minipumps infusing saline or Iso (**figure 4.1**). Echocardiographic parameters were re-measured 4 weeks after implantation followed by surgical exchange of the active minipumps (within the mice) to ineffective minipumps, thereby removing the source of the saline or Iso infusion (due to project licence regulations). As it was unknown how quickly the echocardiographic parameters would change after minipump exchange (if at all) echocardiography was performed daily until the echocardiographic parameters in Iso-treated animals were stable for 3 consecutive days after Iso removal (**figure 4.1**). Mice were harvested the day after 3 consistent echocardiographic readings.

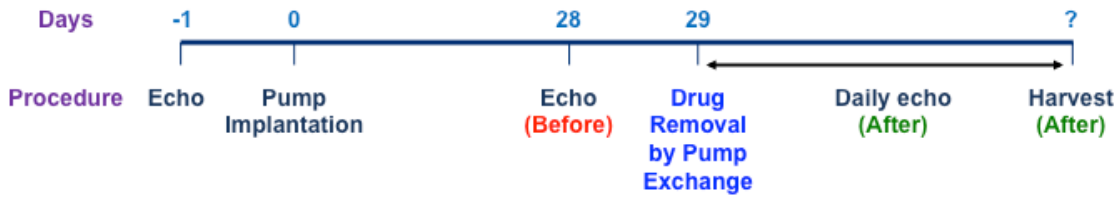

Figure 4.1 Timeline for pilot study for minipump exchange experiments. This study aimed to investigate how quickly the cardiac phenotype after Isoprenaline (Iso) infusion was reversible. 10– 11 –week-old WT (C57Bl/6) male mice (24 - 27 g) were subjected to echocardiography (echo) measurements pre-implantation. Next day, the mice were fitted with minipumps infusing 50 mg/kg/day Iso or saline. 4 weeks later, echo measurements were performed. The following day, the minipumps in the mice were exchanged with ineffective minipumps. Echo measurements were performed daily after minipump exchange until echo measurements were consistent for 3 days. The day after this was achieved, the mice were harvested. 'Before' refers to parameters measured before minipump exchange whilst 'After' signifies measurements recorded after minipump exchange.

As described in **section 3.2.2.3**, 2 methods of anaesthetised echocardiography were performed on these mice. Mice were anaesthetised using 1.5% ISF in which differences in the HR were noted between saline- and Iso-infused mice (method 1) and using different percentages of ISF (1% for saline-infused mice and 2% for Iso-treated mice) to attain HRs between 450 and 550 bpm (method 2).

Although the numbers of experimental replicates were too low to analyse the data statistically (saline, *n* = 1; Iso, *n* = 3), the echocardiographic data using method 1 (**figure 4.2**) demonstrated increases in LVPWd, LV mass and HR 28 days after Iso infusion (before minipump exchange), compared to saline-treated mice, suggesting that Iso infusion induced tachycardia and thickened walls (**figure 4.2b, e, f**). Using method 2, 4 weeks of Iso infusion induced LV chamber dilatation, cardiac dysfunction and heart weight gain as suggested by increased LVIDd, LV mass and decreased FS **(figure 4.3c, d, e),** compared to saline-treatment. However, 1 day after minipump removal, these changes in echocardiographic parameters described above using both echocardiographic methods were no longer present and similar values for all parameters were detected in saline- and Iso- treated mice. These findings suggested potential recovery of tachycardia, LV chamber dilatation, cardiac dysfunction and heart weight gain after removal of Iso.

The changes in echocardiographic parameters using both echocardiographic methods, in Iso treated mice 1 day after minipump exchange (day 30) remained consistent for the following 2 days (**figures 4.2 and 4.3**). Therefore, mice were harvested 4 days after minipump exchange (**table 4.1**). Heart and lung weight appeared greater in Iso-treated mice compared to saline-treated mice, potentially suggesting that Iso-induced heart weight gain and pulmonary congestion may not be recoverable 4 days after minipump exchange.

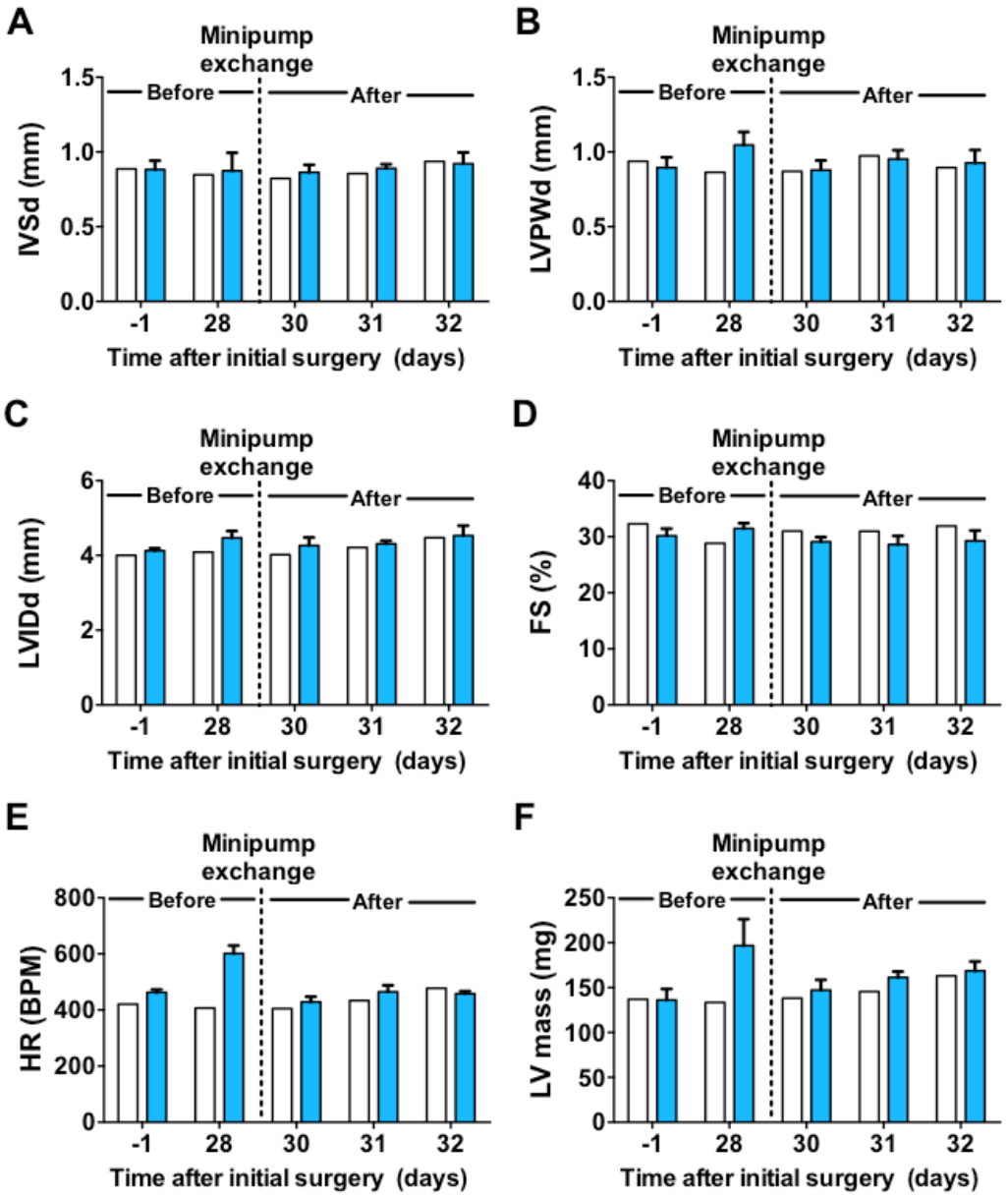

Figure 4.2 Tachycardia and heart weight were potentially recoverable 1 day after removal of Iso.

Echocardiographic parameters using 1.5% isoflurane were determined before (-1), after 4 weeks infusion (day 28) of saline or Iso (Before minipump exchange) and 1,2 and 3 days (days 30, 31, 32) after drug removal by minipump exchange (After). A, IVSd = End-diastolic interventricular septal wall thickness. B, LVPWd = End-diastolic left ventricular posterior wall thickness. C, LVIDd = End-diastolic left ventricle internal dimension. D, FS = Fractional shortening. E, HR = Heart rate. F, LV mass. Before minipump exchange, tachycardia and increased LV mass were observed in Iso-treated mice. However 1 day after pump exchange, the tachycardia and increased LV mass were potentially abolished. Saline-treated mice (open bars) *n*= 1, Iso-treated mice (blue bars) *n*= 3.

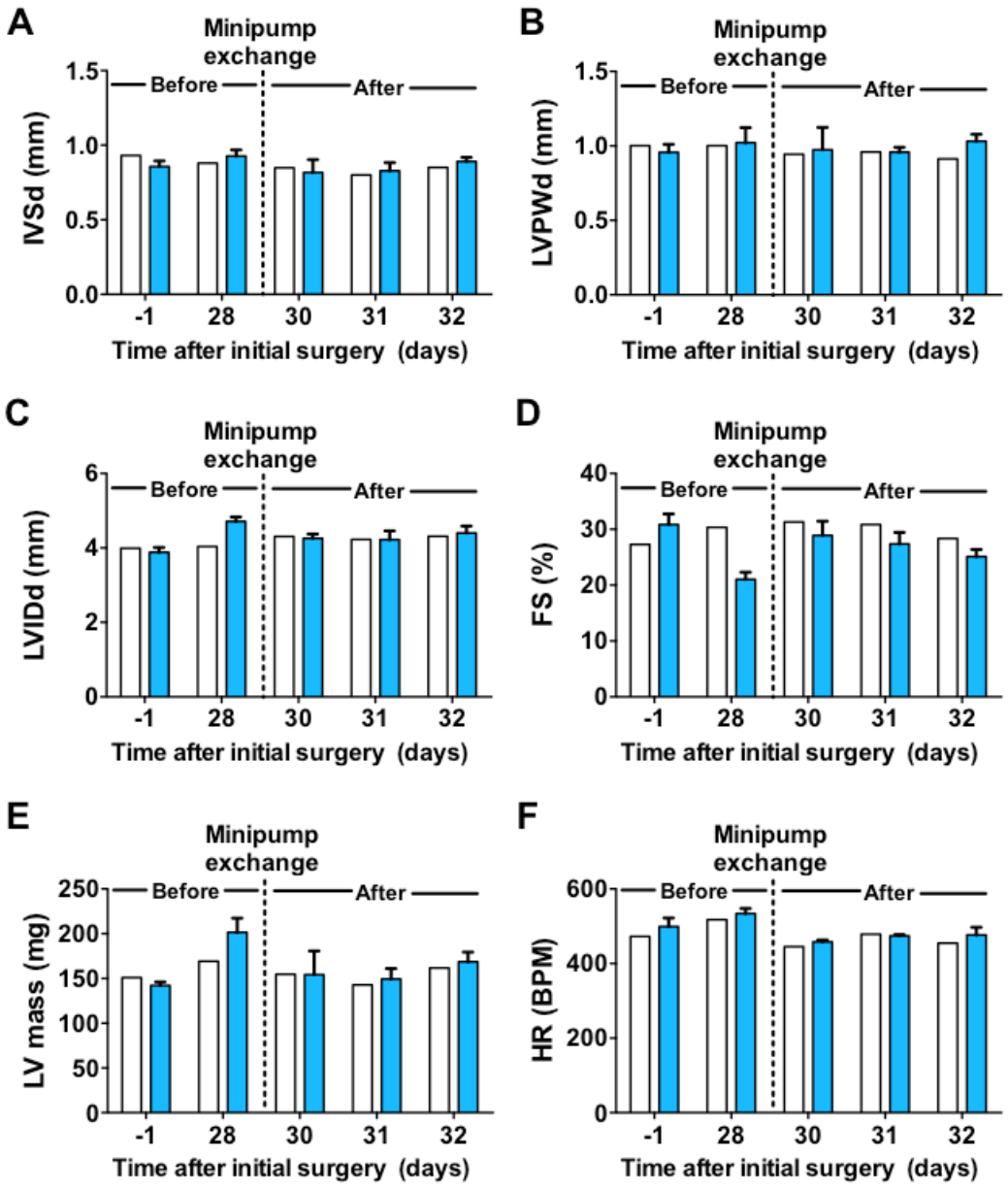

Figure 4.3 Cardiac dysfunction and chamber dilatation were potentially recoverable 1 day after removal of Iso.
Echocardiography was performed to achieve heart rates (HR) between 450 and 550 bpm in mice, before (-1) and after 4 weeks infusion (day 28) of saline or Iso (Before (minipump exchange)) and 1, 2 and 3 days (days 30, 31, 32) after drug removal by minipump exchange (After). A, IVSd = End-diastolic interventricular septal wall thickness. B, LVPWd = End-diastolic left ventricular posterior wall thickness. C, LVIDd = End-diastolic left ventricle internal dimension. D, FS = Fractional shortening. E, HR = Heart rate. F, LV mass. Before minipump exchange, cardiac dysfunction and chamber dilatation were observed in Iso-treated mice. However 1 day after pump exchange, the cardiac dysfunction and chamber dilatation were potentially reversed. Saline-treated mice (open bars) *n*= 1, Iso-treated mice (blue bars) *n*= 3.

Table 4.1 Body and heart weight gain were observed 4 days after Iso removal.
Physiological parameters were measured from mice after 4 days after removal of saline or Iso by minipump exchange. Increased body weight and heart weight were observed in Iso-infused mice compared to saline-treated mice. Saline-treated mice *n*= 1, Iso-treated mice *n*= 3.

Physiological parameters	Saline (*n* = 1)	Iso (*n* = 3)
Body weight (g)	30.90	31.03 ± 0.07
Tibia length (mm)	17.80	17.50 ± 0.15
Heart weight (mg)	159.70	174.50 ± 1.99
Lung weight (mg)	153.10	171.33 ± 1.07
Liver weight (mg)	1517.10	1511.53 ± 59.29
Heart weight / tibia length (mg/mm)	8.97	9.97 ± 0.14
Lung weight / tibia length (mg/mm)	8.60	9.79 ± 0.15

This pilot study suggested that changes in the myocardium induced by Iso infusion could be reversed within 24 hours of Iso removal. Therefore this experiment was repeated with sufficient mice to analyse the data statistically (**figure 4.4**). Similar to the initial study, mice were again subjected to echocardiographic and physiological analysis prior to implantation of minipumps infusing either saline or Iso and again 4 weeks after implantation. Minipumps were exchanged and echocardiography was performed 1 day after minipump exchange. The mice were harvested the following day. An additional cohort of mice were implanted with minipumps and were harvested 29 days after minipump implantation to enable comparison of physiological parameters before and after minipump exchange (**figure 4.4**). Echocardiographic and physiological measurements taken before minipump exchange were termed ‘before’ and those obtained after minipump exchange were labelled ‘after’ (**figure 4.4**).

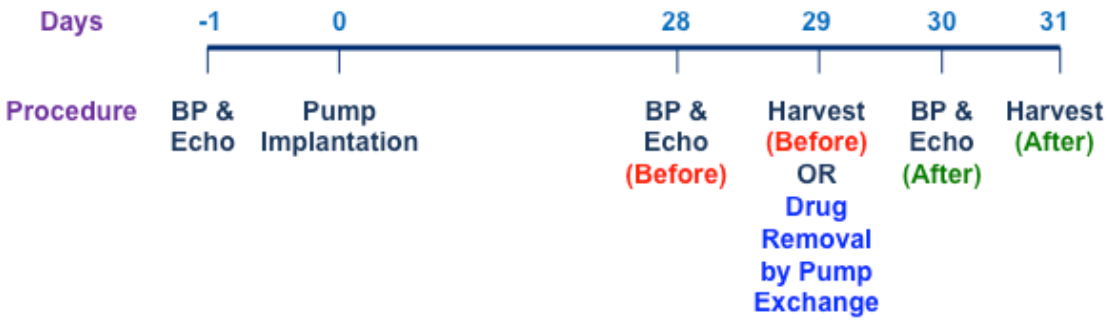

Figure 4.4 Timeline of *in vivo* procedures for drug removal by pump exchange study.
To determine if the cardiac phenotype after Isoprenaline (Iso) infusion was reversible, 10– 11 –week-old WT (C57Bl/6) male mice (24 - 27 g) were subjected to anaesthetised echocardiography (echo) and blood pressure (BP) measurements pre-implantation. Next day, the mice were fitted with minipumps infusing 50 mg/kg/day Iso or saline. 4 weeks later, echo and BP measurements were performed. Next day, half of the mice were sacrificed and physiological parameters were measured. The minipumps in the remaining mice were exchanged with ineffective minipumps. Echo and BP measurements were performed the following day on these mice. The day after, the mice were harvested. 'Before' refers to parameters measured before minipump exchange whilst 'After' signifies measurements recorded after minipump exchange.

4.2.1.1 Tachycardia and cardiac dysfunction recovered 1 day after removal of Iso.

Prior to minipump implantation, the mice were divided into 2 groups and anaesthetised echocardiographic and physiological measurements were similar between these 2 groups (**table 4.2**).

Table 4.3 includes the echocardiographic data 28 days after minipump implantation of all the mice in this study, including the mice that were harvested on day 29. Iso-treated mice mice exhibited increased systolic and diastolic BP, LVPWd and LV mass, decreased EF and FS and increased HR, compared to saline-treated mice. Changes in LVIDd were not observed after Iso treatment, suggesting that chamber dilatation was not observed in Iso-treated mice, though the LVIDs was increased after Iso treatment.

Table 4.2 No difference in echocardiographic or physiological parameters prior to minipump implantation in WT mice.
Anaesthetised echocardiography was performed on 10-11-week-old WT mice to assess cardiac structure and function. No differences were observed in all echocardiographic or physiological parameters at baseline. Data were analysed by student's t-test. BP = Blood pressure, IVSd = End-diastolic interventricular septal wall thickness, IVSs = End-systolic interventricular septal wall thickness, LVPWd = End-diastolic left ventricular posterior wall thickness, LVPWs = End-systolic left ventricular posterior wall thickness, LVIDd = End-diastolic left ventricle internal dimension, LVIDs = End-systolic left ventricle internal dimension, EF = Ejection fraction, FS = Fractional shortening, HR = Heart rate. n.s = no significance.

Parameters	WT Saline (*n*= 12)	WT Iso (*n*= 12)	*P* value	Significance
Body weight (g)	24.50 ± 0.19	24.58 ± 0.23	0.68	n.s
Systolic BP (mmHg)	99.02 ± 3.89	95.37 ± 3.88	0.51	n.s
Diastolic BP (mmHg)	72.60 ± 3.60	66.82 ± 2.74	0.21	n.s
IVSd (mm)	0.92 ± .03	0.86 ± 0.02	0.12	n.s
IVSs (mm)	1.34 ± 0.05	1.26 ± 0.05	0.26	n.s
LVPWd (mm)	1.00 ± 0.03	0.98 ± 0.04	0.61	n.s
LVPWs (mm)	1.24 ± 0.02	1.26 ± 0.04	0.67	n.s
LVIDd (mm)	3.77 ± 0.07	3.84 ± 0.06	0.39	n.s
LVIDs (mm)	2.61 ± 0.06	2.64± 0.06	0.73	n.s
EF (%)	59.28 ± 1.10	60.06 ± 0.99	0.60	n.s
FS (%)	30.92 ± 0.74	31.50 ± 0.66	0.57	n.s
HR (BPM)	468.58 ± 5.15	475.96 ± 9.34	0.50	n.s
LV mass (mg)	137.83 ± 4.90	134.96 ± 5.84	0.66	n.s

Besides this anomaly, these Iso-infused mice were considered to be representable of β-stimulant-induced cardiomyopathy with observations of tachycardia, thickened walls, hypertension and cardiac dysfunction. Therefore 50% of mice were harvested for physiological parameters before minipump exchange.

Table 4.3 Echocardiographic data 28 days after minipump implantation
Anaesthetised echocardiography and blood pressure (BP) measurements were performed on WT mice 4 weeks after saline or Iso infusion. Iso induced hypertension, elevated LV mass, tachycardia and cardiac dysfunction. Saline-treated mice n= 12, Iso-treated mice (blue bars) n= 12. Data were analysed by student's t-test. *p<0.05. BP = Blood pressure, IVSd = End-diastolic interventricular septal wall thickness, IVSs = End-systolic interventricular septal wall thickness, LVPWd = End-diastolic left ventricular posterior wall thickness, LVPWs = End-systolic left ventricular posterior wall thickness, LVIDd = End-diastolic left ventricle internal dimension, LVIDs = End-systolic left ventricle internal dimension, EF = Ejection fraction, FS = Fractional shortening, HR = Heart rate.

Parameters		WT Saline (*n*= 12)	WT Iso (*n*= 12)
Physiological parameters	**SBP (mmHg)**	99.09 ± 2.86	128.24 ± 4.89 *
	DBP (mmHg)	69.92 ± 2.53	98.61 ± 4.69 *
Echocardiographic parameters using 1.5% ISF	**IVSd (mm)**	0.87 ± 0.03	0.96 ± 0.04
	IVSs (mm)	1.24 ± 0.03	1.31 ± 0.05
	LVPWd (mm)	0.99 ± 0.03	1.10 ± 0.03 *
	LVPWs (mm)	1.34 ± 0.04	1.39 ± 0.04
	LVIDd (mm)	4.12 ± 0.08	4.25 ± 0.11
	LVIDs (mm)	2.86 ± 0.08	3.12 ± 0.13
	EF (%)	58.61 ± 1.16	52.83 ± 2.17 *
	FS (%)	30.69 ± 0.78	27.07 ± 1.34 *
	HR (BPM)	436.83 ± 11.46	624.96 ± 9.92 *
	LV mass (mg)	152.35 ± 5.75	186.09 ± 11.20 *
Echocardiographic parameters using 1-2% ISF to achieve similar HR	**IVSd (mm)**	0.83 ± 0.04	0.91 ± 0.04
	IVSs (mm)	1.25 ± 0.05	1.15 ± 0.05
	LVPWd (mm)	1.04 ± 0.02	1.09 ± 0.14
	LVPWs (mm)	1.33 ± 0.03	1.35 ± 0.05
	LVIDd (mm)	4.11 ± 0.04	4.34 ± 0.11
	LVIDs (mm)	2.83 ± 0.04	3.34 ± 0.10 *
	EF (%)	59.27 ± 1.06	46.84 ± 1.37 *
	FS (%)	31.13 ± 0.72	23.30 ± 0.80 *
	HR (BPM)	471.29 ± 8.18	532.04 ± 7.16 *
	LV mass (mg)	152.24 ± 8.31	186.22 ± 9.34 *

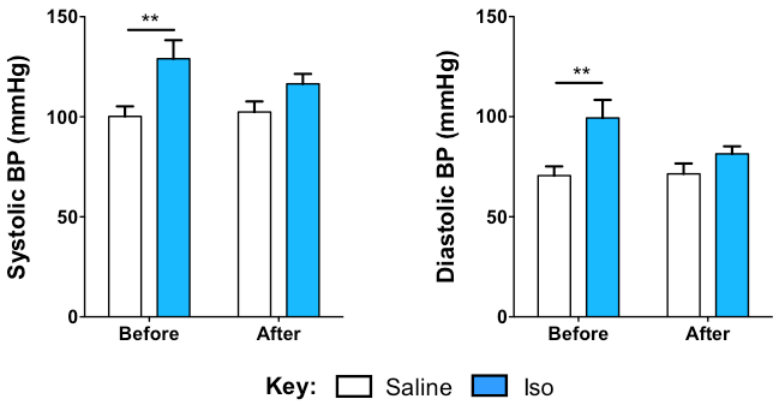

Figure 4.5 Loss of hypertension after removal of Iso.
Blood pressure (BP) of mice were measured after 4 weeks infusion of saline or Iso (Before (minipump exchange)) and 1 day after drug removal by minipump exchange (After). Iso caused hypertension before minipump exchange, however 1 day after its removal, there were no differences in BP parameters between saline- and Iso- treated mice. Saline-treated mice (open bars), Iso-treated mice (blue bars). *n*= 6 for all groups. Data analysed by paired two-way ANOVA with bonferroni's post-hoc test. ***p*<0.01.

Figures 4.5 - 4.7 display the echocardiographic and physiological parameters of the mice that underwent minipump exchange to directly compare mice before and after minipump exchange and to establish the effects of Iso removal. As expected, 4 weeks of Iso infusion (before minipump exchange) induced hypertension compared to saline-treated mice (**figure 4.5**). Interestingly, 1 day after minipump exchange, there were no significant differences in systolic and diastolic BP in the Iso-infused mice compared to saline-treated mice.

Similar to the pilot study, echocardiography method 1 demonstrated an increase in HR (**figure 4.6e**), LVPWd (**figure 4.6b**) and LV mass (**figure 4.6f**) in mice infused with Iso before minipump exchange, compared with saline-infused mice, suggesting tachycardia and cardiac hypertrophy. However 1 day after drug removal by minipump exchange, there were no significant differences in these parameters between saline- and Iso- treated mice. The HR in Iso-treated mice was significantly lowered after minipump exchange, compared to the HR before minipump exchange, indicating that the tachycardia was reversed.

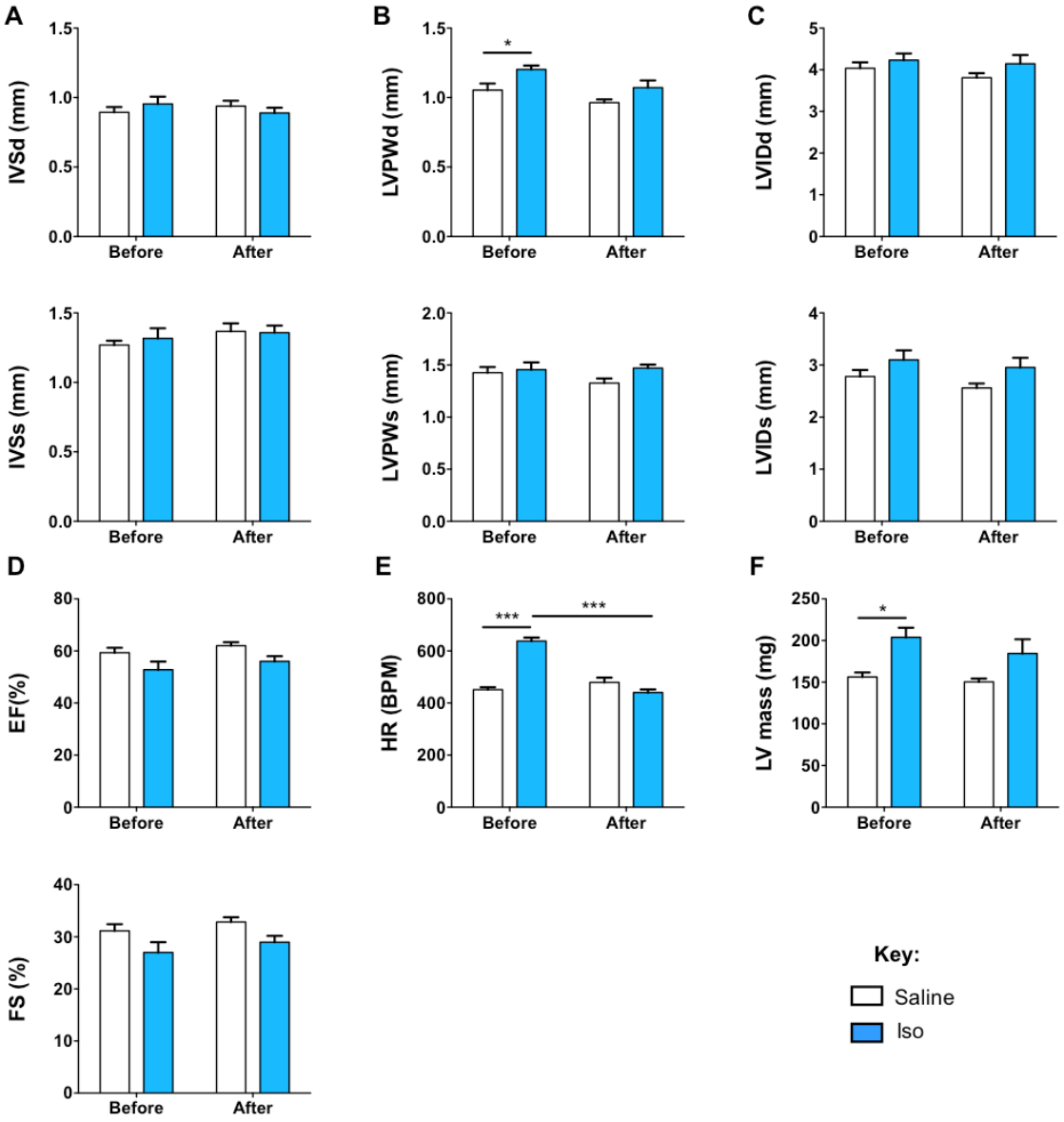

Figure 4.6 Removal of Iso eliminated tachycardia.
Echocardiographic parameters using 1.5% isoflurane were determined after 4 weeks infusion of saline or Iso (Before (minipump exchange)) and 1 day after drug removal by minipump exchange (After). A, IVSd = End-diastolic interventricular septal wall thickness, IVSs = End-systolic interventricular septal wall thickness. B, LVPWd = End-diastolic left ventricular posterior wall thickness, LVPWs = End-systolic left ventricular posterior wall thickness. C, LVIDd = End-diastolic left ventricle internal dimension, LVIDs = End-systolic left ventricle internal dimension. D, EF = Ejection fraction, FS = Fractional shortening. E, HR = Heart rate. F, LV mass. Before minipump exchange, tachycardia, increased LV mass and cardiac dysfunction were observed in Iso-treated mice. However 1 day after pump exchange, the tachycardia was abolished. Saline-treated mice (open bars), Iso-treated mice (blue bars). *n*= 6 for all groups. Data analysed by paired two-way ANOVA with bonferroni's post-hoc test. **p*<0.05, ***p*<0.01, ****p*<0.001.

Using the second method of echocardiography, LVIDs (**figure 4.7c**) and LV mass (**figure 4.7f**) were increased in Iso-infused mice, compared to saline-treated mice. EF and FS were decreased before minipump exchange (**figure 4.7d**) in Iso treated mice compared with saline-infused mice, suggesting cardiac dysfunction. However after minipump exchange, these parameters were no longer different between saline- and Iso- treated mice, with a significant change in LVIDs, EF and FS parameters in Iso-treated mice before and after minipump exchange, suggesting recovery of cardiac function after Iso removal.

Therefore the data presented in this section found that tachycardia and most surprisingly, systolic function, were recoverable 1 day after minipump exchange.

4.2.1.2 Heart weight gain was not recoverable after Iso removal.

Mice were sacrificed 29 days after minipump implantation (before minipump exchange, termed Before) or 2 days after minipump exchange (referred to as After). The heart, lung and liver (tissues were harvested and weighed and the tibia lengths were recorded in order to determine any physiological variations that may be recoverable after minipump exchange (**figure 4.8**). No differences were observed in body weight, tibia length or lung weight / tibia length between saline- and Iso- treated mice before or after minipump exchange. The heart weight / tibia length ratio was increased in Iso-infused mice at both timepoints, compared to saline-treated mice (**figure 4.8c**). This finding suggested that Iso-induced heart weight gain was not recoverable 2 days after minipump exchange.

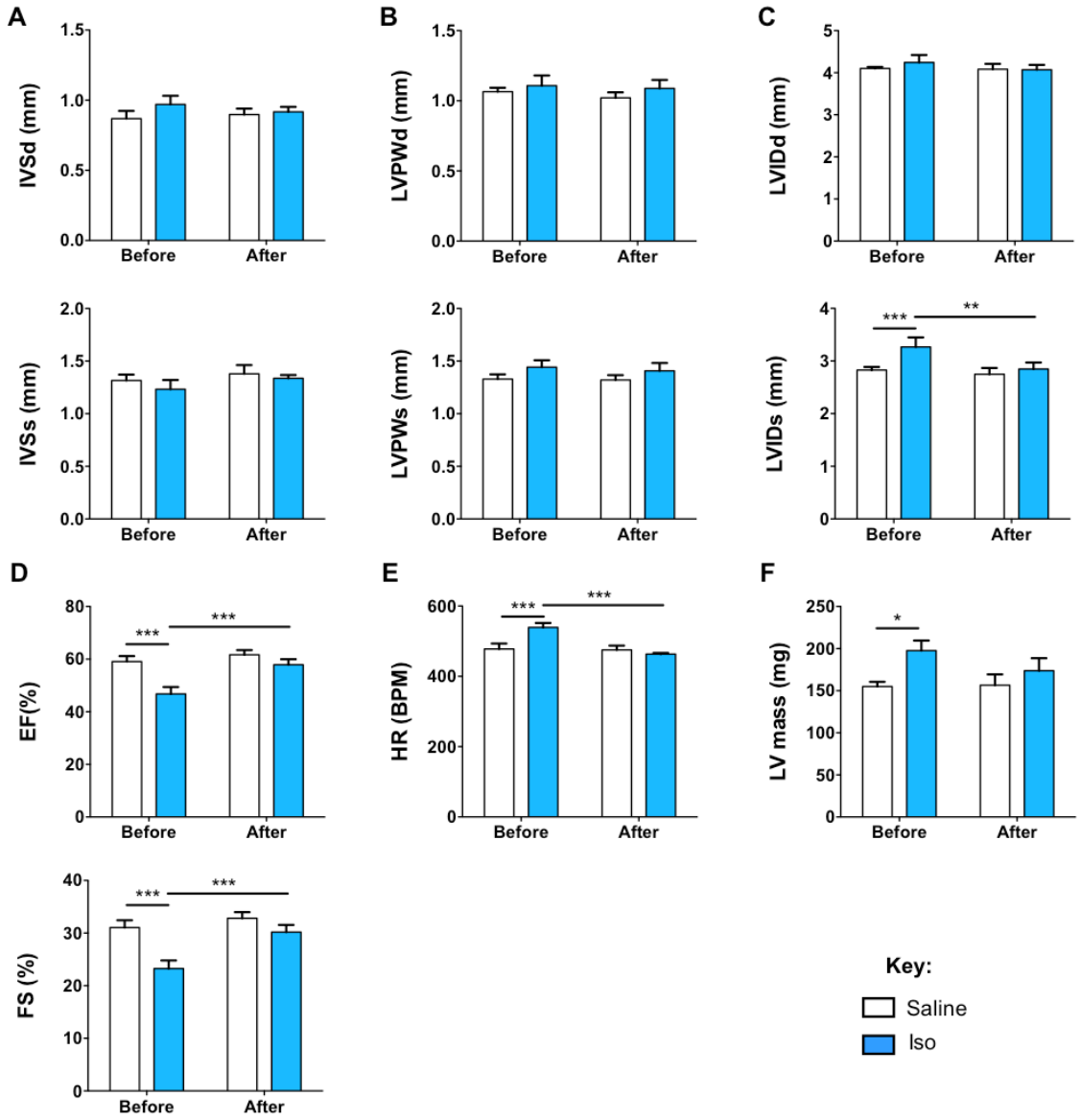

Figure 4.7 Cardiac systolic dysfunction was recovered 1 day after Iso removal.

Echocardiography was performed to achieve heart rates (HR) between 450 and 550 bpm in mice after 4 weeks infusion of saline or Iso (Before (minipump exchange)) and 1 day after drug removal by minipump exchange (After). A, IVSd = End-diastolic interventricular septal wall thickness, IVSs = End-systolic interventricular septal wall thickness. B, LVPWd = End-diastolic left ventricular posterior wall thickness, LVPWs = End-systolic left ventricular posterior wall thickness. C, LVIDd = End-diastolic left ventricle internal dimension LVIDs = End-systolic left ventricle internal dimension. D, EF = Ejection Fraction, FS = Fractional Shortening. E, HR. F, LV mass. Before minipump exchange, tachycardia and systolic cardiac dysfunction were observed in Iso-treated mice. However 1 day after pump exchange, the tachycardia and cardiac dysfunction were rescued. Saline-treated mice (open bars), Iso-treated mice (blue bars). n= 6 for all groups. Data analysed by paired two-way ANOVA with bonferroni's post-hoc test. *p<0.05, **p<0.01, ***p<0.001.

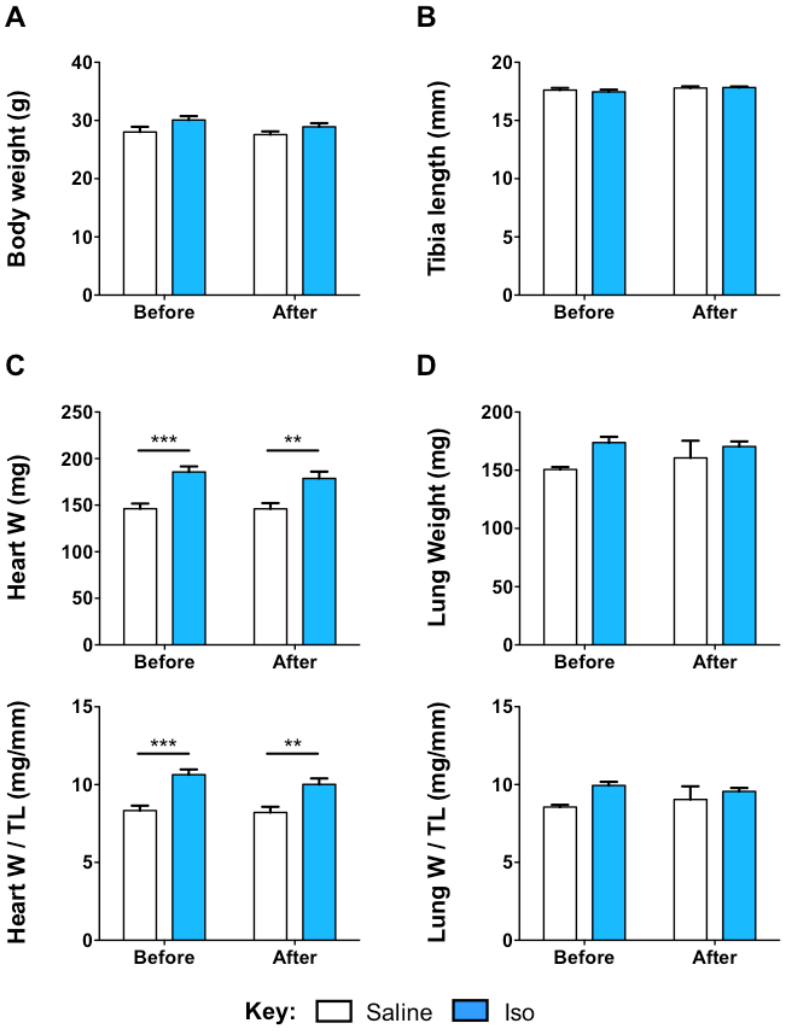

Figure 4.8 Elevated heart weight was not recoverable after Iso removal. Half of the mice were harvested 29 days after minipump infusion of saline or Iso (Before (minipump exchange) whereas the remaining mice were submitted for pump exchange. These surviving mice were harvested 2 days after pump exchange (After). Physiological parameters were measured when harvesting tissues. A, Body weight (W). B, Tibia length (TL). C, Heart W and heart W / TL. D, Lung W and lung W / TL. Heart W / TL ratio was increased before and after pump exchange in Iso-treated mice. Saline-treated mice (open bars), Iso-treated mice (blue bars). Before saline *n*= 6, Before Iso *n*= 6, After saline *n*= 6, After Iso *n*= 6. Data analysed by two-way ANOVA with bonferroni's post-hoc test. **p*<0.05, ***p*<0.01, ****p*<0.001.

Therefore the data presented in this section displayed that Iso-induced tachycardia and systolic function were recoverable 1 day after Iso removal and Iso-induced heart weight gain was not recoverable over the same timecourse. Further study is required to understand the mechanisms of this acute functional recovery (discussed further in **section 4.3.1**) though the recovery of the cardiac

function after Iso removal suggested that the causes of β-stimulant-induced cardiomyopathy were likely to be functional, transient changes that can be reversed very quickly (rather than structural amendments).

4.2.2 Investigation of calcium handling, ischemia, oxidative stress and metabolism in β-stimulant-induced cardiomyopathy in WT mice.

The data from **section 4.2.1** suggested that functional, reversible changes that can be modified very quickly were likely to be the cause of β-stimulant-induced cardiomyopathy. Therefore, the expression of β-ARs, proteins involved in calcium handling, ischemic and oxidative stress markers and metabolic indicators were evaluated in myocardial tissue after 4 weeks saline or Iso infusion, to determine their relative contribution to the development of β-stimulant-induced cardiomyopathy.

4.2.2.1 Iso induced hypertension, chamber dilatation, cardiac dysfunction and increased heart weight.

To further analyse this model of β-stimulant-induced cardiomyopathy, further heart samples were needed from additional cohorts of mice (**figure 4.9**). No differences were observed in echocardiographic and physiological parameters between the 2 groups of mice prior to minipump implantation (**table 4.4**).

Figure 4.9 Timeline of *in vivo* procedures.
10-11-week-old WT male mice (24 - 27 g) were subjected to echocardiography (echo) and BP measurements pre-implantation. Minipumps were implanted into those mice infusing Iso or saline. 4 weeks later, echo and BP measurements were performed and the mice were sacrificed the day after.

Table 4.4 Echocardiography confirms that Iso induces β-stimulant-induced cardiomyopathy.
Echocardiographic and physiological data measured pre-implantation and 4 weeks after infusion of saline and Iso. Increased body weight, hypertension, chamber dilatation, increased LV mass and cardiac dysfunction were observed in mice after 4 weeks of Iso treatment. BP = Blood pressure, IVSd = End-diastolic interventricular septal wall thickness, IVSs = End-systolic interventricular septal wall thickness, LVPWd = End-diastolic left ventricular posterior wall thickness, LVPWs = End-systolic left ventricular posterior wall thickness, LVIDd = End-diastolic left ventricle internal dimension, LVIDs = End-systolic left ventricle internal dimension, EF = Ejection fraction, FS = Fractional shortening, HR = Heart rate. *n*= 4 for all groups. Data analysed by two-way ANOVA with bonferroni's post-hoc test. $^{‡}p<0.05$ compared to pre-implantation values. $^{*}p<0.05$ compared to saline-infused mice 4 weeks post-implantation.

Parameter	Pre-implantation		4 weeks post-implantation	
	Saline (*n*= 4)	Iso (*n*= 4)	Saline (*n*= 4)	Iso (*n*= 4)
Body weight (g)	26.65 ± 0.46	26.58 ± 0.70	30.48 ± 0.89 ‡	32.52 ± 0.15 *‡
Systolic BP (mmHg)	98.80 ± 6.74	99.56 ± 6.12	95.56 ± 5.60	122.35 ± 1.64 *‡
Diastolic BP (mmHg)	69.34 ± 5.16	71.96 ± 5.29	68.16 ± 3.47	94.42 ± 1.15 *‡
IVSd (mm)	0.97 ± 0.05	0.95 ± 0.02	0.96 ± 0.04	0.98 ± 0.05
IVSs (mm)	1.63 ± 0.03	1.63 ± 0.03	1.61 ± 0.06	1.54 ± 0.03
LVPWd (mm)	0.93 ± 0.04	0.88 ± 0.02	1.04 ± 0.03	0.95 ± 0.04
LVPWs (mm)	1.47 ± 0.03	1.48 ± 0.04	1.68 ± 0.06	1.35 ± 0.15
LVIDd (mm)	3.50 ± 0.07	3.61 ± 0.04	3.47 ± 0.08	4.09 ± 0.11 *‡
LVIDs (mm)	1.77 ± 0.07	1.86 ± 0.03	1.75 ± 0.04	2.60 ± 0.16 *‡
EF (%)	81.86 ± 0.98	80.83 ± 0.53	81.93 ± 0.25	66.83 ± 2.97 *‡
FS (%)	49.65 ± 0.99	48.62 ± 0.53	49.64 ± 0.24	36.71 ± 2.21 *‡
HR (BPM)	717.73 ± 13.14	737.92 ± 4.66	754.13 ± 14.89	768.18 ± 15.58
LV mass (mg)	120.96 ± 4.45	119.65 ± 1.87	128.92 ± 9.88	157.01 ± 5.77 *‡

4 weeks after minipump infusion, Iso-infused mice exhibited β-stimulant-induced cardiomyopathy, shown by increased body weight, systolic and diastolic BP, LVIDd and LVIDs, LV mass, body weight and heart weight / tibia length ratio alongside diminished EF and FS, compared to saline-treated mice (**table 4.4** and **4.5**). Tachycardia was not observed after 4 weeks of Iso infusion (**table 4.4**), compared to saline-treated mice, though this could be due to the use of conscious echocardiography for this experiment. Furthermore, no significant

differences in lung weight were observed after Iso infusion (**table 4.5**). Samples from these mice were used for further detailed study of the mechanisms of this model, although no changes in lung weight were observed in Iso-treated mice.

Table 4.5 Body and heart weight gain were observed 4 weeks after Iso infusion.
Physiological parameters were measured from mice after 4 weeks infusion of saline or Iso. Increased body weight and heart weight were observed in Iso-infused mice compared to saline-treated mice. Data were analysed by student's t-test. $^{*}p<0.05$ compared to saline-infused mice.

Physiological parameters	Saline (*n* = 4)	Iso (*n* = 4)
Body weight (g)	30.87 ± 0.55	32.8 ± 0.36 *
Tibia length (mm)	17.37 ± 0.17	17.18 ± 0.16
Heart weight (mg)	158.34 ± 4.86	192.79 ± 8.92 *
Lung weight (mg)	160.1 ± 7.61	170.86 ± 6.35
Heart weight / tibia length (mg/mm)	9.28 ± 0.48	10.61 ± 0.21 *
Lung weight / tibia length (mg/mm)	9.24 ± 0.50	9.95 ± 0.37

4.2.3 Examination of the expression of β-ARs and proteins involved in calcium handling after Iso infusion.

To determine whether alterations in the expression of β-ARs and proteins involved in calcium handling contribute to the development of β-stimulant-induced cardiomyopathy, the expression of β-ARs and calcium handling proteins were evaluated by qRT-PCR and Western blotting.

4.2.3.1 β-AR and SERCA mRNA expression were not different after Iso infusion.

qRT-PCR was performed using LV homogenates from mice infused with saline or Iso for 4 weeks to measure the mRNA levels of 2 different β-ARs expressed in the myocardium, *Adrb1* and *Adrb2.* However, the mRNA expression of *Adrb1* and *Adrb2* was similar between mice infused with saline and Iso (**figure 4.10a**),

suggesting no changes in β-AR expression at the mRNA level after Iso treatment. Furthermore, the mRNA expression of SERCA2 (*Atp2a2*) was evaluated using these samples. However, no differences in *Atp2a2* mRNA expression were detected using these samples (**figure 4.10b**).

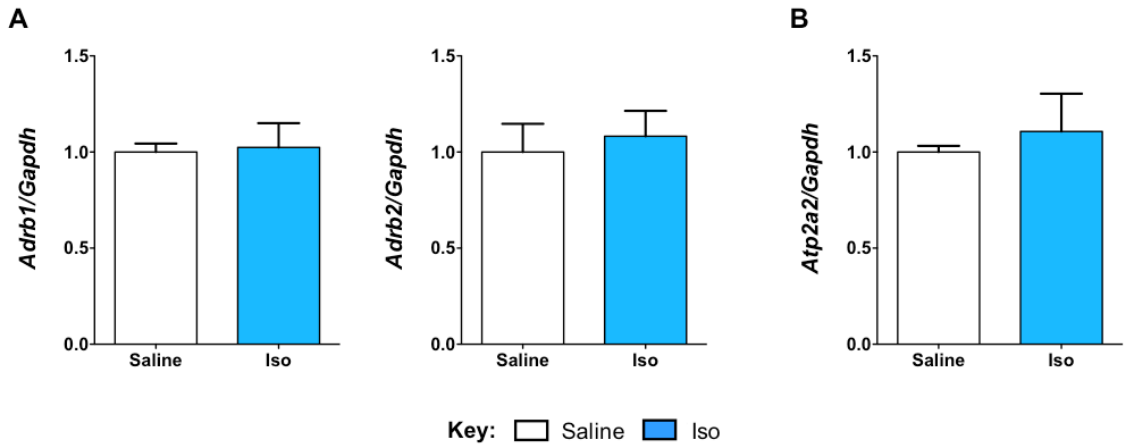

Figure 4.10 mRNA expression of β−adrenergic receptors (β−ARs) were unchanged at the mRNA levels after infusion of Iso.
qRT-PCR was performed on myocardial samples from mice infused for 4 weeks with Iso or saline, to measure the mRNA levels of proteins involved in the β-adrenergic signalling cascade. Using these samples, no differences were found in the expression of these markers. A, Expression of β-adrenergic receptors (*Adrb1* and *Adrb2*), p = 0.87 and p = 0.70, respectively. B, Expression of sarco/endoplasmic reticulum calcium ATPase (SERCA2 or *Atp2a2*), p = 0.63. n= 4. Data analysed by student's t-test.

4.2.3.1.1 Optimisation of antibodies targeting PLN.

Western blotting analysis was performed to evaluate the protein expression of calcium handling proteins, total (t)-PLN and phosphorylated (p)-PLN (Serine-16) using LV homogenates of mice treated with saline or Iso for 4 weeks. The datasheet of the antibodies for tPLN and pPLN stated that PLN exists in 2 forms, as a monomer (6 kDa) or as a phosphorylated pentamer (25 kDa). However, as **figure 4.11** illustrates, many bands were detected using the pPLN and tPLN antibodies and it was unknown which band represented the expression of PLN, although there appears to be no difference in the density of

bands using both pPLN and tPLN antibody between saline- and Iso- treated mice.

Western blotting was therefore performed using LV homogenates of mice treated with saline or Iso for 4 weeks, along with LV homogenates of mice displaying HF after pressure overload and sham-operated controls (kindly provided by Dr Manabu Taneike, King's College London) (**figure 4.12**). In addition there were samples of LV homogenates that were treated with protein phosphatase 1 (PP1) to remove phosphate groups from PLN.

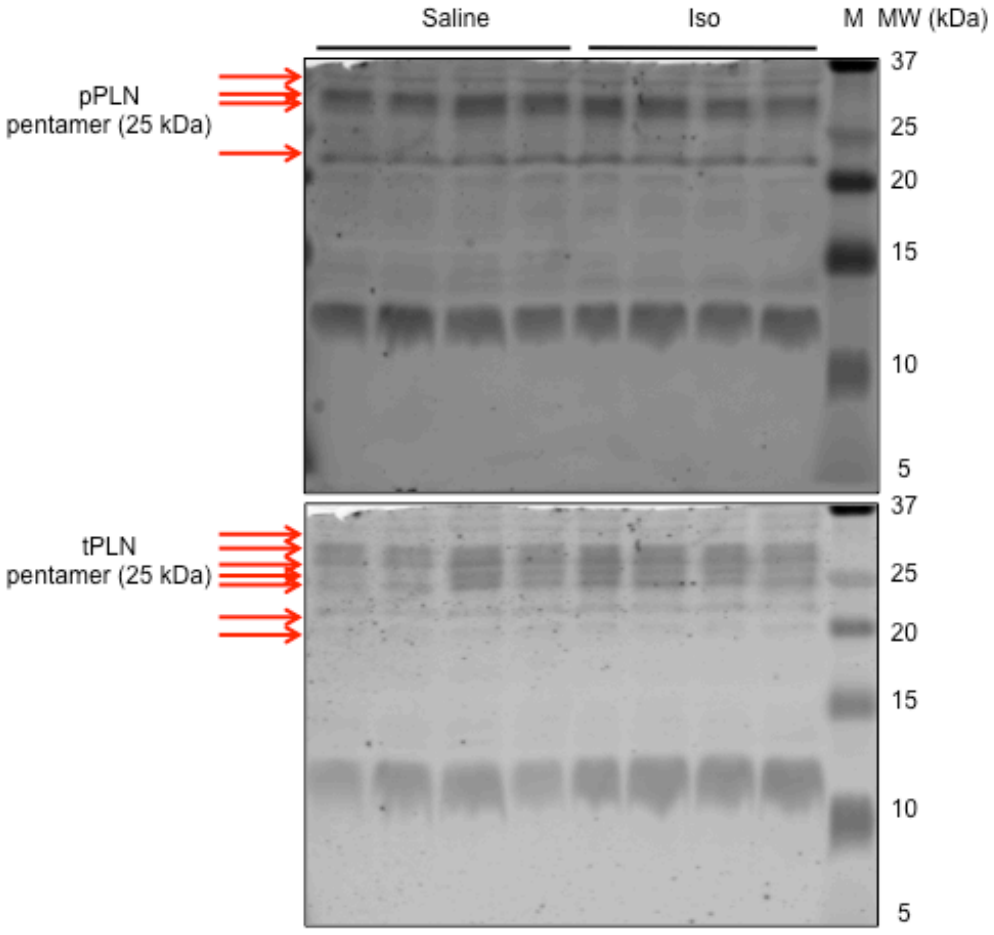

Figure 4.11 Lack of specificity of antibodies used to examine phospholamban expression and post-translational modifications.
Western blotting was performed on LV homogenates harvested from mice infused with Iso for 4 weeks to study expression of phosphorylated-phospholamban (pPLN, Ser16) and total- phospholamban (tPLN). However, many bands were observed using antibodies targeting pPLN and tPLN (illustrated by red arrows), so it was unknown which band related to PLN expression.

The sham-operated heart samples showed higher expression of a wide band at 25 kDa, with pPLN and tPLN antibodies, which was not observed in HF sample, as expected. However, this band, thought to be the pentameric form of PLN, had migrated further than the bands observed in saline- or Iso- treated mice and the intensity of this band was not reduced in PP1-treated samples. Therefore, the true bands for pPLN and tPLN could not be distinguished. Several studies have reported the observation of monomeric or dimeric PLN is at 9-12 kDa [342, 343] and a potential band was seen at this molecular weight (**figure 4.12**).

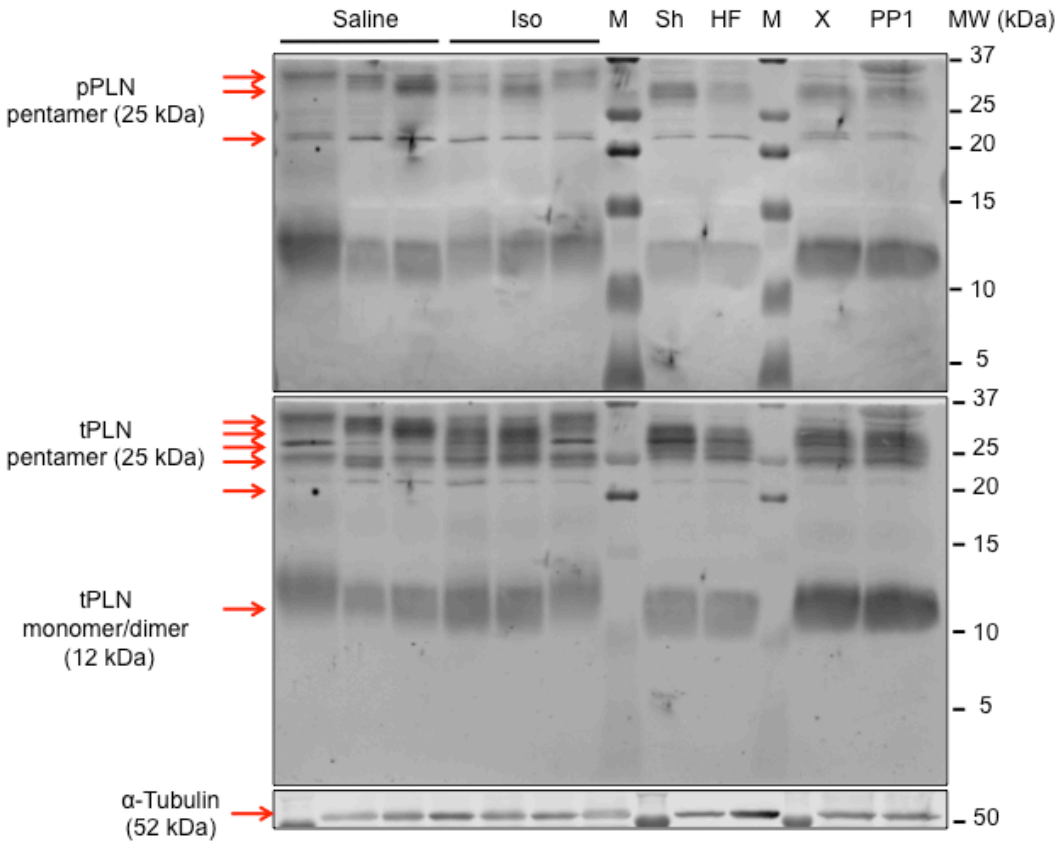

Figure 4.12 Optimisation of antibodies to study phospholamban expression.
Western blotting for phosphorylated phospholamban (pPLN, Serine-16) and total phospholamban (tPLN) were performed using samples of saline- and Iso-treated mice, sham (Sh) mice and mice with failing hearts (HF) induced by pressure overload provided by Dr Manabu Taneike (King's College London) and LV homogenates treated with protein phosphatase 1 (PP1) or untreated (X). As expected, Sh sample showed higher expression of a wide band at 25 kDa, thought to be pPLN, which was not observed in HF sample or the other samples.

4.2.3.1.2 Overexpression of PLN identified representative bands of PLN.

As bands for PLN could not be distinguished using antibodies targeting pPLN and tPLN, it was decided to overexpress PLN to determine the correct bands. My laboratory possessed a vector containing the cDNA sequence encoding murine PLN (mPLN), which was cloned into the cloning vector, pDNR-lib (**figure 4.13a**). Therefore mPLN was subcloned into the mammalian expression vector, pCMV-Sport6 (**figure 4.13b, c**), generating pCMV-Sport6-PLN, which was transfected into HEK293A cells. 24 and 48 hours after transfection, protein was isolated and Western blotting was performed to study pPLN and tPLN expression (**figure 4.13d**). SDS-PAGE was performed with different amounts of protein (20 µg or 40 µg) and different methods of incubating of protein denaturation (95^{o}C for 5 minutes, or RT for 30 minutes). Dose- and time-dependent bands were observed using the tPLN antibody, representing the monomeric (12 kDa) and pentameric (25 kDa) forms of PLN. Faint bands were detected with pPLN (Serine-16) antibody at equivalent positions to those seen with tPLN antibody. Therefore the bands representing pentameric pPLN, pentameric tPLN and monomeric tPLN were identified (**figure 4.14**).

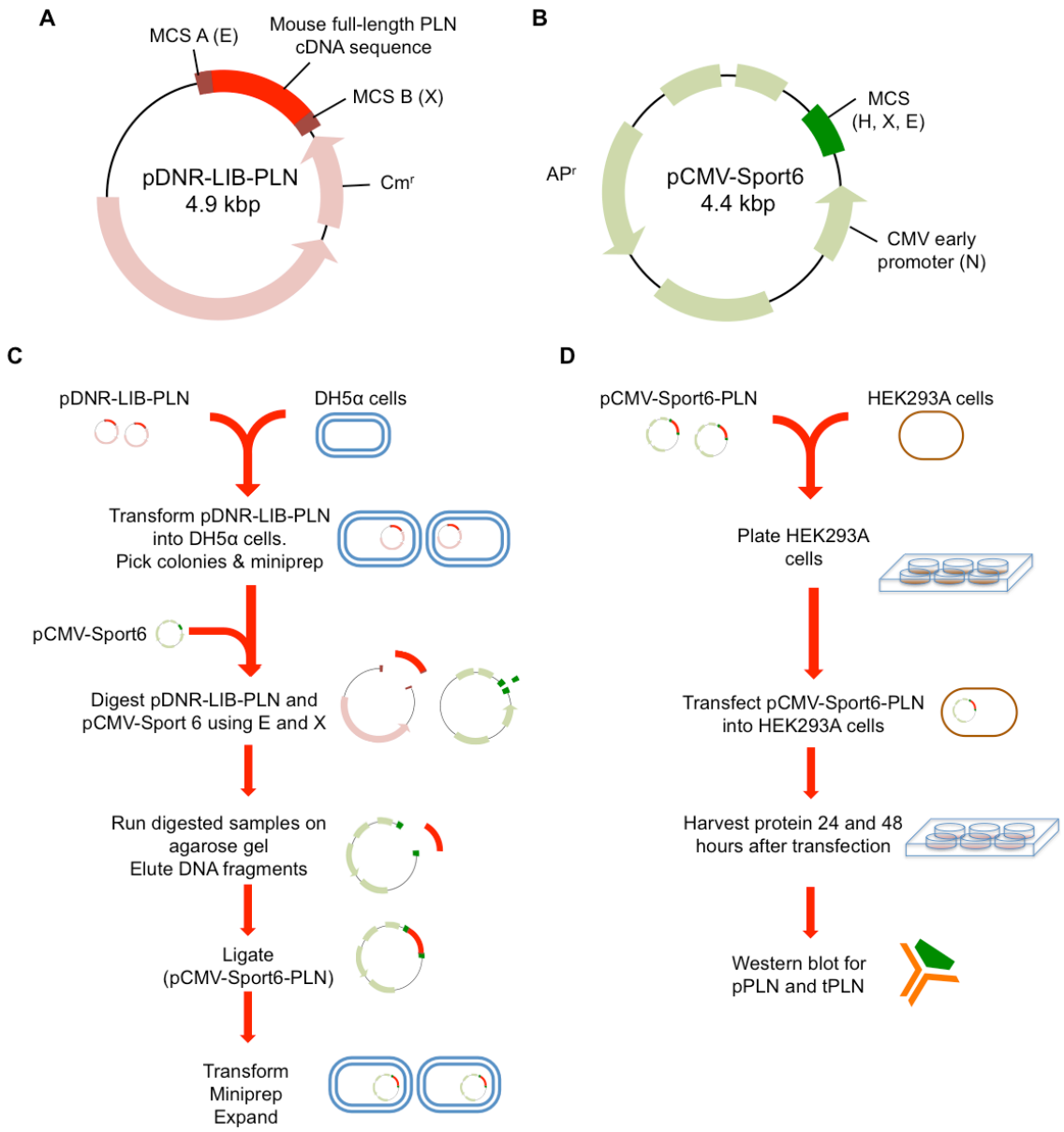

Figure 4.13 Vectors utilised and procedures followed to overexpress phospholamban in HEK293A cells.
A, pDNR-LIB-PLN vector contained chloramphenicol resistance, multiple cloning sites (MCS) which included restriction enzyme (RE) sites for *Eco*RI (E) and *Xho*I (X) and the cDNA sequence encoding murine phospholamban (PLN). B, pCMV-Sport6 vector possessed ampicillin resistance, MCS that contained RE sites for E, X and *Hin*dIII (H) and the CMV early promoter possessed RE site for *Nco*I. C, Procedure used to remove PLN sequence from pDNR-LIB-PLN and insert it into pCMV-Sport6 to generate pCMV-Sport6-PLN. D, Procedure to overexpress PLN by transfecting pCMV-Sport6-PLN into HEK293A cells.

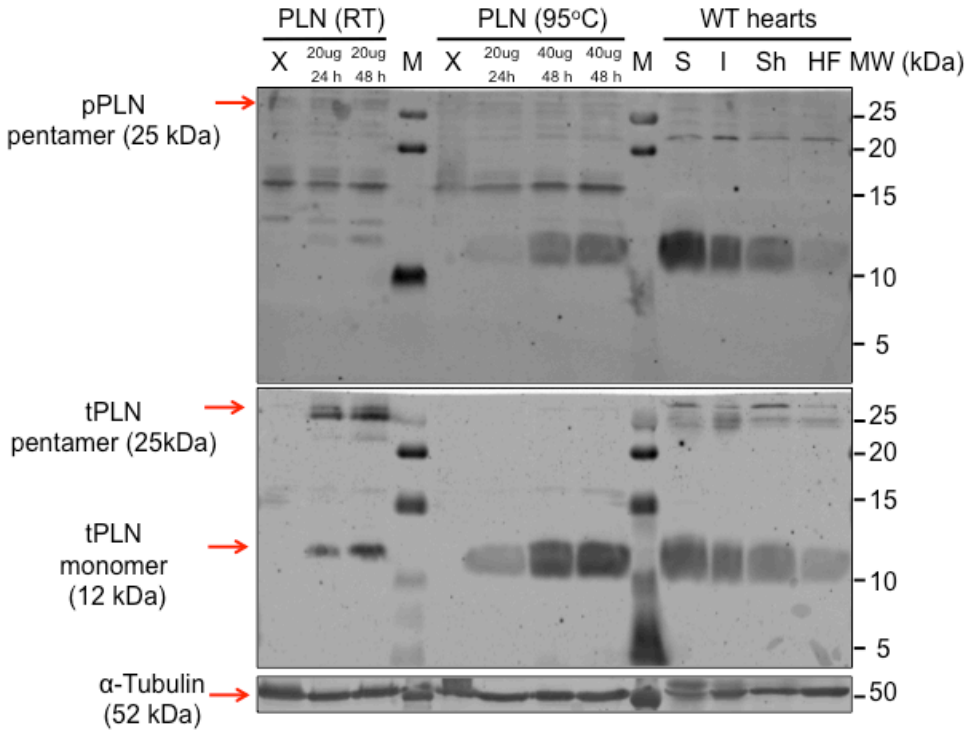

Figure 4.14 Overexpression of phospholamban.
Western blotting was performed using samples of HEK293A cells transfected with pCMV-Sport-PLN. 2 different protein amounts (20 µg or 40 µg) and different methods of denaturing the protein with loading buffer prior to gel loading were performed (95°C for 5 minutes, or room temperature (RT) for 30 minutes). In the membrane for total phospholamban (tPLN), there were clear bands that denoted monomeric (12 kDa) and pentameric (25 kDa) forms of PLN in a dose and time dependent manner. It was also found that incubating samples in loading buffer at RT for 30 minutes would yield clearer bands. Faint bands were observed with phosphorylated-phospholamban (pPLN, Ser16) antibody at same positions as tPLN membrane.

4.2.3.1.3 Expression of proteins involved in calcium handling was unchanged after Iso infusion.

Western blotting for calcium handling proteins, SERCA2, pPLN and tPLN was performed using samples of myocardial tissue harvested from mice after 4 weeks infusion of saline or Iso (**figure 4.15a**). No differences in the protein expression of SERCA2, PLN or pPLN (Serine-16), in pentameric or monomeric form were observed between saline- and Iso- treated mice (**figure 4.15**). However a tendency towards a decrease in the protein expression of SERCA2, pentameric pPLN (Serine-16) and monomeric tPLN between saline- and Iso-treated mice is observed, though further samples would be required to validate

this claim. Therefore, the findings presented in **figure 4.15** suggest that the protein expression of crucial calcium handling proteins were unchanged after the development of β-stimulant-induced cardiomyopathy.

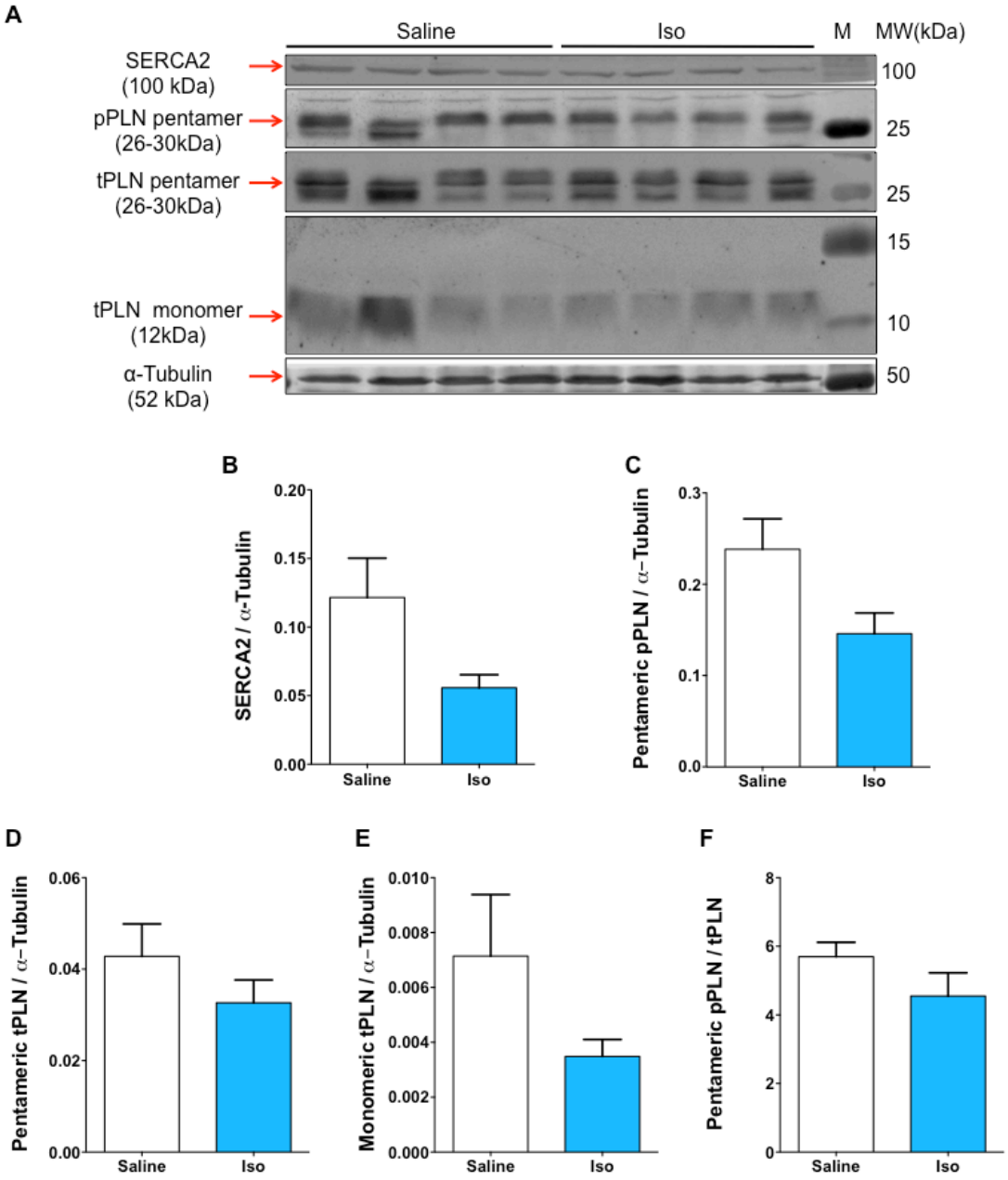

Figure 4.15 Expression of calcium handling proteins were unchanged after Iso infusion.

LV homogenates from mice infused with Iso for 4 weeks were used to determine protein levels of calcium handling proteins - Sarcoplasmic/ endoplasmic reticulum calcium ATPase (SERCA)-2, phosphorylated phospholamban (pPLN, Ser16) and total phospholamban (tPLN). α-Tubulin was used as a loading control. A, Membrane revealed no obvious difference in expression of calcium handling proteins. B-F, Densimetric analysis of membranes in (A). Red arrows in (A) dictate quantified bands. B, p = 0.12. C, p = 0.07. D, p = 0.29. E, p = 0.21. F, p = 0.21. Values expressed as mean ± SEM. n= 4. Data analysed by student t-test.

4.2.3.2 No differences in oxidative stress and ischemic markers after Iso infusion.

As no differences in the expression of β-ARs and calcium handling proteins were observed after Iso infusion, other hypotheses were considered. As mentioned, chronic rapid HRs are proposed to induce ischemia and chronic Iso infusion has previously been shown to cause oxidative stress [301]. Therefore to determine if there was an association between ischemia, oxidative stress and β-stimulant-induced cardiomyopathy, qRT-PCR analysis was performed to look at markers of ischemia and oxidative stress using LV homogenates harvested from mice infused with saline or Iso for 4 weeks. Indicators studied include hypoxia inducible factor 1 α (*Hif1a*), a hypoxic marker whilst heme oxygenase 1 (*Hmox1*), peroxisome proliferator-activated receptor gamma, coactivator 1 alpha (*Ppargc1a*) and superoxide dismutase 2 (*Sod2*) are markers of oxidative stress [344, 345]. However, no differences in *Hif1a, Hmox1, Ppargc1a* and *Sod2* mRNA expression were observed between mice infused with saline and Iso (**figure 4.16**), though a trend towards increased expression of *Hmox1* after Iso infusion could be suggested (p = 0.13). More samples are needed to either prove od disprove this tendency.

Analysis of the transcriptome of SIC patients demonstrated increased expression of Nrf2-induced genes compared to controls [340]. The transcription factor, Nrf2, is triggered by oxidative stress and inflammation and positively regulates the expression of a plethora of antioxidant proteins [346, 347]. Therefore the expression of Nrf2-induced genes were evaluated using LV tissue from mice infused with saline or Iso for 4 weeks.

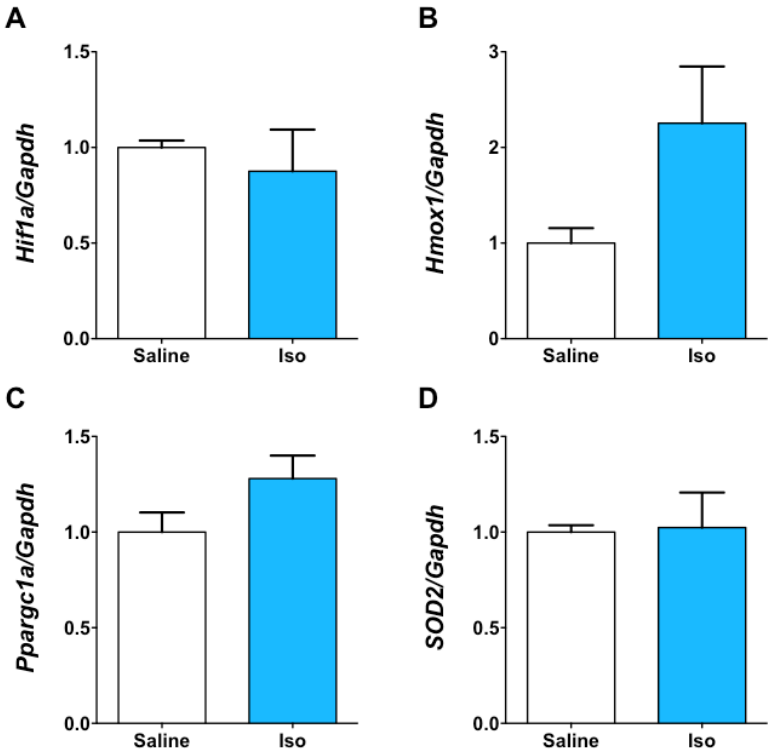

Figure 4.16 Expression of ischemic and oxidative stress markers was unchanged after Iso treatment.
qRT-PCR was performed on LV homogenates from mice after 4 weeks Iso infusion to study mRNA expression of ischemia and oxidative stress markers. A, Hypoxia inducible factor 1 α (*Hif1a*), $p = 0.61$. B, Haem oxygenase 1 (*Hmox1*), $p = 0.13$. C, Peroxisome proliferator-activated receptor Gamma, coactivator 1 Alpha (*Ppargc1a*), $p = 0.14$. D, Superoxide dismutase 2 (*Sod2*), $p = 0.91$. Using these samples, no differences were observed in the expression of these ischemic and oxidative stress markers. Glyceraldehyde 3-phosphate dehydrogenase (*Gapdh*) was used as a housekeeping gene. Values expressed as mean ± SEM. $n = 4$. Data analysed by student t-test.

Using these samples, no differences were observed in the expression of Nrf2-induced genes, glutamate—cysteine ligase (*Gclc*), glutathione S-transferase A2 (*Gsta2*) and thioredoxin reductase 1 (*Txnrd1*) between saline- and Iso- treated mice (**figure 4.17**). Together these results suggest that Iso infusion did not activate these ischemic or oxidative stress signalling pathways.

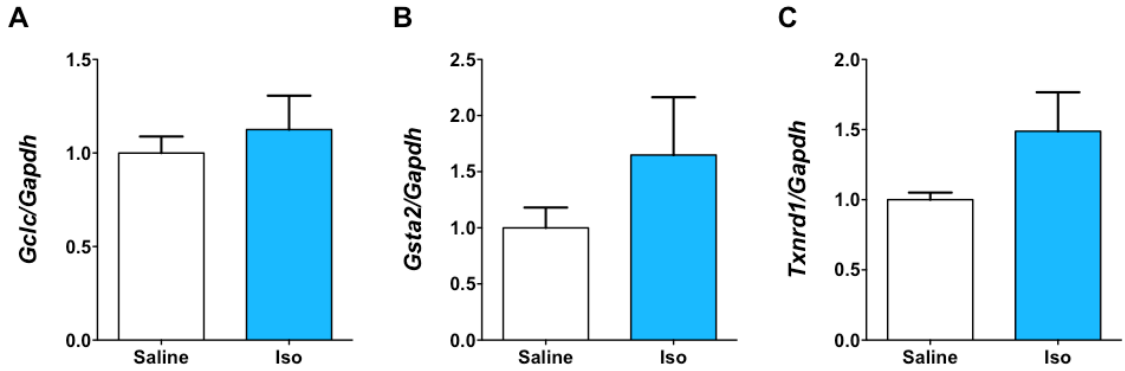

Figure 4.17 Expression of Nrf2-induced genes was unchanged after treatment of Iso.
qRT-PCR was used to measure the mRNA expression of genes upregulated by transcription factor, Nrf2 in myocardial tissue from mice after 4 weeks Iso treatment. A, Glutamate-cysteine ligase, catalytic (Gclc), p = 0.57. B, Glutathione S-transferase A2 (*Gsta2*), p = 0.32. C, Thioredoxin reductase 1 (*Txnrd1*), p = 0.18. No differences were observed in these markers in these samples. Glyceraldehyde 3-phosphate dehydrogenase (*Gapdh*) was used as a housekeeping gene. Values expressed as mean ± SEM. n= 4. Data analysed by student t-test.

4.2.3.3 Cytoskeletal protein expression were similar between mice infused with saline and Iso.

Decreased protein expression of cytoskeletal scaffolds, α-actinin, desmin and spectrin were observed in the stunned myocardium of guinea pigs [348]. Thus the protein expression of α-actinin and desmin was explored in LV homogenates harvested from mice 4 weeks after saline or Iso infusion (**figure 4.18**). There were no significant differences in cytoskeletal protein expression of α-actinin and desmin after 4 weeks infusion of saline or Iso.

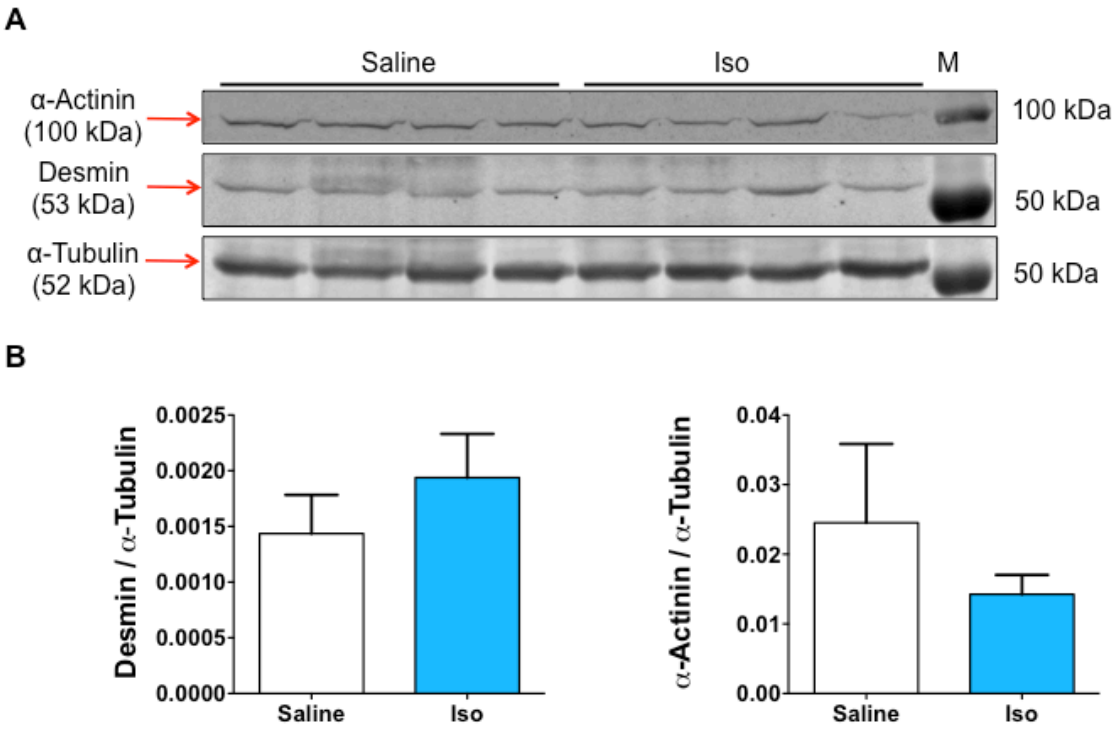

Figure 4.18 Cytoskeletal protein expression was unchanged after Iso treatment.
Protein expression of cytoskeletal proteins, α-actinin and desmin, were evaluated by Western blotting using LV homogenates from mice infused for 4 weeks with saline or Iso. α-Tubulin was used as a loading control. A, Membrane revealed no obvious difference in expression of α-actinin and desmin. B, Densimetric analysis of membranes in (A). Red arrows in (A) dictate quantified bands. Values expressed as mean ± SEM. *n*= 4. Data analysed by student t-test. Desmin, $p = 0.34$, α-actinin, $p = 0.89$.

4.2.3.4 Maintained mitochondrial morphology and sarcomere alignment after Iso infusion.

To investigate potential changes in sarcomere alignment and mitochondrial shape, size and internal structure, heart tissue from mice infused with saline or Iso were submitted for TEM analysis. Under low magnification (5,000x), sarcomere structure and alignment appear maintained after Iso infusion compared to saline-infused mice (**figure 4.19**). Under higher magnification (40,000x), mitochondrial shape and size (not quantified) also appear to be consistent between saline- and Iso- infused myocardium, with no obvious

differences in the cristae or inner mitochondrial structure. As mitochondrial shape, size and cristae structure were maintained after Iso infusion, this suggests that mitochondrial function is not changed as a result of Iso infusion.

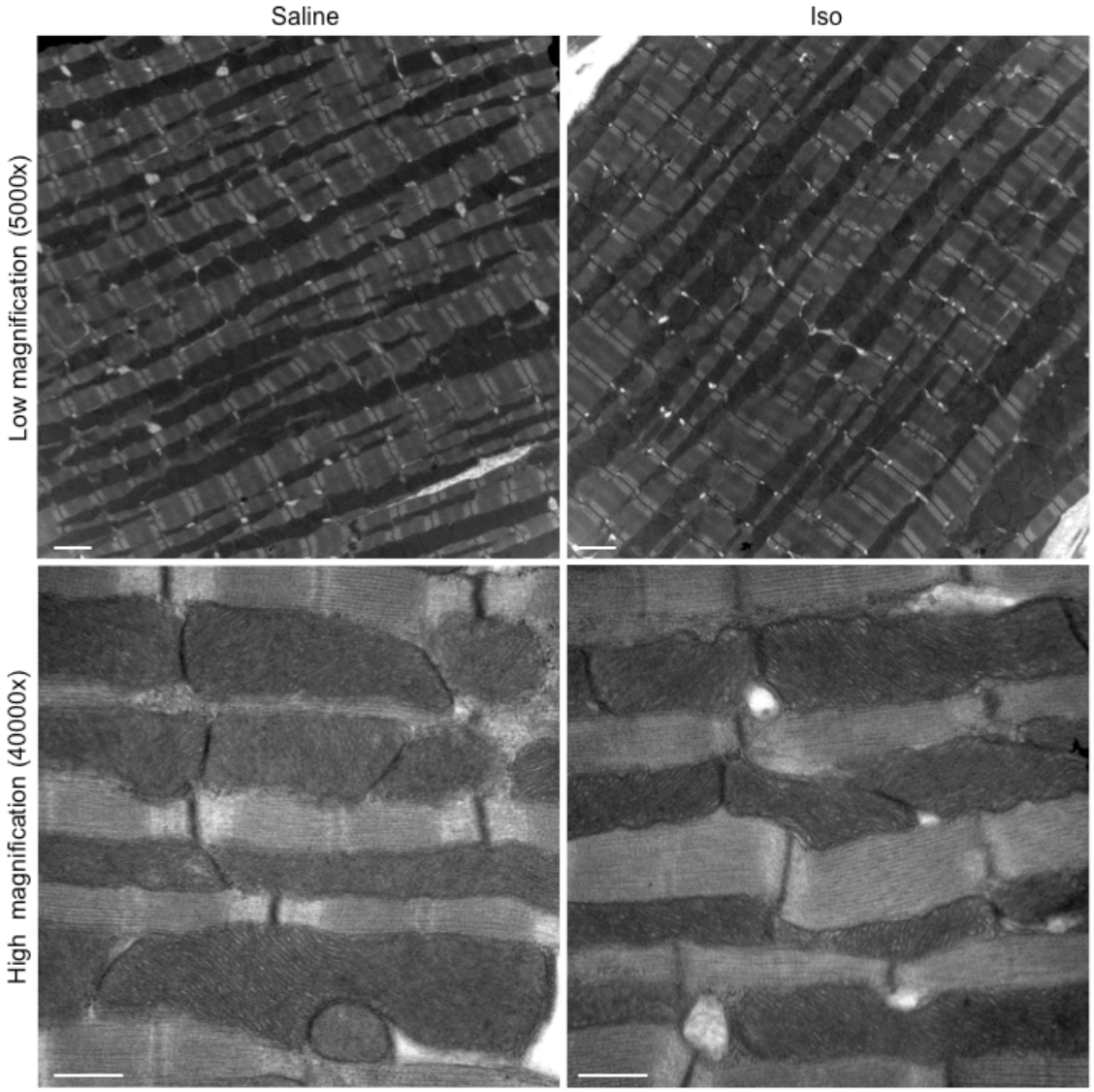

Figure 4.19 Appearance of maintained sarcomeric alignment and mitochondrial structure were observed after 4 weeks Iso treatment.
Electron microscopy was performed on myocardium harvested from mice after 4 weeks infusion with Iso (*n*= 2). Low magnification images (scale bar = 2 μm) show conserved sarcomeric alignment whilst high magnification images (scale bar = 500 nm) reveal consistent mitochondrial structure, shape and size (not quantified) in Iso-treated mice compared with mice infused with saline.

4.2.3.5 Study of cellular energetics, glucose metabolism and FA metabolism after Iso infusion.

As metabolic abnormalities, such as decreasing FA and glucose metabolism have been reported after Iso infusion [302], histology, Western blotting and qRT-PCR analyses were performed to evaluate any alterations in FA metabolism and glucose metabolism that may contribute to the development of β-stimulant-induced cardiomyopathy.

4.2.3.5.1 Lipid deposition and FA metabolism were unchanged after Iso infusion.

To determine any differences in lipid deposition in the myocardium, Oil Red O staining was performed on cryosections of myocardium harvested from mice after 4 weeks infusion of saline or Iso (**figure 4.20a**). Image J software was used to quantify the lipid deposition in 5 images per section and expressed as a percentage of lipid deposition. No differences in lipid deposition were observed in the myocardium between saline- and Iso- treated mice (**figure 4.20b**).

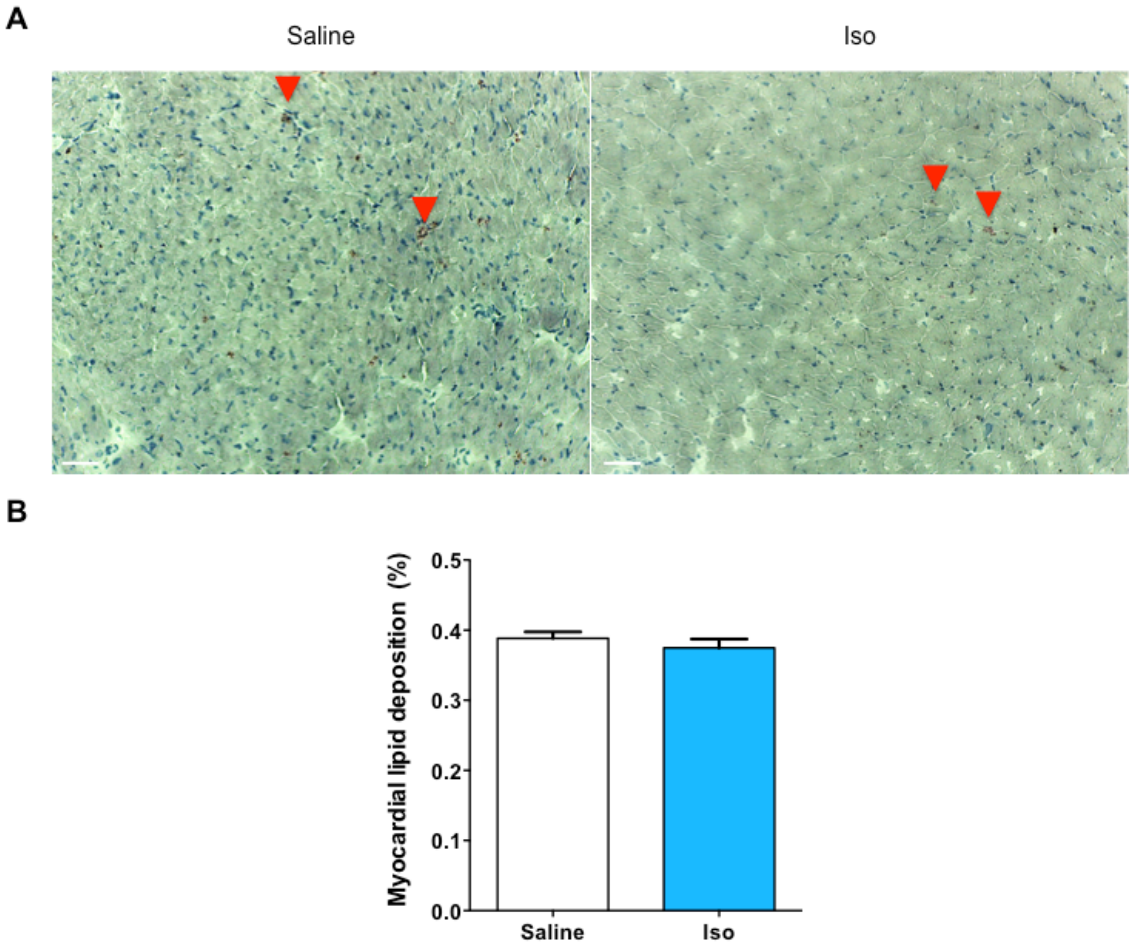

Figure 4.20 No differences in lipid deposition after Iso treatment.
A, Cryosections of myocardial tissue harvested from mice infused with saline or Iso for 4 weeks were subjected to Oil-Red-O staining. B, Quantification of Oil-Red-O staining of 5 images per section to determine percentage of lipid deposition in myocardium using Image J software. p = 0.40. No differences in lipid deposition were observed. Values expressed as mean ± SEM. n= 4. Data were analysed by student t-test. Scale bar = 30 μm.

The mRNA expression of proteins involved in FA transport and metabolism were evaluated by qRT-PCR using samples from mice after 4 weeks Iso treatment. The expression of markers of β-oxidation of long chain FAs, carnitine palmitoyltransferase (*Cpt*)-*1b*, *Cpt2*, carnitine O-acetyltransferase (*Crat*) and Acetyl-CoA carboxylase b (*Acacb*) were assessed, as well as indicators of FA synthesis, *Acaca* and FA synthase (*Fasn*). However no differences were observed in the expression of these markers between saline- and Iso- infused

mice (**figure 4.21**). Together with the histological data, these finding suggests that FA metabolism is unchanged in this model and does not contribute to β-stimulant-induced cardiomyopathy.

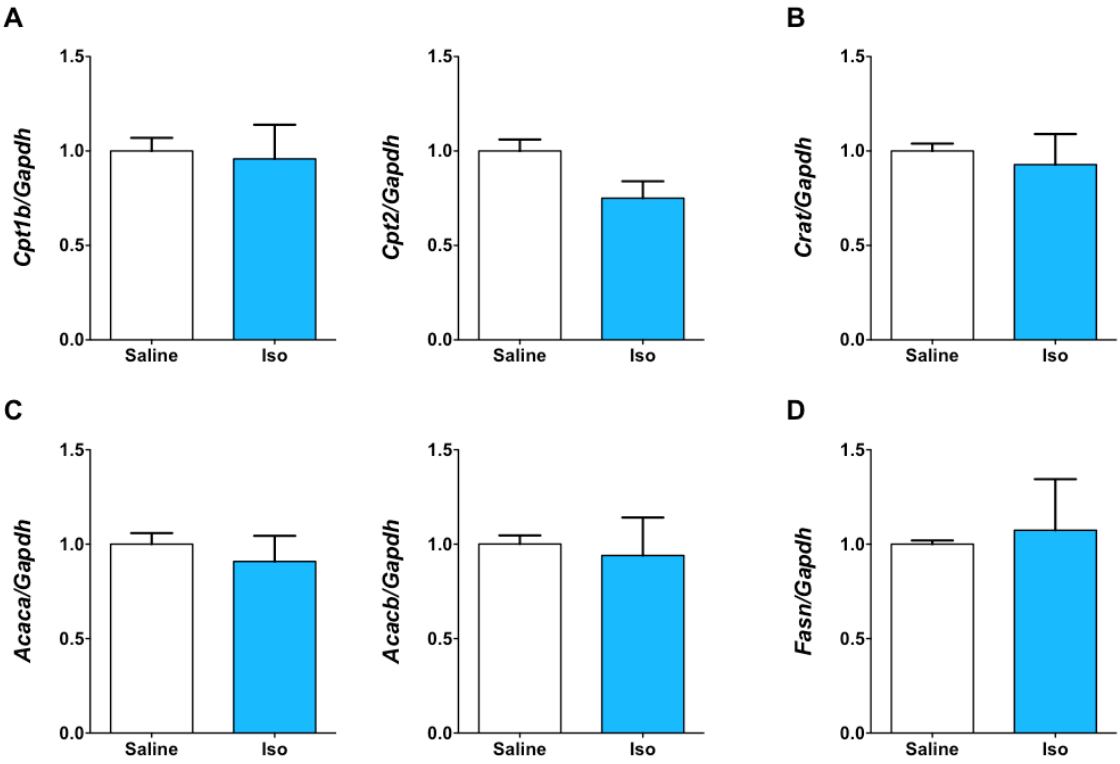

Figure 4.21 Expression of fatty acid (FA) transport and metabolism markers was unchanged after Iso infusion.
mRNA expression of proteins involved in FA transport and metabolism were evaluated by qRT-PCR using samples from mice after 4 weeks Iso treatment. A, Carnitine palmitoyltransferase (*Cpt*)-*1* and *Cpt2*, p = 0.84 and p = 0.07, respectively. B, Carnitine O-acetyltransferase (*Crat*), p = 0.70. C, Acetyl-CoA carboxylase (*Acac*)-a and *Acacb, p* = 0.57 and p = 0.79, respectively. D, Datty acid synthase (*Fasn*), p = 0.80. Using LV homogenates from mice after 4 weeks Iso treatment no differences were observed in the expression of these markers. Indicators of β-oxidation of long chain FAs include carnitine palmitoyltransferase (*Cpt*)-*1*, *Cpt2*, carnitine O-acetyltransferase (*Crat*) and Acetyl-CoA carboxylase b (*Acacb*) whilst (*Acac*)-a and FA synthase (*Fasn*) are considered to be markers of FA synthesis. Glyceraldehyde 3-phosphate dehydrogenase (*Gapdh*) was used as a housekeeping gene. Values expressed as mean ± SEM. *n*= 4. Data analysed by student t-test.

4.2.3.5.2 Cellular energy production was unchanged after Iso infusion.

To estimate changes in cellular energy production, the expression of AMPKα was studied. AMPKα is a subunit of heterotrimeric protein, AMPK. This protein acts as a cellular fuel sensor and is an essential regulator of cellular energy homeostasis [349]. AMPK is activated when ATP levels are diminishing, which may occur under circumstances such as low glucose, hypoxia, ischemia and heat shock. Stimulation of AMPK boosts cellular energy levels by inhibiting anabolic energy consuming pathways (FA and protein synthesis) and activating energy producing, catabolic pathways (FA oxidation, glucose transport, and autophagy).

Therefore, total (t) AMPKα and phosphorylated (p) AMPKα (Threonine-172) expression were evaluated by Western blotting in samples of myocardial tissues harvested from mice infused with Iso or saline for 4 weeks (**figure 4.22a**). Using these samples, no differences in the expression of pAMPKα or tAMPKα were found, signifying there were potentially no changes in energy homeostasis after Iso infusion or in β-stimulant-induced cardiomyopathy.

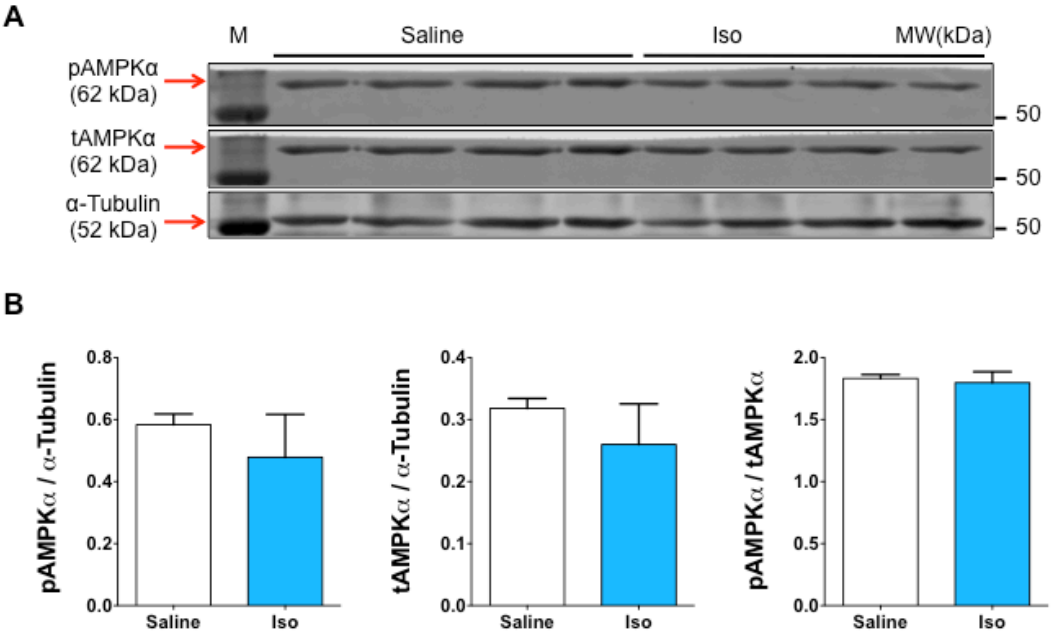

Figure 4.22 Adenosine monophosphate-activated protein kinase subunit alpha (AMPKα) protein expression was unchanged after Iso treatment. Protein expression of total (tAMPKα) and phosphorylated levels (pAMPKα, Thr172), were evaluated by Western blotting using LV homogenates from mice infused for 4 weeks with saline or Iso. α-Tubulin was used as a loading control. A, Membrane revealed no obvious difference in expression pAMPKα or tAMPKα. B, Densimetric analysis of membranes in (A). Red arrows in (A) dictate quantified bands. Values expressed as mean ± SEM. n= 4. Data were analysed by student t-test. pAMPKα, p = 0.51; tAMPKα, p = 0.45; pAMPKα/ tAMPKα, p = 0.74.

4.2.3.5.3 Glucose transport and metabolism were unchanged after Iso infusion.

Next, potential changes in the mRNA expression of proteins involved in glucose transport and metabolism were evaluated by qRT-PCR using LV homogenates from mice after 4 weeks infusion of saline or Iso. The expression of markers of pyruvate decarboxylation, such as pyruvate dehydrogenase kinase isozyme 1 (*Pdk1*), *Pdk4* and pyruvate dehydrogenase alpha 1 (*Pdha1*) were assessed to provide information about the relevant levels of aerobic metabolism. Additionally, the expression of glucose transporter 1 (GLUT 1 or solute carrier family 2 facilitated glucose transporter member 1 (*Slc2a1*)) and GLUT 4 (*Slc2a4*) were investigated as markers of glucose transport, whilst levels of

lactate dehydrogenase a (*Ldha*) were assessed as an indicator of anaerobic metabolism. Once again, no differences were observed in the mRNA expression of these markers of glucose transport and metabolism between mice infused with saline and Iso for 4 weeks (**figure 4.23**), suggesting that glucose transport and metabolism remained unchanged after Iso infusion. However, a tendency towards an increase in *Ldha* expression could be noted between saline and Iso infused hearts (p = 0.18), though more samples are required.

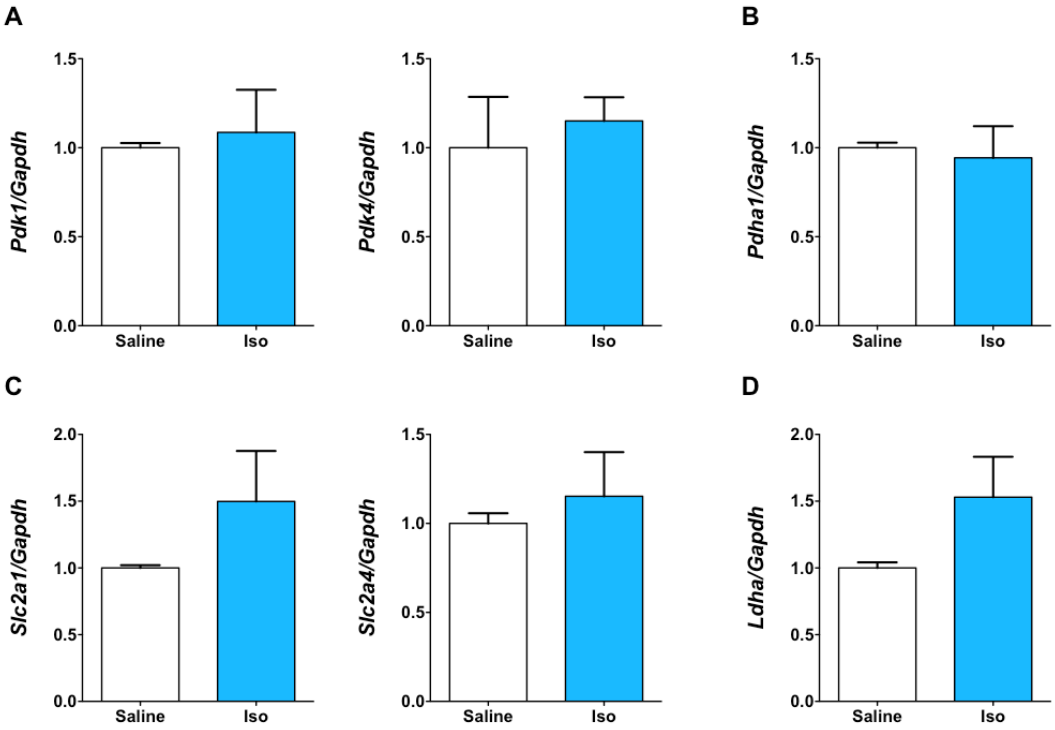

Figure 4.23 No differences in mRNA expression of markers involved in glucose transport and metabolism.
qRT-PCR was performed on LV homogenates from mice after 4 weeks Iso infusion to study mRNA expression of proteins involved in glucose acid transport and metabolism. A, Pyruvate dehydrogenase kinase isozyme 1 (*Pdk1*) and *Pdk4, p* = 0.74 and *p* = 0.66, respectively. B, Pyruvate dehydrogenase alpha 1 (*Pdha1*), *p* = 0.77. C, Glucose transporter 1 or Solute carrier family 2 facilitated glucose transporter member 4, (GLUT1 or *Slc2a1*) and Glucose transporter 4 (GLUT4 or *Slc2a4*), *p* = 0.28 and *p* = 0.59, respectively. D, Lactate dehydrogenase a (*Ldha*), *p* = 0.18. Pdk1, Pdk 4 and Pdha1 are involved in pyruvate decarboxylation, therefore are markers of aerobic metabolism. Ldha is a marker of anaerobic metabolism whilst Glut 1 and Glut 4 are markets of glucose transport and insulin-sensitivities. No differences were observed in the mRNA expression of these markers of glucose transport and metabolism between saline- and Iso- treated mice. Glyceraldehyde 3-phosphate dehydrogenase (*Gapdh*) was used as a housekeeping gene. Values expressed as mean ± SEM. *n*= 4. Data were analysed by student's t-test.

4.2.3.6 Degradation of IκB after Iso infusion

Iso has been reported to induce NF-κB translocation into the nucleus [350]. While NFκB is notorious for its role within the immune system, it also regulates the expression of genes involved in cell survival and stress responses to ischemia, hypoxia and cellular stretch [185, 186, 351]. Therefore it is considered to be both cardioprotective and cardiotoxic.

To provide an insight into NFκB activity after Iso infusion, Western blotting was performed to examine the expression of IκB and phosphorylated (p)IκB. As mentioned in **section 1.5.2**) IκB binds to NFκB, preventing the translocation of NFκB into the nucleus. However phosphorylation of IκB targets IκB for ubiquitination and degradation, permitting the translocation of NFκB into the nucleus to bind to DNA and induce expression of NFκB-regulated genes.

Expression of IκB and pIκB (Serine-32 / Serine-36) was evaluated using LV homogenates from mice infused with saline or Iso for 4 weeks (**figure 4.24a**). No differences in pIκB levels were observed between saline- and Iso- treated mice. However decreased IκB expression was noted in Iso-treated mice compared with saline-infused mice, inducing an increase in the pIκB / IκB ratio in Iso-treated mice (**figure 4.24b**), subsequently suggesting degradation of IκB. This consequently implies potential increased translocation of NFκB into the nucleus after Iso infusion, which may contribute to the development of β-stimulant-induced cardiomyopathy, though further study is required.

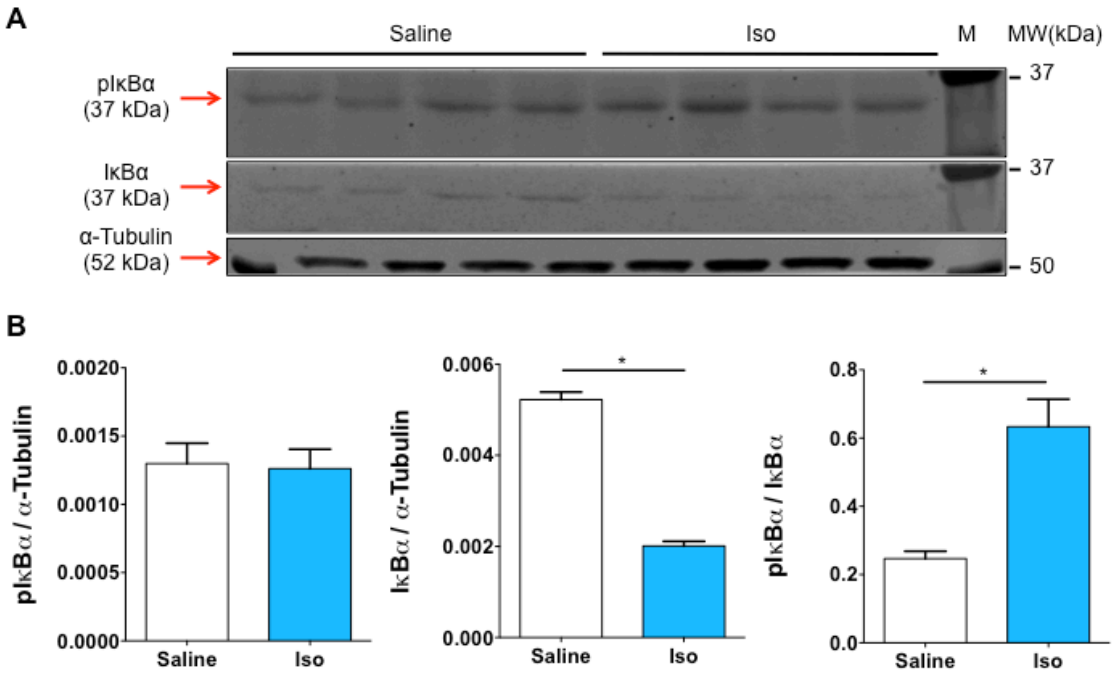

Figure 4.24 IκBα protein expression was reduced after Iso treatment. Protein expression of inhibitor of kappa B (IκBα) and phosphorylated levels (pIκBα, Ser32/Ser36) were determined by Western blotting using LV homogenates from mice infused with saline or Iso for 4 weeks. α-Tubulin was used as a loading control. A, Membrane revealed decreased expression of IκBα after Iso infusion. B, Densimetric analysis of membranes in (A). Red arrows in (A) dictate quantified bands. Values expressed as mean ± SEM. *n*= 4. Data were analysed by student t-test. **p*<0.05.

4.3 Discussion

Intriguingly, the data presented in this chapter suggest that the tachycardia and cardiac dysfunction observed in β-stimulant-induced cardiomyopathy were recoverable 1 day after Iso removal. Additionally, the data suggested that genes induced by NFκB may contribute to the development of β-stimulant-induced cardiomyopathy. However the mechanism behind this model of reversible β-stimulant-induced cardiomyopathy remains unknown.

4.3.1 Iso-induced tachycardia and cardiac dysfunction were reversible

The cardiac phenotype observed after β-stimulant-induced cardiomyopathy was reversible. Changes in HR and cardiac function after 4 weeks of Iso infusion, were partially recoverable 1 day after removal of Iso (**figures 4.2, 4.3, 4.5 - 4.7** summarised in **table 4.6**). Furthermore, heart weight normalised to tibia length was consistently increased in Iso-treated mice before and after minipump exchange (**figure 4.8c**), suggesting that gain in heart weight was not recoverable 2 days after minipump exchange. It is unlikely that the gain in heart weight would be recoverable so acutely and it should also be noted that these measurements were taken 1 - 2 days after minipump exchange and further changes or complete recovery of changes in HR and cardiac function may become apparent after longer recovery times. It has been reported that cardiac function in SIC patients improves 1 week after the manifestation of SIC, with complete recovery within 3 weeks [59]. In rats, reversible effects of Iso-induced hypertrophy were observed 3 days after minipump exchange, although the LV weight remained significantly increased compared with saline-treated mice [352]. This is in broad agreement with some of the findings of this current study, although the rate of reversibility was quicker in the model used in this chapter.

There were some inconsistencies in the echocardiographic and physiological data obtained in the minipump exchange experiments, compared with that described in chapter 3 (**figures 3.3, 3.4**) after 4 weeks infusion of Iso. Chamber dilatation, measured by LVIDd and LVIDs parameters and pulmonary congestion, as assessed by lung weight, were not observed in these experiments (**figures 4.6 – 4.8**). The reason for these discrepancies is not known, but could be due to environmental factors such as the time of year that these experiments were performed.

Table 4.6 Summary table of minipump exchange study.
Table to review differences in echocardiographic and physiological parameters at baseline, before minipump exchange (after 4 weeks minipump infusion) and after minipump exchange to remove drugs. Findings recorded in this table are relative to saline-treated mice at same timepoint (✓ = significant difference, X = no difference). Before minipump exchange, Iso induced hypertension, tachycardia, cardiac dysfunction, thickened posterior walls, heavier hearts and systemic congestion. However, 1 day after minipump exchange, these phenotypes had been abolished, except for heart weight, suggesting that aspects of β-stimulant-induced cardiomyopathy are recoverable. HR = Heart rate, LVIDd = End-diastolic left ventricle internal dimension, LVIDs = End-systolic left ventricle internal dimension, EF = Ejection fraction, FS = Fractional shortening, IVSd = End-diastolic interventricular septal wall thickness, LVPWd = End-diastolic left ventricular posterior wall thickness, W = Weight, TL = Tibia length. * relative to data in table 4.2 and figures 4.5, 4.6, 4.7 and 4.8.

Phenotype	Baseline	Pump exchange	
		Before	After
Hypertension			
Increased systolic and diastolic BP	X	✓	X
Tachycardia			
Increased HR	X	✓	X
Cardiac dilatation			
Increased LVIDd and LVIDs	X	X	X
Cardiac dysfunction			
Decreased EF and FS	X	✓	X
Cardiac structure and weight			
Increased IVSd and LVPWd	X	✓*	X
Increased LV mass	X	✓	X
Increased Heart W / TL	X	✓	✓
Pulmonary congestion			
Increased Lung W / TL	X	X	X

Another interesting feature of this study was how quickly the cardiac function depicted by EF and FS improved and recovered after Iso removal (**figure 4.7d**). *Nef* et al (2008) reported that genes involved in FA metabolism and oxidative phosphorylation were upregulated in patients that had recovered from SIC, compared with patients suffering from SIC [340]. Though the mechanisms which facilitated this acute recovery of Iso-induced tachycardia and cardiac dysfunction was not evaluated in this thesis, this report by *Nef* et al (2008) indicate one possible mechanism that may induce rapid recovery of the myocardium after Iso removal. Therefore, further study is required to identify the causes of this acute recovery and could focus upon the gene expression of proteins involved in FA metabolism and oxidative phosphorylation.

These experiments identified that Iso-induced tachycardia and cardiac dysfunction were recoverable 1 day after Iso removal, yet Iso-induced gain of heart weight was not recoverable within this same timeframe. Whilst the cause of the acute recovery remains unstudied, these findings suggested that 4 weeks of Iso infusion caused reversible changes to the function of the myocardium, which were likely to be functional amendments rather than structural modifications.

4.3.2 Infusion of Iso does not change calcium handling, oxidative stress-signalling or metabolism in mice

The reversibility of β-stimulant-induced cardiomyopathy suggested that functional, reversible changes had occurred in the myocardium after Iso infusion. Therefore it was hypothesised that desensitisation and changes in β-AR expression and calcium handling were likely causes of the phenotype observed and this may impact oxidative stress-related proteins and metabolism.

New samples were obtained which exhibited β-stimulated cardiomyopathy, excluding the tachycardia and pulmonary congestion associated with this condition. As mentioned, echocardiography was performed on conscious mice, which could be the reason why the HR was unchanged after Iso infusion. Furthermore, no differences in lung weight (similar to **figure 4.3**) were observed after 4 weeks of Iso infusion. This highlights the inconsistency of this model and it remains unknown whether Iso actually induces pulmonary congestion.

In this model of β-stimulant-induced cardiomyopathy the mRNA expression of the β-ARs were unchanged (**figure 4.10a**). However the protein expression and localisation of these receptors should be evaluated, as qRT-PCR experiments do not consider post-transcriptional regulation of mRNA, β-AR localisation and the phosphorylation status of the receptors.

Calcium handling is often impaired in clinical HF cases, preclinical HF models and in models of Iso infusion and is proposed to contribute to TIC and SIC. However in the experiments described here, no differences in the protein expression of calcium handling proteins were observed after Iso infusion, though a decreased tendency was observed in the expression of SERCA2, pentameric pPLN (Serine-16) and monomeric tPLN between saline- and Iso-treated mice was observed. Further samples are required to validate that tendency. One study reported differences in calcium activity after Iso infusion whilst the protein expression of calcium handling proteins (PLN, SERCA2 or RyR2) remained unchanged [299] whilst another study reported similar findings using samples from DCM patients [242]. Therefore, although expression of the proteins involved in calcium handling have been analysed, activity of the enzymes and receptors should be examined and calcium transients and amplitudes should be studied.

Attempts to measure RyR2 protein expression by Western blotting after Iso infusion were endeavoured (not shown). However, after multiple attempts to optimise the Western blotting procedure (SDS-PAGE, transfer, antibody incubations), RyR2 was undetectable. This could be due to the difficulties associated with transferring large molecular weight proteins (565 kDa) from SDS-PAGE gel to nitrocellulose membrane or due to degradation of RyR2 within the samples.

Next it was demonstrated that the expression of ischemic and oxidative stress markers after Iso infusion was unchanged in this model of β-stimulant-induced cardiomyopathy (**figure 4.16**). A trend towards increased expression of *Hmox1* after Iso infusion could be observed but more samples are required to validate that claim. Furthermore, the unchanged expression of hypoxic marker, *Hif1a,* after Iso infusion, compared to saline treatment, implied that the cardiomyocytes were not hypoxic after treatment with Iso.

It was reported that Nrf2-induced genes were elevated in SIC patients [340], however, no differences were observed in the mRNA levels of Nrf2-induced genes (*Gclc, Gsta2, Txnrd1*) between saline- and Iso- treated mice (**figure 4.15**). These findings were corroborated after examination of *Hmox1* expression, another gene regulated by Nrf2 (used as oxidative stress marker in this current study) (**figure 4.16b**). In the original report [340], changes were highest in glutathione peroxidase (*Gpx1*) and catalase (*Cat*) which were not examined in this model. Therefore the expression of these and other Nrf2-induced genes should be measured in this model of β-stimulant-induced cardiomyopathy.

Iso has been reported to lessen oxidative metabolism, boost oxidative stress and reduce FA oxidation [299, 302], all of which would be affected by abnormal

mitochondrial function. In SIC patients, damage to contractile proteins, contraction band necrosis and hypercontracted sarcomeres were reported [58, 63]. Together all these parameters suggest that the mitochondrial function and sarcomere alignment may be impaired after Iso treatment. TEM analysis found that overall mitochondrial shape and structure was maintained after Iso infusion (**figure 4.19,** not quantified). However, quantitative analysis of the images to analyse mitochondrial shape and structure would support and confirm this statement. The 'observed' conservation of mitochondrial shape and structure after Iso infusion also suggested that mitochondrial function would be unchanged after Iso infusion. This was supported by unchanged expression of *Ppargc1a* (oxidative stress marker and regulator of mitochondrial biogenesis and function) (**figure 4.16c**), *Cpt1b* and *Cpt2* (markers of FA oxidation located in mitochondria) (**figure 4.21a**), *Pdk1, Pdk 4* and *Pdha1* (markers of glycolytic metabolism, also located in mitochondria) (**figure 4.23a, b**) between saline- and Iso- treated mice.

Reports that Iso induced metabolic abnormalities [302] compelled the investigation to study the expression of several markers of lipid and glucose metabolism and transporters after Iso infusion. However, no differences were observed in markers for FA synthesis, β-oxidation of long chain FAs, aerobic metabolism, anaerobic metabolism and glucose uptake between mice infused with saline or Iso (**figure 4.21** and **4.23**). In addition, *Hif1a* expression is also considered a marker of FA β-oxidation [335] and its expression after Iso infusion concurs with the findings of the other markers (**figure 4.16a**). However, a trend towards increased expression of *Ldha* was noted between saline and Iso infused hearts (p = 0.18), though more samples are required to support this assertion.

Whilst no differences were observed after Iso infusion in the metabolic parameters mentioned above as well as in lipid deposition and cellular energetics, it is important to note that other aspects of metabolism (such as protein synthesis and oxidative phosphorylation) should be measured, alongside the levels of metabolites (ATP, FAs, glucose).

In summary, no differences in β-AR expression, calcium handling proteins and markers of ischemia and oxidative stress and metabolism were observed in this model of β-stimulant-induced cardiomyopathy, highlighting its unusualness. However more samples for each experiment are required to further support these assertions.

One limitation of this study was the lack of power calculations to ensure that the data was irrefutable. The number of samples needs to be increased for several experiments to validate the claims made (discussed further in **section 6.4)**. Other limitations include the differential methods of echocardiography yielding different findings and the use of qRT-PCR to determine expression of particular proteins (discussed further in **section 6.4)**. Further experiments would focus upon studying the protein expression of markers measured by qPCR in this chapter (if antibodies are available) and the activity of these proteins as well as measuring metabolite levels.

4.3.3 Potential role of NFκB in β-stimulant-induced cardiomyopathy.

Iso was reported to induce NFκB translocation into the nucleus [350] and interestingly, in this model of β-stimulant-induced cardiomyopathy, the expression of IκB was decreased after Iso infusion (**figure 4.24b**). This finding suggests that Iso infusion induces degradation of IκB, enabling the translocation

of NFκB into the nucleus. However the upstream and/or downstream effects of this remain unanswered.

To validate these findings, attempts to study the expression and localisation of NFκB and IκB after Iso infusion by IF using tissue samples were undertaken, as demonstrated by several studies [353, 354]. However, very few cells on each section emitted fluorescent signal representing NFκB and IκB. This was unexpected as NFκB is ubiquitously expressed, suggesting that this IF protocol requires optimisation. Alternatively, another experiment using inhibitors of NFκB may be designed and used to prove an association between β-AR signalling and NFκB. Treatment of Iso-infused mice with NFκB inhibitors may be used to prove such an association.

To determine the upstream signalling that induced degradation of IκB, the signalling cascade upstream of NFκB and IκB should be considered. The kinases reported to phosphorylate IκB include IKKα, IKKβ or c-Jun N-terminal kinases (JNK), all of which are activated by different signalling pathways. Therefore if the kinase that phosphorylates IκB is identified, then it is possible to identify the signalling pathway upstream and possible stimuli that induced the phenotype observed in β-stimulant-induced cardiomyopathy. However, cellular conditions that are known to induce NFκB activity include inflammation, cell death, hypoxia or ischemia. As demonstrated by chapter 3 and this chapter, inflammation, apoptosis and ischemia were not upregulated in this model of β-stimulant-induced cardiomyopathy, therefore other pathways which activate NFκB activity should be evaluated such as cellular stretch and cell survival.

Additionally, to determine whether there is increased translocation of NFκB into the nucleus, the expression of genes downstream of NFκB should be evaluated. NFκB is a transcription factor for genes involved in immune activation and

regulation, including cytokines and chemokines, regulators of apoptosis, growth factors and other transcription factors [355].

In the report that demonstrated Iso stimulated DNA binding activity of NFκB, that same report also demonstrated Iso induced DNA binding activity of AP-1 and JNK [350]. Therefore expression and translocation of both AP-1 and JNK should also be evaluated.

In summary, this chapter demonstrated that continuous, excessive and chronic infusion of Iso may induce NFκB activity and its downstream effects may contribute to the development of reversible β-stimulant-induced cardiomyopathy.

5 Imperative and novel functions of TLR9 in wound healing during acute ventricular remodelling post-MI.

5.1 Introduction

MI is a leading cause of HF [356, 357]. Rupture of atherosclerotic plaques is the most common cause of MI, restricting the flow of blood through the coronary artery and hence inducing myocardial ischemia. This subsequently disrupts cardiomyocyte function, provoking cell death, inflammation and scar formation, which sequentially causes permanent damage to the myocardium that may contribute to the progression of HF [263].

In mice, several models that mimic MI have been generated in order to understand the molecular mechanisms that contribute to the myocardial damage observed after MI [358]. The best-characterised model involves complete ligation of the LAD coronary artery, which fully restricts the blood flow to the anterior and apical regions of the heart [359]. This area, known as the ischemic area at risk, subsequently develops into an infarct associated with a cross-linked collagen scar (**figure 5.1**).

A multitude of studies using samples from HF patients and various preclinical models have demonstrated a distinct role for inflammation in the pathogenesis of HF [19, 20, 360, 361]. Whilst the mechanisms that underlie the stimulation of inflammatory responses within the myocardium are currently unresolved [20], this subject is presently an area of intense study. It was recently reported that the immune sensor, TLR9, instigates an inflammatory response during the pathogenesis of HF in a murine model of cardiac pressure overload [173].

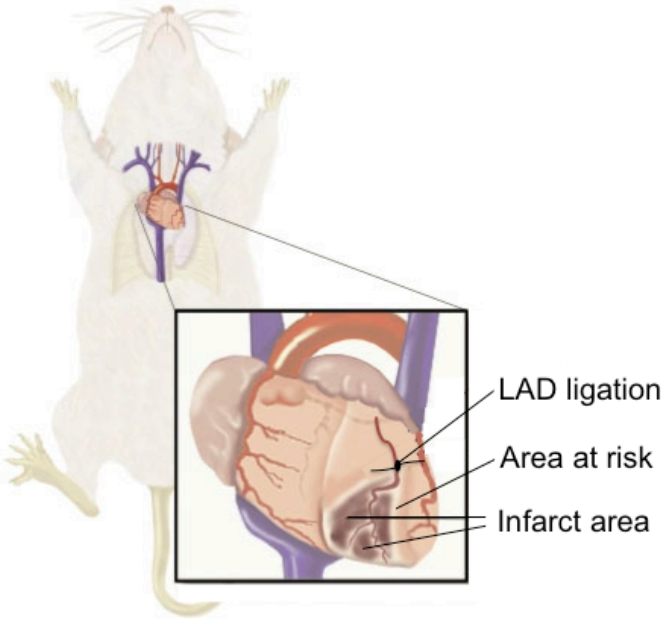

Figure 5.1 Murine model of MI.
To investigate the pathophysiology of MI, a model was established by ligating the left anterior descending (LAD) coronary artery, completely occluding the supply of blood to a region of the myocardium, termed the ischemic area at risk.

Several reports have demonstrated that inflammatory responses are elicited post-MI [362, 363, 364, 365]. Although, the impact of TLR9 stimulation on LV remodelling after MI has thus far not been elucidated, mice deficient in TLR2, TLR3 or TLR4 exhibited smaller infarcts, diminished cardiac remodelling and reduced inflammation after MI and I/R injury [366, 367, 368, 369]. These studies insinuate that inflammation is detrimental to LV remodelling post-MI, causing damage to the myocardium. However, inflammation is reported to play a crucial role during LV remodelling post-MI by aiding the clearance of dead cells from the infarcted myocardium and promoting tissue repair [32, 36, 362]. Therefore inflammatory responses must be tightly balanced.

Increased levels of circulating mtDNA, a known stimulus for TLR9, have been recorded in acute MI patients [305], which could potentially activate TLR9 to induce an inflammatory response post-MI. In a model of cardiac pressure overload, mtDNA was incompletely digested by autolysosomes within cardiomyocytes, leading to TLR9-mediated inflammation [173]. By contrast, after

MI mtDNA is released extracellularly from necrotic cells and may be internalised by other cell-types (fibroblasts, endothelial cells, leukocytes) within the myocardium or systemic circulation. Thus these 2 models mimic different myocardial conditions, which could confer distinct TLR9-mediated inflammatory responses. Additionally, the prevalence of cell death is greater after MI than in response to pressure overload and therefore a more intense inflammatory response may be required after MI to remove dead cells. Thus both the regulation and role of TLR9-mediated inflammation induced by mtDNA may be different between these 2 murine models.

It was therefore hypothesised that TLR9 might contribute to the inflammation associated with ventricular remodelling post-MI and this chapter will explore whether TLR9-mediated inflammation is beneficial or detrimental after MI. The aim of this study was to investigate the role of TLR9-mediated inflammation in the infarcted myocardium. The differences in LV remodelling between WT and TLR9KO mice, subjected to ligation of the LAD, were assessed to inform on the contribution of TLR9-mediated inflammation to cardiac remodelling after MI.

5.2 Results

5.2.1 TLR9KO mice had higher mortality after MI compared with WT mice.

To study the contribution of TLR9 signalling to the inflammatory response post-MI, 8 – 10-week old male C57Bl/6 (WT) and global TLR9KO mice were subjected to MI by ligation of the LAD (**figure 5.1**) or sham surgery. Prior to surgery, the physiological and echocardiographic parameters were measured to ensure there were no differences at baseline between WT and TLR9KO mice (**table 5.1**).

Table 5.1 Echocardiographic and physiological parameters were not different between WT and TLR9KO mice prior to surgery.
Conscious echocardiography and blood pressure measurements were performed on 8-10-week old WT and TLR9KO mice before surgery to reveal no difference between groups. Values are expressed as mean ± SEM. Data were analysed by one-way ANOVA with bonferroni's post-hoc test. Sig. = significance, n.s = no significance, IVSd = End-diastolic interventricular septal wall thickness, LVPWd = End-diastolic left ventricular posterior wall thickness, LVIDd = End-diastolic left ventricle internal dimension, LVIDs = End-systolic left ventricle internal dimension, EF = Ejection fraction, FS = Fractional shortening, HR = Heart rate, BW = Body weight, MBP = Mean blood pressure.

Parameters	WT Sham (*n*= 6)	WT MI (*n*= 9)	TLR9KO Sham (*n*= 7)	TLR9KO MI (*n*= 11)	Sig.
IVSd (mm)	0.79 ± 0.05	0.72 ± 0.04	0.74 ± 0.02	0.75 ± 0.01	n.s
LVIDd (mm)	2.89 ± 0.07	3.02 ± 0.06	3.14 ± 0.12	3.13 ± 0.07	n.s
LVIDs (mm)	1.54 ± 0.10	1.48 ± 0.05	1.51 ± 0.09	1.60 ± 0.07	n.s
LVPWd (mm)	0.76 ± 0.05	0.72 ± 0.02	0.72 ± 0.03	0.73 ± 0.01	n.s
EF (%)	82.84 ± 0.94	83.59 ± 0.78	84.22 ± 1.30	81.50 ± 1.24	n.s
FS (%)	50.17 ± 1.09	51.13 ± 0.88	52.10 ± 1.52	49.13 ± 1.36	n.s
HR (BPM)	725.89 ± 6.03	723.72 ± 6.64	700.69 ± 10.94	699.54 ± 8.86	n.s
LV mass (mg)	62.71 ± 3.43	64.91± 1.62	69.98 ± 3.57	70.77 ± 2.33	n.s
BW (g)	24.20 ± 0.63	24.30 ± 0.40	24.61 ± 0.47	24.81 ± 0.31	n.s
MBP (mmHg)	105.53 ± 0.63	113.61 ± 2.93	109.68 ± 4.09	113.54 ± 3.81	n.s

Operations to induce MI or sham surgery were performed on WT and TLR9KO mice. The mice were observed closely for 2 weeks for signs of stress or injury after surgery. Surprisingly, 4 days after operation, MI-operated TLR9KO mice began to die, whilst MI-operated WT mice persisted. Only 4/11 TLR9KO mice survived until 14 days following MI operation, whilst 8/9 WT mice survived this period (36.4% versus 88.9% survival rate) (**figure 5.2**). All WT- and TLR9KO-sham mice survived throughout the experiment. The cause of death for the WT and TLR9KO mice subjected to MI was cardiac rupture, indicated by blood coagula in the chest cavity and small slits located on the free wall of the LV ascertained by post-mortem analyses (**figure 5.3**). These intriguing results indicate that TLR9 is fundamental for LV remodelling post MI, during the acute phase 4 - 6 days after operation.

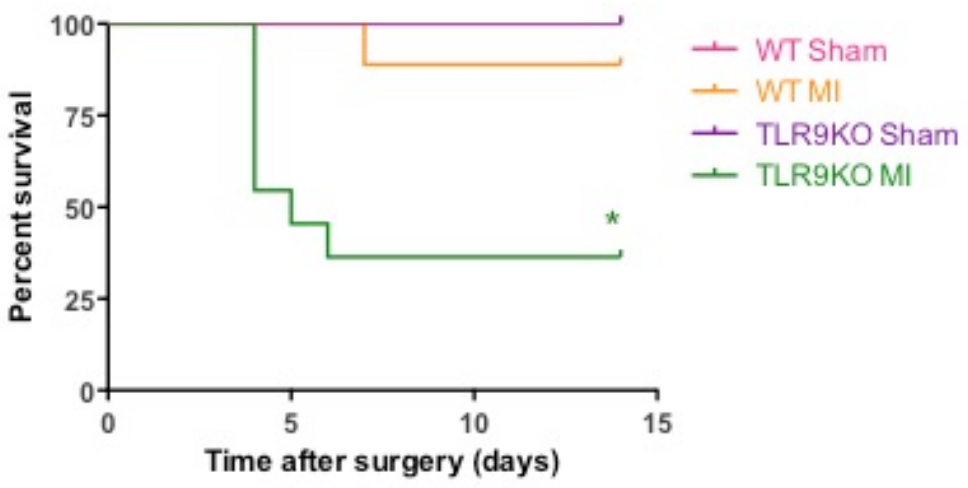

Figure 5.2 TLR9KO mice have a lower survival rate after MI.
WT and TLR9KO mice were followed for 14 days after sham or MI surgery. TLR9KO mice subjected to MI showed significantly higher mortality than WT mice 4 days after surgery. WT Sham (pink, *n* = 6, 100% survival), WT MI (orange, *n*= 9, 88.9% survival), TLR9KO Sham (purple, *n* = 7, 100% survival) and TLR9KO MI (green, *n* = 11, 36.4% survival). Data were analysed by Mantel-Cox Log-Rank test. *$p<0.05$ versus all other murine groups.

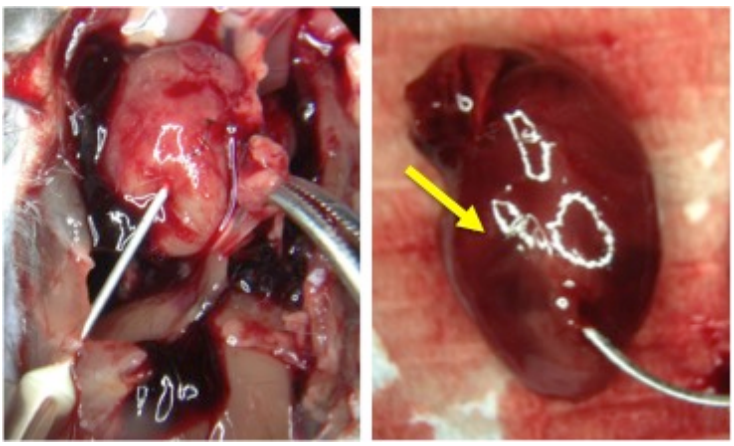

Figure 5.3 Cardiac rupture was the cause of mortality after MI in WT and TLR9KO mice.
Post-mortem analysis revealed that cause of death of WT (n=1) and TLR9KO (n=7) mice was cardiac rupture indicated by blood in the chest cavity and small slits observed in the free wall of the left ventricle (indicated by the arrow).

5.2.2 Ischemic area at risk, wall thicknesses and haemodynamic parameters were consistent between WT and TLR9KO mice after MI.

To ensure there were no differences in the ischemic area at risk between WT and TLR9KO mice after MI operation, which may influence infarction size and incidence of cardiac rupture, Evans Blue staining was performed on a separate cohort of animals. Evans Blue reagent was directly injected into the inferior vena cava of WT and TLR9KO mice immediately after ligation of the coronary artery. The hearts were harvested, sliced and imaged (**figure 5.4a**).

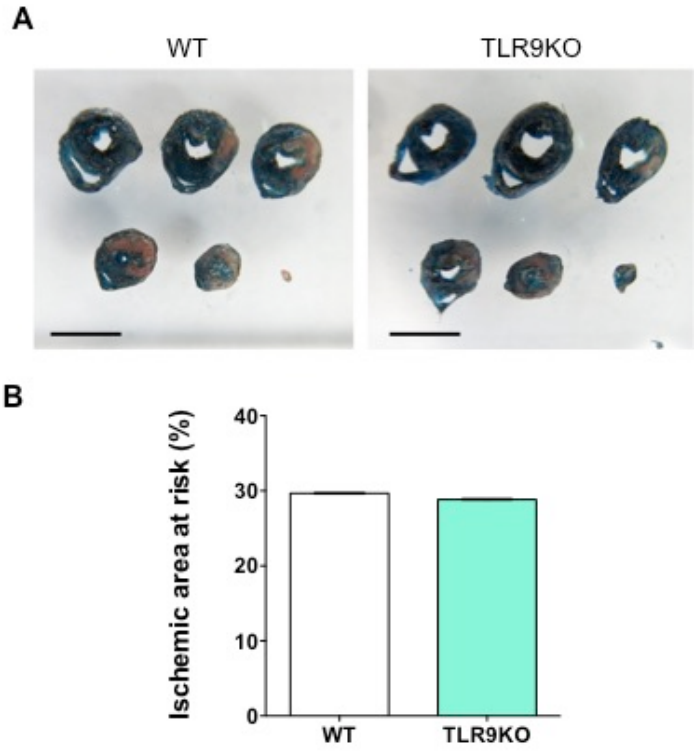

Figure 5.4 No difference in the ischemic area of risk between WT and TLR9KO mice subjected to MI.
Evans Blue reagent was injected into the inferior vena cava to determine the ischemic area at risk immediately after operating to induce MI. The ischemic area at risk represents the area of the myocardium that is no longer connected to the circulation. A, Images of stained heart; areas stained blue are healthy and viable, whereas unstained areas represent the ischemic area at risk. Scale bar = 5 mm. B, Graphical representation of the ischemic area at risk calculated as a percentage of the whole heart. There was no difference in the ischemic area at risk between WT and TLR9KO mice. Values are expressed as mean ± SEM. WT MI (open, *n*= 5), TLR9KO Sham (green, *n* = 6). Data were analysed by student's t-test.

The unstained area represented the ischemic area at risk that was disconnected from the circulation and may have developed into an infarct, whilst the healthy, viable myocardium was stained blue. Image quantification indicated no significant differences in the ischemic area at risk between WT and TLR9KO mice after MI (**figure 5.4b**).

Cardiac rupture is an adverse consequence of thinning of the myocardial walls, and is also a common feature of MI [370, 371]. Thus cardiac MRI was performed on WT and TLR9KO mice 3 days after induction of MI to determine if there were any changes in cardiac structural and functional parameters and infarct size (**figure 5.5**). However, no significant differences were observed in the thickness of the walls in the border or infarct zones, infarct size or haemodynamic parameters between WT and TLR9KO mice subjected to MI (**table 5.2**).

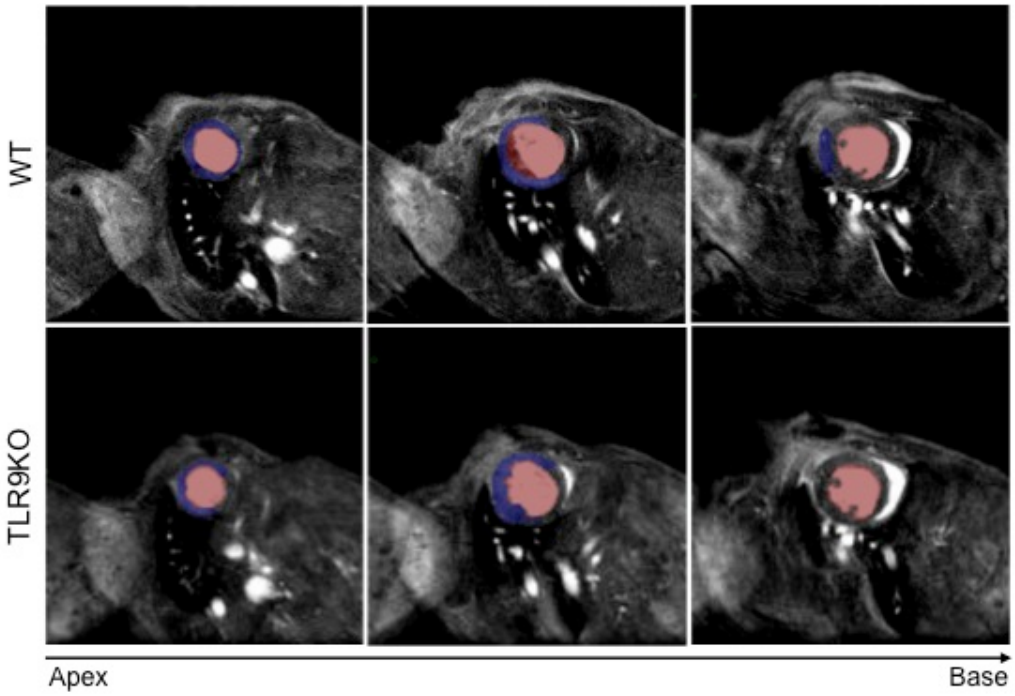

Figure 5.5 Cardiac MRI revealed no difference in cardiac structure 3 days after MI between WT and TLR9KO mice.
Representative images of cardiac MRI performed on WT and TLR9KO mice 3 days after surgery to induce MI. LV cavity = Red area, Infarct area = blue area. *n*= 4 for both groups.

Table 5.2 No differences in left ventricular structure and function 3 days post MI between WT and TLR9KO mice revealed by cardiac MRI.
Cardiac MRI was performed on anaesthetised MI-operated WT and TLR9KO mice. Wall thickness was measured in 10 random points in the border and infarct regions from images acquired 3 mm from the apex. The other parameters were calculated from 7 – 9 images taken at 1 mm intervals along the short axis. No differences were observed in the wall thickness, infarct size, LV mass and functional parameters of WT and TLR9KO mice 3 days after MI. Values are expressed as mean ± SEM. Data were analysed by student's t-test. Sig. = Significance, n.s = no significance.

Parameters	WT (*n*= 4)	TLR9KO (*n*= 4)	*p* value	Sig.
Wall thickness (border) (mm)	0.52 ± 0.01	0.52 ± 0.01	0.99	n.s
Wall thickness (infarct) (mm)	0.53 ± 0.02	0.55 ± 0.04	0.72	n.s
LV mass (mg)	65.42 ± 4.86	79.38 ± 2.85	0.09	n.s
Infarct size (%)	50.18 ± 4.01	51.17 ± 4.89	0.90	n.s
End-diastolic LV volume (µl)	74.21 ± 2.40	81.49 ± 8.33	0.55	n.s
End-systolic LV volume (µl)	53.79 ± 2.59	56.85 ± 7.90	0.79	n.s
Stroke Volume (ml/min)	20.42 ± 1.46	24.64 ± 1.05	0.10	n.s
Cardiac Output (µl)	9.53 ± 0.50	13.59 ± 1.24	0.08	n.s
Ejection Fraction (%)	27.57 ± 2.08	31.71 ± 3.01	0.33	n.s

5.2.3 Lack of fibrosis in infarcted myocardium of WT and TLR9KO mice.

To investigate the molecular mechanisms that boosted the incidence of cardiac rupture in TLR9KO mice after MI, histological and biochemical analyses were performed on the myocardium harvested from WT and TLR9KO mice. Hearts were harvested from WT and TLR9KO mice, 1 day and 3 days after operation, to examine the progression of cardiac remodelling after MI (**figure 5.6**).

Figure 5.6 Timecourse of experiments.
To investigate the cause of higher mortality seen in TLR9KO mice after MI, WT and TLR9KO mice were harvested 1 and 3 days after sham or MI operations.

H & E staining was executed on myocardial cryosections obtained from WT and TLR9KO mice to assess overall cell infiltration (leukocytes or fibroblasts) into the myocardium post-MI (**figure 5.7**). The hearts of WT and TLR9KO mice subjected to MI at both timepoints were highly heterogeneous, compared to sham-operated animals. The healthy parts of the MI-operated heart, termed the remote area, had similar myocardial structure as sham-operated animals.

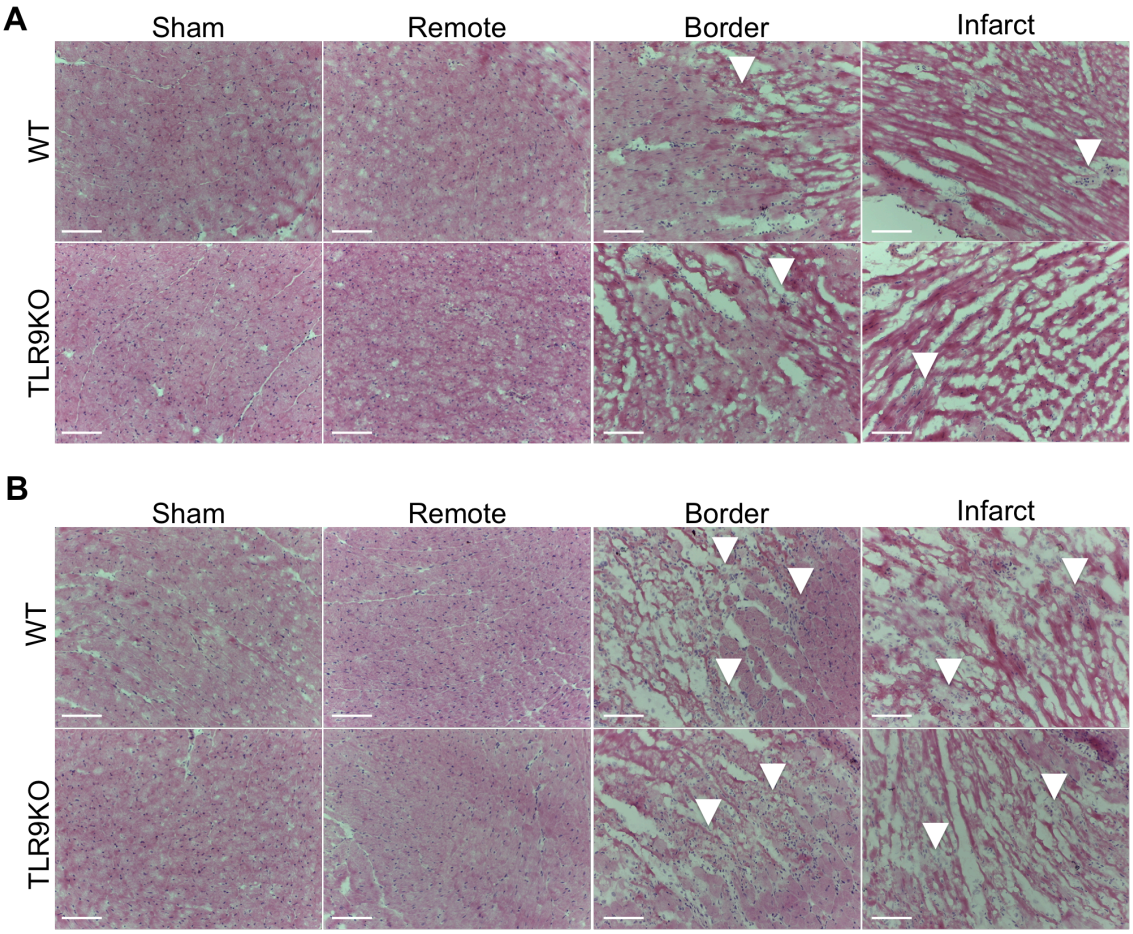

Figure 5.7 H & E staining revealed increased infiltration of cells into the myocardium in WT and TLR9KO subjected to MI.
H & E staining was performed on cryosections from WT and TLR9KO mice after MI. 3 different regions of mice subjected to MI are shown – remote, border and infarct. There appears to be excessive infiltration of cells into the border and infarcted regions 1 day after MI, but more so after 3 days (shown by arrow heads). *n*= 4 for all groups. A, Myocardium 1 day after surgery. B, Myocardium 3 days after surgery. Scale bar = 60 μm.

However, in the infarct area there was excessive cell infiltration and/or cardiomyocyte death, suggested by the presence of haematoxylin stain (blue) but not eosin (red) stain (not quantified). The transitional zone from the remote area to infarcted myocardium, termed the border zone, displayed a substantially greater number of these infiltrating or necrotic cells (not quantified). Thus it was decided that future staining performed on MI-operated hearts should be analysed in 3 different areas, remote, border and infarct areas.

After myocardial injury, the wounded area matures into a collagen- and connective tissue- containing fibrotic scar. Thus, histological staining and qRT-PCR analyses were implemented to study the extent of fibrosis in WT and TLR9KO mice after surgery. MT staining was performed on WT and TLR9KO hearts harvested 1 and 3 days after MI surgery (**figure 5.8**). Areas stained blue by MT reagent represented fibrotic areas, however there was very little blue staining observed in the myocardium of WT and TLR9KO mice at both time points after sham or MI surgery (not quantified), suggesting no difference in fibrosis between WT and TLR9KO mice, 1 or 3 days after sham or MI surgery.

To determine if there were changes in fibrotic markers at the mRNA level, the quantity of *Col1a, Col3a1*, transforming growth factor (*Tgf*)*b1* and *Tgfb2* was measured by qRT-PCR using LV homogenates from WT and TLR9KO mice after sham or MI surgery (**figure 5.9**). Using these samples, there were no differences in the levels of *Col1a2* and *Col3a1* 1 day after operation between sham- and MI- operated WT mice, but levels were significantly increased after 3 days in MI-operated WT mice, compared to sham-operated WT mice.

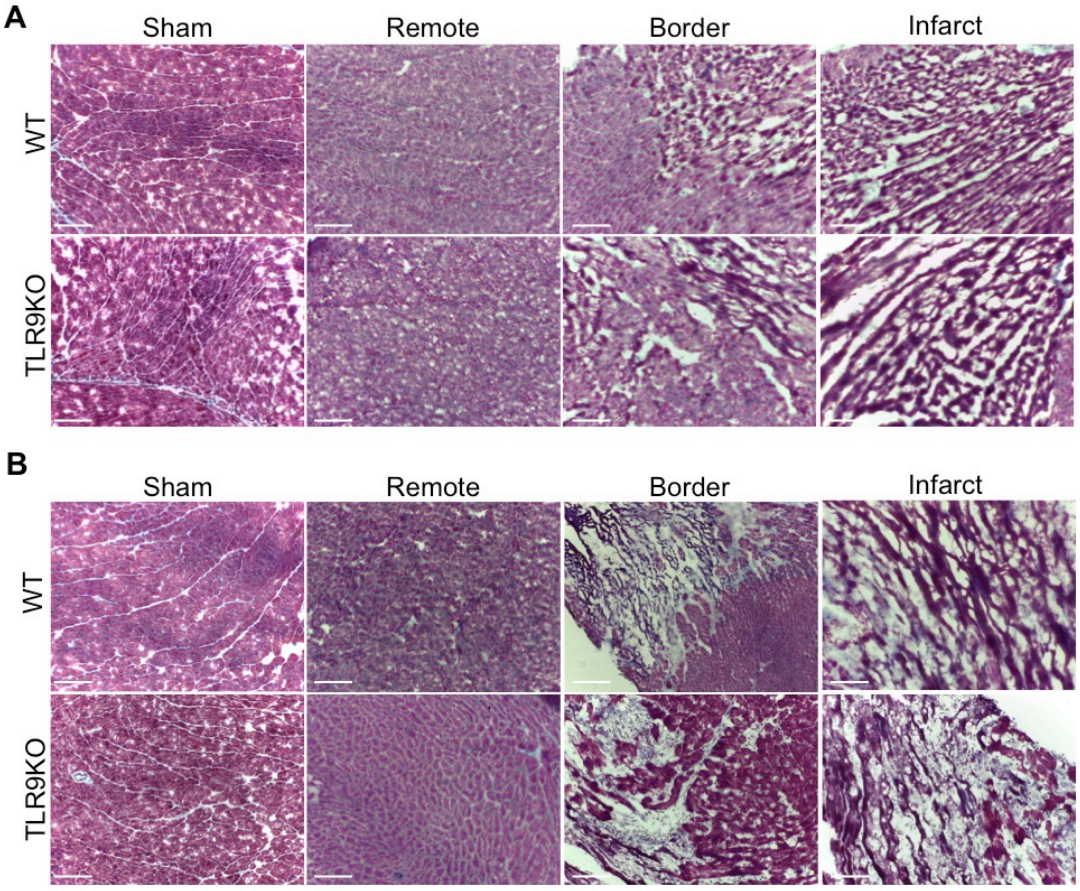

Figure 5.8 Masson's Trichrome staining found no difference in fibrosis in WT and TLR9KO mice after MI.
3 different areas of MI-operated mice are shown – remote, border and infarct. Although excessive infiltration of cells can be seen in these images (white grey areas) in the border and infarcted regions of mice 3 days after operation, WT and TLR9KO mice did not show any fibrosis (blue signal) after MI at both timepoints. *n*= 4 for all groups. A, Myocardium 1 day after surgery. B, Myocardium 3 days after surgery. Scale bars = 60 μm.

Surprisingly, these markers were elevated in sham-operated WT mice 3 days after operation compared with sham-operated WT mice harvested 1 day after surgery. Additionally, mRNA levels of *Tgfb1* and *Tgfb2* were elevated 1 and 3 days after MI in WT mice compared to sham-operated mice. Whilst levels of *Tgfb2* remained consistent in MI-operated WT mice between 1 and 3 days after surgery, *Tgfb1* expression increased between these timepoints. Finally, the expression of fibrotic markers between sham- and MI- operated TLR9KO mice

was analogous to WT sham- and MI- operated mice at 1 and 3 days after operation and no differences were identified in the levels of *Col1a, Col3a1*, *Tgfb1* and *Tgfb2* between WT and TLR9KO mice subjected to MI. Therefore these findings infer that fibrosis did not contribute to the increased incidence of cardiac rupture in TLR9KO mice after MI.

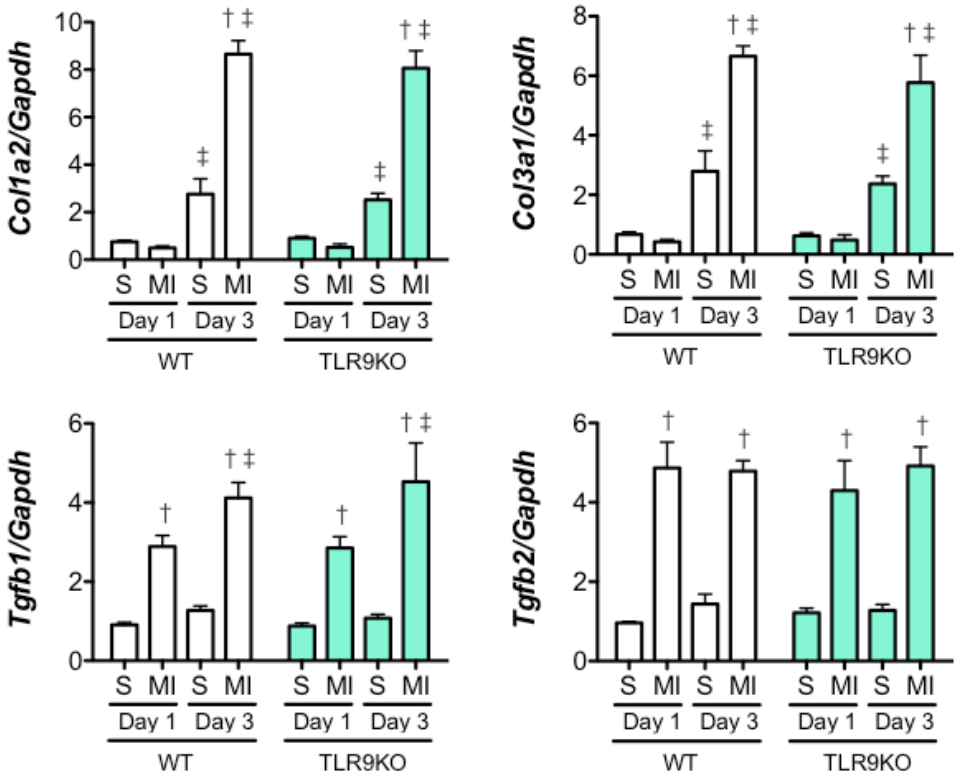

Figure 5.9 mRNA levels of fibrotic markers were similar between WT and TLR9KO mice after MI.
qRT-PCR was performed on LV samples of mice to measure levels of fibrotic markers. Levels of collagen type 1 alpha 2 (*Col1a2*) and *Col3a1* were increased 3 days after MI whereas levels of transforming growth factor β1 (*Tgfb1)* and *Tgfb2* were increased 1 and 3 days after surgery compared to sham (S)- operated mice. Yet no difference was observed between WT (open bars) and TLR9KO (green bars) mice after MI. Glyceraldehyde 3-phosphate dehydrogenase (*Gapdh*) was used as a housekeeping gene. Values are expressed as mean ± SEM; Day 1 WT sham *n*= 6, Day 1 WT MI *n*= 7, Day 3 WT sham *n*= 5, Day 3 WT MI *n*= 6, Day 1 TLR9KO sham *n*= 6, Day 1 TLR9KO MI *n*= 5, Day 3 TLR9KO sham *n*= 5, Day 3 TLR9KO MI *n*= 5. Data were analysed by two-way ANOVA with bonferroni post-hoc test. † $p<0.05$ versus corresponding sham animals at same timepoint, ‡ $p<0.05$ versus same treatment at different timepoints.

5.2.4 Investigation of the wound healing response after MI.

To comprehend the cause of cardiac rupture in TLR9KO mice after infarction, other avenues were explored. It was stated that myocardial inflammation, impaired ECM remodelling and dampened fibrotic healing are fundamental mechanisms for acute ventricular remodelling and for the pathogenesis of cardiac rupture [36]. Thus these components were investigated by biochemical and histological experiments to determine whether they contribute to the greater frequency of cardiac rupture observed in TLR9KO mice after MI.

5.2.4.1 Inflammation did not influence the mortality of TLR9KO mice subjected to MI.

The hypothesis postulated that TLR9-mediated inflammation may contribute to LV remodelling post-MI. The increased incidence of cardiac rupture in MI-operated TLR9KO mice, compared to WT mice observed in **figure 5.2**, suggested that TLR9 is beneficial in acute-remodelling post MI. TLR9-mediated inflammation may therefore be critically vital for LV remodelling post-MI, by potentially facilitating the clearance of dead cells and initiating would healing. However, previous studies have shown to correlate inflammation with increased occurrence of cardiac rupture [372, 373], highlighting the detrimental effects of inflammatory responses within the myocardium. It could be speculated that although the overall inflammatory response is detrimental for risk of cardiac rupture, TLR9-mediated inflammation may be a very specific response that is crucial for the removal of dead cells and the activation of tissue repair processes.

Thus the inflammatory response was evaluated in this model by IHC staining and qRT-PCR analysis to determine the infiltration of inflammatory cells and

levels of pro-inflammatory chemokines and cytokines in the myocardium. IHC staining of cryosections of cardiac tissue from WT and TLR9KO mice subjected to MI, were performed to assess the levels of leukocytes (CD45) in addition to macrophages (CD68), neutrophils (Ly6G/C) and T cells (CD3). Sham-operated WT animals and the remote region of MI-operated WT animals comprised of a similar number of inflammatory cells at all timepoints (**figures 5.10, 5.11 and 5.12**). In MI-operated WT sections, compared to the remote region, infiltration of inflammatory cells (CD45-, CD68- and Ly6G/C- positive cells) was greatest in the border regions at both timepoints followed by the infarct areas, indicating the active recruitment of cells to the damaged myocardium post-MI. A day after MI surgery, an increase in CD45-positive and CD68-positive cells in the border and infarct regions were seen in WT mice, compared to sham-operated WT mice and this was vastly enhanced 3 days after MI operation. The numbers of Ly6G/C-positive cells were consistently elevated in the infarct and border regions of MI-operated WT mice 1 and 3 days after surgery, compared to sham-operated mice. Minimal changes in the numbers of CD3-positive cells were observed between WT sham and all distinct regions of MI-operated animals, although a slight increase was seen in the border region 3 days after MI, compared to sham-operated animals. The differences between WT sham- and MI- operated mice mentioned above, were consistent with sham- and MI-operated TLR9KO mice at all timepoints, yet there were no significant differences in the number of CD45-, CD68-, Ly6G/C- and CD3- positive cells between WT and TLR9KO mice subjected to MI (**figures 5.10, 5.11 and 5.12**).

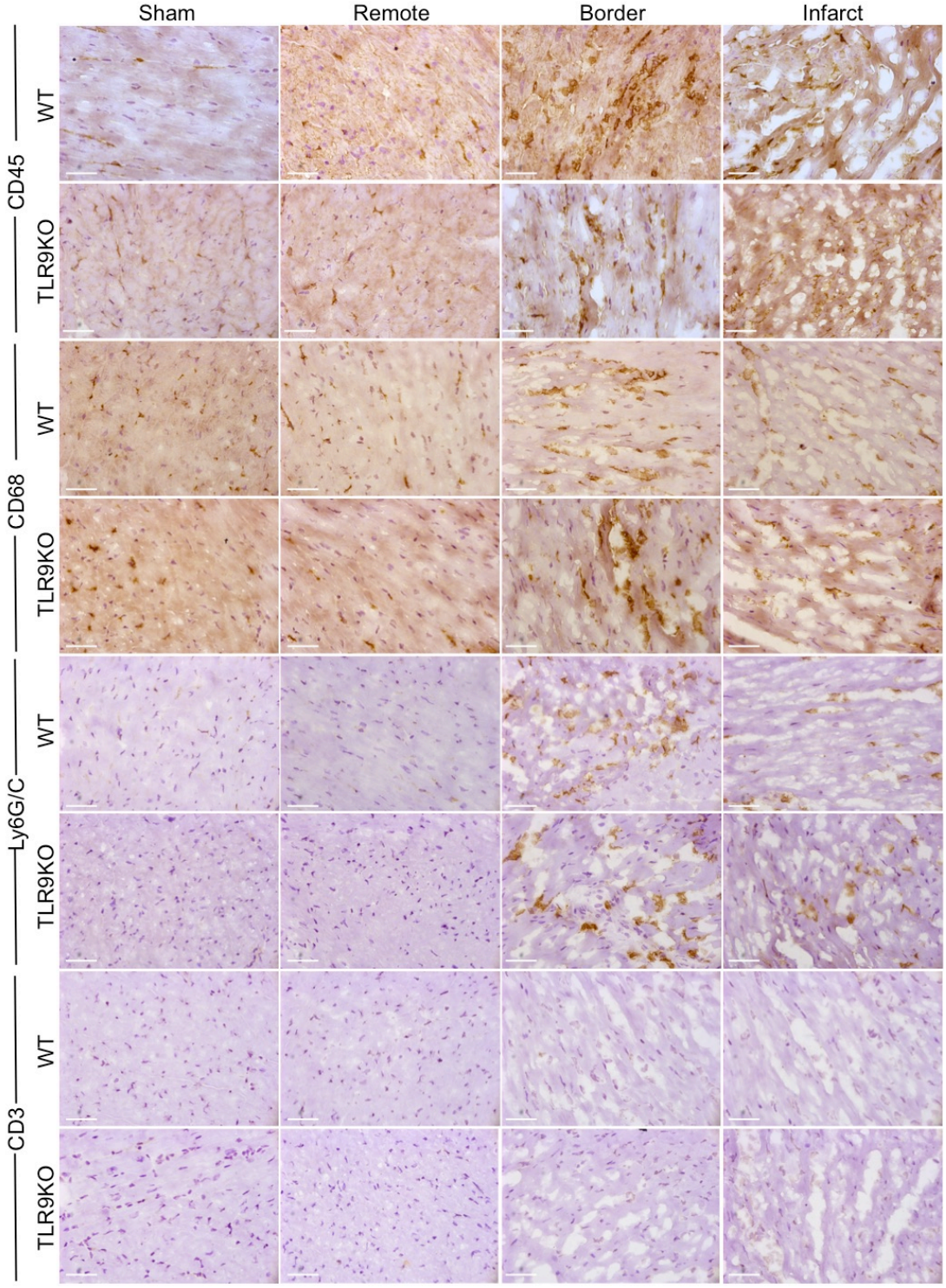

Figure 5.10 Immunohistochemical staining suggests no differences in the number of inflammatory cells in the myocardium in WT and TLR9KO mice 1 day after MI.

Staining was performed to detect cells expressing CD45 = leukocytes, CD68 = macrophages, Ly6G/C = neutrophils and CD3 = T-cells. 3 different regions of MI-operated hearts are displayed – remote, border and infarct. In the border and infarct regions of MI-operated hearts, there appears to be greater infiltration of CD45-, CD68- and Ly6G/C- positive cells, compared to sham-operated hearts, however no obvious difference in the filtration of inflammatory cells into the myocardium of WT and TLR9KO mice 1 day after surgery. *n*= 4 for all groups. Scale bars = 30 μm.

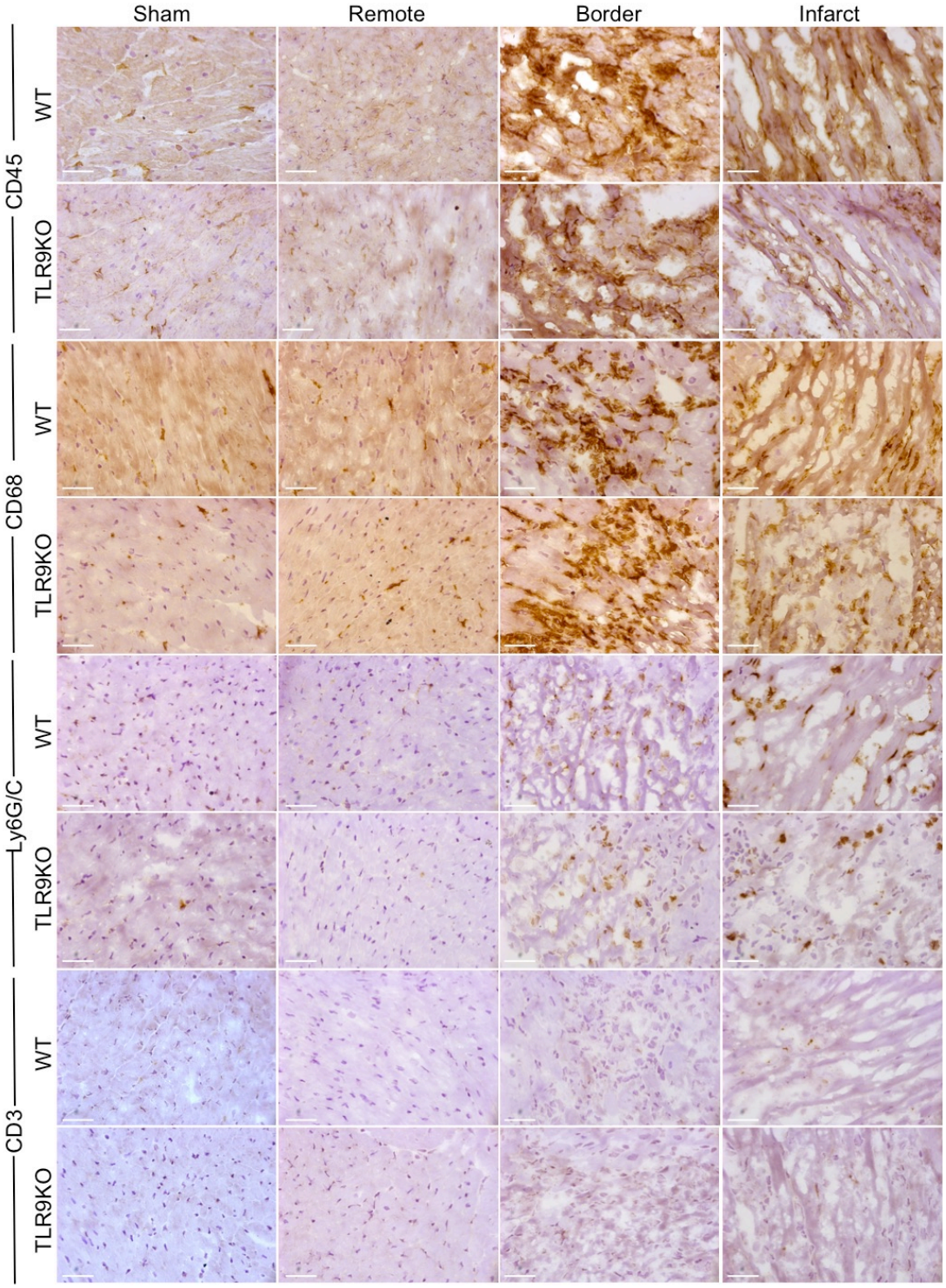

Figure 5.11 No disparities in the number of inflammatory cells in the myocardium in WT and TLR9KO mice 3 days after MI suggested by IHC staining.

Staining was performed to detect cell-specific markers; CD45 = leukocytes, CD68 = macrophages, Ly6G/C = neutrophils and CD3 = T-cells. 3 different areas of hearts subjected to MI are shown – remote, border and infarct. Similar to day 1 (figure 5.10) there appears to be greater infiltration of CD45-, CD68- and Ly6G/C- positive cells into the border and infarct regions of MI-operated hearts. No obvious difference in the filtration of inflammatory cells into the myocardium of WT and TLR9KO mice. *n*= 4 for all groups. Scale bars = 30 μm.

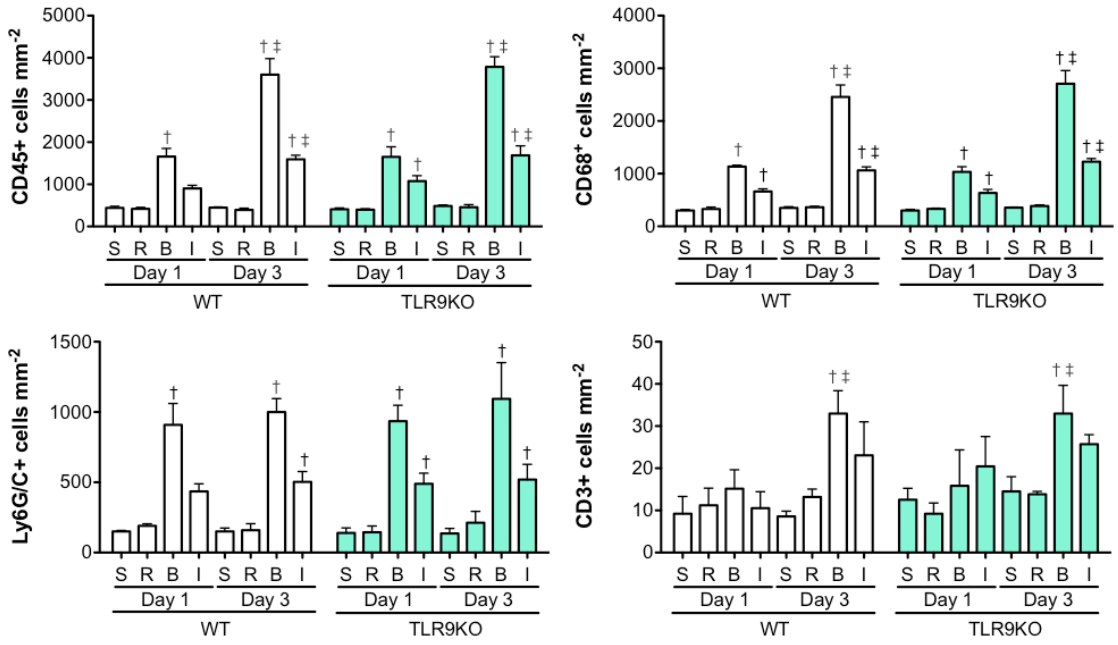

Figure 5.12 Quantification of infiltrating inflammatory cells into the myocardium of WT and TLR9KO mice revealed no difference between WT and TLR9KO mice subjected to MI.
Number of positive cells were counted from 5 different images per heart section in sham (S) mice and per region (R = Remote, B = Border, I = Infarct) in MI-operated animals (figures 5.10 and 5.11). Cell markers that were investigated include: CD45 = leukocytes, CD68 = macrophages, Ly6G/C = neutrophils and CD3 = T-cells. Number of CD45-, CD68- and Ly6G/C- positive cells were increased in the border and infarct regions of MI-operated hearts 1 and 3 days after MI. CD3-positive cells were increased in the border region of mice 3 days after MI. No differences in the quantity of inflammatory cells in the myocardium of WT and TLR9KO mice. Values are expressed as mean ± SEM. *n*= 4 for all groups. Data were analysed by two-way ANOVA with bonferroni's post-hoc test. † $p<0.05$ versus corresponding sham animals at same timepoint, ‡ $p<0.05$ versus same treatment at different timepoints.

To confirm these findings, the mRNA levels of pro-inflammatory chemokines and cytokines were measured by qRT-PCR in LV homogenates of WT and TLR9KO mice after MI surgery (**figure 5.13**). Expression of *Ccl2*, *Tnfa, Il1b* and *Il6* were increased 1 and 3 days after MI in WT mice compared with sham-operated mice. The anti-inflammatory marker, *Il10,* was not elevated 1 day after MI, but was significantly upregulated 3 days after surgery in MI-operated WT mice compared to sham-operated WT mice.

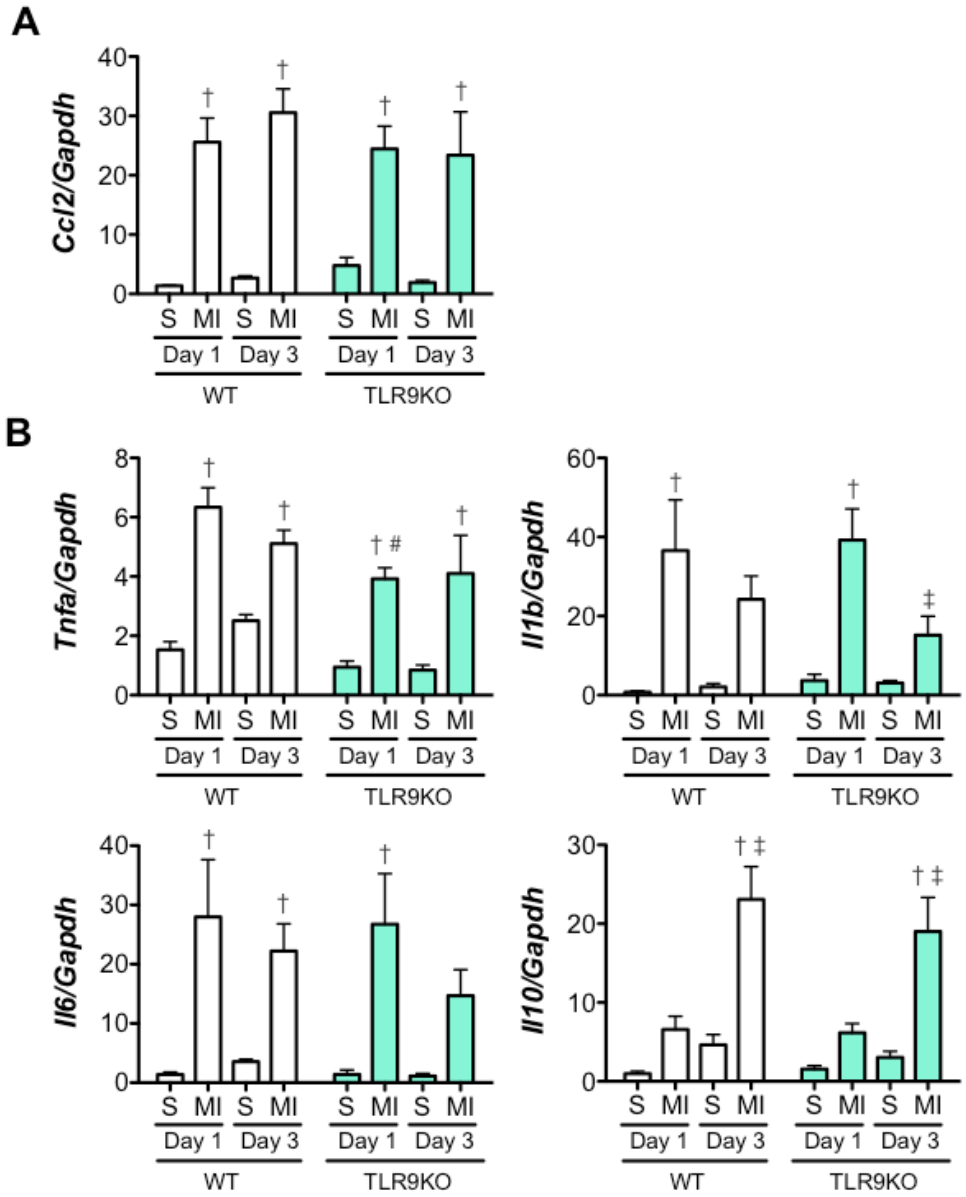

Figure 5.13 mRNA expression levels of chemokine and cytokines were not different between WT and TLR9KO mice after MI.
Levels of pro-inflammatory chemokine and cytokines mRNA were measured by qRT- PCR. Expression of chemokine (C-C motif) ligand (*Ccl2)*, tumour necrosis factor (*Tnf*)*a,* interleukin *(Il)1b* and *Il6* were upregulated in WT and TLR9KO mice subjected to MI compared with sham (S) mice. The anti-inflammatory marker, *Il10,* was increased 3 days after MI in WT and TLR9KO mice compared to sham mice. *Tnfa* expression was different between WT and TLR9KO 1 day after MI, however the other markers displayed no difference between WT and TLR9KO mice subjected to MI. A, mRNA expression of chemokines. B, mRNA levels of cytokines. Glyceraldehyde 3-phosphate dehydrogenase (*Gapdh*) was used as a housekeeping gene. Values expressed as mean ± SEM.; Day 1 WT sham *n*= 6, Day 1 WT MI *n*= 7, Day 3 WT sham *n*= 5, Day 3 WT MI *n*= 6*,* Day 1 TLR9KO sham *n*= 6, Day 1 TLR9KO MI *n*= 5*,* Day 3 TLR9KO sham *n*= 5, Day 3 TLR9KO MI *n*= 5*.* Data were analysed by two-way ANOVA with bonferroni's post-hoc test. † $p<0.05$ versus corresponding sham animals at same timepoint, ‡ $p<0.05$ versus same treatment at different timepoints. # $p<0.05$ versus WT animal at same timepoint with same treatment.

TLR9KO mice expressed similar mRNA levels of cytokines and chemokines (excluding *Tnfa*) as WT mice mentioned above, after sham and MI surgery at both timepoints. Interestingly, the increase in *Tnfa* expression in TLR9KO mice 1 day after MI was significantly less than WT mice 1 day after MI. However no significant differences in *Tnfa* levels were detected between MI-operated WT and TLR9KO mice 3 days after surgery. Therefore the qRT-PCR results, excluding *Tnfa*, corroborated the findings of the IHC staining, implying that inflammation may not contribute to the increased mortality of TLR9KO mice after MI.

5.2.4.2 Decreased *Timp1* mRNA expression may diminish survival of TLR9KO mice after MI.

Injury to the myocardium instigates remodelling of the ECM by MMPs to facilitate infiltration of inflammatory cells to remove necrotic cells [374, 375]. MMP activity is profoundly regulated by TIMPs, although an imbalance between MMPs and TIMPs has been reported in various cardiac diseases [376, 377, 378].

To determine whether alterations in the remodelling of the ECM contributed to the survival of TLR9KO after MI, the mRNA levels of two primary MMPs (*Mmp2 and Mmp9*) involved in cardiac remodelling were measured by qRT-PCR using LV homogenates of WT and TLR9KO mice 1 and 3 days after MI (**figure 5.14a**). *Mmp2*, which is constitutively expressed in the myocardium, was significantly decreased in MI-operated WT mice compared to relative sham-operated mice 1 and 3 days after surgery. In contrast, *Mmp9* expression was increased in WT mice subjected to MI compared with sham-operated WT mice at both timepoints.

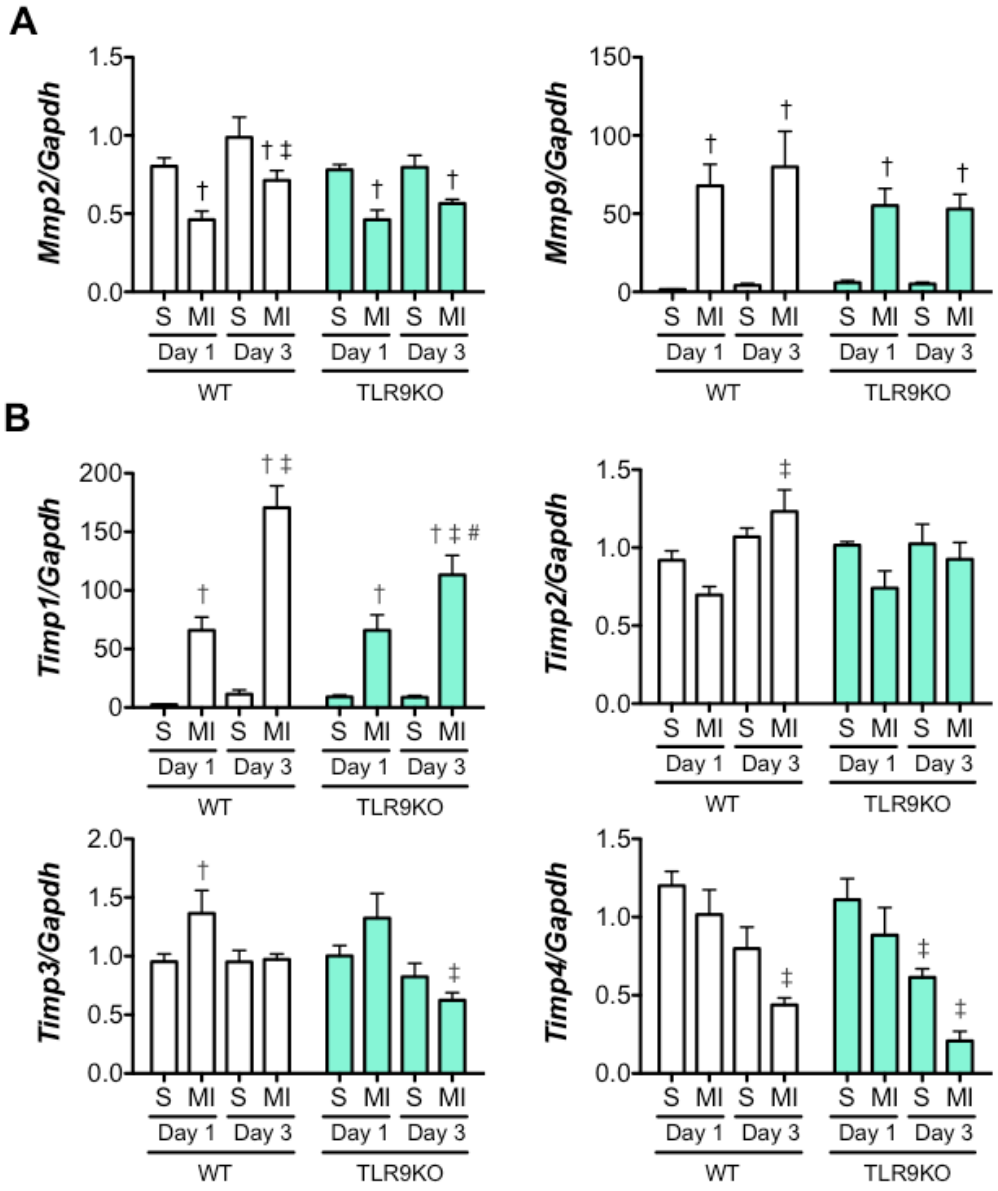

Figure 5.14 mRNA expression of tissue inhibitor of metalloproteinases (TIMP) 1 was decreased in TLR9KO mice 3 days after MI.
qRT-PCR was performed to evaluate the mRNA expression of A, Matrix metalloproteinases and B, TIMPs. *Mmp2* expression was decreased in mice subjected to MI compared to sham mice at both timepoints, whereas *Mmp9* levels were increased in MI-operated hearts compared with sham (S) -operated mice. *Timp1* was increased 1 and 3 days after MI compared to sham mice and a difference in *Timp1* expression was observed 3 days after MI between WT and TLR9KO mice. Minor changes were present in the expression of *Timp2*, *Timp3* and *Timp4* were observed after MI in WT and TLR9KO mice. Glyceraldehyde 3-phosphate dehydrogenase (*Gapdh*) was used as a housekeeping gene. Values expressed as mean ± SEM.; Day 1 WT sham *n*= 6, Day 1 WT MI *n*= 7, Day 3 WT sham *n*= 5, Day 3 WT MI *n*= 6, Day 1 TLR9KO sham *n*= 6, Day 1 TLR9KO MI *n*= 5, Day 3 TLR9KO sham *n*= 5, Day 3 TLR9KO MI *n*= 5. Data were analysed by two way ANOVA with bonferroni post-hoc test. † $p<0.05$ versus corresponding sham animals at same timepoint, ‡ $p<0.05$ versus same treatment at different timepoints. # $p<0.05$ versus WT animal at same timepoint with same treatment.

The expression of *Mmp2* and *Mmp9* between sham- and MI- operated TLR9KO mice followed similar tendencies to WT sham- and MI- operated mice and no differences in *Mmp2* and *Mmp9* expression were observed between WT and TLR9KO mice 1 and 3 days after MI.

Following this, the expression of *Timp1, -2, -3* and *-4* was studied by qRT-PCR using these samples (**figure 5.14b**). *Timp1* expression increased in a time specific manner in MI-induced WT hearts compared to sham-operated mice. Elevated *Timp2* and decreased *Timp4* expression was observed in WT MI-operated hearts between 1 and 3 days after operation. *Timp3* levels were increased in WT MI–operated hearts compared to sham-operated mice at day 1. MI-operated TLR9KO mice exhibited decreased *Timp3* and *Timp4* expression between 1 and 3 days after MI, whilst sham-operated TLR9KO mice unexpectedly displayed decreased *Timp4* expression between these two timepoints. *Timp1* expression in MI-operated TLR9KO mice, showed similar trend to MI-operated WT mice, compared to relative sham animals. However, most intriguingly, the increase in *Timp1* expression was significantly less in TLR9KO mice 3 days after MI, compared to WT mice 3 days after MI. Conversely, *Timp2, -3* and *-4* mRNA levels were consistent between MI-operated WT and TLR9KO mice at all timepoints. The exciting difference in *Timp1* expression 3 days after MI between WT and TLR9KO mice suggests potential alterations in ECM remodelling which may contribute to the increased incidence of cardiac rupture in TLR9KO mice. However further supporting evidence measuring MMP activity is required to validate this (**section 5.3.2** for further discussion).

5.2.4.3 Fewer fibroblasts and myofibroblasts in the infarcted myocardium of TLR9KO mice may promote cardiac rupture.

The wound healing response also encompasses the formation of granulation tissue at the wound site to promote angiogenesis as well as accommodating inflammatory cells and connective tissue cells. Predominately, fibroblasts facilitate construction of granulation tissue, although macrophages and myofibroblasts also participate [36]. IHC and IF staining were implemented to evaluate the infiltration of fibroblasts and myofibroblasts into the infarcted myocardium of WT and TLR9KO mice to determine whether there were any changes in the development of the granulation tissue.

Fibroblast specific protein 1 (FSP1) was used as a marker for fibroblasts [379] to estimate the number of fibroblasts after MI by IHC staining (**figure 5.15a**). The number of FSP1-positive cells were quantified in 5 different regions per heart section and expressed as cells per mm^2 (**figure 5.15b**). Compared to sham-operated WT mice, no changes in the number of FSP1-positive cells were observed 1 day after MI operation in WT mice. However there were dramatic increases in the number of positive cells in the border and infarct areas of WT mice 3 days after MI surgery, compared to sham-operated WT mice. TLR9KO mice subjected to sham and MI operation displayed similar patterns regarding the number of FSP1-positive cells, as sham- and MI- operated WT mice; both WT and TLR9KO exhibited an increase in the numbers of FSP1-positive cells in the border areas 3 days after MI, compared to sham-operated mice. However at this timepoint, there were fewer FSP1-positive cells counted in the border and infarct regions in MI-operated TLR9KO mice compared to WT mice subjected to MI. This exciting discovery suggests that there were less fibroblasts in the

border zone and infarct regions of TLR9KO mice compared to WT mice 3 days after MI, which may contribute to the increased incidence of cardiac rupture.

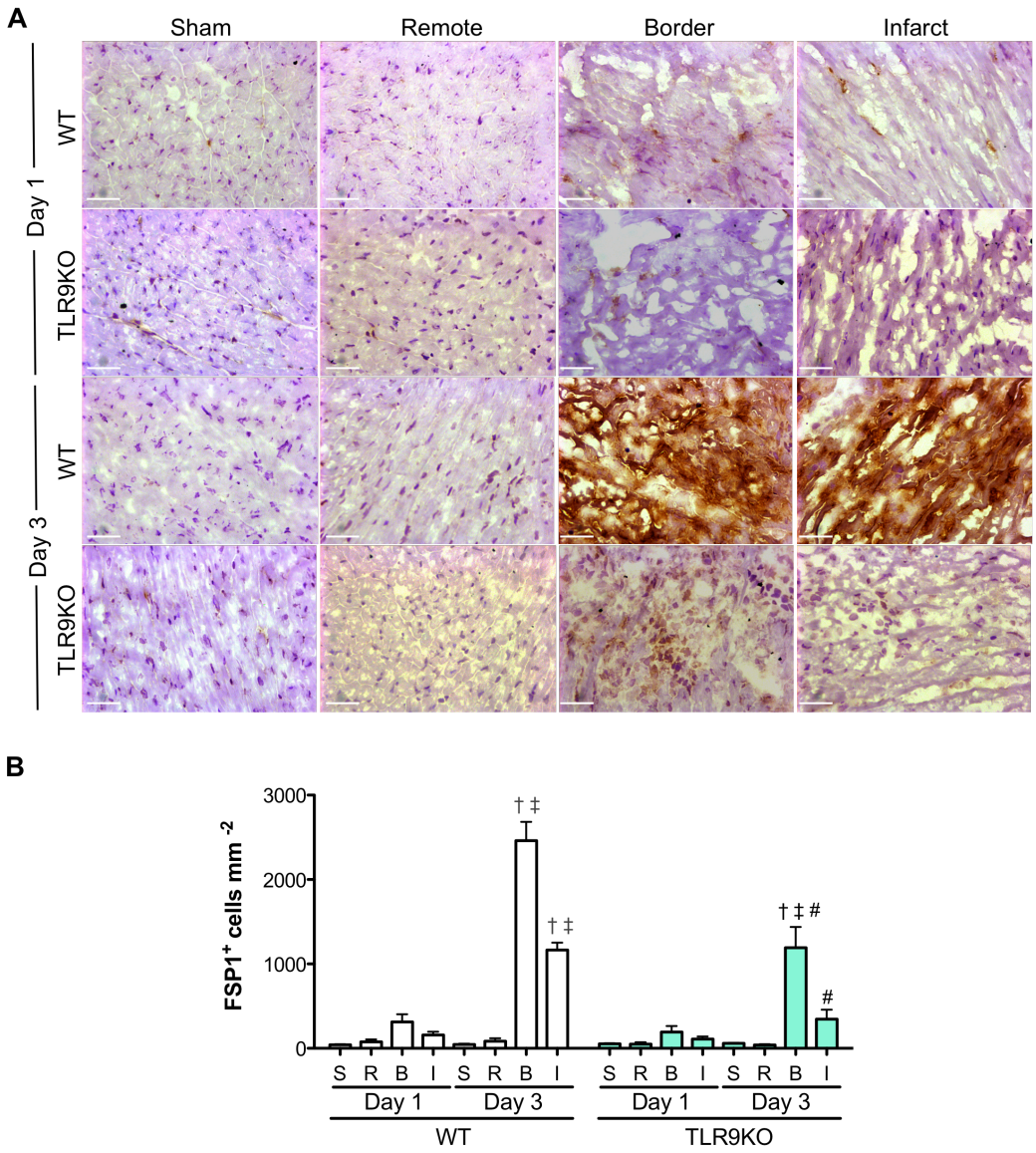

Figure 5.15 Fibroblast specific protein 1 (FSP1) staining revealed a decrease in the number of fibroblasts in TLR9KO hearts subjected to MI. Immunohistochemical analysis for FSP-1 was performed on cryosections of WT and TLR9KO hearts after MI. 3 different regions of hearts subjected to MI are shown – R = Remote, B = Border, I = Infarct. There are few FSP1-positive cells 1 day after surgery, however 3 days after MI; there is a significant increase in both MI-operated WT and TLR9KO mice. However, there were fewer FSP1-positive cells counted in TLR9KO mice compared to WT mice 3 days after MI. A, Scale bars = 30 µm. B, Quantification of FSP1-postive cells. Number of positive cells were counted from 5 different images per heart section in Sham (S) mice and per region (R, B and I) in MI operated animals. Values are expressed as mean ± SEM. *n*= 4 for all groups. Data were analysed by two-way ANOVA with bonferroni's post-hoc test. † $p<0.05$ versus corresponding sham animals at same timepoint, ‡ $p<0.05$ versus same treatment at different timepoints. # $p<0.05$ versus WT animal at same timepoint with same treatment.

To support these results, IF staining of cryosections with α-smooth muscle actin (α-SMA) and Ki67 was performed on WT and TLR9KO mice after MI (**figures 5.16 and 5.17**). α-SMA is considered a marker of myofibroblasts [32] whereas Ki67 is utilised as an indicator of proliferation [380]. The numbers of α-SMA-positive (myofibroblasts) and double positive cells (α-SMA and Ki67, proliferating myofibroblasts) were quantified from 5 different areas of each section (**figure 5.18**). Similar to FSP-1 staining, no differences in the number of positive cells were exhibited 1 day after surgery between sham- and MI-operated WT mice. The numbers of α-SMA-positive and double positive cells was increased in the border and infarct regions 3 days post-MI in WT mice, compared to sham-operated animals. TLR9KO mice presented similar tendencies as WT mice after sham and MI operation 1 day after operation. However, the numbers of α-SMA-positive and double positive cells was not significantly increased in the border and infarct regions of MI-operated TLR9KO 3 days, compared to sham animals and the numbers of α-SMA-positive and double positive cells was significantly less in MI-operated TLR9KO mice 3 days after surgery, suggesting there were fewer myofibroblasts and proliferative fibroblasts in TLR9KO mice 3 days after MI.

Therefore the intriguing data demonstrated in this section indicates a diminished number of fibroblasts, myofibroblasts and proliferative myofibroblasts in the infarcted myocardium of TLR9KO mice, compared to WT mice may impair the formation of granulation tissue and contribute to the increased occurrence of cardiac rupture.

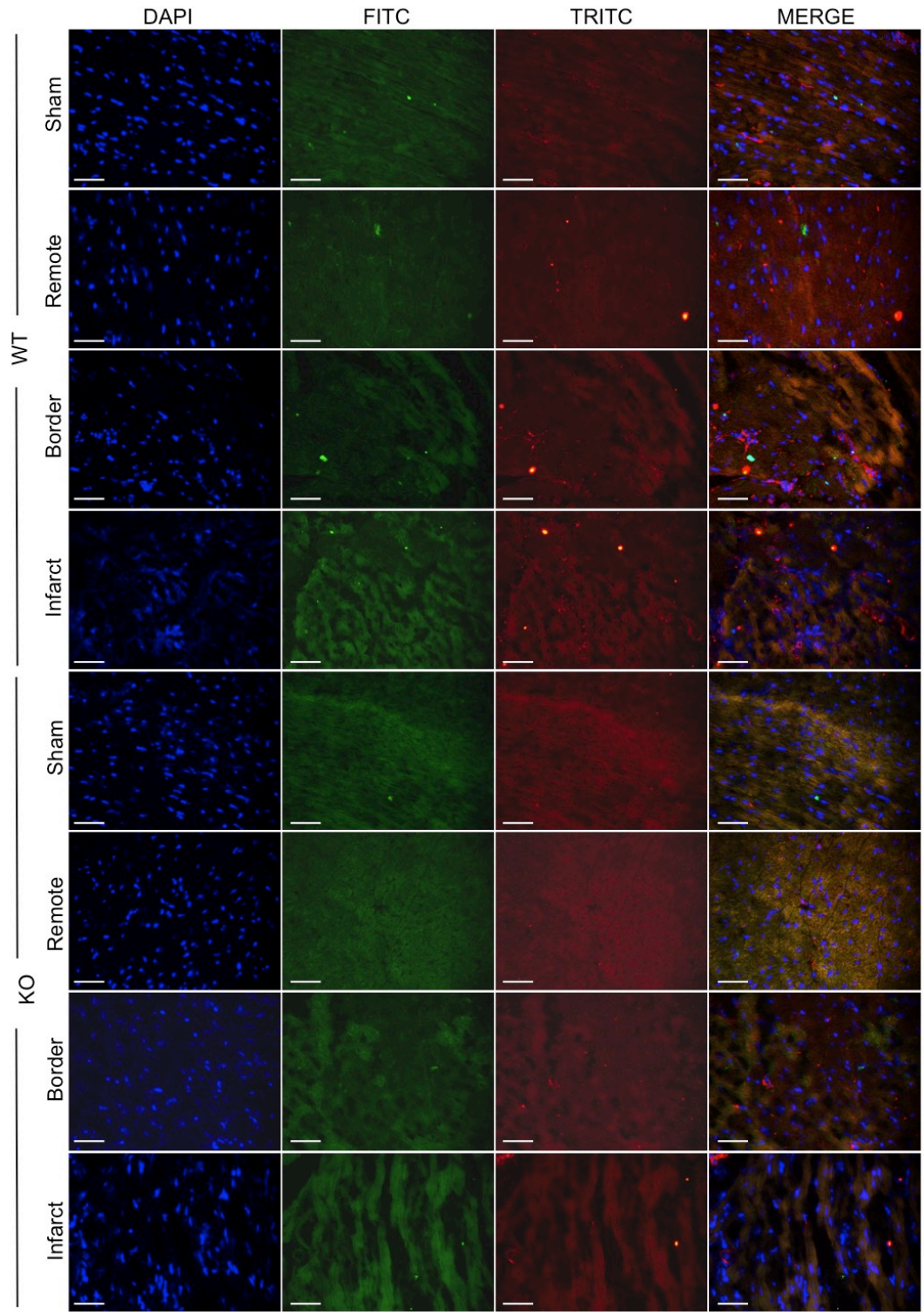

Figure 5.16 Immunofluorescence (IF) staining suggests no differences in the number of fibroblasts in the infarcted myocardium 1 day after surgery. IF analysis for α-smooth muscle actin (αSMA) and Ki67 was performed on cryosections of WT and TLR9KO hearts 1 day after MI. 3 different regions of mice subjected to MI are shown – remote, border and infarct. No differences in the expression of αSMA and Ki67 were detected in all groups. DAPI (DNA), FITC (Ki67 for proliferation), TRITC (αSMA for myofibroblasts). Scale bar = 60 μm. *n*= 4 for all groups.

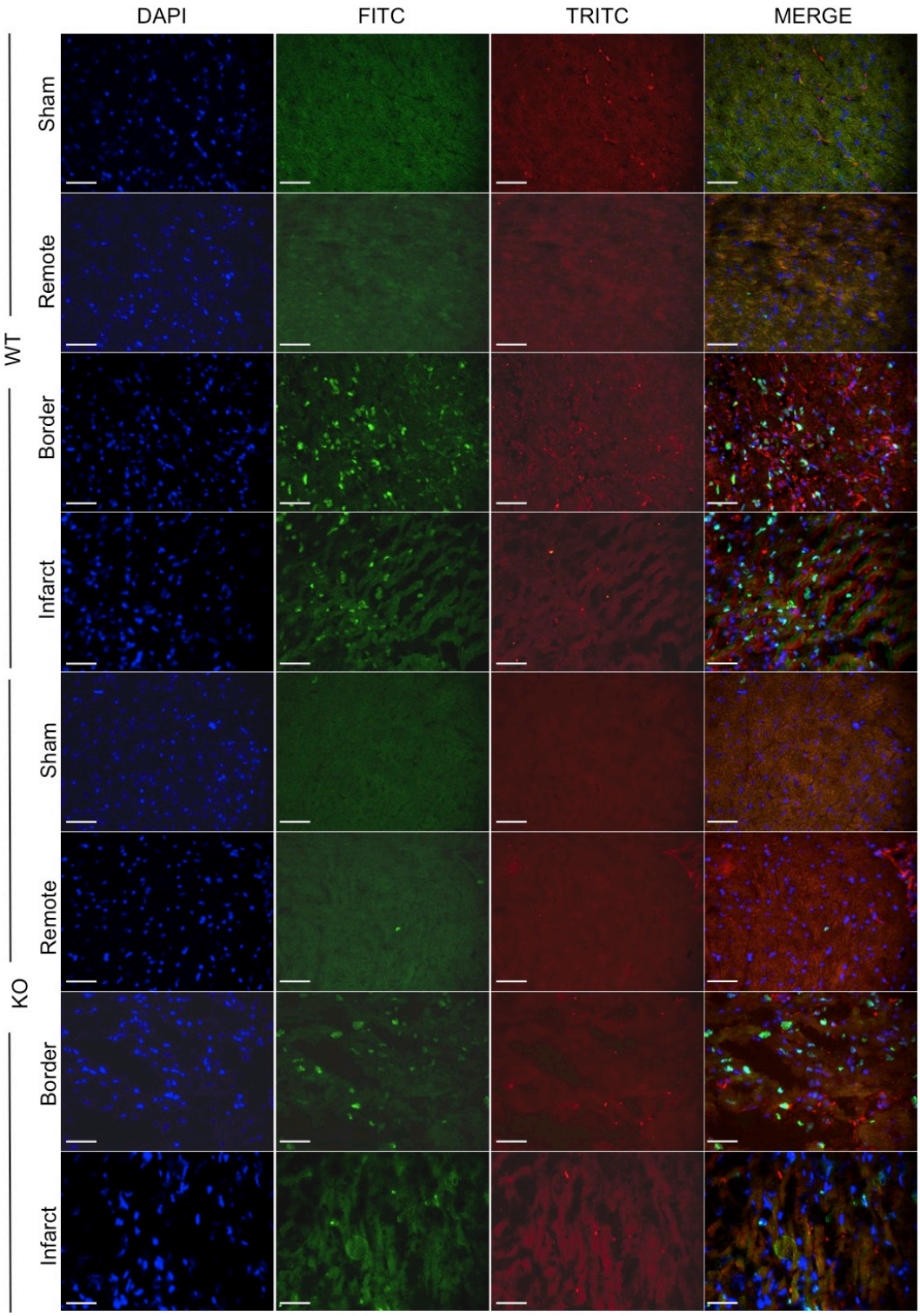

Figure 5.17 Immunofluorescence (IF) staining reveals a reduced number of proliferative myofibroblasts in TLR9KO mice 3 days after MI.
α-smooth muscle actin (αSMA) and Ki67 staining was performed on cryosections of WT and TLR9KO hearts 3 days after MI. 3 different regions of MI-operated hearts are shown – remote, border and infarct. There appears to be a reduction in αSMA-positive and Ki67-positive cells in the border and infarct regions on TLR9KO mice compared with WT mice. DAPI (DNA), FITC (Ki67 for proliferation), TRITC (αSMA for myofibroblasts). Scale bar = 60 μm. *n*= 4 for all groups.

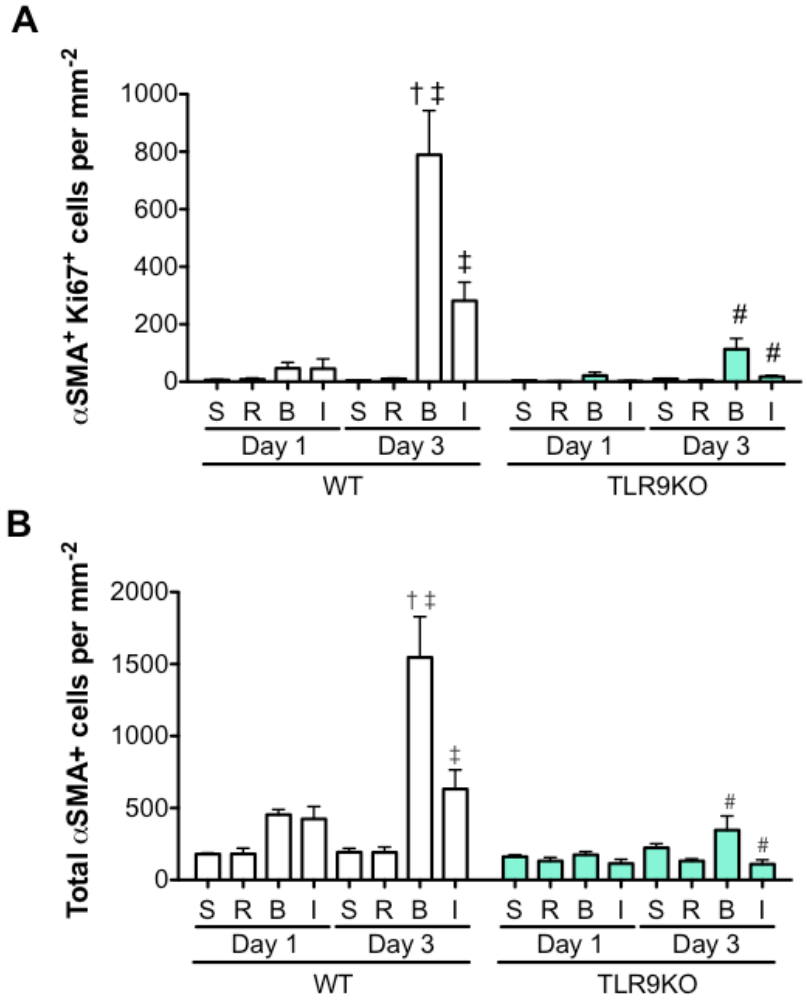

Figure 5.18 Quantification of IF staining confirms reduced numbers of proliferative myofibroblasts in TLR9KO mice 3 days after MI.
Quantification of α-smooth muscle actin (αSMA)-positive and Ki67-postive cells (A) and total number of αSMA-positive cells (B). Number of positive cells were counted from 2 different images per heart section (as shown in figures 5.16 and 5.17) in sham (S) mice and per region (R = Remote, B = Border, I = Infarct) in MI-operated animals. There were no differences in the number of αSMA-positive-Ki67-postive cells and number of αSMA-positive cells 1 day after operation. 3 days after MI, there was a significant increase in these cells in the border and infarct regions of WT mice subjected to MI, which was not observed in TLR9KO mice. Values are expressed as mean ± SEM. *n*= 4 for all groups. Data were analysed by two-way ANOVA with bonferroni post-hoc test. † $p<0.05$ versus corresponding sham animals at same timepoint, ‡ $p<0.05$ versus same treatment at different timepoints. # $p<0.05$ versus WT animal at same timepoint with same treatment.

5.3 Discussion

Overall this chapter demonstrates the beneficial functions of TLR9 during post-MI acute LV remodelling (**table 5.3**). After MI surgery, the incidence of cardiac rupture and mortality was substantially elevated in TLR9KO mice, compared to WT mice. This reduced rate of survival may be attributable to impaired wound healing with the observation of decreased levels of *Timp1* mRNA and fewer fibroblasts and myofibroblasts in TLR9KO mice post-MI. Most unexpectedly, TLR9-mediated inflammation may not contribute to the mortality of TLR9KO mice after MI. Collectively, these findings suggest novel and vital, yet life-preserving roles of TLR9 that potentially influences *Timp1* mRNA expression and numbers of fibroblasts and myofibroblasts that are fundamental to post-MI acute LV remodelling.

5.3.1 ECM remodelling, inflammation and initiation of scar formation were observed after MI in WT mice.

Cardiac rupture is a common observation in both acute-MI patients and preclinical models. After MI induction by LAD ligation, incidence of cardiac rupture in C57Bl/6 mice was reported to be between 20 – 31% [372, 381, 382]. However in this study a rupture incidence of 11.1% was achieved in WT (C57Bl/6) mice (**figure 5.2**). The low value for rupture incidence is possibly due to the experienced surgical technique of Dr Shigemiki Omiya (King's College London).

As TLR9KO mice began to die 4 days after MI operation, mice were harvested 1 and 3 days after MI. Acute LV remodelling post-MI involves the recruitment of inflammatory cells and fibroblasts to facilitate removal of dead cells and ECM remodelling. Yang *et al* (2002) demonstrated infiltration of neutrophils 1 - 2 days

after MI whilst the number of macrophages increased between 1 - 3 days after MI [382]. Additionally, the same report showed that lymphocytes, such as T-cells, were expressed in the myocardium 4 days after infarction and that fibrosis was detected 1 week after MI. In other studies levels of inflammatory mediators such as *Tnfa* and *Il6* have been described to be upregulated 24 hours after MI [365, 383, 384]. Furthermore, in terms of ECM remodelling, it was reported that *Mmp9* expression was detected 1 day after MI and peaks 2 days later [385] whereas *Mmp2* and *Timp1-4* expression was elevated 4 days after MI [386, 387]. Additionally it was demonstrated that fibroblasts are observed at all stages of LV remodelling post-MI, yet are most prominent, along with myofibroblasts during the proliferative stage that occurs roughly 3 days after MI [381, 388].

It was therefore anticipated that in the mouse model described here, a robust inflammatory response entailing leukocyte recruitment and increased pro-inflammatory cytokine expression would be observed after both harvesting timepoints (1 and 3 days after MI), but very few T-cells and little fibrosis would be observed at these timepoints. Additionally, upregulation of *Mmp9* levels might be expected at both 1 and 3 days after MI in this model alongside infiltration of fibroblasts and myofibroblasts, particularly 3 days after operation. By contrast, expression of *Mmp2* and *Timp1-4* was expected to remain unchanged, as exhibited by previous studies.

As predicted, MT staining revealed little overt fibrosis in the myocardium of MI-operated mice at both 1 and 3 days after operation (**figure 5.8**). qRT-PCR analysis detected a time-specific increase in the mRNA levels of fibrotic molecular markers, *Col1a2*, *Col3a1* and *Tgfb1* (**figure 5.9)**, suggesting that fibrosis would be observed after the timepoints which mice were harvested. Unexpectedly, *Col1a2* and *Col3a1* mRNA levels were also increased between 1

and 3 days after operation in sham-operated mice. The elevated levels could be a consequence of the operation and thus highlights the necessity for appropriate controls.

Table 5.3 Summary table for findings in this chapter.
After MI, TLR9KO mice had a higher incidence of cardiac rupture 4 days than WT mice. No differences were found in the ischemic area at risk, infarct size, LV wall thickness, levels of fibrosis, inflammation or MMP expression. Interestingly, mRNA expression of *Tnfa* (tumour necrosis factor α), *Timp1* (an inhibitor of ECM remodelling) and the number of fibroblasts and proliferative myofibroblasts were decreased in TLR9KO mice 3 days post MI compared to WT mice.

Analysis		WT Sham vs WT MI	TLR9KO Sham vs TLR9KO MI	WT MI vs TLR9KO MI
Incidence of cardiac rupture		n.s	* 4-5 days	* 4-5 days
Infarction size				
Ischemic area at risk		NA	NA	n.s
Infarct size		NA	NA	n.s
Cardiac function		NA	NA	n.s
LV remodelling				
Wall thickness		NA	NA	n.s
Fibrosis	**- collagen deposition**	n.s	n.s	n.s
	- collagen markers	* 1-3 days	* 1-3 days	n.s
Inflammation	**- cell infiltration**	* 1-3 days	* 1-3 days	n.s
	- mediators	* 1-3 days	* 1-3 days	* 1 days (*Tnfa* only)
ECM remodelling	**- MMP mRNA expression**	* 1-3 days	* 1-3 days	n.s
	-TIMP mRNA expression	* 1-3 days (*TIMP1* only)	* 1-3 days (*TIMP1* only)	* 3 days (*TIMP1* only)
Cell infiltration	**- fibroblasts**	* 3 days	* 3 days	* 3 days
	- myofibroblasts	* 3 days	* 3 days	* 3 days

The data presented in this study regarding inflammatory cell recruitment and expression of pro-inflammatory and anti-inflammatory mediators concur with previous studies (**figures 5.10 – 5.13**) [365, 382, 383, 384, 389]. Although pro-inflammatory cytokines were expressed 3 days post-MI, the enhanced expression of the anti-inflammatory marker, *Il10,* between 1 and 3 days post-MI (**figure 5.13b, table 3.1**), suggested a transition from an inflammatory phase to a proliferative phase of LV remodelling 3 days post-MI [32, 33]. This was additionally supported by the time-specific increase of fibroblasts, myofibroblasts and proliferating myofibroblasts between 1 and 3 days after MI (**figures 5.15 – 5.18**) as myofibroblasts, in particular, are known to appear during the phenotypic switch between the 2 phases [32, 381, 388].

Mmp2 expression in MI-operated WT mice unexpectedly decreased significantly, compared with sham mice, at all timepoints (**figure 5.14a**). This surprising result suggested possible transcriptional regulation of the *Mmp2* gene in MI-operated mice, during the acute phase of LV remodelling. *Mmp9* expression was upregulated at both harvest points after MI as expected. Whilst there were only small changes in *Timp2, -3* and *-4* mRNA levels*, Timp1* expression was significantly elevated in MI-operated mice at both timepoints (**figure 5.14b, table 3.1**). However, it has been reported that although *Timp1* mRNA increases 3 days after MI and peaks at day 7, an increase in TIMP1 protein levels was only detected 2 weeks after MI [390, 391], suggesting post-translational processing of the TIMP1 protein. Therefore protein expression of TIMP1 should be evaluated in this current model to validate its increase in expression at the protein level.

Together, these experiments demonstrate the induction of a robust inflammatory response, ECM remodelling and tissue repair processes in this model of MI, which corroborates with previous reports.

5.3.2 Diminished wound healing contributes to increased incidence of cardiac rupture in TLR9KO mice after MI.

The surprising and intriguing mortality of TLR9KO mice, 4 – 6 days after MI (**figure 5.2, table 3.1**) indicated that TLR9 was fundamental for acute LV remodelling post-MI. Post-mortem analysis revealed that cardiac rupture of the LV free wall was the cause of death of MI-operated TLR9KO mice (**figure 5.3**), which is frequently observed in patients and murine MI models [36]. Previous reports demonstrate that cardiac rupture is commonly observed 2 – 6 days after MI surgery in mice, with a peak seen at 3 - 4 days [392], which corroborates with incidence of mortality of TLR9KO mice in this model (**figure 5.2**).

No preceding cardiac phenotypes that may increase susceptibility to cardiac rupture were ascertained by echocardiography or physiological measurements prior to MI operation in TLR9KO mice (**table 5.1**). Thus the cause of cardiac rupture was investigated and included factors such as; enlargened infarct size, decreased wall thickness, inflammation, altered ECM remodelling and modified granulation tissue formation. The BP of WT and TLR9KO mice was not measured prior to and after surgery. Baseline BP should be similar between WT and TLR9KO mice (as shown in **table 3.3**), however as differences in BP is another contributing factor to the increased incidence of cardiac rupture, BP should be investigated in future studies between WT and TLR9KO mice.

A previous investigation demonstrated that activation of TLR9 by administration of CpG ODN did not influence infarct size in WT mice subjected to I/R injury [356].

Although the I/R injury is distinctive to LAD ligation, it could potentially suggest that there would be no differences in infarct size in this current model. Assessment of the ischemic area at risk (**figure 5.4**) and infarct size (**table 5.2**) by Evans Blue staining and cardiac MRI (**figure 5.5**) demonstrated this expectation to be true, indicating that infarct size was unrelated to the incidence of cardiac rupture in TLR9KO.

The increased susceptibility of cardiac rupture in TLR9KO mice, suggested that TLR9 and potentially TLR9-mediated inflammation were important for tissue repair and debris removal after MI. Surprisingly in this study, no differences in the inflammatory response (except *Tnfa* mRNA expression) between WT and TLR9KO mice after MI were observed at all timepoints (**figures 5.10 - 5.13, table 3.1**). Although, *Tnfa* expression was reduced 1 day after MI in TLR9KO mice compared to WT mice, the levels of *Tnfa* were similar 3 days after MI between MI-operated WT and TLR9KO mice, prior to occurrence of cardiac rupture (**figure 5.13b**). One report stated that MI-operated TNFαKO mice had a lower incidence of rupture compared to WT controls with a reduced inflammatory response [393]. Therefore it was unlikely that inflammation or *Tnfa* itself contributed to the incidence of cardiac rupture as the levels of *Tnfa* were similar 3 days after MI. However due to the time required for translation, protein levels of TNFα expression should be evaluated 3 days after MI in WT and TLR9KO mice to determine any differences in the protein expression of TNFα, that may contribute to the increased incidence of cardiac rupture in TLR9KO mice. Additionally, the comparable inflammatory response between MI-operated WT and TLR9KO mice implied that inflammation observed after MI is independent of TLR9 and may be mediated by other immune sensors, such as TLR2, TLR3 and TLR4 [366, 367, 368, 369].

Investigation of ECM remodelling found no differences in the mRNA levels of *Mmp2, Mmp9, Timp2, 3 and 4* between WT and TLR9KO mice 1 and 3 days after MI. Interestingly, *Timp1* mRNA expression measured by qRT-PCR was significantly different between WT and TLR9KO mice 3 days after MI (**figure 5.14**, **table 3.1**). It remains unclear how differences in *Timp1* expression may contribute to the incidence of cardiac rupture. One report observed accelerated LV remodelling 14 days after MI in TIMP1KO mice compared to WT mice, however the incidence of cardiac rupture was unchanged [394]. As TIMP1 is an inhibitor of MMPs, it affects MMP activity rather than their expression. As previously mentioned, it was reported that TIMP1 may undergo post-translation processing [390, 391]. Thus zymography should be performed to measure MMP activity in the myocardium of MI-operated WT and TLR9KO mice to determine and validate any differences in ECM remodelling.

In this study, fewer fibroblasts and proliferative myofibroblasts were observed in the infarcted myocardium of TLR9KO mice 3 days after MI, compared to WT mice after MI (**figures 5.15 – 5.18, table 3.1**). This may have diminished the formation of granulation tissue post-MI in TLR9KO mice, impairing the tissue repair process, provoking rupture of the myocardium. Possible reasons for observing fewer fibroblasts within the myocardium of TLR9KO mice include differences in fibroblast activation or differentiation or recruitment of fibroblasts. Myofibroblasts are differentiated from different categories of fibroblasts as well as other cell types [32] and it has been demonstrated that TLR9 activation contributes to the differentiation of pulmonary fibroblasts into myofibroblasts [395]. Conversely, *in vitro* experiments conducted by Ohm et al (2014) found that TLR9 had no effect on CF differentiation into myofibroblasts, but reduced the proliferation and migration of CFs which opposes the findings presented in

figures 5.16 - 5.18 [176]. Reports that TIMP1 can stimulate the growth of fibroblasts [112], may provide a mechanism in which TLR9 signalling may regulate fibroblast migration by altering TIMP1 expression (**figure 5.19**). Nonetheless further studies are needed to uncover a possible association between TLR9 and myofibroblast differentiation.

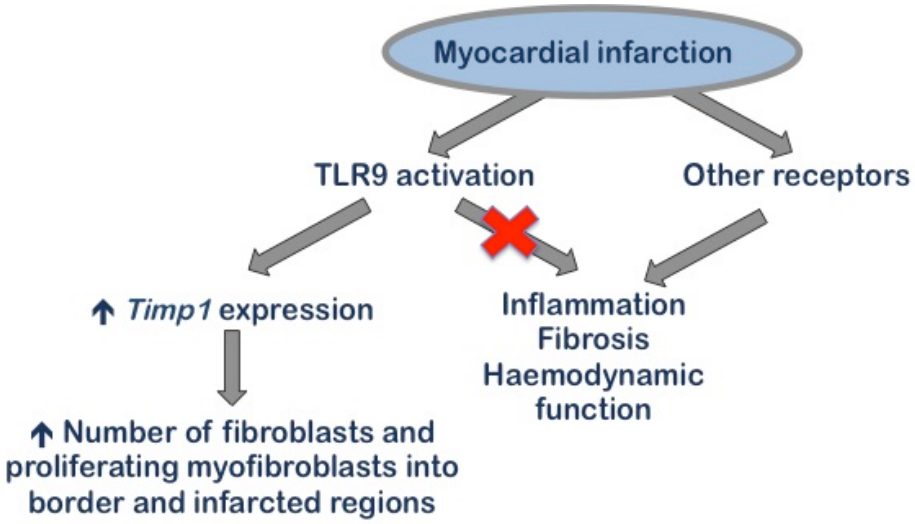

Figure 5.19 The proposed mechanism of TLR9-signalling in acute left ventricular remodelling after MI.
Induction of MI leads to stimulation of TLR9, which sequentially increases expression of *Timp1*. This consequently increases the number of fibroblasts and induces proliferation of fibroblasts into myofibroblasts. However, TLR9 does not contribute to the inflammation observed in acute left ventricular post-MI.

One limitation of this study was the use of C57Bl/6 mice as the WT control. Though TLR9KO mice have been bred onto Bl/6 background, littermate controls are the most appropriate control and this is further discussed in **section 6.4.** Another limitation involves the use of a global TLR9KO mice, as this does not relay much information about which cell type(s) mediate the observed effect, whether it be cardiomyocytes, fibroblasts or endothelial cells. Further, MMP activity needs to be measured by zymography to validate any claims about TLR9 influencing ECM remodelling (mentioned above). Also, due to the heterogeneity of the heart post-MI, qRT-PCR of inflammatory, fibrotic and ECM

remodelling markers should have been performed using LV samples that had been dissected into remote, border and infarct areas. However it may be difficult to dissect a heart 3 days post- surgery as the infarct areas may be difficult to see. Further work could focus upon the effects of TLR9 after reperfusion to determine whether similar or alternate effects are observed and this may be more relevant to clinical MI cases in which reperfusion of a blocked artery has been achieved.

In summary, this chapter identified novel, beneficial downstream functions of TLR9 in tissue repair after myocardial injury. These life-preserving functions of TLR9 may influence MMP activity and the numbers of fibroblast and myofibroblasts, preventing the induction of cardiac rupture and adverse consequences. However more supporting evidence is required to validate these claims and to identify the mechanism by which TLR9 mediates these functions.

6 General Discussion

HF is associated with increased levels of pro-inflammatory cytokines and inflammation [19, 20, 21]. Although, the mechanisms of cardiac inflammation remain unclear, it was proposed that 'sterile inflammation' contributes to the pathogenesis and progression of HF [20]. Previous data identified that the immune sensor and inflammatory instigator, TLR9 is associated with pressure overload-induced myocardial inflammation and cardiac remodelling [173]. However, the mechanisms by which TLR9-mediated inflammation contribute to HF remain unknown, though reports of the immunomodulatory properties of β-AR signalling [224, 225], which is also impaired in pressure overload and HF, suggested a potential avenue to investigate. Furthermore the role of TLR9 in MI, a common cause of HF has not yet been elucidated. As the role of TLR9 within the failing heart is unclear, this thesis aimed to investigate the potential role of TLR9-mediated inflammation in the pathogenesis of HF, with particular focus on β-AR signalling and in MI.

Using an Iso infusion model, it was shown that TLR9 induced cardiac dysfunction, thickened posterior walls and heart weight gain. These interactions suggest a detrimental role of TLR9 in β-AR-induced cardiac remodelling. Furthermore, the Iso infusion model used to stimulate the β-AR signalling cascade, appeared to be unique and warranted further study. Iso infusion caused β-stimulant-induced cardiomyopathy that was devoid of changes to β-AR signalling and calcium handling, oxidative stress, metabolic abnormalities and cardiac remodelling (fibrosis, apoptosis or inflammation). However, β-stimulant-induced cardiomyopathy exhibited IκB degradation, suggesting NFκB activation. Furthermore, 1 day after removal of Iso, recovery of cardiac

dysfunction and tachycardia associated with β-stimulant-induced cardiomyopathy was observed.

A beneficial role of TLR9 in post-MI acute LV remodelling was uncovered, which prevented cardiac rupture. This function was associated with differences in *Timp1* mRNA expression and the number of fibroblasts and myofibroblasts. These findings highlight two things: firstly, the opposing roles of TLR9 in these two different circumstances and secondly, that the role of TLR9 in these two situations was independent of inflammation. However, whilst these findings are highly exciting, unfortunately, neither of the models used in this thesis enabled the study of TLR9-mediated inflammation in the pathogenesis of HF, which was the original aim of this thesis. Both models have been reported to induce HF [33, 224, 362, 375], however notable phenotypes were observed in these models before HF was recognised. Therefore this thesis transferred its focus to investigate the roles of TLR9 in cardiac dysfunction, LV remodelling and tissue repair.

6.1 The multifunctional role of TLR9 in cardiac remodelling.

The data presented in this thesis demonstrated the double-edged nature of TLR9 in cardiac remodelling. Although cardiac remodelling aims to alleviate increased workload, these remodelling processes eventually lead to cardiac dysfunction and the development of HF [66]. Further study to comprehend the transition from adaptive to maladaptive remodelling is required to highlight potential therapeutic targets that could manipulate pathways to preserve adaptive mechanisms and reverse maladaptive remodelling. It often appears that the same pathway is involved in both adaptive and maladaptive processes, though the observed phenotype depends on its balance, such as NFκB and TNFα [185, 186, 187]. Additionally, components of cardiac remodelling appear to

interact with one another, for example, inflammation is connected to fibrosis and cell death, whilst fibrosis in turn is connected to cell death and inflammation [32, 131]. Therefore dissecting and targeting one process may influence the effects of other components.

The presented data identified the detrimental function of TLR9 in β-AR-induced cardiac remodelling, alongside its beneficial role in post-MI acute LV tissue repair. Furthermore the nature of remodelling disrupted by TLR9 activation in these two models was different; in chapter 3, heart weight and function were influenced by TLR9 whereas in chapter 5, TLR9 manipulated *Timp1* mRNA expression and the number of fibroblasts and myofibroblasts. These findings propose novel roles of TLR9 in cardiac remodelling after Iso infusion or post-MI. These functions are added to its well-documented function within the immune system as a sensor [177, 181] and its newly reported protective role against stress by modulating energy metabolism in cardiomyocytes [183, 184] (**figure 6.1**).

In a model of pressure overload, TLR9KO mice displayed reduced chamber dilatation and improved cardiac function and the authors suggested this was due to the observation of fewer infiltrated myocardial macrophages, less fibrosis and reduced hypertrophy compared to control mice [173]. This report indicated additional roles of TLR9 in cardiac remodelling, suggesting a potential role of TLR9-mediated inflammation in pressure overload-induced cardiac remodelling. Many signalling pathways are activated during pressure overload and it was hypothesised that the β-AR signalling pathway, a major regulator of calcium handling and cardiac contractility, could be involved in mediating the observed rescue of chamber dilatation and cardiac dysfunction measured after pressure overload.

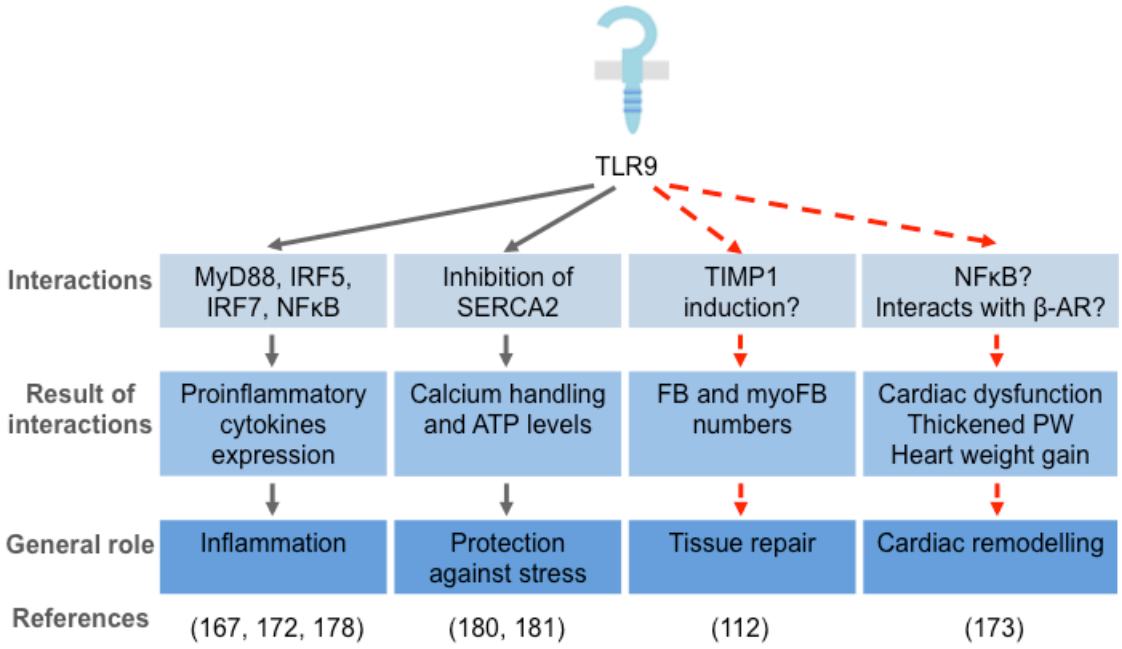

Figure 6.1 Reported and potential roles of TLR9 within the myocardium. Known (grey arrows) functions of TLR9 include its role as an immune sensor stimulating inflammation as well as providing protection against CpG-induced stress. Novel potential functions of TLR9 observed in this thesis (red arrows), suggest that TLR9 is involved in tissue repair and cardiac remodelling and potential mechanisms have been outlined, supported by data from other reports.

The current data suggests that an interaction between the TLR9 signalling pathway and the β-AR signalling cascade, which was detrimental to cardiac function and structure, could partially contribute to the rescued phenotype observed in the pressure overload model in TLR9KO mice. In addition, fibrosis is a typical consequence of cardiomyocyte death and the reduced fibrosis detected after pressure overload in TLR9KO mice compared to control mice could be due to diminished cell death. However it may also potentially be due to the reduced number of fibroblasts and myofibroblasts in TLR9KO mice after myocardial injury (which was observed in the acute MI model). Therefore, TLR9-mediated regulation of fibroblast and myofibroblast numbers may be beneficial after MI for tissue repair, but could have adverse consequences after pressure overload and induce fibrosis. Thus the signalling pathways

downstream of TLR9 that mediate these observations should be studied in further detail.

The opposing nature of TLR9 after Iso infusion or MI is not uncommon as many proteins play various roles under different physiological and pathological conditions. It was reported that MAPK p38, calpains and NFkB signalling are protective against pressure overload-induced haemodynamic stress [306, 396, 397] whereas in I/R injury, these proteins are suggested to be detrimental [398, 399, 400, 401, 402, 403]. In combination with the findings of this thesis, these reports highlight that the aetiologies of the cardiac remodelling should be considered, as it is likely that remodelling is mediated through different mechanisms and induced by different causes.

6.2 Role of TLR9-mediated inflammation in the failing heart

TLR9 is recognised for its role in inflammation with many papers documenting that the stimulation of TLR9 induces expression of pro-inflammatory cytokines [181, 404]. However the data presented here demonstrated that TLR9-mediated inflammation was not involved in influencing cardiac function and heart weight in a model of β-stimulant-induced cardiomyopathy and was not implicated in acute tissue repair post-MI. These findings were surprising as both MI and the β-AR signalling cascade have been reported to involve inflammation [33, 224, 362, 375]. One factor that should be considered is the temporal aspects of inflammation, the acute versus chronic inflammatory periods and the rise / fall of different inflammatory mediators at different stages of myocardial injury and inflammation. In comparison with the pressure overload study [173], the measurements were performed 9 weeks after the induction of pressure-overload, whereas similar measurements were recorded 4 weeks after Iso

infusion or 3 days after MI surgery. Therefore temporal myocardial inflammatory activities and the timepoint of harvest may advocate one reason as to why no differences in inflammation were observed in the models utilised in this thesis and may indicate a role of TLR9 in chronic myocardial inflammation, rather than acute inflammation. Moreover, pressure overload is known to damage the structure of mitochondria and induce mitochondrial dysfunction [405, 406], which in turn, could provoke a TLR9-mediated inflammatory response due to incomplete degradation of mtDNA [173]. However after Iso infusion no mitochondrial structural damage was observed by electron microscopy, which could suggest why no inflammation was observed in this model. It is also plausible that pressure overload and Iso infusion induce cardiac remodelling by different stimuli, which activate different pathways. The cardiac phenotype observed after pressure overload is a culmination of the activation of many signalling pathways, whereas the Iso infusion model focuses on one signalling pathway. Therefore the data from this thesis suggests that TLR9-mediated inflammation observed after pressure overload may possibly be independent of β-AR signalling.

Though the pressure overload model suggested a role of TLR9-mediated inflammation to induce chamber dilatation and cardiac dysfunction, this was based on the observation of mild infiltration of $CD68^+$ macrophages 10 weeks after pressure overload. However, no significant differences were detected in the cytokine mRNA levels between pressure overload control and TLR9KO mice at this timepoint. This questions the activity of these macrophages as no changes in cytokine expression were detected.

Additionally, it could be postulated from this current data that TLR9-mediated inflammation may not be involved in the progression of HF, but inflammation may be stimulated by other immune receptors and pathways including TLR2,

TLR3, TLR4 and the inflammasome [169]. However TLR9 may contribute to the pathogenesis and progression of HF with the novel roles involved in tissue repair and cardiac remodelling demonstrated by this thesis. Therefore the data from this thesis questions the influence of TLR9-mediated inflammation on cardiac remodelling and the failing heart.

6.3 Uniqueness of Iso infusion model

The renounced Iso infusion model was utilised to model HF. However this current Iso model could be considered unusual and unique as it developed into a condition referred to as β-stimulant-induced cardiomyopathy, which exhibited cardiac dysfunction and heart weight gain but no other aspects of cardiac remodelling (fibrosis or apoptosis). Additionally, as the data stands no changes where observed in the metabolic state, oxidative stress, β-AR expression or calcium handling of Iso-infused myocardium. Although trends were observed in some of these parameters, more samples are required to confirm and validate these statements. These findings conflicted with previous reports as discussed (**sections 3.3.2 and 4.3.2**) and could be due to the dose of Iso used, duration of treatment, method of administration, age and strain of mouse and species of animal (**table 6.1**).

Additionally, reports of polymorphisms within the AR signalling cascade have been described in humans, which can affect ligand binding and the activity of proteins [407]. Though there are no reports as of yet, it is possible that polymorphisms in the AR signalling cascade may exist between different strains of mice, as well as between animals which may contribute to the unique phenotype observed in this thesis in comparison with previous reports.

Table 6.1 Features of reported models of Iso infusion

Table to illustrate doses and durations of Iso infusion alongside, age, weight and sex of animal utilised in reported models and the associated effects in comparison to the findings of this thesis (in red). MP= minipump, LV(W)/BW = left ventricular weight / body weight, HW/BW = heart weight / body weight, LVPW = left ventricular posterior wall, IVS = intraventricular septum, TL = tibia length, Lung W = lung weight, LVID = left ventricular internal diameter. FS = fractional shortening, EF = ejection fraction, β-AR = β- adrenergic receptor, AC = adenylate cyclase, Ca^{2+} = calcium, FA = fatty acids, *Tgfb* = transforming growth factor-beta, *Il6* = interleukin-6, *Col1* = collagen type 1, *Col3* = collagen type 3, *Nppa* = natriuretic peptide A, *Nppb* = natriuretic peptide B

Species	Sex, age and weight of animal	Administration, duration and dose of Iso	Features of myocardium	**Ref**
Mouse (C57Bl/6)	Male, 10 - 11 weeks, 24 – 27g	50 mg/kg/day, 28 days, MP	Hypertrophy (↑ HW/TL, CSA), chamber dilatation (↑ LVID), cardiac dysfunction (↓ EF, FS), hypertension, tachycardia, weight gain, pulmonary congestion (↑ LungW/TL), IκB degradation.	
Mouse (CD-1)	7 weeks	30 mg/kg/day, 13 days, MP	Hypertrophy (↑ LV/BW ratio), fibrosis (histology), ↓ β-AR expression, ↓AC activity.	300
Mouse (C57Bl/6)	Male, 20 g	15 mg/kg/day 1 week, MP	Hypertrophy (↑ LVPW, HW/BW), fibrosis (↑*Tgfb, Col1, Col3* mRNA), inflammation (↑ *Il6* mRNA)	408
Mouse (C57Bl/6)	Male, 12 weeks	30 mg/kg/day, 4 days, MP	Hypertrophy (↑ LV/BW, IVS, LVPW, *Nppa, Nppb* mRNA), tachycardia	409
Mouse (C57Bl/6)	6 months	60 mg/kg/day 10 days, MP	Hypertrophy (↑ HW/TL and histology)	313
Mouse (C57Bl/6)	Male, 8 weeks old	40 mg/kg/day, 10 days, MP	Hypertrophy (↑ HW/BW, histology), tachycardia, fibrosis (histology), inflammation (↑ immune cells)	315
Mouse (Swiss Webster)	Male, 8 months, 40 g	Daily 100 mg/kg, 5 days SC injection	Hypertrophy (↑ LVW) fibrosis (histology)	311
Mouse	4 months	60 mg/kg/day, 3 weeks, MP	Hypertrophy (↑ HW/BW), cardiac dysfunction (↓ EF), fibrosis, apoptosis (histology)	410
Mouse (FVB)	Male, 6 weeks old	15 mg/kg/day, 7 days, MP	Hypertrophy (↑HW, CSA, *Nppa* mRNA)	331
Rat (Sprague-Dawley)	Female, 6 weeks, 180-200 g	150 mg/kg, once, SC injection	Hypertrophy (↑ LVPW), chamber dilatation (↑ LVID), hypertension, fibrosis, necrosis (histology)	304
Rats (Wistar)	Male, 250 -350 g	67 mg/kg/day SC injection	Cardiac dysfunction (↓ EF, FS), oxidative stress, Ca^{2+} mishandling	299
Rats (Wistar)	Male, 300 g	5 mg/kg/day, 7 days, MP	Hypertrophy (LVW), cardiac dysfunction (↓ EF), fibrosis (histology), impaired metabolism (↓ FA and glucose metabolism)	302
Rat	Male, 280 – 290 g	1-15 mg/kg/day for 15 days	Hypertrophy (↑ HW), fibrosis (histology)	296

These potential polymorphisms could alter signalling downstream of the receptor and thereby mediate different effects after Iso infusion between different species of animals or even between strains of mice.

As well as cardiac dysfunction, this current Iso infusion model induced both tachycardia and hypertension. Both of these are risk factors for the development of HF and may induce diastolic dysfunction and pulmonary congestion leading to HFpEF [25, 26]. Additionally, tachycardia itself can reverse cardiac dysfunction once the tachycardia is corrected, as seen in TIC patients, [50, 51]. Therefore it is probable that Iso-induced cardiac dysfunction was due to tachycardia and that removal of Iso ceased the tachycardia and enabled recovery of cardiac function. Another potential cause for Iso-induced cardiac dysfunction could be catecholamine-induced stunning, which is described as a cause for SIC [65]. Interestingly, several of the characteristics of this model resemble features of rapid-pacing models performed in dogs, which is used to model aspects of TIC and atrial fibrillation [411, 412]. Rapid-pacing models have been shown to induce LV systolic dysfunction, cardiomyocyte contractile dysfunction and neurohormonal activation and upon cessation of the pacing, the myocardium recovers [413]. Whilst fibrosis is not a common attribute of this model, elevated ANP levels, reduced β−AR density and apoptosis are molecular and cellular features of rapid-pacing [412]. Therefore, whilst there are similarities between the Iso infusion model presented in this thesis and rapid-pacing, there are several distinctions.

Therefore, the model of Iso infusion utilised in this study contradicts the findings of previous reports, which use lower doses of Iso for shorter time periods (**table 6.1**). As a stronger dose and longer infusion period of Iso was utilised in this current model, it is plausible that a different cardiac response was activated,

yielding the unusual response observed. In addition, the current Iso infusion model, correlates with some, but not all features of other models (rapid-pacing). Therefore this model of Iso infusion is unique and further investigation to understand the mechanisms by which Iso induces cardiac dysfunction is required.

6.3.1 Role of NFκB in Iso infusion model

After treatment of Iso, degradation of IκB was observed, suggesting increased nuclear translocation of the transcription factor, NFκB. The stimuli and downstream effects of this observation have not yet been uncovered, however NFκB is known for its pleiotropic nature. Stimuli that induce NFκB activity include cytokines, oxidative stress, inflammatory stimuli, stress, growth factors and DNA damage which mediate responses such as stress, growth, inflammation and cell survival/ death [414].

Neither oxidative stress or inflammation were detected after Iso infusion and were therefore unlikely to induce NFκB translocation. However NFκB activation can be induced by other stimuli such as cellular stretch and cell survival pathways [351, 415]. Whilst, *Nppa* expression, a marker of cellular stretch, was decreased after Iso infusion, dilation of the LV chamber was observed, which is the resulting phenomena of cellular stretch. Though NFκB activation has been reported after Iso infusion [350], there are no reports that address the possible associations of NFκB activation with the β-AR signalling cascade. Therefore, the expression and activity of other markers of cell survival and cellular stretch could be examined to determine whether these pathways stimulated NFκB activation.

In addition, the downstream response of NFκB activation remains unanswered. Therefore, the expression of genes downstream of NFκB should be evaluated after Iso infusion. Neither inflammation nor apoptosis, both of which are downstream responses to NFκB activation, were observed after Iso infusion, implying that these were not the responses induced by NFκB translocation. However reports that NFκB is associated with the development of cardiac hypertrophy [416], which was potentially observed in this model of Iso infusion (though further study is required), indicate a pathway that could be pursued.

6.3.2 An unreliable and inconsistent Iso infusion model?

The Iso infusion model developed in this thesis is inconsistent, as there have been discrepancies in echocardiographic and physiological data in and between chapters of this thesis. There were inconsistencies in LV chamber size, body weight, lung weight and liver weight which were increased after Iso infusion, compared to saline-treated mice in several studies and unchanged in other studies. Whilst Iso has been reported to induce chamber dilatation, weight gain and pulmonary congestion as measured by lung weight [304, 317], increased liver weight, which is an indicator for systemic congestion has not been previously reported in mice after Iso infusion. These inconsistencies question the reproducibility of this model and it remains unknown why these parameters were different on different occasions. The C57Bl/6 mice used for experiments reported in this thesis were ordered from the same company and mice of the same gender, age and body weight were utilised for experiments. The experimental protocol was consistent for all studies. However external environmental factors, such as time of day and/or time of year in which the experiments were conducted as well as the number of mice in a cage may

cause some discrepancies in the data, therefore further evaluation of this model and a higher number of samples per experiment is required to confirm these findings.

6.4 Study limitations

One major limitation of the experiments performed in this thesis were the lack of power calculations to establish and validate the data. With the challenging issue surrounding the ethical use of animals in scientific research, experiments are required to be performed with enough animals to prove beyond reasonable doubt a hypothesis, without using an excessive number to limit the number of animals sacrificed. Therefore power calculations are used to calculate the number of animals required for an experiment and the current data shown in this thesis requires more samples for several experiments to support and validate the claims made.

Several studies employing Iso infusion were performed (pilot study, WT versus TLR9KO, minipump exchange and new samples) in this thesis. However the echocardiographic data was difficult to analyse, comprehend and compare between these different studies as multiple forms of echocardiography were performed. Conscious and anaesthetised echocardiographic analyses were performed, with 2 methods employed for anaesthetised echocardiography, using the same percentage of ISF (1.5%) and secondly, using different percentages of ISF to obtain HRs between 450-550 bpm. Mice were scruffed to perform conscious echocardiography, which may induce stress, and alter the cardiac function through increased catecholamine levels. However, anaesthetised echocardiography subdued the cardiac function and therefore did not represent the physiological cardiac phenotype. Additionally, awake

echocardiography had to be performed very quickly with images taken from one viewpoint (short-axis M-mode) whereas with anaesthetised echocardiography, the heart can be analysed more thoroughly by difference viewpoints (long axis, short axis, four chamber view), enabling more information regarding cardiac function and structure. Performing echocardiography using same ISF%, detected differences in the HR between saline and Iso treated mice. However, as echocardiographic parameters are HR dependent, echocardiography was performed to match the HR using different ISF%, therefore the mice were under different depths of anaesthesia, which again may influence the cardiac function. Therefore, there was no ideal way to analyse the cardiac parameters of mice after Iso infusion so the echocardiographic data from the different methods of analysis were collated to provide an overall view of the effects of Iso infusion.

Moreover, C57Bl/6 mice were used as WT controls for experiments using TLR9KO mice. Ideally, experiments would have been performed using littermates, comparing $TLR9^{+/+}$ versus $TLR9^{-/-}$ (TLR9KO) mice to eliminate any differences in the genetic background between the mice. However, as TLR9KO mice were bred onto a C57Bl/6 background for more than five generations, this permitted the use of C57Bl/6 as the WT control. Additionally, to minimise the influence of external environmental effects, WT and TLR9KO mice would be bred and maintained under similar conditions.

Furthermore, global TLR9KO mice were used in these experiments. Though it can be speculated that TLR9 expressed within cardiomyocytes may contribute to TLR9-mediated cardiac remodelling whereas TLR9 in fibroblasts influences tissue repair, use of a cell-specific knockout would substantiate which cell-type is involved and validate these postulations.

In this study, in order to investigate the signalling pathways involved in cardiac hypertrophy, calcium handling and apoptosis, q-RT PCR and Western blot analysis was performed to study mRNA and protein expression. However the level of mRNA and protein does not always correlate with their functionality and/or activity. Additionally, great care should be taken when harvesting tissue in order to study protein expression and/or phosphorylation. In this current study, weighing the heart was an important parameter for analysis so harvested heart samples remained at room temperature, which could affect protein expression, phosphorylation levels and its activity. Moreover the availability of specific and reliable antibodies to detect the protein can be challenging. Therefore evaluating the activity of different enzymes, pumps or transporters, and/or translocation of proteins to different cellular compartments would further investigate the roles of these proteins in various models and would be considered as future work for these projects.

Furthermore, DAB^+ cell staining in IHC experiments was used to quantify cells that expressed specific markers. Though this method is considered to be semi-quantitative, it provides an approximation on the number of positively stained cells. However flow cytometry, which accurately quantifies the number of cells with a specific marker, would have been an ideal tool to use.

6.5 Future directions

Further experiments would focus upon validating the current findings by increasing the number of samples in experiments where mentioned. Also, the function of NFκB activation after Iso infusion in the model created in this thesis. DNA microarray analysis could be used to identify the downstream effects of NFκB activation after Iso infusion. Moreover, Western blotting and

immunoprecipitation experiments may distinguish the signalling pathways that are activated to induce IκB degradation and NFκB activity downstream of Iso stimulation.

Additionally other avenues that could be explored as causes for the development of β-stimulant-induced cardiomyopathy include measurements of contractile function and the expression of contractile proteins as well as mitochondrial function and ATP levels. Decreased ATP levels and reduced mitochondrial function are both an observation and potential cause of TIC. Although mitochondrial structure, pyruvate decarboxylation and β-oxidation of FAs appear to be maintained after Iso infusion, suggesting intact mitochondrial function, activity of the complexes within the electron transport chain would validate this speculation. Therefore further investigation is required to understand the molecular mechanisms of β-stimulant-induced cardiomyopathy. Also identification of the mechanisms by which acute reversal of Iso-induced tachycardia and cardiac dysfunction was observed requires further study. However as mentioned, one possible mechanism is amendments to the expression of proteins involved in FA metabolism and oxidative phosphorylation.

Cell-specific function and expression is a common trait of many proteins. As TLR9 is expressed in both cardiomyocytes and fibroblasts, further investigations would be directed to identify and comprehend the cell-types that mediate the various functions of TLR9. One experiment involves the use of isolated cells (cardiomyocytes, fibroblasts, endothelial cells), which could be treated with synthetic CpG ODNs that either stimulate or inhibit TLR9. From this the proteins that interact with TLR9 and the downstream signalling pathways that mediate the responses observed after Iso infusion or LAD ligation (mimicked by using

Iso treatment or ischemic cell culture conditions) could be identified by western blotting or immunoprecipitation. Also co-cultures (cardiomyocytes, fibroblasts, macrophages) could also be utilised in the aforementioned experiments to determine the relative association and interactions between different cell types to influence TLR9 activity as well as cell-specific TLR9KO mice. Cre-Lox P technology would be employed to delete TLR9 in these cells by expressing Cre under the promoter of α-myosin heavy chain (cardiomyocytes), periostin (activated fibroblasts) and tie2 (endothelial cells), generating cell-specific TLR9KO mice. By identifying the cell-type that mediates these roles of TLR9, this may possibly allude to the proteins or the pathways that connect TLR9 signalling to its observed impact on cardiac function, heart weight, *Timp1* mRNA expression and numbers of fibroblasts and myofibroblasts. Co-immunoprecipitation and mass spectrometry experiments of proteins involved in the TLR9 signalling cascade and DNA microarrays may identify potential mediators.

6.6 Clinical implications

Using Iso as a β-AR stimulant has validated the importance of the β-AR signalling cascade in the development of cardiac dysfunction and heart weight gain, emphasising the benefits of utilising β-blockers as a common treatment for HF.

Combining the data of *Oka* et al (2012) demonstrating that TLR9 ablation attenuated pressure overload-induced HF [173] and the data from this Iso model, the impact of TLR9 on cardiac function could potentially be a therapeutic target. Furthermore, *in vivo* experiments have exhibited that TLR9 inhibition attenuated pressure overload-induced HF [173]. Therefore, inhibition of TLR9 may prevent or

reduce cardiac dysfunction in patients associated with hypertension or aortic stenosis, as these are known causes of myocardial pressure overload. Additionally *in vivo* inhibition of TLR9 diminished CpG-induced myocardial dysfunction associated with sepsis [203], suggesting another potential use of therapeutics which inhibit TLR9. Furthermore, whilst findings from this thesis suggest that β-AR signalling interacts with NFκB and therefore IκB/NFκB could be considered as a potential therapeutic target, further work is needed to understand its pleiotropic role within the myocardium.

However, the consequences of TLR9 inhibition could be detrimental if the patients treated with TLR9 inhibitors suffered from a MI, especially during the acute phase of remodelling post-MI. The data presented in this thesis has demonstrated that the incidence of cardiac rupture was increased in TLR9KO mice after MI due to impaired tissue repair, eluding that inhibition of TLR9 may have adverse outcomes. Therefore, further study is required to identify the downstream mechanisms involved in TLR9-mediated cardiac dysfunction and tissue repair, so the molecules downstream of the TLR9 receptor that cause cardiac dysfunction could be therapeutically targeted and not those involved in TLR9-mediated tissue repair.

Also, the temporal and spatial aspects of inflammation and TLR9 activity need to be considered in terms of treatment design and duration. Though the data presented in this thesis saw no difference in TLR9-mediated inflammation in the models used in this thesis (discussed in **section 6.2**), TLR9-mediated inflammation may be a chronic affect. Therefore a therapy targeting TLR9 would need to consider the varied roles of TLR9 and their temporal regulation as well as the targeting approach (systemic or directed towards a particular cell-type or organ.

6.7 Concluding remarks

The sensory nature of TLR9 recognising unmethylated CpG motifs on DNA and provoking the initiation of an inflammatory response is well acknowledged. However the data presented here proposes novel roles for TLR9 in cardiac remodelling that are independent of inflammation. One role of TLR9 identified from this project was its ability to induce cardiac dysfunction in β-stimulant-induced cardiomyopathy, whilst, another role of TLR9 has been described in tissue repair processes post-MI. To identify the intricate pathways that connect TLR9 to the observed phenomena, further study is required.

Moreover, chronic, excessive infusion of Iso induces a reversible cardiac dysfunctional phenotype, which may be mediated by NFκB signalling, however further investigation is needed to evaluate this model.

Finally, though the contribution of the TLR9-mediated inflammation in the pathogenesis of HF remains unanswered, novel roles of TLR9 were identified in the multifaceted and complex process of cardiac remodelling.

7 References

1. Nag AC. Study of non-muscle cells of the adult mammalian heart: a fine structural analysis and distribution. *Cytobios*. 1980;28:41-61.
2. Bernardo BC, Weeks KL, Pretorius L and McMullen JR. Molecular distinction between physiological and pathological cardiac hypertrophy: experimental findings and therapeutic strategies. *Pharmacology & Therapeutics*. 2010;128:191-227.
3. Zak R. Development and proliferative capacity of cardiac muscle cells. *Circulation Research*. 1974;35:suppl II:17-26.
4. Souders CA, Bowers SL and Baudino TA. Cardiac fibroblast: the renaissance cell. *Circulation Research*. 2009;105:1164-76.
5. Fan D, Takawale A, Lee J and Kassiri Z. Cardiac fibroblasts, fibrosis and extracellular matrix remodeling in heart disease. *Fibrogenesis & Tissue Repair*. 2012;5:15.
6. Huxley H and Hanson J. Changes in the cross-striations of muscle during contraction and stretch and their structural interpretation. *Nature*. 1954;173:973-6.
7. Huxley AF and Niedergerke R. Structural changes in muscle during contraction; interference microscopy of living muscle fibres. *Nature*. 1954;173:971-3.
8. Szent-Gyorgyi AG. Calcium regulation of muscle contraction. *Biophysical Journal*. 1975;15:707-23.
9. McMullen JR, Shioi T, Zhang L, Tarnavski O, Sherwood MC, Kang PM and Izumo S. Phosphoinositide 3-kinase(p110alpha) plays a critical role for the induction of physiological, but not pathological, cardiac hypertrophy. *Proceedings of the National Academy of Sciences of the United States of America*. 2003;100:12355-60.
10. Pazos-Lopez P, Peteiro-Vazquez J, Carcia-Campos A, Garcia-Bueno L, de Torres JPA and Castro-Beiras A. The causes, consequences, and treatment of left or right heart failure. *Vascular Health and Risk Management*. 2011;7:237-54.
11. Hunt SA, Abraham WT, Chin MH, Feldman AM, Francis GS, Ganiats TG, Jessup M, Konstam MA, Mancini DM, Michl K, Oates JA, Rahko PS, Silver MA, Stevenson LW and Yancy CW. 2009 focused update incorporated into the ACC/AHA 2005 Guidelines for the Diagnosis and Management of Heart Failure in Adults: a report of the American College of Cardiology Foundation/American Heart Association Task Force on Practice Guidelines: developed in collaboration with the International Society for Heart and Lung Transplantation. *Circulation*. 2009;119:e391-479.
12. Klein L, O'Connor CM, Gattis WA, Zampino M, de Luca L, Vitarelli A, Fedele F and Gheorghiade M. Pharmacologic therapy for patients with chronic heart failure and reduced systolic function: review of trials and practical considerations. *American Journal of Cardiology*. 2003;91:18f-40f.
13. Lips DJ, deWindt LJ, van Kraaij DJ and Doevendans PA. Molecular determinants of myocardial hypertrophy and failure: alternative pathways for beneficial and maladaptive hypertrophy. *European Heart Journal*. 2003;24:883-96.
14. Heineke J and Molkentin JD. Regulation of cardiac hypertrophy by intracellular signalling pathways. *Nature Reviews Molecular Cell Biology*. 2006;7:589-600.
15. Levy D, Labib SB, Anderson KM, Christiansen JC, Kannel WB and Castelli WP. Determinants of sensitivity and specificity of electrocardiographic criteria for left ventricular hypertrophy. *Circulation*. 1990;81:815-20.
16. Jessup M and Brozena S. Heart failure. *New England Journal of Medicine* 2003;348:2007-18.
17. Viquerat CE, Daly P, Swedberg K, Evers C, Curran D, Parmley WW and Chatterjee K. Endogenous catecholamine levels in chronic heart failure. Relation to the severity of hemodynamic abnormalities. *American Journal of Medicine*. 1985;78:455-60.
18. Lefkowitz RJ, Rockman HA and Koch WJ. Catecholamines, cardiac beta-adrenergic receptors, and heart failure. *Circulation*. 2000;101:1634-7.
19. Levine B, Kalman J, Mayer L, Fillit HM and Packer M. Elevated circulating levels of tumor necrosis factor in severe chronic heart failure. *New England Journal of Medicine*. 1990;323:236-41.
20. Mann DL. Inflammatory mediators and the failing heart: past, present, and the foreseeable future. *Circulation Research*. 2002;91:988-98.
21. Yndestad A, Damas JK, Oie E, Ueland T, Gullestad L and Aukrust P. Systemic inflammation in heart failure--the whys and wherefores. *Heart Failure Reviews*. 2006;11:83-92.

22. Fowler MB, Laser JA, Hopkins GL, Minobe W and Bristow MR. Assessment of the beta-adrenergic receptor pathway in the intact failing human heart: progressive receptor down-regulation and subsensitivity to agonist response. *Circulation*. 1986;74:1290-302.
23. McMurray JJ, Adamopoulos S, Anker SD, Auricchio A, Bohm M, Dickstein K, Falk V, Filippatos G, Fonseca C, Gomez-Sanchez MA, Jaarsma T, Kober L, Lip GY, Maggioni AP, Parkhomenko A, Pieske BM, Popescu BA, Ronnevik PK, Rutten FH, Schwitter J, Seferovic P, Stepinska J, Trindade PT, Voors AA, Zannad F, Zeiher A and Guidelines ESCCfP. ESC Guidelines for the diagnosis and treatment of acute and chronic heart failure 2012: The Task Force for the Diagnosis and Treatment of Acute and Chronic Heart Failure 2012 of the European Society of Cardiology. Developed in collaboration with the Heart Failure Association (HFA) of the ESC. *European Heart Journal*. 2012;33:1787-847.
24. Chatterjee K and Massie B. Systolic and diastolic heart failure: differences and similarities. *Journal of Cardiac Failure*. 2007;13:569-76.
25. Sharma K and Kass DA. Heart failure with preserved ejection fraction: mechanisms, clinical features, and therapies. *Circulation Research*. 2014;115:79-96.
26. Quiroz R, Doros G, Shaw P, Liang CS, Gauthier DF and Sam F. Comparison of characteristics and outcomes of patients with heart failure preserved ejection fraction versus reduced left ventricular ejection fraction in an urban cohort. *American Journal of Cardiology*. 2014;113:691-6.
27. Hernandez AF, Hammill BG, O'Connor CM, Schulman KA, Curtis LH and Fonarow GC. Clinical effectiveness of beta-blockers in heart failure: findings from the OPTIMIZE-HF (Organized Program to Initiate Lifesaving Treatment in Hospitalized Patients with Heart Failure) Registry. *Journal of the American College of Cardiology*. 2009;53:184-92.
28. Flather MD, Yusuf S, Kober L, Pfeffer M, Hall A, Murray G, Torp-Pedersen C, Ball S, Pogue J, Moye L and Braunwald E. Long-term ACE-inhibitor therapy in patients with heart failure or left-ventricular dysfunction: a systematic overview of data from individual patients. ACE-Inhibitor Myocardial Infarction Collaborative Group. *Lancet*. 2000;355:1575-81.
29. Chandrasekaran B and Kurbaan AS. Myocardial infarction with angiographically normal coronary arteries. *Journal of the Royal Society of Medicine*. 2002;95:398-400.
30. Laflamme MA and Murry CE. Regenerating the heart. *Nature Biotechnology*. 2005;23:845-56.
31. Luepker RV, Apple FS, Christenson RH, Crow RS, Fortmann SP, Goff D, Goldberg RJ, Hand MM, Jaffe AS, Julian DG, Levy D, Manolio T, Mendis S, Mensah G, Pajak A, Prineas RJ, Reddy KS, Roger VL, Rosamond WD, Shahar E, Sharrett AR, Sorlie P, Tunstall-Pedoe H, Epidemiology AHACo, Prevention, Committee AHAS, World Heart Federation Council on E, Prevention, European Society of Cardiology Working Group on E, Prevention, Centers for Disease C, Prevention, National Heart L and Blood I. Case definitions for acute coronary heart disease in epidemiology and clinical research studies: a statement from the AHA Council on Epidemiology and Prevention; AHA Statistics Committee; World Heart Federation Council on Epidemiology and Prevention; the European Society of Cardiology Working Group on Epidemiology and Prevention; Centers for Disease Control and Prevention; and the National Heart, Lung, and Blood Institute. *Circulation*. 2003;108:2543-9.
32. Shinde AV and Frangogiannis NG. Fibroblasts in myocardial infarction: a role in inflammation and repair. *Journal of Molecular and Cellular Cardiology*. 2014;70:74-82.
33. Frangogiannis NG. The inflammatory response in myocardial injury, repair, and remodelling. *Nature Reviews Cardiology*. 2014;11:255-65.
34. Kramer CM, Sinusas AJ, Sosnovik DE, French BA and Bengel FM. Multimodality imaging of myocardial injury and remodeling. *Journal of Nuclear Medicine*. 2010;51 Suppl 1:107S-121S.
35. Thygesen K, Alpert JS, Jaffe AS, Simoons ML, Chaitman BR, White HD and Task Force for the Universal Definition of Myocardial I. Third universal definition of myocardial infarction. *Nature Reviews Cardiology*. 2012;9:620-33.
36. Gao XM, White DA, Dart AM and Du XJ. Post-infarct cardiac rupture: recent insights on pathogenesis and therapeutic interventions. *Pharmacology & Therapeutics*. 2012;134:156-79.
37. Coffman TM. Under pressure: the search for the essential mechanisms of hypertension. *Nature Medicine*. 2011;17:1402-9.
38. Redwood H. Hypertension, society, and public policy. *European Heart Journal Supplements*. 2007;9:B13-B18.
39. Paulis L and Unger T. Novel therapeutic targets for hypertension. *Nature Reviews Cardiology*. 2010;7:431-41.
40. Te Riet L, van Esch JH, Roks AJ, van den Meiracker AH and Danser AH. Hypertension: renin-angiotensin-aldosterone system alterations. *Circulation Research*. 2015;116:960-75.

41. Dolci A, Dominici R, Cardinale D, Sandri MT and Panteghini M. Biochemical markers for prediction of chemotherapy-induced cardiotoxicity: systematic review of the literature and recommendations for use. *American Journal of Clinical Pathology*. 2008;130:688-95.
42. Iacovoni A, De Maria R and Gavazzi A. Alcoholic cardiomyopathy. *Journal of Cardiovascular Medicine* 2010;11:884-92.
43. Harvey PA and Leinwand LA. The cell biology of disease: cellular mechanisms of cardiomyopathy. *Journal of Cell Biology*. 2011;194:355-65.
44. Wang L, Seidman JG and Seidman CE. Narrative review: harnessing molecular genetics for the diagnosis and management of hypertrophic cardiomyopathy. *Annals of Internal Medicine*. 2010;152:513-20, W181.
45. Luk A, Ahn E, Soor GS and Butany J. Dilated cardiomyopathy: a review. *Journal of Clinical Pathology*. 2009;62:219-25.
46. Maron BJ, Gardin JM, Flack JM, Gidding SS, Kurosaki TT and Bild DE. Prevalence of hypertrophic cardiomyopathy in a general population of young adults. Echocardiographic analysis of 4111 subjects in the CARDIA Study. Coronary Artery Risk Development in (Young) Adults. *Circulation*. 1995;92:785-9.
47. Marian AJ. Pathogenesis of diverse clinical and pathological phenotypes in hypertrophic cardiomyopathy. *Lancet*. 2000;355:58-60.
48. Soor GS, Luk A, Ahn E, Abraham JR, Woo A, Ralph-Edwards A and Butany J. Hypertrophic cardiomyopathy: current understanding and treatment objectives. *Journal of Clinical Pathology*. 2009;62:226-35.
49. Patel H, Madanieh R, Kosmas CE, Vatti SK and Vittorio TJ. Reversible Cardiomyopathies. *Clinical Medicine Insights: Cardiology*. 2015;9:7-14.
50. Patel JJ and Whittaker CT. Tachycardia-induced heart failure. *Permanente Journal*. 2007;11:50-2.
51. Shinbane JS, Wood MA, Jensen DN, Ellenbogen KA, Fitzpatrick AP and Scheinman MM. Tachycardia-induced cardiomyopathy: a review of animal models and clinical studies. *Journal of the American College of Cardiology*. 1997;29:709-15.
52. Spinale FG, Zellner JL, Tomita M, Crawford FA and Zile MR. Relation between ventricular and myocyte remodeling with the development and regression of supraventricular tachycardia-induced cardiomyopathy. *Circulation Research*. 1991;69:1058-67.
53. Kajstura J, Zhang X, Liu Y, Szoke E, Cheng W, Olivetti G, Hintze TH and Anversa P. The cellular basis of pacing-induced dilated cardiomyopathy. Myocyte cell loss and myocyte cellular reactive hypertrophy. *Circulation*. 1995;92:2306-17.
54. Moe GW, Montgomery C, Howard RJ, Grima EA and Armstrong PW. Left ventricular myocardial blood flow, metabolism, and effects of treatment with enalapril: further insights into the mechanisms of canine experimental pacing-induced heart failure. *Journal of Laboratory and Clinical Medicine*. 1993;121:294-301.
55. Shannon RP, Komamura K, Shen YT, Bishop SP and Vatner SF. Impaired regional subendocardial coronary flow reserve in conscious dogs with pacing-induced heart failure. *American Journal of Physiology*. 1993;265:H801-9.
56. Perreault CL, Shannon RP, Komamura K, Vatner SF and Morgan JP. Abnormalities in intracellular calcium regulation and contractile function in myocardium from dogs with pacing-induced heart failure. *Journal of Clinical Investigation*. 1992;89:932-8.
57. Shite J, Qin F, Mao W, Kawai H, Stevens SY and Liang C. Antioxidant vitamins attenuate oxidative stress and cardiac dysfunction in tachycardia-induced cardiomyopathy. *Journal of the American College of Cardiology*. 2001;38:1734-40.
58. Akashi YJ, Nef HM and Lyon AR. Epidemiology and pathophysiology of Takotsubo syndrome. *Nature Reviews Cardiology*. 2015;12:387-97.
59. Wittstein IS. Stress cardiomyopathy: a syndrome of catecholamine-mediated myocardial stunning? *Cellular and Molecular Neurobiology*. 2012;32:847-57.
60. Nef HM, Mollmann H, Hilpert P, Masseli F, Kostin S, Troidl C, Rolf A, Dill T, Weber M, Hamm C and Elsasser A. Sympathoadrenergic overstimulation in Tako-Tsubo cardiomyopathy triggered by physical and emotional stress. *International Journal of Cardiology*. 2008;130:266-8.
61. Wittstein IS, Thiemann DR, Lima JA, Baughman KL, Schulman SP, Gerstenblith G, Wu KC, Rade JJ, Bivalacqua TJ and Champion HC. Neurohumoral features of myocardial stunning due to sudden emotional stress. *New England Journal of Medicine* 2005;352:539-48.
62. Santoro F, Ieva R, Musaico F, Ferraretti A, Triggiani G, Tarantino N, Di Biase M and Brunetti ND. Lack of efficacy of drug therapy in preventing takotsubo cardiomyopathy recurrence: a meta-analysis. *Clinical Cardiology*. 2014;37:434-9.

63. Nef HM, Mollmann H, Kostin S, Troidl C, Voss S, Weber M, Dill T, Rolf A, Brandt R, Hamm CW and Elsasser A. Tako-Tsubo cardiomyopathy: intraindividual structural analysis in the acute phase and after functional recovery. *European Heart Journal*. 2007;28:2456-64.
64. Szardien S, Mollmann H, Willmer M, Liebetrau C, Voss S, Troidl C, Hoffmann J, Rixe J, Elsasser A, Hamm CW and Nef HM. Molecular basis of disturbed extracellular matrix homeostasis in stress cardiomyopathy. *International Journal of Cardiology*. 2013;168:1685-8.
65. Lyon AR, Rees PS, Prasad S, Poole-Wilson PA and Harding SE. Stress (Takotsubo) cardiomyopathy--a novel pathophysiological hypothesis to explain catecholamine-induced acute myocardial stunning. *Nature Clinical Practice Cardiovascular Medicine*. 2008;5:22-9.
66. Cohn JN, Ferrari R and Sharpe N. Cardiac remodeling--concepts and clinical implications: a consensus paper from an international forum on cardiac remodeling. Behalf of an International Forum on Cardiac Remodeling. *Journal of the American College of Cardiology*. 2000;35:569-82.
67. Pfeffer MA and Braunwald E. Ventricular remodeling after myocardial infarction. Experimental observations and clinical implications. *Circulation*. 1990;81:1161-72.
68. Mann DL. *Heart Failure: A Companion to Braunwald's Heart Disease.* 1 ed. Pennsylvania: Saunders; 2004.
69. McMullen JR and Jennings GL. Differences between pathological and physiological cardiac hypertrophy: novel therapeutic strategies to treat heart failure. *Clinical and Experimental Pharmacology and Physiology*. 2007;34:255-62.
70. Kehat I and Molkentin JD. Molecular pathways underlying cardiac remodeling during pathophysiological stimulation. *Circulation*. 2010;122:2727-35.
71. Oudit GY, Sun H, Kerfant BG, Crackower MA, Penninger JM and Backx PH. The role of phosphoinositide-3 kinase and PTEN in cardiovascular physiology and disease. *Journal of Molecular and Cellular Cardiology* 2004;37:449-71.
72. Shioi T, Kang PM, Douglas PS, Hampe J, Yballe CM, Lawitts J, Cantley LC and Izumo S. The conserved phosphoinositide 3-kinase pathway determines heart size in mice. *EMBO Journal*. 2000;19:2537-48.
73. Bueno OF, De Windt LJ, Tymitz KM, Witt SA, Kimball TR, Klevitsky R, Hewett TE, Jones SP, Lefer DJ, Peng CF, Kitsis RN and Molkentin JD. The MEK1-ERK1/2 signaling pathway promotes compensated cardiac hypertrophy in transgenic mice. *EMBO Journal*. 2000;19:6341-50.
74. Bueno OF and Molkentin JD. Involvement of extracellular signal-regulated kinases 1/2 in cardiac hypertrophy and cell death. *Circulation Research*. 2002;91:776-81.
75. Molkentin JD, Lu JR, Antos CL, Markham B, Richardson J, Robbins J, Grant SR and Olson EN. A calcineurin-dependent transcriptional pathway for cardiac hypertrophy. *Cell*. 1998;93:215-28.
76. Haq S, Choukroun G, Lim H, Tymitz KM, del Monte F, Gwathmey J, Grazette L, Michael A, Hajjar R, Force T and Molkentin JD. Differential activation of signal transduction pathways in human hearts with hypertrophy versus advanced heart failure. *Circulation*. 2001;103:670-7.
77. Passier R, Zeng H, Frey N, Naya FJ, Nicol RL, McKinsey TA, Overbeek P, Richardson JA, Grant SR and Olson EN. CaM kinase signaling induces cardiac hypertrophy and activates the MEF2 transcription factor in vivo. *Journal of Clinical Investigation*. 2000;105:1395-406.
78. Zhang T, Maier LS, Dalton ND, Miyamoto S, Ross J, Jr., Bers DM and Brown JH. The deltaC isoform of CaMKII is activated in cardiac hypertrophy and induces dilated cardiomyopathy and heart failure. *Circulation Research*. 2003;92:912-9.
79. Komuro I and Yazaki Y. Control of cardiac gene expression by mechanical stress. *Annual Review of Physiology*. 1993;55:55-75.
80. Frey N, Katus HA, Olson EN and Hill JA. Hypertrophy of the Heart: A New Therapeutic Target? *Circulation*. 2004;109:1580-1589.
81. Haider AW, Larson MG, Benjamin EJ and Levy D. Increased left ventricular mass and hypertrophy are associated with increased risk for sudden death. *Journal of the American College of Cardiology*. 1998;32:1454-9.
82. Hill JA and Olson EN. Cardiac plasticity. *New England Journal of Medicine* 2008;358:1370-80.
83. Cook SA, Sugden PH and Clerk A. Activation of c-Jun N-terminal kinases and p38-mitogen-activated protein kinases in human heart failure secondary to ischaemic heart disease. *Journal of Molecular and Cellular Cardiology*. 1999;31:1429-34.
84. Nicol RL, Frey N, Pearson G, Cobb M, Richardson J and Olson EN. Activated MEK5 induces serial assembly of sarcomeres and eccentric cardiac hypertrophy. *EMBO Journal*. 2001;20:2757-67.

85. Porter KE and Turner NA. Cardiac fibroblasts: at the heart of myocardial remodeling. *Pharmacology & Therapeutics*. 2009;123:255-78.
86. Ross RS. The extracellular connections: the role of integrins in myocardial remodeling. *Journal of Cardiac Failure*. 2002;8:S326-31.
87. Norris RA, Borg TK, Butcher JT, Baudino TA, Banerjee I and Markwald RR. Neonatal and adult cardiovascular pathophysiological remodeling and repair: developmental role of periostin. *Annals of the New York Academy of Sciences*. 2008;1123:30-40.
88. Krenning G, Zeisberg EM and Kalluri R. The origin of fibroblasts and mechanism of cardiac fibrosis. *Journal of Cellular Physiology*. 2010;225:631-7.
89. Munoz-Chapuli R, Perez-Pomares JM, Macias D, Garcia-Garrido L, Carmona R and Gonzalez-Iriarte M. The epicardium as a source of mesenchyme for the developing heart. *Italian Journal of Anatomy and Embryology*. 2001;106:187-96.
90. Zeisberg EM, Tarnavski O, Zeisberg M, Dorfman AL, McMullen JR, Gustafsson E, Chandraker A, Yuan X, Pu WT, Roberts AB, Neilson EG, Sayegh MH, Izumo S and Kalluri R. Endothelial-to-mesenchymal transition contributes to cardiac fibrosis. *Nature Medicine*. 2007;13:952-61.
91. Camelliti P, Green CR and Kohl P. Structural and functional coupling of cardiac myocytes and fibroblasts. *Advances in Cardiology*. 2006;42:132-49.
92. Kohl P, Camelliti P, Burton FL and Smith GL. Electrical coupling of fibroblasts and myocytes: relevance for cardiac propagation. *Journal of Electrocardiology*. 2005;38:45-50.
93. Petrov VV, Fagard RH and Lijnen PJ. Stimulation of collagen production by transforming growth factor-beta1 during differentiation of cardiac fibroblasts to myofibroblasts. *Hypertension*. 2002;39:258-63.
94. Willems IE, Havenith MG, De Mey JG and Daemen MJ. The alpha-smooth muscle actin-positive cells in healing human myocardial scars. *American Journal of Pathology*. 1994;145:868-75.
95. Sun Y and Weber KT. Angiotensin converting enzyme and myofibroblasts during tissue repair in the rat heart. *Journal of Molecular and Cellular Cardiology*. 1996;28:851-8.
96. Sun Y and Weber KT. RAS and connective tissue in the heart. *International Journal of Biochemistry & Cell Biology* 2003;35:919-31.
97. Gabbiani G. The myofibroblast in wound healing and fibrocontractive diseases. *Journal of Pathology*. 2003;200:500-3.
98. Ljungqvist A and Unge G. The proliferative activity of the myocardial tissue in various forms of experimental cardiac hypertrophy. *Acta Pathologica Microbiologica Scandinavica Series A*. 1973;81:233-40.
99. Mandache E, Unge G, Appelgren LE and Ljungqvist A. The proliferative activity of the heart tissues in various forms of experimental cardiac hypertrophy studied by electron microscope autoradiography. *Virchows Archiv B Cell Pathology*. 1973;12:112-22.
100. Tao H, Yang JJ, Shi KH, Deng ZY and Li J. DNA methylation in cardiac fibrosis: new advances and perspectives. *Toxicology*. 2014;323:125-9.
101. Phatharajaree W, Phrommintikul A and Chattipakorn N. Matrix metalloproteinases and myocardial infarction. *Canadian Journal of Cardiology*. 2007;23:727-33.
102. Spinale FG. Matrix metalloproteinases: regulation and dysregulation in the failing heart. *Circulation Research*. 2002;90:520-30.
103. Aderem A and Ulevitch RJ. Toll-like receptors in the induction of the innate immune response. *Nature*. 2000;406:782-7.
104. Mann DL and Spinale FG. Activation of matrix metalloproteinases in the failing human heart: breaking the tie that binds. *Circulation*. 1998;98:1699-702.
105. Kelly D, Khan S, Cockerill G, Ng LL, Thompson M, Samani NJ and Squire IB. Circulating stromelysin-1 (MMP-3): a novel predictor of LV dysfunction, remodelling and all-cause mortality after acute myocardial infarction. *European Journal of Heart Failure*. 2008;10:133-9.
106. Zucker S, Lysik RM, Zarrabi HM, Moll U, Tickle SP, Stetler-Stevenson W, Baker TS and Docherty AJ. Plasma assay of matrix metalloproteinases (MMPs) and MMP-inhibitor complexes in cancer. Potential use in predicting metastasis and monitoring treatment. *Annals of the New York Academy of Sciences*. 1994;732:248-62.
107. Greene J, Wang M, Liu YE, Raymond LA, Rosen C and Shi YE. Molecular cloning and characterization of human tissue inhibitor of metalloproteinase 4. *Journal of Biological Chemistry*. 1996;271:30375-80.
108. Cox MJ, Hawkins UA, Hoit BD and Tyagi SC. Attenuation of oxidative stress and remodeling by cardiac inhibitor of metalloproteinase protein transfer. *Circulation*. 2004;109:2123-8.

109. Siwik DA, Chang DL and Colucci WS. Interleukin-1beta and tumor necrosis factor-alpha decrease collagen synthesis and increase matrix metalloproteinase activity in cardiac fibroblasts in vitro. *Circulation Research*. 2000;86:1259-65.
110. Xie Z, Singh M and Singh K. Differential regulation of matrix metalloproteinase-2 and -9 expression and activity in adult rat cardiac fibroblasts in response to interleukin-1beta. *Journal of Biological Chemistry*. 2004;279:39513-9.
111. Deschamps AM and Spinale FG. Pathways of matrix metalloproteinase induction in heart failure: bioactive molecules and transcriptional regulation. *Cardiovascular Research*. 2006;69:666-76.
112. Lovelock JD, Baker AH, Gao F, Dong JF, Bergeron AL, McPheat W, Sivasubramanian N and Mann DL. Heterogeneous effects of tissue inhibitors of matrix metalloproteinases on cardiac fibroblasts. *American Journal of Physiology - Heart and Circulatory Physiology*. 2005;288:H461-8.
113. Thomas CV, Coker ML, Zellner JL, Handy JR, Crumbley AJ, 3rd and Spinale FG. Increased matrix metalloproteinase activity and selective upregulation in LV myocardium from patients with end-stage dilated cardiomyopathy. *Circulation*. 1998;97:1708-15.
114. Heymans S, Schroen B, Vermeersch P, Milting H, Gao F, Kassner A, Gillijns H, Herijgers P, Flameng W, Carmeliet P, Van de Werf F, Pinto YM and Janssens S. Increased cardiac expression of tissue inhibitor of metalloproteinase-1 and tissue inhibitor of metalloproteinase-2 is related to cardiac fibrosis and dysfunction in the chronic pressure-overloaded human heart. *Circulation*. 2005;112:1136-44.
115. Laviades C, Varo N, Fernandez J, Mayor G, Gil MJ, Monreal I and Diez J. Abnormalities of the extracellular degradation of collagen type I in essential hypertension. *Circulation*. 1998;98:535-40.
116. Zervoudaki A, Economou E, Stefanadis C, Pitsavos C, Tsioufis K, Aggeli C, Vasiliadou K, Toutouza M and Toutouzas P. Plasma levels of active extracellular matrix metalloproteinases 2 and 9 in patients with essential hypertension before and after antihypertensive treatment. *Journal of Human Hypertension*. 2003;17:119-24.
117. Tziakas DN, Chalikias GK, Parissis JT, Hatzinikolaou EI, Papadopoulos ED, Tripsiannis GA, Papadopoulou EG, Tentes IK, Karas SM and Chatseras DI. Serum profiles of matrix metalloproteinases and their tissue inhibitor in patients with acute coronary syndromes. The effects of short-term atorvastatin administration. *International Journal of Cardiology*. 2004;94:269-77.
118. Wagner DR, Delagardelle C, Ernens I, Rouy D, Vaillant M and Beissel J. Matrix metalloproteinase-9 is a marker of heart failure after acute myocardial infarction. *Journal of Cardiac Failure*. 2006;12:66-72.
119. Spach MS and Boineau JP. Microfibrosis produces electrical load variations due to loss of side-to-side cell connections: a major mechanism of structural heart disease arrhythmias. *Pacing and Clinical Electrophysiology*. 1997;20:397-413.
120. Kinoshita T, Ishikawa Y, Arita M, Akishima-Fukasawa Y, Fujita K, Inomata N, Suzuki T, Namiki A, Mikami T, Ikeda T, Yamazaki J, Ishii T and Akasaka Y. Antifibrotic response of cardiac fibroblasts in hypertensive hearts through enhanced TIMP-1 expression by basic fibroblast growth factor. *Cardiovascular Pathology*. 2014;23:92-100.
121. Sarrazy V, Koehler A, Chow ML, Zimina E, Li CX, Kato H, Caldarone CA and Hinz B. Integrins alphavbeta5 and alphavbeta3 promote latent TGF-beta1 activation by human cardiac fibroblast contraction. *Cardiovascular Research*. 2014;102:407-17.
122. Leask A and Abraham DJ. TGF-beta signaling and the fibrotic response. *FASEB Journal*. 2004;18:816-27.
123. Hatamochi A, Mori K and Ueki H. Role of cytokines in controlling connective tissue gene expression. *Archives of Dermatological Research*. 1994;287:115-21.
124. Ghosh AK, Yuan W, Mori Y, Chen S and Varga J. Antagonistic regulation of type I collagen gene expression by interferon-gamma and transforming growth factor-beta. Integration at the level of p300/CBP transcriptional coactivators. *Journal of Biological Chemistry*. 2001;276:11041-8.
125. Schaper J and Speiser B. The extracellular matrix in the failing human heart.
126. Zannad F, Rossignol P and Iraqi W. Extracellular matrix fibrotic markers in heart failure. *Heart Failure Reviews*. 2010;15:319-29.
127. Zannad F, Alla F, Dousset B, Perez A and Pitt B. Limitation of excessive extracellular matrix turnover may contribute to survival benefit of spironolactone therapy in patients with congestive heart failure: insights from the randomized aldactone evaluation study (RALES). Rales Investigators. *Circulation*. 2000;102:2700-6.

128. Querejeta R, Varo N, Lopez B, Larman M, Artinano E, Etayo JC, Martinez Ubago JL, Gutierrez-Stampa M, Emparanza JI, Gil MJ, Monreal I, Mindan JP and Diez J. Serum carboxy-terminal propeptide of procollagen type I is a marker of myocardial fibrosis in hypertensive heart disease. *Circulation*. 2000;101:1729-35.
129. Whelan RS, Kaplinskiy V and Kitsis RN. Cell death in the pathogenesis of heart disease: mechanisms and significance. *Annual Review of Physiology*. 2010;72:19-44.
130. Chiong M, Wang ZV, Pedrozo Z, Cao DJ, Troncoso R, Ibacache M, Criollo A, Nemchenko A, Hill JA and Lavandero S. Cardiomyocyte death: mechanisms and translational implications. *Cell Death & Disease*. 2011;2:e244.
131. Konstantinidis K, Whelan RS and Kitsis RN. Mechanisms of cell death in heart disease. *Arteriosclerosis, Thrombosis and Vascular Biology*. 2012;32:1552-62.
132. Kerr JF. Shrinkage necrosis: a distinct mode of cellular death. *Journal of Pathology*. 1971;105:13-20.
133. Walker NI, Harmon BV, Gobe GC and Kerr JF. Patterns of cell death. *Methods and Achievements in Experimental Pathology*. 1988;13:18-54.
134. Pop C and Salvesen GS. Human caspases: activation, specificity, and regulation. *Journal of Biological Chemistry*. 2009;284:21777-81.
135. Mughal W and Kirshenbaum LA. Cell death signalling mechanisms in heart failure. *Experimental & Clinical Cardiology*. 2011;16:102-8.
136. Kischkel FC, Hellbardt S, Behrmann I, Germer M, Pawlita M, Krammer PH and Peter ME. Cytotoxicity-dependent APO-1 (Fas/CD95)-associated proteins form a death-inducing signaling complex (DISC) with the receptor. *EMBO Journal*. 1995;14:5579-88.
137. Boatright KM, Renatus M, Scott FL, Sperandio S, Shin H, Pedersen IM, Ricci JE, Edris WA, Sutherlin DP, Green DR and Salvesen GS. A unified model for apical caspase activation. *Molecular Cell*. 2003;11:529-41.
138. Chipuk JE, Moldoveanu T, Llambi F, Parsons MJ and Green DR. The BCL-2 family reunion. *Molecular Cell*. 2010;37:299-310.
139. Li P, Nijhawan D, Budihardjo I, Srinivasula SM, Ahmad M, Alnemri ES and Wang X. Cytochrome c and dATP-dependent formation of Apaf-1/caspase-9 complex initiates an apoptotic protease cascade. *Cell*. 1997;91:479-89.
140. Yang QH, Church-Hajduk R, Ren J, Newton ML and Du C. Omi/HtrA2 catalytic cleavage of inhibitor of apoptosis (IAP) irreversibly inactivates IAPs and facilitates caspase activity in apoptosis. *Genes & Development* 2003;17:1487-96.
141. Du C, Fang M, Li Y, Li L and Wang X. Smac, a mitochondrial protein that promotes cytochrome c-dependent caspase activation by eliminating IAP inhibition. *Cell*. 2000;102:33-42.
142. Li LY, Luo X and Wang X. Endonuclease G is an apoptotic DNase when released from mitochondria. *Nature*. 2001;412:95-9.
143. Leist M, Single B, Castoldi AF, Kuhnle S and Nicotera P. Intracellular adenosine triphosphate (ATP) concentration: a switch in the decision between apoptosis and necrosis. *Journal of Experimental Medicine*. 1997;185:1481-6.
144. Micheau O and Tschopp J. Induction of TNF receptor I-mediated apoptosis via two sequential signaling complexes. *Cell*. 2003;114:181-90.
145. Bertrand MJ, Milutinovic S, Dickson KM, Ho WC, Boudreault A, Durkin J, Gillard JW, Jaquith JB, Morris SJ and Barker PA. cIAP1 and cIAP2 facilitate cancer cell survival by functioning as E3 ligases that promote RIP1 ubiquitination. *Molecular Cell*. 2008;30:689-700.
146. Mahoney DJ, Cheung HH, Mrad RL, Plenchette S, Simard C, Enwere E, Arora V, Mak TW, Lacasse EC, Waring J and Korneluk RG. Both cIAP1 and cIAP2 regulate TNFalpha-mediated NF-kappaB activation. *Proceedings of the National Academy of Sciences of the United States of America*. 2008;105:11778-83.
147. Kajstura J, Cheng W, Sarangarajan R, Li P, Li B, Nitahara JA, Chapnick S, Reiss K, Olivetti G and Anversa P. Necrotic and apoptotic myocyte cell death in the aging heart of Fischer 344 rats. *American Journal of Physiology*. 1996;271:H1215-28.
148. van Empel VP, Bertrand AT, Hofstra L, Crijns HJ, Doevendans PA and De Windt LJ. Myocyte apoptosis in heart failure. *Cardiovascular Research*. 2005;67:21-9.
149. Guerra S, Leri A, Wang X, Finato N, Di Loreto C, Beltrami CA, Kajstura J and Anversa P. Myocyte death in the failing human heart is gender dependent. *Circulation Research*. 1999;85:856-66.
150. Kostin S, Pool L, Elsasser A, Hein S, Drexler HC, Arnon E, Hayakawa Y, Zimmermann R, Bauer E, Klovekorn WP and Schaper J. Myocytes die by multiple mechanisms in failing human hearts. *Circulation Research*. 2003;92:715-24.
151. Nishida K and Otsu K. Autophagy during cardiac remodeling. *Journal of Molecular and Cellular Cardiology*. 2015.

152. Nakai A, Yamaguchi O, Takeda T, Higuchi Y, Hikoso S, Taniike M, Omiya S, Mizote I, Matsumura Y, Asahi M, Nishida K, Hori M, Mizushima N and Otsu K. The role of autophagy in cardiomyocytes in the basal state and in response to hemodynamic stress. *Nature Medicine*. 2007;13:619-24.
153. Zhu H, Tannous P, Johnstone JL, Kong Y, Shelton JM, Richardson JA, Le V, Levine B, Rothermel BA and Hill JA. Cardiac autophagy is a maladaptive response to hemodynamic stress. *Journal of Clinical Investigation*. 2007;117:1782-93.
154. Miyata S, Takemura G, Kawase Y, Li Y, Okada H, Maruyama R, Ushikoshi H, Esaki M, Kanamori H, Li L, Misao Y, Tezuka A, Toyo-Oka T, Minatoguchi S, Fujiwara T and Fujiwara H. Autophagic cardiomyocyte death in cardiomyopathic hamsters and its prevention by granulocyte colony-stimulating factor. *American Journal of Pathology*. 2006;168:386-97.
155. Nakahira K and Choi AM. Autophagy: a potential therapeutic target in lung diseases. *American Journal of Physiology - Lung Cellular and Molecular Physiology*. 2013;305:L93-107.
156. Yamaguchi O, Higuchi Y, Hirotani S, Kashiwase K, Nakayama H, Hikoso S, Takeda T, Watanabe T, Asahi M, Taniike M, Matsumura Y, Tsujimoto I, Hongo K, Kusakari Y, Kurihara S, Nishida K, Ichijo H, Hori M and Otsu K. Targeted deletion of apoptosis signal-regulating kinase 1 attenuates left ventricular remodeling. *Proceedings of the National Academy of Sciences of the United States of America*. 2003;100:15883-8.
157. Pfeifer U, Fohr J, Wilhelm W and Dammrich J. Short-term inhibition of cardiac cellular autophagy by isoproterenol. *Journal of Molecular and Cellular Cardiology*. 1987;19:1179-84.
158. Matsui Y, Takagi H, Qu X, Abdellatif M, Sakoda H, Asano T, Levine B and Sadoshima J. Distinct roles of autophagy in the heart during ischemia and reperfusion: roles of AMP-activated protein kinase and Beclin 1 in mediating autophagy. *Circulation Research*. 2007;100:914-22.
159. Kanamori H, Takemura G, Goto K, Maruyama R, Tsujimoto A, Ogino A, Takeyama T, Kawaguchi T, Watanabe T, Fujiwara T, Fujiwara H, Seishima M and Minatoguchi S. The role of autophagy emerging in postinfarction cardiac remodelling. *Cardiovascular Research*. 2011;91:330-9.
160. Kassiotis C, Ballal K, Wellnitz K, Vela D, Gong M, Salazar R, Frazier OH and Taegtmeyer H. Markers of autophagy are downregulated in failing human heart after mechanical unloading. *Circulation*. 2009;120:S191-7.
161. Akira S, Uematsu S and Takeuchi O. Pathogen recognition and innate immunity. *Cell*. 2006;124:783-801.
162. Mogensen TH. Pathogen recognition and inflammatory signaling in innate immune defenses. *Clinical Microbiology Reviews*. 2009;22:240-73, Table of Contents.
163. Epelman S, Liu PP and Mann DL. Role of innate and adaptive immune mechanisms in cardiac injury and repair. *Nature Reviews Immunology*. 2015;15:117-29.
164. Medzhitov R. Origin and physiological roles of inflammation. *Nature*. 2008;454:428-35.
165. Pinto AR, Paolicelli R, Salimova E, Gospocic J, Slonimsky E, Bilbao-Cortes D, Godwin JW and Rosenthal NA. An abundant tissue macrophage population in the adult murine heart with a distinct alternatively-activated macrophage profile. *PLoS One*. 2012;7:e36814.
166. Ahmad-Nejad P, Hacker H, Rutz M, Bauer S, Vabulas RM and Wagner H. Bacterial CpG-DNA and lipopolysaccharides activate Toll-like receptors at distinct cellular compartments. *European Journal of Immunology*. 2002;32:1958-1968.
167. Kawai T and Akira S. The role of pattern-recognition receptors in innate immunity: update on Toll-like receptors. *Nature Immunology*. 2010;11:373-84.
168. Marchant DJ, Boyd JH, Lin DC, Granville DJ, Garmaroudi FS and McManus BM. Inflammation in myocardial diseases. *Circulation Research*. 2012;110:126-44.
169. Nakayama H and Otsu K. Translation of hemodynamic stress to sterile inflammation in the heart. *Trends in Endocrinology & Metabolism*. 2013;24:546-53.
170. Schroder K and Tschopp J. The inflammasomes. *Cell*. 2010;140:821-32.
171. Martinon F, Burns K and Tschopp J. The inflammasome: a molecular platform triggering activation of inflammatory caspases and processing of proIL-beta. *Molecular Cell*. 2002;10:417-26.
172. Mann DL. The Emerging Role of Innate Immunity in the Heart and Vascular System For Whom the Cell Tolls. *Circulation Research*. 2011;108:1133-U201.
173. Oka T, Hikoso S, Yamaguchi O, Taneike M, Takeda T, Tamai T, Oyabu J, Murakawa T, Nakayama H, Nishida K, Akira S, Yamamoto A, Komuro I and Otsu K. Mitochondrial DNA that escapes from autophagy causes inflammation and heart failure. *Nature*. 2012;485:251-5.
174. Velten M, Duerr GD, Pessies T, Schild J, Lohner R, Mersmann J, Dewald O, Zacharowski K, Klaschik S, Hilbert T, Hoeft A, Baumgarten G, Meyer R, Boehm O and

Knuefermann P. Priming with synthetic oligonucleotides attenuates pressure overload-induced inflammation and cardiac hypertrophy in mice. *Cardiovascular Research*. 2012;96:422-32.
175. Boyd JH, Mathur S, Wang Y, Bateman RM and Walley KR. Toll-like receptor stimulation in cardiomyoctes decreases contractility and initiates an NF-kappaB dependent inflammatory response. *Cardiovasc Res*. 2006;72:384-93.
176. Ohm IK, Alfsnes K, Belland Olsen M, Ranheim T, Sandanger O, Dahl TB, Aukrust P, Finsen AV, Yndestad A and Vinge LE. Toll-like receptor 9 mediated responses in cardiac fibroblasts. *PLoS One*. 2014;9:e104398.
177. Hemmi H, Takeuchi O, Kawai T, Kaisho T, Sato S, Sanjo H, Matsumoto M, Hoshino K, Wagner H, Takeda K and Akira S. A Toll-like receptor recognizes bacterial DNA. *Nature*. 2000;408:740-745.
178. Zhang Q, Raoof M, Chen Y, Sumi Y, Sursal T, Junger W, Brohi K, Itagaki K and Hauser CJ. Circulating mitochondrial DAMPs cause inflammatory responses to injury. *Nature*. 2010;464:104-7.
179. Wesche H, Henzel WJ, Shillinglaw W, Li S and Cao ZD. MyD88: An adapter that recruits IRAK to the IL-1 receptor complex. *Immunity*. 1997;7:837-847.
180. Takaoka A, Yanai H, Kondo S, Duncan G, Negishi H, Mizutani T, Kano S, Honda K, Ohba Y, Mak TW and Taniguchi T. Integral role of IRF-5 in the gene induction programme activated by Toll-like receptors. *Nature*. 2005;434:243-9.
181. Akira S and Takeda K. Toll-like receptor signalling. *Nature Reviews Immunology*. 2004;4:499-511.
182. Pagni PP, Traub S, Demaria O, Chasson L and Alexopoulou L. Contribution of TLR7 and TLR9 signaling to the susceptibility of MyD88-deficient mice to myocarditis. *Autoimmunity*. 2010;43:275-87.
183. Shintani Y, Kapoor A, Kaneko M, Smolenski RT, D'Acquisto F, Coppen SR, Harada-Shoji N, Lee HJ, Thiemermann C, Takashima S, Yashiro K and Suzuki K. TLR9 mediates cellular protection by modulating energy metabolism in cardiomyocytes and neurons. *Proceedings of the National Academy of Sciences of the United States of America*. 2013;110:5109-14.
184. Shintani Y, Drexler HC, Kioka H, Terracciano CM, Coppen SR, Imamura H, Akao M, Nakai J, Wheeler AP, Higo S, Nakayama H, Takashima S, Yashiro K and Suzuki K. Toll-like receptor 9 protects non-immune cells from stress by modulating mitochondrial ATP synthesis through the inhibition of SERCA2. *EMBO Reports*. 2014;15:438-45.
185. Higuchi Y, Otsu K, Nishida K, Hirotani S, Nakayama H, Yamaguchi O, Matsumura Y, Ueno H, Tada M and Hori M. Involvement of reactive oxygen species-mediated NF-kappa B activation in TNF-alpha-induced cardiomyocyte hypertrophy. *Journal of Molecular and Cellular Cardiology*. 2002;34:233-40.
186. Hirotani S, Otsu K, Nishida K, Higuchi Y, Morita T, Nakayama H, Yamaguchi O, Mano T, Matsumura Y, Ueno H, Tada M and Hori M. Involvement of nuclear factor-kappaB and apoptosis signal-regulating kinase 1 in G-protein-coupled receptor agonist-induced cardiomyocyte hypertrophy. *Circulation*. 2002;105:509-15.
187. Gupta S. A decision between life and death during TNF-alpha-induced signaling. *Journal of Clinical Immunology*. 2002;22:185-94.
188. Le DE, Pascotto M, Leong-Poi H, Sari I, Micari A and Kaul S. Anti-inflammatory and pro-angiogenic effects of beta blockers in a canine model of chronic ischemic cardiomyopathy: comparison between carvedilol and metoprolol. *Basic Research in Cardiology*. 2013;108:384.
189. Li B, Liao YH, Cheng X, Ge H, Guo H and Wang M. Effects of carvedilol on cardiac cytokines expression and remodeling in rat with acute myocardial infarction. *International Journal of Cardiology*. 2006;111:247-55.
190. Chung ES, Packer M, Lo KH, Fasanmade AA, Willerson JT and Anti TNFTACHFI. Randomized, double-blind, placebo-controlled, pilot trial of infliximab, a chimeric monoclonal antibody to tumor necrosis factor-alpha, in patients with moderate-to-severe heart failure: results of the anti-TNF Therapy Against Congestive Heart Failure (ATTACH) trial. *Circulation*. 2003;107:3133-40.
191. Mann DL, McMurray JJ, Packer M, Swedberg K, Borer JS, Colucci WS, Djian J, Drexler H, Feldman A, Kober L, Krum H, Liu P, Nieminen M, Tavazzi L, van Veldhuisen DJ, Waldenstrom A, Warren M, Westheim A, Zannad F and Fleming T. Targeted anticytokine therapy in patients with chronic heart failure: results of the Randomized Etanercept Worldwide Evaluation (RENEWAL). *Circulation*. 2004;109:1594-602.
192. Gullestad L, Ueland T, Fjeld JG, Holt E, Gundersen T, Breivik K, Folling M, Hodt A, Skardal R, Kjekshus J, Andreassen A, Kjekshus E, Wergeland R, Yndestad A, Froland SS,

Semb AG and Aukrust P. Effect of thalidomide on cardiac remodeling in chronic heart failure: results of a double-blind, placebo-controlled study. *Circulation*. 2005;112:3408-14.
193. Orea-Tejeda A, Arrieta-Rodriguez O, Castillo-Martinez L, Rodriguez-Reyna T, Asensio-Lafuente E, Granados-Arriola J and Dorantes-Garcia J. Effects of thalidomide treatment in heart failure patients. *Cardiology*. 2007;108:237-42.
194. Sliwa K, Skudicky D, Candy G, Wisenbaugh T and Sareli P. Randomised investigation of effects of pentoxifylline on left-ventricular performance in idiopathic dilated cardiomyopathy. *Lancet*. 1998;351:1091-3.
195. Bahrmann P, Hengst UM, Richartz BM and Figulla HR. Pentoxifylline in ischemic, hypertensive and idiopathic-dilated cardiomyopathy: effects on left-ventricular function, inflammatory cytokines and symptoms. *European Journal of Heart Failure*. 2004;6:195-201.
196. Yamazaki T, Seko Y, Tamatani T, Miyasaka M, Yagita H, Okumura K, Nagai R and Yazaki Y. Expression of intercellular adhesion molecule-1 in rat heart with ischemia/reperfusion and limitation of infarct size by treatment with antibodies against cell adhesion molecules. *American Journal of Pathology*. 1993;143:410-8.
197. Simpson PJ, Todd RF, 3rd, Fantone JC, Mickelson JK, Griffin JD and Lucchesi BR. Reduction of experimental canine myocardial reperfusion injury by a monoclonal antibody (anti-Mo1, anti-CD11b) that inhibits leukocyte adhesion. *Journal of Clinical Investigation*. 1988;81:624-9.
198. Christia P and Frangogiannis NG. Targeting inflammatory pathways in myocardial infarction. *European Journal of Clinical Investigation*. 2013;43:986-95.
199. Nakao A. Temporal regulation of cytokines by the circadian clock. *J Immunol Res*. 2014;2014:614529.
200. Blum A and Miller H. Pathophysiological role of cytokines in congestive heart failure. *Annual Review of Medicine*. 2001;52:15-27.
201. Yang L, Cai X, Liu J, Jia Z, Jiao J, Zhang J, Li C, Li J and Tang XD. CpG-ODN attenuates pathological cardiac hypertrophy and heart failure by activation of PI3Kalpha-Akt signaling. *PLoS One*. 2013;8:e62373.
202. Knuefermann P, Schwederski M, Velten M, Krings P, Ehrentraut H, Rudiger M, Boehm O, Fink K, Dreiner U, Grohe C, Hoeft A, Baumgarten G, Koch A, Zacharowski K and Meyer R. Bacterial DNA induces myocardial inflammation and reduces cardiomyocyte contractility: role of toll-like receptor 9. *Cardiovascular Research*. 2008;78:26-35.
203. Boehm O, Markowski P, van der Giet M, Gielen V, Kokalova A, Brill C, Hoeft A, Baumgarten G, Meyer R and Knuefermann P. In vivo TLR9 inhibition attenuates CpG-induced myocardial dysfunction. *Mediators of Inflammation*. 2013;2013:217297.
204. Post SR, Hammond HK and Insel PA. Beta-adrenergic receptors and receptor signaling in heart failure. *Annual Review of Pharmacology and Toxicology*. 1999;39:343-360.
205. Lou Q, Janardhan A and Efimov IR. Remodeling of calcium handling in human heart failure. *Advances in Experimental Medicine and Biology*. 2012;740:1145-74.
206. Ashrafian H, Frenneaux MP and Opie LH. Metabolic mechanisms in heart failure. *Circulation*. 2007;116:434-48.
207. Burgoyne JR, Mongue-Din H, Eaton P and Shah AM. Redox signaling in cardiac physiology and pathology. *Circulation Research*. 2012;111:1091-106.
208. Rockman HA, Koch WJ and Lefkowitz RJ. Seven-transmembrane-spanning receptors and heart function. *Nature*. 2002;415:206-12.
209. Ahlquist RP. A study of the adrenotropic receptors. *American Journal of Pathology*. 1948;153:586-600.
210. Bristow MR, Ginsburg R, Umans V, Fowler M, Minobe W, Rasmussen R, Zera P, Menlove R, Shah P, Jamieson S and et al. Beta 1- and beta 2-adrenergic-receptor subpopulations in nonfailing and failing human ventricular myocardium: coupling of both receptor subtypes to muscle contraction and selective beta 1-receptor down-regulation in heart failure. *Circulation Research*. 1986;59:297-309.
211. Barki-Harrington L, Perrino C and Rockman HA. Network integration of the adrenergic system in cardiac hypertrophy. *Cardiovascular Research*. 2004;63:391-402.
212. Sprang SR. G protein mechanisms: insights from structural analysis. *Annual Review of Biochemistry*. 1997;66:639-78.
213. Lohse MJ. G-protein-coupled receptor kinases and the heart. *Trends in Cardiovascular Medicine*. 1995;5:63-8.
214. Brum PC, Rolim NP, Bacurau AV and Medeiros A. Neurohumoral activation in heart failure: the role of adrenergic receptors. *Anais da Academia Brasileira de Ciências*. 2006;78:485-503.

215. Vidal M, Wieland T, Lohse MJ and Lorenz K. Beta-Adrenergic receptor stimulation causes cardiac hypertrophy via a G-betagamma/Erk-dependent pathway. *Cardiovascular Research*. 2012;96:255-64.
216. Xiao RP, Avdonin P, Zhou YY, Cheng H, Akhter SA, Eschenhagen T, Lefkowitz RJ, Koch WJ and Lakatta EG. Coupling of beta2-adrenoceptor to Gi proteins and its physiological relevance in murine cardiac myocytes. *Circulation Research*. 1999;84:43-52.
217. Saito S, Hiroi Y, Zou Y, Aikawa R, Toko H, Shibasaki F, Yazaki Y, Nagai R and Komuro I. Beta-Adrenergic pathway induces apoptosis through calcineurin activation in cardiac myocytes. *Journal of Biological Chemistry*. 2000;275:34528-33.
218. Vinge LE, Oie E, Andersson Y, Grogaard HK, Andersen G and Attramadal H. Myocardial distribution and regulation of GRK and beta-arrestin isoforms in congestive heart failure in rats. *American Journal of Physiology - Heart and Circulatory Physiology*. 2001;281:H2490-9.
219. Koch WJ, Lefkowitz RJ and Rockman HA. Functional consequences of altering myocardial adrenergic receptor signaling. *Annual Review of Physiology*. 2000;62:237-60.
220. Lohse MJ, Engelhardt S and Eschenhagen T. What is the role of beta-adrenergic signaling in heart failure? *Circulation Research*. 2003;93:896-906.
221. Ungerer M, Parruti G, Bohm M, Puzicha M, DeBlasi A, Erdmann E and Lohse MJ. Expression of beta-arrestins and beta-adrenergic receptor kinases in the failing human heart. *Circulation Research*. 1994;74:206-13.
222. Choi D-J, Koch WJ, Hunter JJ and Rockman HA. Mechanism of β-Adrenergic Receptor Desensitization in Cardiac Hypertrophy Is Increased β-Adrenergic Receptor Kinase. *Journal of Biological Chemistry*. 1997;272:17223-17229.
223. Eschenhagen T, Mende U, Nose M, Schmitz W, Scholz H, Haverich A, Hirt S, Doring V, Kalmar P, Hoppner W and et al. Increased messenger RNA level of the inhibitory G protein alpha subunit Gi alpha-2 in human end-stage heart failure. *Circulation Research*. 1992;70:688-96.
224. Murray DR, Prabhu SD and Chandrasekar B. Chronic beta-adrenergic stimulation induces myocardial proinflammatory cytokine expression. *Circulation*. 2000;101:2338-41.
225. Werner C, Werdan K, Ponicke K and Brodde OE. Impaired beta-adrenergic control of immune function in patients with chronic heart failure: reversal by beta1-blocker treatment. *Basic Research in Cardiology*. 2001;96:290-8.
226. Wang SQ, Song LS, Lakatta EG and Cheng H. Ca2+ signalling between single L-type Ca2+ channels and ryanodine receptors in heart cells. *Nature*. 2001;410:592-6.
227. Fabiato A. Calcium-induced release of calcium from the cardiac sarcoplasmic reticulum. *American Journal of Physiology*. 1983;245:C1-14.
228. Catterall WA. Structure and regulation of voltage-gated Ca2+ channels. *Annual Review of Cell and Developmental Biology* 2000;16:521-55.
229. Fearnley CJ, Roderick HL and Bootman MD. Calcium signaling in cardiac myocytes. *Cold Spring Harbor Perspectives in Biology*. 2011;3:a004242.
230. Zalk R, Clarke OB, des Georges A, Grassucci RA, Reiken S, Mancia F, Hendrickson WA, Frank J and Marks AR. Structure of a mammalian ryanodine receptor. *Nature*. 2015;517:44-9.
231. Yan Z, Bai XC, Yan C, Wu J, Li Z, Xie T, Peng W, Yin CC, Li X, Scheres SH, Shi Y and Yan N. Structure of the rabbit ryanodine receptor RyR1 at near-atomic resolution. *Nature*. 2015;517:50-5.
232. Serysheva, II, Schatz M, van Heel M, Chiu W and Hamilton SL. Structure of the skeletal muscle calcium release channel activated with Ca2+ and AMP-PCP. *Biophysical Journal*. 1999;77:1936-44.
233. Valdivia HH, Kaplan JH, Ellis-Davies GC and Lederer WJ. Rapid adaptation of cardiac ryanodine receptors: modulation by Mg2+ and phosphorylation. *Science*. 1995;267:1997-2000.
234. Marx SO, Reiken S, Hisamatsu Y, Gaburjakova M, Gaburjakova J, Yang YM, Rosemblit N and Marks AR. Phosphorylation-dependent regulation of ryanodine receptors: a novel role for leucine/isoleucine zippers. *Journal of Cell Biology*. 2001;153:699-708.
235. Lytton J, Westlin M, Burk SE, Shull GE and MacLennan DH. Functional comparisons between isoforms of the sarcoplasmic or endoplasmic reticulum family of calcium pumps. *Journal of Biological Chemistry*. 1992;267:14483-9.
236. Movsesian MA, Nishikawa M and Adelstein RS. Phosphorylation of phospholamban by calcium-activated, phospholipid-dependent protein kinase. Stimulation of cardiac sarcoplasmic reticulum calcium uptake. *Journal of Biological Chemistry*. 1984;259:8029-32.

237. Iwamoto T, Pan Y, Wakabayashi S, Imagawa T, Yamanaka HI and Shigekawa M. Phosphorylation-dependent regulation of cardiac Na+/Ca2+ exchanger via protein kinase C. *Journal of Biological Chemistry*. 1996;271:13609-15.
238. Ruknudin A, He S, Lederer WJ and Schulze DH. Functional differences between cardiac and renal isoforms of the rat Na+-Ca2+ exchanger NCX1 expressed in Xenopus oocytes. *Journal of Physiology*. 2000;529 Pt 3:599-610.
239. Zhang XQ, Ahlers BA, Tucker AL, Song J, Wang J, Moorman JR, Mounsey JP, Carl LL, Rothblum LI and Cheung JY. Phospholemman inhibition of the cardiac Na+/Ca2+ exchanger. Role of phosphorylation. *Journal of Biological Chemistry*. 2006;281:7784-92.
240. Chen X, Piacentino V, 3rd, Furukawa S, Goldman B, Margulies KB and Houser SR. L-type Ca2+ channel density and regulation are altered in failing human ventricular myocytes and recover after support with mechanical assist devices. *Circulation Research*. 2002;91:517-24.
241. Marx SO, Reiken S, Hisamatsu Y, Jayaraman T, Burkhoff D, Rosemblit N and Marks AR. PKA phosphorylation dissociates FKBP12.6 from the calcium release channel (ryanodine receptor): defective regulation in failing hearts. *Cell*. 2000;101:365-76.
242. Schwinger RH, Bohm M, Schmidt U, Karczewski P, Bavendiek U, Flesch M, Krause EG and Erdmann E. Unchanged protein levels of SERCA II and phospholamban but reduced Ca2+ uptake and Ca(2+)-ATPase activity of cardiac sarcoplasmic reticulum from dilated cardiomyopathy patients compared with patients with nonfailing hearts. *Circulation*. 1995;92:3220-8.
243. Hasenfuss G, Reinecke H, Studer R, Meyer M, Pieske B, Holtz J, Holubarsch C, Posival H, Just H and Drexler H. Relation between myocardial function and expression of sarcoplasmic reticulum Ca(2+)-ATPase in failing and nonfailing human myocardium. *Circulation Research*. 1994;75:434-42.
244. Weber CR, Piacentino V, 3rd, Houser SR and Bers DM. Dynamic regulation of sodium/calcium exchange function in human heart failure. *Circulation*. 2003;108:2224-9.
245. Stanley WC, Recchia FA and Lopaschuk GD. Myocardial substrate metabolism in the normal and failing heart. *Physiological Reviews*. 2005;85:1093-129.
246. Wisneski JA, Gertz EW, Neese RA, Gruenke LD and Craig JC. Dual carbon-labeled isotope experiments using D-[6-14C] glucose and L-[1,2,3-13C3] lactate: a new approach for investigating human myocardial metabolism during ischemia. *Journal of the American College of Cardiology*. 1985;5:1138-46.
247. Gertz EW, Wisneski JA, Stanley WC and Neese RA. Myocardial substrate utilization during exercise in humans. Dual carbon-labeled carbohydrate isotope experiments. *Journal of Clinical Investigation*. 1988;82:2017-25.
248. Doenst T, Nguyen TD and Abel ED. Cardiac metabolism in heart failure: implications beyond ATP production. *Circulation Research*. 2013;113:709-24.
249. van der Vusse GJ, van Bilsen M and Glatz JF. Cardiac fatty acid uptake and transport in health and disease. *Cardiovascular Research*. 2000;45:279-93.
250. Lopaschuk GD, Ussher JR, Folmes CD, Jaswal JS and Stanley WC. Myocardial fatty acid metabolism in health and disease. *Physiological Reviews*. 2010;90:207-58.
251. Kolwicz SC, Jr. and Tian R. Glucose metabolism and cardiac hypertrophy. *Cardiovascular Research*. 2011;90:194-201.
252. Russell RR, 3rd and Taegtmeyer H. Changes in citric acid cycle flux and anaplerosis antedate the functional decline in isolated rat hearts utilizing acetoacetate. *Journal of Clinical Investigation*. 1991;87:384-90.
253. Allard MF, Schonekess BO, Henning SL, English DR and Lopaschuk GD. Contribution of oxidative metabolism and glycolysis to ATP production in hypertrophied hearts. *American Journal of Pathology*. 1994;267:H742-50.
254. Nascimben L, Ingwall JS, Lorell BH, Pinz I, Schultz V, Tornheim K and Tian R. Mechanisms for increased glycolysis in the hypertrophied rat heart. *Hypertension*. 2004;44:662-7.
255. Sack MN, Rader TA, Park S, Bastin J, McCune SA and Kelly DP. Fatty acid oxidation enzyme gene expression is downregulated in the failing heart. *Circulation*. 1996;94:2837-42.
256. Depre C, Shipley GL, Chen W, Han Q, Doenst T, Moore ML, Stepkowski S, Davies PJ and Taegtmeyer H. Unloaded heart in vivo replicates fetal gene expression of cardiac hypertrophy. *Nature Medicine*. 1998;4:1269-75.
257. Tian R. Transcriptional regulation of energy substrate metabolism in normal and hypertrophied heart. *Current Hypertension Reports*. 2003;5:454-8.
258. Karbowska J, Kochan Z and Smolenski RT. Peroxisome proliferator-activated receptor alpha is downregulated in the failing human heart. *Cellular & Molecular Biology Letters*. 2003;8:49-53.

259. Bashore TM, Magorien DJ, Letterio J, Shaffer P and Unverferth DV. Histologic and biochemical correlates of left ventricular chamber dynamics in man. *Journal of the American College of Cardiology*. 1987;9:734-42.
260. Beer M, Seyfarth T, Sandstede J, Landschutz W, Lipke C, Kostler H, von Kienlin M, Harre K, Hahn D and Neubauer S. Absolute concentrations of high-energy phosphate metabolites in normal, hypertrophied, and failing human myocardium measured noninvasively with (31)P-SLOOP magnetic resonance spectroscopy. *Journal of the American College of Cardiology*. 2002;40:1267-74.
261. Maulik SK and Kumar S. Oxidative stress and cardiac hypertrophy: a review. *Toxicology Mechanisms and Methods*. 2012;22:359-66.
262. Suematsu N, Tsutsui H, Wen J, Kang D, Ikeuchi M, Ide T, Hayashidani S, Shiomi T, Kubota T, Hamasaki N and Takeshita A. Oxidative stress mediates tumor necrosis factor-alpha-induced mitochondrial DNA damage and dysfunction in cardiac myocytes. *Circulation*. 2003;107:1418-23.
263. Perricone AJ and Vander Heide RS. Novel therapeutic strategies for ischemic heart disease. *Pharmacological Research*. 2014;89:36-45.
264. Barcellos-Hoff MH and Dix TA. Redox-mediated activation of latent transforming growth factor-beta 1. *Molecular Endocrinology*. 1996;10:1077-83.
265. Spinale FG. Myocardial matrix remodeling and the matrix metalloproteinases: influence on cardiac form and function. *Physiological Reviews*. 2007;87:1285-342.
266. Zima AV and Blatter LA. Redox regulation of cardiac calcium channels and transporters. *Cardiovascular Research*. 2006;71:310-21.
267. Diaz-Velez CR, Garcia-Castineiras S, Mendoza-Ramos E and Hernandez-Lopez E. Increased malondialdehyde in peripheral blood of patients with congestive heart failure. *American Heart Journal*. 1996;131:146-52.
268. Mak S, Lehotay DC, Yazdanpanah M, Azevedo ER, Liu PP and Newton GE. Unsaturated aldehydes including 4-OH-nonenal are elevated in patients with congestive heart failure. *Journal of Cardiac Failure*. 2000;6:108-14.
269. Tang WH, Brennan ML, Philip K, Tong W, Mann S, Van Lente F and Hazen SL. Plasma myeloperoxidase levels in patients with chronic heart failure. *American Journal of Cardiology*. 2006;98:796-9.
270. Mallat Z, Philip I, Lebret M, Chatel D, Maclouf J and Tedgui A. Elevated levels of 8-iso-prostaglandin F2alpha in pericardial fluid of patients with heart failure: a potential role for in vivo oxidant stress in ventricular dilatation and progression to heart failure. *Circulation*. 1998;97:1536-9.
271. Koyama Y, Takeishi Y, Arimoto T, Niizeki T, Shishido T, Takahashi H, Nozaki N, Hirono O, Tsunoda Y, Nitobe J, Watanabe T and Kubota I. High serum level of pentosidine, an advanced glycation end product (AGE), is a risk factor of patients with heart failure. *Journal of Cardiac Failure*. 2007;13:199-206.
272. Kono Y, Nakamura K, Kimura H, Nishii N, Watanabe A, Banba K, Miura A, Nagase S, Sakuragi S, Kusano KF, Matsubara H and Ohe T. Elevated levels of oxidative DNA damage in serum and myocardium of patients with heart failure. *Circulation Journal*. 2006;70:1001-5.
273. Sakai H, Tsutamoto T, Tsutsui T, Tanaka T, Ishikawa C and Horie M. Serum level of uric acid, partly secreted from the failing heart, is a prognostic marker in patients with congestive heart failure. *Circulation Journal*. 2006;70:1006-11.
274. Remme WJ. Overview of the relationship between ischemia and congestive heart failure. *Clinical Cardiology*. 2000;23:IV4-8.
275. Sanada S, Komuro I and Kitakaze M. Pathophysiology of myocardial reperfusion injury: preconditioning, postconditioning, and translational aspects of protective measures. *American Journal of Physiology - Heart and Circulatory Physiology*. 2011;301:H1723-41.
276. Orrenius S, Zhivotovsky B and Nicotera P. Regulation of cell death: the calcium-apoptosis link. *Nature Reviews Molecular Cell Biology*. 2003;4:552-65.
277. Jennings RB, Sommers HM, Smyth GA, Flack HA and Linn H. Myocardial necrosis induced by temporary occlusion of a coronary artery in the dog. *Archives of Pathology & Laboratory Medicine* 1960;70:68-78.
278. Yellon DM and Hausenloy DJ. Myocardial reperfusion injury. *New England Journal of Medicine* 2007;357:1121-35.
279. Inserte J, Hernando V and Garcia-Dorado D. Contribution of calpains to myocardial ischaemia/reperfusion injury. *Cardiovascular Research*. 2012;96:23-31.
280. Zweier JL and Talukder MA. The role of oxidants and free radicals in reperfusion injury. *Cardiovascular Research*. 2006;70:181-90.

281. Zorov DB, Filburn CR, Klotz LO, Zweier JL and Sollott SJ. Reactive oxygen species (ROS)-induced ROS release: a new phenomenon accompanying induction of the mitochondrial permeability transition in cardiac myocytes. *Journal of Experimental Medicine*. 2000;192:1001-14.
282. Hasenfuss G. Animal models of human cardiovascular disease, heart failure and hypertrophy. *Cardiovascular Research*. 1998;39:60-76.
283. Breckenridge R. Heart failure and mouse models. *Disease Models & Mechanisms*. 2010;3:138-43.
284. Houser SR, Margulies KB, Murphy AM, Spinale FG, Francis GS, Prabhu SD, Rockman HA, Kass DA, Molkentin JD, Sussman MA, Koch WJ, American Heart Association Council on Basic Cardiovascular Sciences CoCC, Council on Functional G and Translational B. Animal models of heart failure: a scientific statement from the American Heart Association. *Circulation Research*. 2012;111:131-50.
285. Rockman HA, Ross RS, Harris AN, Knowlton KU, Steinhelper ME, Field LJ, Ross J, Jr. and Chien KR. Segregation of atrial-specific and inducible expression of an atrial natriuretic factor transgene in an in vivo murine model of cardiac hypertrophy. *Proceedings of the National Academy of Sciences of the United States of America*. 1991;88:8277-81.
286. Rothermel BA, Berenji K, Tannous P, Kutschke W, Dey A, Nolan B, Yoo KD, Demetroulis E, Gimbel M, Cabuay B, Karimi M and Hill JA. Differential activation of stress-response signaling in load-induced cardiac hypertrophy and failure. *Physiological Genomics*. 2005;23:18-27.
287. Toischer K, Rokita AG, Unsold B, Zhu W, Kararigas G, Sossalla S, Reuter SP, Becker A, Teucher N, Seidler T, Grebe C, Preuss L, Gupta SN, Schmidt K, Lehnart SE, Kruger M, Linke WA, Backs J, Regitz-Zagrosek V, Schafer K, Field LJ, Maier LS and Hasenfuss G. Differential cardiac remodeling in preload versus afterload. *Circulation*. 2010;122:993-1003.
288. Scheuermann-Freestone M, Freestone NS, Langenickel T, Hohnel K, Dietz R and Willenbrock R. A new model of congestive heart failure in the mouse due to chronic volume overload. *European Journal of Heart Failure*. 2001;3:535-43.
289. Zolotareva AG and Kogan ME. Production of experimental occlusive myocardial infarction in mice. *Cor et Vasa*. 1978;20:308-14.
290. Michael LH, Entman ML, Hartley CJ, Youker KA, Zhu J, Hall SR, Hawkins HK, Berens K and Ballantyne CM. Myocardial ischemia and reperfusion: a murine model. *American Journal of Physiology*. 1995;269:H2147-54.
291. Fisher SG and Marber MS. An in vivo model of ischaemia-reperfusion injury and ischaemic preconditioning in the mouse heart. *Journal of Pharmacological and Toxicological Methods*. 2002;48:161-9.
292. Vandervelde S, van Amerongen MJ, Tio RA, Petersen AH, van Luyn MJ and Harmsen MC. Increased inflammatory response and neovascularization in reperfused vs. non-reperfused murine myocardial infarction. *Cardiovascular Pathology*. 2006;15:83-90.
293. Ytrehus K. The ischemic heart--experimental models. *Pharmacological Research*. 2000;42:193-203.
294. Stiles GL and Lefkowitz RJ. Cardiac adrenergic receptors. *Annual Review of Medicine*. 1984;35:149-64.
295. Rona G, Zsoter T, Chappel C and Gaudry R. Myocardial lesions, circulatory and electrocardiographic changes produced by isoproterenol in the dog. *Reviews of Canadian Biology*. 1959;18:83-94.
296. Bartosova D, Chvapil M, Korecky B, Poupa O, Rakusan K, Turek Z and Vizek M. The growth of the muscular and collagenous parts of the rat heart in various forms of cardiomegaly. *Journal of Physiology*. 1969;200:285-95.
297. Beznak M. Hemodynamics during the acute phase of myocardial damage caused by isoproterenol. *Canadian Journal of Physiology and Pharmacology*. 1962;40:25-30.
298. Beznak M and Hacker P. Hemodynamics during the chronic stage of myocardial damage caused by isoproterenol. *Canadian Journal of Physiology and Pharmacology*. 1964;42:269-74.
299. Willis BC, Salazar-Cantu A, Silva-Platas C, Fernandez-Sada E, Villegas CA, Rios-Argaiz E, Gonzalez-Serrano P, Sanchez LA, Guerrero-Beltran CE, Garcia N, Torre-Amione G, Garcia-Rivas GJ and Altamirano J. Impaired oxidative metabolism and calcium mishandling underlie cardiac dysfunction in a rat model of post-acute isoproterenol-induced cardiomyopathy. *American Journal of Physiology - Heart and Circulatory Physiology*. 2015;308:H467-77.
300. Kudej RK, Iwase M, Uechi M, Vatner DE, Oka N, Ishikawa Y, Shannon RP, Bishop SP and Vatner SF. Effects of chronic beta-adrenergic receptor stimulation in mice. *Journal of Molecular and Cellular Cardiology*. 1997;29:2735-46.

301. Zhang GX, Kimura S, Nishiyama A, Shokoji T, Rahman M, Yao L, Nagai Y, Fujisawa Y, Miyatake A and Abe Y. Cardiac oxidative stress in acute and chronic isoproterenol-infused rats. *Cardiovascular Research*. 2005;65:230-8.
302. Heather LC, Catchpole AF, Stuckey DJ, Cole MA, Carr CA and Clarke K. Isoproterenol induces in vivo functional and metabolic abnormalities: similar to those found in the infarcted rat heart. *Journal of Physiology and Pharmacology*. 2009;60:31-9.
303. Oudit GY, Crackower MA, Eriksson U, Sarao R, Kozieradzki I, Sasaki T, Irie-Sasaki J, Gidrewicz D, Rybin VO, Wada T, Steinberg SF, Backx PH and Penninger JM. Phosphoinositide 3-kinase gamma-deficient mice are protected from isoproterenol-induced heart failure. *Circulation*. 2003;108:2147-52.
304. Grimm D, Elsner D, Schunkert H, Pfeifer M, Griese D, Bruckschlegel G, Muders F, Riegger GA and Kromer EP. Development of heart failure following isoproterenol administration in the rat: role of the renin-angiotensin system. *Cardiovascular Research*. 1998;37:91-100.
305. Bliksoen M, Mariero LH, Ohm IK, Haugen F, Yndestad A, Solheim S, Seljeflot I, Ranheim T, Andersen GO, Aukrust P, Valen G and Vinge LE. Increased circulating mitochondrial DNA after myocardial infarction. *International Journal of Cardiology*. 2012;158:132-4.
306. Taneike M, Mizote I, Morita T, Watanabe T, Hikoso S, Yamaguchi O, Takeda T, Oka T, Tamai T, Oyabu J, Murakawa T, Nakayama H, Nishida K, Takeda J, Mochizuki N, Komuro I and Otsu K. Calpain protects the heart from hemodynamic stress. *Journal of Biological Chemistry*. 2011;286:32170-7.
307. Protti A, Sirker A, Shah AM and Botnar R. Late gadolinium enhancement of acute myocardial infarction in mice at 7T: cine-FLASH versus inversion recovery. *Journal of Magnetic Resonance Imaging*. 2010;32:878-86.
308. Protti A, Dong X, Sirker A, Botnar R and Shah AM. MRI-based prediction of adverse cardiac remodeling after murine myocardial infarction. *American Journal of Physiology - Heart and Circulatory Physiology*. 2012;303:H309-14.
309. Francis GS. Neurohumoral mechanisms involved in congestive heart failure. *American Journal of Cardiology*. 1985;55:15A-21A.
310. Ohtsuka T, Hamada M, Hiasa G, Sasaki O, Suzuki M, Hara Y, Shigematsu Y and Hiwada K. Effect of beta-blockers on circulating levels of inflammatory and anti-inflammatory cytokines in patients with dilated cardiomyopathy. *Journal of the American College of Cardiology*. 2001;37:412-7.
311. Brooks WW and Conrad CH. Isoproterenol-induced myocardial injury and diastolic dysfunction in mice: structural and functional correlates. *Comparative Medicine*. 2009;59:339-43.
312. Leenen FH, White R and Yuan B. Isoproterenol-induced cardiac hypertrophy: role of circulatory versus cardiac renin-angiotensin system. *American Journal of Physiology - Heart and Circulatory Physiology*. 2001;281:H2410-6.
313. Jaehnig EJ, Heidt AB, Greene SB, Cornelissen I and Black BL. Increased susceptibility to isoproterenol-induced cardiac hypertrophy and impaired weight gain in mice lacking the histidine-rich calcium-binding protein. *Molecular and Cellular Biology*. 2006;26:9315-26.
314. Chen X, Zeng S, Zou J, Chen Y, Yue Z, Gao Y, Zhang L, Cao W and Liu P. Rapamycin attenuated cardiac hypertrophy induced by isoproterenol and maintained energy homeostasis via inhibiting NF-kappaB activation. *Mediators of Inflammation*. 2014;2014:868753.
315. Galindo CL, Skinner MA, Errami M, Olson LD, Watson DA, Li J, McCormick JF, McIver LJ, Kumar NM, Pham TQ and Garner HR. Transcriptional profile of isoproterenol-induced cardiomyopathy and comparison to exercise-induced cardiac hypertrophy and human cardiac failure. *BMC Physiology*. 2009;9:23.
316. Booysen HL, Norton GR, Opie LH and Woodiwiss AJ. Reverse chamber remodelling following adrenergic-induced advanced cardiac dilatation and pump dysfunction. *Basic Research in Cardiology*. 2012;107:238.
317. Rassler B. Contribution of alpha - and beta -Adrenergic Mechanisms to the Development of Pulmonary Edema. *Scientifica*. 2012;2012:829504.
318. Rassler B, Marx G, Schierle K and Zimmer HG. Catecholamines can induce pulmonary remodeling in rats. *Cellular Physiology and Biochemistry*. 2012;30:1134-47.
319. Yancy CW, Jessup M, Bozkurt B, Butler J, Casey DE, Jr., Drazner MH, Fonarow GC, Geraci SA, Horwich T, Januzzi JL, Johnson MR, Kasper EK, Levy WC, Masoudi FA, McBride PE, McMurray JJ, Mitchell JE, Peterson PN, Riegel B, Sam F, Stevenson LW, Tang WH, Tsai EJ and Wilkoff BL. 2013 ACCF/AHA guideline for the management of heart failure: executive summary: a report of the American College of Cardiology Foundation/American Heart Association Task Force on practice guidelines. *Circulation*. 2013;128:1810-52.

320. Heart Failure Society of A, Lindenfeld J, Albert NM, Boehmer JP, Collins SP, Ezekowitz JA, Givertz MM, Katz SD, Klapholz M, Moser DK, Rogers JG, Starling RC, Stevenson WG, Tang WH, Teerlink JR and Walsh MN. HFSA 2010 Comprehensive Heart Failure Practice Guideline. *Journal of Cardiac Failure*. 2010;16:e1-194.
321. Nakano A, Harada T, Morikawa S and Kato Y. Expression of leukocyte common antigen (CD45) on various human leukemia/lymphoma cell lines. *Acta Pathologica Japonica*. 1990;40:107-15.
322. Holness CL and Simmons DL. Molecular cloning of CD68, a human macrophage marker related to lysosomal glycoproteins. *Blood*. 1993;81:1607-13.
323. Shi C, Hohl TM, Leiner I, Equinda MJ, Fan X and Pamer EG. Ly6G+ neutrophils are dispensable for defense against systemic Listeria monocytogenes infection. *Journal of Immunology*. 2011;187:5293-8.
324. van Dongen JJ, Krissansen GW, Wolvers-Tettero IL, Comans-Bitter WM, Adriaansen HJ, Hooijkaas H, van Wering ER and Terhorst C. Cytoplasmic expression of the CD3 antigen as a diagnostic marker for immature T-cell malignancies. *Blood*. 1988;71:603-12.
325. Yin W, Zhang P, Huang JH, Zhang QY, Fan R, Li J, Zhou JJ, Hu YZ, Guo HT, Zhang SM, Wang YM, Kaye AD, Gu CH, Liu JC, Cheng L, Cui Q, Yi DH and Pei JM. Stimulation of kappa-opioid receptor reduces isoprenaline-induced cardiac hypertrophy and fibrosis. *European Journal of Pharmacology*. 2009;607:135-42.
326. Benjamin IJ, Jalil JE, Tan LB, Cho K, Weber KT and Clark WA. Isoproterenol-induced myocardial fibrosis in relation to myocyte necrosis. *Circulation Research*. 1989;65:657-70.
327. Wyllie AH. Glucocorticoid-induced thymocyte apoptosis is associated with endogenous endonuclease activation. *Nature*. 1980;284:555-6.
328. Hikoso S, Yamaguchi O, Higuchi Y, Hirotani S, Takeda T, Kashiwase K, Watanabe T, Taniike M, Tsujimoto I, Asahi M, Matsumura Y, Nishida K, Nakajima H, Akira S, Hori M and Otsu K. Pressure overload induces cardiac dysfunction and dilation in signal transducer and activator of transcription 6-deficient mice. *Circulation*. 2004;110:2631-7.
329. Li P, Sur SH, Mistlberger RE and Morris M. Circadian blood pressure and heart rate rhythms in mice. *American Journal of Physiology*. 1999;276:R500-4.
330. Zimmer HG. Catecholamine-induced cardiac hypertrophy: significance of proto-oncogene expression. *Journal of Molecular Medicine*. 1997;75:849-59.
331. Friddle CJ, Koga T, Rubin EM and Bristow J. Expression profiling reveals distinct sets of genes altered during induction and regression of cardiac hypertrophy. *Proceedings of the National Academy of Sciences of the United States of America*. 2000;97:6745-50.
332. Thomsen JK, Fogh-Andersen N, Jaszczak P and Giese J. Atrial natriuretic peptide (ANP) decrease during normal pregnancy as related to hemodynamic changes and volume regulation. *Acta Obstetricia et Gynecologica Scandinavica*. 1993;72:103-10.
333. Bonventre PF, Saelinger CB and Imhoff JG. Studies on the effect of diphtheria toxin on protein synthesis in mice. *Journal of Medical Microbiology*. 1973;6:169-76.
334. Abraham J, Mudd JO, Kapur NK, Klein K, Champion HC and Wittstein IS. Stress cardiomyopathy after intravenous administration of catecholamines and beta-receptor agonists. *Journal of the American College of Cardiology*. 2009;53:1320-5.
335. Shao Y, Redfors B, Stahlman M, Tang MS, Miljanovic A, Mollmann H, Troidl C, Szardien S, Hamm C, Nef H, Boren J and Omerovic E. A mouse model reveals an important role for catecholamine-induced lipotoxicity in the pathogenesis of stress-induced cardiomyopathy. *European Journal of Heart Failure*. 2013;15:9-22.
336. Jocken JW and Blaak EE. Catecholamine-induced lipolysis in adipose tissue and skeletal muscle in obesity. *Physiology & Behavior*. 2008;94:219-30.
337. Jocken JW, Goossens GH, van Hees AM, Frayn KN, van Baak M, Stegen J, Pakbiers MT, Saris WH and Blaak EE. Effect of beta-adrenergic stimulation on whole-body and abdominal subcutaneous adipose tissue lipolysis in lean and obese men. *Diabetologia*. 2008;51:320-7.
338. Obunai K, Misra D, Van Tosh A and Bergmann SR. Metabolic evidence of myocardial stunning in takotsubo cardiomyopathy: a positron emission tomography study. *Journal of Nuclear Cardiology*. 2005;12:742-4.
339. Castillo Rivera AM, Ruiz-Bailen M and Rucabado Aguilar L. Takotsubo cardiomyopathy--a clinical review. *Medical Science Monitor*. 2011;17:RA135-47.
340. Nef HM, Mollmann H, Troidl C, Kostin S, Bottger T, Voss S, Hilpert P, Krause N, Weber M, Rolf A, Dill T, Schaper J, Hamm CW and Elsasser A. Expression profiling of cardiac genes in Tako-Tsubo cardiomyopathy: insight into a new cardiac entity. *Journal of Molecular and Cellular Cardiology*. 2008;44:395-404.

341. Nef HM, Mollmann H, Troidl C, Kostin S, Voss S, Hilpert P, Behrens CB, Rolf A, Rixe J, Weber M, Hamm CW and Elsasser A. Abnormalities in intracellular Ca2+ regulation contribute to the pathomechanism of Tako-Tsubo cardiomyopathy. *European Heart Journal*. 2009;30:2155-64.
342. Simmerman HK and Jones LR. Phospholamban: protein structure, mechanism of action, and role in cardiac function. *Physiological Reviews*. 1998;78:921-47.
343. Wegener AD and Jones LR. Phosphorylation-induced mobility shift in phospholamban in sodium dodecyl sulfate-polyacrylamide gels. Evidence for a protein structure consisting of multiple identical phosphorylatable subunits. *Journal of Biological Chemistry*. 1984;259:1834-41.
344. Cherry AD, Suliman HB, Bartz RR and Piantadosi CA. Peroxisome proliferator-activated receptor gamma co-activator 1-alpha as a critical co-activator of the murine hepatic oxidative stress response and mitochondrial biogenesis in Staphylococcus aureus sepsis. *Journal of Biological Chemistry*. 2014;289:41-52.
345. Majmundar AJ, Wong WJ and Simon MC. Hypoxia-inducible factors and the response to hypoxic stress. *Molecular Cell*. 2010;40:294-309.
346. Nguyen T, Nioi P and Pickett CB. The Nrf2-antioxidant response element signaling pathway and its activation by oxidative stress. *Journal of Biological Chemistry*. 2009;284:13291-5.
347. Ma Q. Role of nrf2 in oxidative stress and toxicity. *Annual Review of Pharmacology and Toxicology*. 2013;53:401-26.
348. Matsumura Y, Saeki E, Inoue M, Hori M, Kamada T and Kusuoka H. Inhomogeneous disappearance of myofilament-related cytoskeletal proteins in stunned myocardium of guinea pig. *Circulation Research*. 1996;79:447-54.
349. Mihaylova MM and Shaw RJ. The AMPK signalling pathway coordinates cell growth, autophagy and metabolism. *Nature Cell Biology*. 2011;13:1016-23.
350. Takemoto Y, Yoshiyama M, Takeuchi K, Omura T, Komatsu R, Izumi Y, Kim S and Yoshikawa J. Increased JNK, AP-1 and NF-kappa B DNA binding activities in isoproterenol-induced cardiac remodeling. *Journal of Molecular and Cellular Cardiology*. 1999;31:2017-30.
351. de Moissac D, Zheng H and Kirshenbaum LA. Linkage of the BH4 domain of Bcl-2 and the nuclear factor kappaB signaling pathway for suppression of apoptosis. *Journal of Biological Chemistry*. 1999;274:29505-9.
352. Kitagawa Y, Yamashita D, Ito H and Takaki M. Reversible effects of isoproterenol-induced hypertrophy on in situ left ventricular function in rat hearts. *American Journal of Physiology - Heart and Circulatory Physiology*. 2004;287:H277-85.
353. Go YM, Son DJ, Park H, Orr M, Hao L, Takabe W, Kumar S, Kang DW, Kim CW, Jo H and Jones DP. Disturbed flow enhances inflammatory signaling and atherogenesis by increasing thioredoxin-1 level in endothelial cell nuclei. *PLoS One*. 2014;9:e108346.
354. Tavora B, Reynolds LE, Batista S, Demircioglu F, Fernandez I, Lechertier T, Lees DM, Wong PP, Alexopoulou A, Elia G, Clear A, Ledoux A, Hunter J, Perkins N, Gribben JG and Hodivala-Dilke KM. Endothelial-cell FAK targeting sensitizes tumours to DNA-damaging therapy. *Nature*. 2014;514:112-6.
355. Pahl HL. Activators and target genes of Rel/NF-kappaB transcription factors. *Oncogene*. 1999;18:6853-66.
356. Ohm IK, Gao E, Belland Olsen M, Alfsnes K, Bliksoen M, Ogaard J, Ranheim T, Nymo SH, Holmen YD, Aukrust P, Yndestad A and Vinge LE. Toll-like receptor 9-activation during onset of myocardial ischemia does not influence infarct extension. *PLoS One*. 2014;9:e104407.
357. Keeley EC, Boura JA and Grines CL. Primary angioplasty versus intravenous thrombolytic therapy for acute myocardial infarction: a quantitative review of 23 randomised trials. *Lancet*. 2003;361:13-20.
358. Klocke R, Tian W, Kuhlmann MT and Nikol S. Surgical animal models of heart failure related to coronary heart disease. *Cardiovascular Research*. 2007;74:29-38.
359. Gao XM, Dart AM, Dewar E, Jennings G and Du XJ. Serial echocardiographic assessment of left ventricular dimensions and function after myocardial infarction in mice. *Cardiovascular Research*. 2000;45:330-8.
360. Testa M, Yeh M, Lee P, Fanelli R, Loperfido F, Berman JW and LeJemtel TH. Circulating levels of cytokines and their endogenous modulators in patients with mild to severe congestive heart failure due to coronary artery disease or hypertension. *Journal of the American College of Cardiology*. 1996;28:964-71.
361. Bozkurt B, Mann DL and Deswal A. Biomarkers of inflammation in heart failure. *Heart Failure Reviews*. 2010;15:331-41.

362. Nian M, Lee P, Khaper N and Liu P. Inflammatory cytokines and postmyocardial infarction remodeling. *Circulation Research*. 2004;94:1543-53.
363. Neumann FJ, Ott I, Gawaz M, Richardt G, Holzapfel H, Jochum M and Schomig A. Cardiac release of cytokines and inflammatory responses in acute myocardial infarction. *Circulation*. 1995;92:748-55.
364. Yan X, Anzai A, Katsumata Y, Matsuhashi T, Ito K, Endo J, Yamamoto T, Takeshima A, Shinmura K, Shen W, Fukuda K and Sano M. Temporal dynamics of cardiac immune cell accumulation following acute myocardial infarction. *Journal of Molecular and Cellular Cardiology* 2013;62:24-35.
365. Deten A, Volz HC, Briest W and Zimmer HG. Cardiac cytokine expression is upregulated in the acute phase after myocardial infarction. Experimental studies in rats. *Cardiovascular Research*. 2002;55:329-40.
366. Lu C, Ren D, Wang X, Ha T, Liu L, Lee EJ, Hu J, Kalbfleisch J, Gao X, Kao R, Williams D and Li C. Toll-like receptor 3 plays a role in myocardial infarction and ischemia/reperfusion injury. *Biochimica et Biophysica Acta*. 2014;1842:22-31.
367. Fallach R, Shainberg A, Avlas O, Fainblut M, Chepurko Y, Porat E and Hochhauser E. Cardiomyocyte Toll-like receptor 4 is involved in heart dysfunction following septic shock or myocardial ischemia. *Journal of Molecular and Cellular Cardiology*. 2010;48:1236-44.
368. Shishido T, Nozaki N, Yamaguchi S, Shibata Y, Nitobe J, Miyamoto T, Takahashi H, Arimoto T, Maeda K, Yamakawa M, Takeuchi O, Akira S, Takeishi Y and Kubota I. Toll-like receptor-2 modulates ventricular remodeling after myocardial infarction. *Circulation*. 2003;108:2905-10.
369. Timmers L, Sluijter JP, van Keulen JK, Hoefer IE, Nederhoff MG, Goumans MJ, Doevendans PA, van Echteld CJ, Joles JA, Quax PH, Piek JJ, Pasterkamp G and de Kleijn DP. Toll-like receptor 4 mediates maladaptive left ventricular remodeling and impairs cardiac function after myocardial infarction. *Circulation Research*. 2008;102:257-64.
370. Weisman HF, Bush DE, Mannisi JA and Bulkley BH. Global cardiac remodeling after acute myocardial infarction: a study in the rat model. *Journal of the American College of Cardiology*. 1985;5:1355-62.
371. Firth BG and Dunnmon PM. Left ventricular dilatation and failure post-myocardial infarction: pathophysiology and possible pharmacologic interventions. *Cardiovascular Drugs and Therapy Journal*. 1990;4:1363-74.
372. Gao XM, Ming Z, Su Y, Fang L, Kiriazis H, Xu Q, Dart AM and Du XJ. Infarct size and post-infarct inflammation determine the risk of cardiac rupture in mice. *International Journal of Cardiology*. 2010;143:20-8.
373. Fang L, Gao XM, Moore XL, Kiriazis H, Su Y, Ming Z, Lim YL, Dart AM and Du XJ. Differences in inflammation, MMP activation and collagen damage account for gender difference in murine cardiac rupture following myocardial infarction. *Journal of Molecular and Cellular Cardiology*. 2007;43:535-44.
374. Vanhoutte D, Schellings M, Pinto Y and Heymans S. Relevance of matrix metalloproteinases and their inhibitors after myocardial infarction: a temporal and spatial window. *Cardiovascular Research*. 2006;69:604-13.
375. Frangogiannis NG, Smith CW and Entman ML. The inflammatory response in myocardial infarction. *Cardiovascular Research*. 2002;53:31-47.
376. Li H, Simon H, Bocan TM and Peterson JT. MMP/TIMP expression in spontaneously hypertensive heart failure rats: the effect of ACE- and MMP-inhibition. *Cardiovascular Research*. 2000;46:298-306.
377. Webb CS, Bonnema DD, Ahmed SH, Leonardi AH, McClure CD, Clark LL, Stroud RE, Corn WC, Finklea L, Zile MR and Spinale FG. Specific temporal profile of matrix metalloproteinase release occurs in patients after myocardial infarction: relation to left ventricular remodeling. *Circulation*. 2006;114:1020-7.
378. Tyagi SC, Kumar SG, Haas SJ, Reddy HK, Voelker DJ, Hayden MR, Demmy TL, Schmaltz RA and Curtis JJ. Post-transcriptional regulation of extracellular matrix metalloproteinase in human heart end-stage failure secondary to ischemic cardiomyopathy. *Journal of Molecular and Cellular Cardiology*. 1996;28:1415-28.
379. Strutz F, Okada H, Lo CW, Danoff T, Carone RL, Tomaszewski JE and Neilson EG. Identification and characterization of a fibroblast marker: FSP1. *Journal of Cell Biology*. 1995;130:393-405.
380. Scholzen T and Gerdes J. The Ki-67 protein: from the known and the unknown. *Journal of Cellular Physiology*. 2000;182:311-22.
381. van den Borne SW, van de Schans VA, Strzelecka AE, Vervoort-Peters HT, Lijnen PM, Cleutjens JP, Smits JF, Daemen MJ, Janssen BJ and Blankesteijn WM. Mouse strain

determines the outcome of wound healing after myocardial infarction. *Cardiovascular Research*. 2009;84:273-82.
382. Yang F, Liu YH, Yang XP, Xu J, Kapke A and Carretero OA. Myocardial infarction and cardiac remodelling in mice. *Experimental Physiology* 2002;87:547-55.
383. Fahim MR, Halim SM and Kamel I. Tumor necrosis factor alpha in patients with acute myocardial infarction. *Egyptian Journal of Immunology*. 2004;11:31-7.
384. Jacobs M, Staufenberger S, Gergs U, Meuter K, Brandstatter K, Hafner M, Ertl G and Schorb W. Tumor necrosis factor-alpha at acute myocardial infarction in rats and effects on cardiac fibroblasts. *Journal of Molecular and Cellular Cardiology*. 1999;31:1949-59.
385. Chen J, Tung CH, Allport JR, Chen S, Weissleder R and Huang PL. Near-infrared fluorescent imaging of matrix metalloproteinase activity after myocardial infarction. *Circulation*. 2005;111:1800-5.
386. Matsumura S, Iwanaga S, Mochizuki S, Okamoto H, Ogawa S and Okada Y. Targeted deletion or pharmacological inhibition of MMP-2 prevents cardiac rupture after myocardial infarction in mice. *Journal of Clinical Investigation*. 2005;115:599-609.
387. Wilson EM, Moainie SL, Baskin JM, Lowry AS, Deschamps AM, Mukherjee R, Guy TS, St John-Sutton MG, Gorman JH, 3rd, Edmunds LH, Jr., Gorman RC and Spinale FG. Region- and type-specific induction of matrix metalloproteinases in post-myocardial infarction remodeling. *Circulation*. 2003;107:2857-63.
388. Ma Y, de Castro Bras LE, Toba H, Iyer RP, Hall ME, Winniford MD, Lange RA, Tyagi SC and Lindsey ML. Myofibroblasts and the extracellular matrix network in post-myocardial infarction cardiac remodeling. *Pflügers Archiv: European Journal of Physiology*. 2014;466:1113-27.
389. Krishnamurthy P, Rajasingh J, Lambers E, Qin G, Losordo DW and Kishore R. IL-10 inhibits inflammation and attenuates left ventricular remodeling after myocardial infarction via activation of STAT3 and suppression of HuR. *Circulation Research*. 2009;104:e9-18.
390. Lu L, Zhang JQ, Ramires FJ and Sun Y. Molecular and cellular events at the site of myocardial infarction: from the perspective of rebuilding myocardial tissue. *Biochemical and Biophysical Research Communications*. 2004;320:907-13.
391. Peterson JT, Li H, Dillon L and Bryant JW. Evolution of matrix metalloprotease and tissue inhibitor expression during heart failure progression in the infarcted rat. *Cardiovascular Research*. 2000;46:307-15.
392. Gao XM, Xu Q, Kiriazis H, Dart AM and Du XJ. Mouse model of post-infarct ventricular rupture: time course, strain- and gender-dependency, tensile strength, and histopathology. *Cardiovascular Research*. 2005;65:469-77.
393. Sun M, Dawood F, Wen WH, Chen M, Dixon I, Kirshenbaum LA and Liu PP. Excessive tumor necrosis factor activation after infarction contributes to susceptibility of myocardial rupture and left ventricular dysfunction. *Circulation*. 2004;110:3221-8.
394. Creemers EE, Davis JN, Parkhurst AM, Leenders P, Dowdy KB, Hapke E, Hauet AM, Escobar PG, Cleutjens JP, Smits JF, Daemen MJ, Zile MR and Spinale FG. Deficiency of TIMP-1 exacerbates LV remodeling after myocardial infarction in mice. *American Journal of Physiology - Heart and Circulatory Physiology*. 2003;284:H364-71.
395. Meneghin A, Choi ES, Evanoff HL, Kunkel SL, Martinez FJ, Flaherty KR, Toews GB and Hogaboam CM. TLR9 is expressed in idiopathic interstitial pneumonia and its activation promotes in vitro myofibroblast differentiation. *Histochemistry and Cell Biology*. 2008;130:979-92.
396. Hikoso S, Yamaguchi O, Nakano Y, Takeda T, Omiya S, Mizote I, Taneike M, Oka T, Tamai T, Oyabu J, Uno Y, Matsumura Y, Nishida K, Suzuki K, Kogo M, Hori M and Otsu K. The I{kappa}B kinase {beta}/nuclear factor {kappa}B signaling pathway protects the heart from hemodynamic stress mediated by the regulation of manganese superoxide dismutase expression. *Circulation Research*. 2009;105:70-9.
397. Nishida K, Yamaguchi O, Hirotani S, Hikoso S, Higuchi Y, Watanabe T, Takeda T, Osuka S, Morita T, Kondoh G, Uno Y, Kashiwase K, Taniike M, Nakai A, Matsumura Y, Miyazaki J, Sudo T, Hongo K, Kusakari Y, Kurihara S, Chien KR, Takeda J, Hori M and Otsu K. p38alpha mitogen-activated protein kinase plays a critical role in cardiomyocyte survival but not in cardiac hypertrophic growth in response to pressure overload. *Molecular and Cellular Biology*. 2004;24:10611-20.
398. Iwamoto H, Miura T, Okamura T, Shirakawa K, Iwatate M, Kawamura S, Tatsuno H, Ikeda Y and Matsuzaki M. Calpain inhibitor-1 reduces infarct size and DNA fragmentation of myocardium in ischemic/reperfused rat heart. *J Cardiovasc Pharmacol*. 1999;33:580-6.
399. Chen M, Won DJ, Krajewski S and Gottlieb RA. Calpain and mitochondria in ischemia/reperfusion injury. *Journal of Biological Chemistry*. 2002;277:29181-6.

400. Khalil PN, Neuhof C, Huss R, Pollhammer M, Khalil MN, Neuhof H, Fritz H and Siebeck M. Calpain inhibition reduces infarct size and improves global hemodynamics and left ventricular contractility in a porcine myocardial ischemia/reperfusion model. *European Journal of Pharmacology*. 2005;528:124-31.
401. Otsu K, Yamashita N, Nishida K, Hirotani S, Yamaguchi O, Watanabe T, Hikoso S, Higuchi Y, Matsumura Y, Maruyama M, Sudo T, Osada H and Hori M. Disruption of a single copy of the p38alpha MAP kinase gene leads to cardioprotection against ischemia-reperfusion. *Biochem Biophys Res Commun*. 2003;302:56-60.
402. Li C, Browder W and Kao RL. Early activation of transcription factor NF-kappaB during ischemia in perfused rat heart. *American Journal of Pathology*. 1999;276:H543-52.
403. Morishita R, Sugimoto T, Aoki M, Kida I, Tomita N, Moriguchi A, Maeda K, Sawa Y, Kaneda Y, Higaki J and Ogihara T. In vivo transfection of cis element "decoy" against nuclear factor-kappaB binding site prevents myocardial infarction. *Nature Medicine*. 1997;3:894-9.
404. Takeda K and Akira S. TLR signaling pathways. *Semin Immunol*. 2004;16:3-9.
405. Dai DF, Hsieh EJ, Liu Y, Chen T, Beyer RP, Chin MT, MacCoss MJ and Rabinovitch PS. Mitochondrial proteome remodelling in pressure overload-induced heart failure: the role of mitochondrial oxidative stress. *Cardiovascular Research*. 2012;93:79-88.
406. Rosca MG and Hoppel CL. Mitochondrial dysfunction in heart failure. *Heart Fail Rev*. 2013;18:607-22.
407. Johnson JA, Cavallari LH, Beitelshees AL, Lewis JP, Shuldiner AR and Roden DM. Pharmacogenomics: application to the management of cardiovascular disease. *Clinical Pharmacology & Therapeutics*. 2011;90:519-31.
408. Cha HN, Choi JH, Kim YW, Kim JY, Ahn MW and Park SY. Metformin Inhibits Isoproterenol-induced Cardiac Hypertrophy in Mice. *Korean Journal of Physiology & Pharmacology*. 2010;14:377-84.
409. Zahabi A, Picard S, Fortin N, Reudelhuber TL and Deschepper CF. Expression of constitutively active guanylate cyclase in cardiomyocytes inhibits the hypertrophic effects of isoproterenol and aortic constriction on mouse hearts. *Journal of Biological Chemistry*. 2003;278:47694-9.
410. Zhang X, Szeto C, Gao E, Tang M, Jin J, Fu Q, Makarewich C, Ai X, Li Y, Tang A, Wang J, Gao H, Wang F, Ge XJ, Kunapuli SP, Zhou L, Zeng C, Xiang KY and Chen X. Cardiotoxic and cardioprotective features of chronic beta-adrenergic signaling. *Circulation Research*. 2013;112:498-509.
411. Morillo CA, Klein GJ, Jones DL and Guiraudon CM. Chronic rapid atrial pacing. Structural, functional, and electrophysiological characteristics of a new model of sustained atrial fibrillation. *Circulation*. 1995;91:1588-95.
412. Moe GW and Armstrong P. Pacing-induced heart failure: a model to study the mechanism of disease progression and novel therapy in heart failure. *Cardiovascular Research*. 1999;42:591-9.
413. Avitall B, Urbonas A, Millard S, Urboniene D and Helms R. Ablation of atrial fibrillation in the rapid pacing canine model using a multi-electrode loop catheter. *Journal of the American College of Cardiology*. 2001;37:1733-40.
414. Gordon JW, Shaw JA and Kirshenbaum LA. Multiple facets of NF-kappaB in the heart: to be or not to NF-kappaB. *Circulation Research*. 2011;108:1122-32.
415. Leychenko A, Konorev E, Jijiwa M and Matter ML. Stretch-induced hypertrophy activates NFkB-mediated VEGF secretion in adult cardiomyocytes. *PLoS One*. 2011;6:e29055.
416. Zelarayan L, Renger A, Noack C, Zafiriou MP, Gehrke C, van der Nagel R, Dietz R, de Windt L and Bergmann MW. NF-kappaB activation is required for adaptive cardiac hypertrophy. *Cardiovascular Research*. 2009;84:416-24.